DESIGN OF NOVEL ELECTRON-RICH ORGANOMETALLIC FRAMEWORKS INVOLVING METAL-ISOCYANIDE JUNCTIONS

By

Tiffany Rene Maher

Submitted to the Department of Chemistry and the
Graduate Faculty of the University of Kansas
in partial fulfillment of the requirements for the degree of
Doctor of Philosophy.

_____
Dr. Mikhail V. Barybin – Chairperson

_____
Dr. Cindy L. Berrie

_____
Dr. Kristin Bowman-James

_____
Dr. Timothy A. Jackson

_____
Dr. Susan M. Williams

Date defended: April 16, 2009

The Dissertation Committee for Tiffany Maher certifies
this is the approved version of the following dissertation:

DESIGN OF NOVEL ELECTRON-RICH ORGANOMETALLIC FRAMEWORKS INVOLVING METAL-ISOCYANIDE JUNCTIONS

_____
Dr. Mikhail V. Barybin – Chairperson

_____
Dr. Cindy L. Berrie

_____
Dr. Kristin Bowman-James

_____
Dr. Timothy A. Jackson

_____
Dr. Susan M. Williams

Date approved: April 23, 2009

Abstract

Aromatic diisocyanides are extensively employed as building blocks in coordination and surface chemistry as charge transport mediators for nanotechnology applications. The first diisocyanoarene-bridged bimetallate system, $[\{(CO)_5V\}_2(\mu\text{-}CNC_6Me_4NC)]^{2-}$, was synthesized from $V(CO)_6$ through a neutral $[(CO)_5V]_2(\mu\text{-}CNC_6Me_4NC)$ intermediate, or, less conveniently, directly from subvalent $[V(CO)_6]^-$. In the solid state, the bimetallic dianions $[\{(CO)_5V\}_2(\mu\text{-}CNC_6Me_4NC)]^{2-}$ undergo regular π-stacking aggregation and exhibit strong contact ion association with cobaltocenium counter-ions. This results in an unusual electron-rich polymeric supramolecular ensemble held together exclusively via non-covalent interactions. The chemistry of a second vanadium(-I) bimetallate featuring the 1,1'-diisocyanoferrocene bridge is described as well.

Synthesis of 2,2'-diisocyano-1,1',3,3'-tetraethoxycarbonyl-6,6'-biazulene involving Pd-catalyzed coupling of monoazulenic precursors was developed. The single crystal X-ray analysis of this nearly 2 nm-long linear ditopic diisocyanobiazulene linker revealed an interplanar angle of 67° between the two azulene rings. The two-electron reduction of this diisocyanobiazulene is perfectly reversible, at least on the electrochemical scale, and occurs in a single step at an unusually mild potential of *ca*. 1.0 V vs. ferrocene/ferrocenium couple. Generation of a closed-shell biazulenic dianion accompanied by a substantial decrease in the interplanar angle between the two azulenic halves of this novel ligand is strongly

suggested. Mono- and bimetallic complexation of the 2,2'-diisocyano-6,6'-biazulene allowed assessment of the change in the metal-to-diisocyanobiazulene charge transfer energy upon binucleation of the linker by electronic spectroscopy. In addition, efficient regioselective mono-isocyanide functionalization of the perfectly planar, symmetric 2,2'-biazulene and initial organometallic chemistry of the resulting long nonbenzenoid aryl isocyanide is described.

The first examples of biazulenic self-assembled monolayers (SAMs) on a metal surface were prepared and characterized by FTIR and ellipsometric techniques. The organic substrates feature symmetric linear 2,2'- or 6,6'-biazulenic motif functionalized with one or two isocyanide "alligator clips". In all cases, terminal upright η^1 coordination to gold is realized. The gold-isocyanide junction in these biazulenic films appears to be much less prone to gold-assisted oxidation of isocyanide to isocyanate under ambient conditions compared to SAMs of many benzenoid aryl isocyanides on Au(111). The kinetic stability of adsorbed benzenoid aryl isocyanides on gold can be substantially improved by linking several coordinated isocyanoarene moieties together. This is demonstrated by the adsorption of 8,16,24,32-tetraisocyano[2.2.2.2]metacyclophane on the gold(111) surface via all four of its isocyanide groups to form an air-stable SAM that features approximately upright orientation of the aryl isocyanide units with respect to the surfaces as evidenced by FTIR and optical ellipsometry measurements. The energetic gain upon chemisorption of the tetraisocyanide to the gold surface in the μ_4-η^1: η^1: η^1: η^1 fashion substantially outweighs the cost of the metacyclophane conformational

change required for such coordination. Thus, the isocyanide groups function as effective two-atom long anchors for self-assembling stable monolayers of cyclophanes on metallic gold and the strategy developed herein should be of general utility.

Acknowledgements

First and foremost, I would like to thank Professor Mikhail (Misha) Barybin. He has been an amazing mentor and truly shown what it takes to be not just a chemist but a scientist in all regards. I will continually strive to reach his level of civic responsibility, which he demonstrates in so many ways, in my own life.

I would also like to thank the entire faculty in the Department of Chemistry at KU, especially Professor Cindy Berrie, Professor Kristin Bowman-James, and Professor Timothy Jackson, for their continued assistance in research, willingness to serve on my committee, and general dedication to improving scientific knowledge. I particularly must thank Dr. Cindy Berrie for all the help that she has given as a collaborator to the Barybin Group. She and her students provided so much assistance and knowledge relating to the surface chemistry work. The faculty set a tremendous example of service and commitment, which I hope to carry forward in my own career as a mentor. I also must thank Professor Susan Williams, from Chemical and Petroleum Engineering, for her service to my committee.

I have been fortunate to have really great people to work with, including Dr. Randall (Randy) Robinson, Dave McGinnis. Randy taught me about patience in the lab and desperation in research. Dave has been a great friend in and out of the lab and I am so grateful that he chose to join the Barybin group on his adventure through graduate school. I would also like to acknowledge Kolbe Scheetz, Brad Neal, Andrew Spaeth, John Meyers, and Alexander Vorushilov, my current lab mates. I also thank

Dr. Thomas Holovics, Dr. Stephan Deplazes, Krista Lemley, Garrett Glover and Sergio Perez-Conesa, former lab mates and REU students.

In the course of this work, much assistance has come from various labs around the University. I need to thank Dr. Douglas Powell and Dr. Victor Day for their work on the X-ray structures. Victor has been a tremendous help in interpreting and finding methods to collect data on very difficult crystals. Dr. Ward Thompson and his group made a significant contribution to the theoretical work relating to biazulenes and the surface calculations for the tetraisocyano[2.2.2.2]metacyclophane. A thousand thanks go to Sarah Neuenswander, who managed to keep the NMR lab running and was ever reliable when NMR services were needed. Thanks also to Dr. David Vandervelde, former NMR lab director, and Dr. Justin Douglas, the new NMR lab director and Dr. Matt Benning of Bruker-AXS in Madison, WI for collecting the diffraction data for compound **2.1c**. I also must thank Dr. Masaharu (Masa) Toriyama as a collaborator for much of this work. Without Masa, the metacyclophane work may never have happened and he was a wonderfully reliable source for starting materials relating to the 2,2'-biazulene chemistry.

Finally, I would like to thank my family and friends. My mom, Dianne, and my dad, Mike, have provided so much support despite being long distances away. I think they must have always known what I was capable of accomplishing, and I am quite proud to prove them correct. To my brother, Greg, and his wife, Khrystle, I thank both of you for being there when I needed someone to talk to. To my dear friends, Erica Roth and Janice May, although we no longer live close to one another, we have

managed to never seem that far away and without both of your faith in my abilities, I would not have gotten this far. Lastly, I thank my cats, Fish and Kiki, who were always a warm cuddle away on a day when chemistry didn't work and things seemed to difficult to bear.

TABLE OF CONTENTS

LIST OF TABLES

LIST OF FIGURES

LIST OF SCHEMES

CHAPTER I

I. First Diisocyanoarene-Bridged Bimetallates

I.1. Introduction

Isocyanides, also known as isonitriles and carbylamines, are molecules that feature a lone pair of electrons on a terminal carbon atom. In this sense, isocyanides are similar to carbon monoxide (Figure I.1). Aromatic isocyanides have been extensively studied as potentially conductive bridging molecules for molecular electronics. Current investigations into organic isocyanides as conducting molecules to be used as molecular wires has focused on the development of aromatic diisocyanides that provide significant orbital overlap between the isocyanide and the organic bridge to make a conducting wire that bridges two electronic centers. Previous contributions to this area of study have been limited to benzenoid aromatic molecules bound as a self-assembled monolayer to a metal surface or as a bridging molecule that is bound between two metal centers of low oxidation state. To date, however, there have been no reports of binding a bridging aromatic diisocyanide to two metal centers in negative oxidation states.

Figure I.1. Resonance structures of an isocyanide and carbon monoxide.

Isocyanides can behave in two fashions when coordinating to a metal center. In 1959, Malatesta reported on the potential donating and accepting properties of isocyanides.[1] Isocyanides may use the lone pair of electrons on the carbon atom to form a σ-bond to a transition metal center of almost any oxidation state. The nature of this bond is highly polar (nearly ionic) in character; however, the bond strength increases with the charge/radius ratio of the metal center. σ-Bonding is seen in coordination complexes

of amines, alcohols, etc. By 1947, coordination chemists had reported on the formation of σ-bonded isocyanides to a variety of metal ions in positive oxidation states, including Cr(III), Fe(II), Fe(III), Co(III), Cu(I), Zn(II), Mo(IV), Ag(I), Cd(II), Pt(II), W(IV), and Hg(II).[1]

Figure I.2. Donor/Acceptor nature of metal-isocyanide interactions.

Because of the presence of a π-system in the isocyanide functionality, isocyanides may also behave as acceptor ligands with transition metals, as shown in Figure I.2. These complexes will often follow the 18-electron rule.[2] The bonds formed between the isocyanide and the metal atom or ion in these complexes are much more covalent and typically the carbon-metal bond exhibits some double-bond character. Similar bonding modes are seen with carbonyls and cyanides. In fact, isocyanides are isoelectronic with the carbonyl ligand, which is typically involved in coordination chemistry of electron-rich transition metal complexes. Therefore, isocyanides have been explored in relation to metal carbonyl chemistry. However, while a large number of subvalent metal carbonyl complexes are known,[3] analogous isocyanide complexes are not as abundant.[4]

The ability to participate in π-backbonding interactions with metal centers allows ligands such as carbonyls and isocyanides to stabilize metals with a low oxidation state or a higher d-shell electron count. Prior to 1947, no reports of binary metal isocyanides existed. Based on the similarities to the metal-carbonyl chemistry, it was proposed that isocyanides should be capable of forming homoleptic complexes with transition metals.

As such, researchers began to try substitution reactions of metal carbonyls in attempts to obtain homoleptic metal isocyanides. The first reported complex of this type was with Ni(0) using $Ni(CO)_4$ as the starting material.[1] The homoleptic aryl and alkyl isocyanide Ni(0) complexes were later also formed from Ni(II) salts.[1] Advancement in the coordination chemistry of zero-valent metal isocyanide complexes, including Group 6 metals (Cr, Mo, W), followed these early discoveries. However, because of the polar nature of the isocyanide framework, isocyanides appeared to be incapable of stabilizing metal centers to the same extent as the far less polar isoelectronic carbon monoxide. Thus, it was posed that metallates (metal complexes in sub-zero oxidation states) of isocyanides may not be stable. In fact, in Malatesta's review, no reports of isocyanides with transition metals from group 1-5 had been reported as of 1959.[1]

Figure I.3. Line drawing of 1,4-diisocyanobenzene (DIB).

In 1988, Bennett and coworkers began investigating the use of 1,4-diisocyanobenzene (**DIB)** as a potential structural and electronic bridge between two electron rich metal centers for the purpose of studying charge transfer from one metal onto the other.[5] Two tungsten(0) centers were bridged by **DIB**. The ancillary ligands on the metal centers consisted of carbonyls and phosphines. Phosphines were chosen as the other ligands in the coordination sphere to enhance solubility of the bimetallic complex and increase the overall electron richness of the metal centers.[5] Upon probing the geometry and electronic properties of the bimetallic framework, Bennett and coworkers

determined that the C-N-C angles within the isocyanide groups appeared to deviate slightly from linearity in the solid state when bound to a W(0) center, possibly due to an increased charge density on the metal center due to the presence of the PR_3 groups.[5] IR and NMR data were consistent with observations afforded by the solid state structure.

Figure I.4. Electron-rich bimetallic complexes studied by Bennett and coworkers.[5]

By 1992, Bennett and coworkers continued their studies on the bimetallic W(0) **DIB** system.[6] In particular, they probed the ability for the isocyanide ligand to function as both a σ-donor and a π-acceptor by systematically varying the ancillary ligands in the coordination sphere of a bimetallic $W(CO)_x(PR_3)_y(CNR)$ system.[6] As seen in Table I.1, IR spectroscopy can be used to elucidate the extent of backbonding interactions between the metal and isocyanide group in relation to changing electron density of the metal center.[6] As the electron density on the metal center was increased by either adding more phosphine ligands or decreasing the charge on the metal center, the energy of the isonitrile stretching band appeared to decrease, thereby indicating stronger backbonding interactions.[6] For example by substituting a triarylphosphine for a carbonyl in $W(CO)_5CNC_6H_4NC$, the ν_{CN} band shifted from 2130 cm^{-1} to 2109 cm^{-1} for the isocyanide ligand bound to a metal and from 2144 to 2118 cm^{-1} for the uncoordinated isocyanide.[6] This also indicates the participation of the aromatic framework in delocalizing charge density within the complex.[6] Interestingly, however, the energy of the isocyanide stretch was not changed in the mixed-valent $(CO)_5WCNC_6H_4NCW(CO)_2(PEt_3)_2Br_2$ compared to

the analogous homo-valent complexes, indicating that, on the IR time scale, the delocalization is minute at best. [6] In the electronic spectra, the mixed-valent complex showed a single broad band that was intermediate in energy to the analogous single valent bimetallic complexes. [6]

Table I.1. Comparison of Isonitrile and Carbonyl stretching frequencies for tungsten complexes. [6]

Compound	$\nu_{CN}(cm^{-1})$	$\nu_{CO}(cm^{-1})$					
CNC_6H_4NC	2128						
$(CO)_5WCNC_6H_4NC$	2130 2144			1925		1990	2056
$(CO)_4(PPh_3)WCNC_6H_4NC$	2109 2118	1898		1942	1953	2005	
$W(CO)_3(PEt_3)_2Br_2$		1894		1921			
$(CO)_5WCNC6H4NCW(CO)_5$	2132			1925		1990	2055
$(CO)_4(PPh_3)WCNC_6H_4NC$ $W(PPh_3)(CO)_4$	2111	1884	1907	1926		1999	
$Br_2(PEt_3)_2(CO)_2WCNC_6H_4NC$ $W(CO)_2(PEt_3)_2Br_2$	2083	1870		1928			
$(CO)_5WCNC_6H_4NC$ $W(CO)_2(PEt_3)Br_2$	2092 2141	1873		1926	1950	1992	2056
$(CO)_4(PPh_3)WCNC_6H_4NC$ $W(CO)_2(PEt_3)Br_2$	2094 2110		1913			2003	

During this time period, researchers were also using **DIB** in studies of macrocyclic complexes with applications towards luminescent sensors and light harvesting materials. In 1996, Hanack reported that **DIB** could be used to bridge two iron centers trapped in phthalocyanine units to form macrocyclophane complexes with the aim of forming Langmuir-Blodgett films, sensors for organic vapors, or nonlinear optical applications.[7] The isocyanide stretching frequencies indicated the participation of the **DIB** bridge in backbonding interactions with the metal centers. Likewise, Hanack and coworkers reported in 1998 that **DIB** could be used to bridge ruthenium phthalocyanine units to create stacked transition metal macrocycles.[8] In 1999, Mirkin and coworkers described

using **DIB** to link the metal centers of two metallocyclophanes and analyzed the influence of the **DIB** linker on the luminescence of the resulting supramolecular assembly.[9] **DIB** had no quenching effect on the fluorescence of the phthalocyanine units and the supramolecular assembly exhibited a broad structure-less charge transfer band that was consistent with molecules that behave as donor-acceptor complexes.[9]

Figure I.5. Example of a phthalocyanine complex bridged by DIB.

Although Bennett and coworkers extensively studied metal complexes containing W(0) and **DIB**, little other chemistry involving electron rich metal centers with this bridging aromatic isocyanide has been investigated. However, monoisocyanide congeners have been investigated in reactions of low-valent Group 5 and 6 transition metals. Ellis and coworkers reported in 1982 the first metallate containing an isocyanide ligand in $[V(CO)_5(CNR)]^-$ where R= phenyl, ^{n}butyl, methyl, ^{t}butyl, and cyclohexyl.[10] The synthesis of this metallate was accomplished by using labile ligand addition to the

extremely electron-rich anion $[V(CO)_5]^{3-}$.[10] In this reaction sequence, $[V(CO)_5]^{3-}$ was combined with ammonia to form monoanion $[V(CO)_5NH_3]^-$, the ammonia ligand of which was then displaced by an aryl or alkyl isocyanide.[10] The reaction sequence, which starts from $[V(CO)_6]^-$ is somewhat more facile than previous substitution reactions using the neutral $V(CO)_6$, as the latter 17-electron vanadium carbonyl complex is formed by one electron oxidation of $[V(CO)_6]^-$.[10]

By 1985, Rehder had expanded the above chemistry by employing photolysis of $[V(CO)_6]^-$ in the presence of a labile ligand or solvent followed by ligand exchange to form pentacarbonylisocyanovanadate(I-) complexes with alkyl and aryl isocyanides.[11] The photolytic substitution allows for synthesis of substituted organometallic carbonyl vanadates without the use of liquid ammonia. In 1989, Cooper reported the first binary transition metal isonitrilate, $K[Co(CNXyl)_4]$, where CNXyl is 2,6-dimethylphenylisocyanide.[12] This reaction was accomplished by first forming the tetraethene complex of Co(-I) and then performing ligand substitution with the appropriate aryl isocyanide.[12] In 1994, Cooper also reported the formation of this cobaltate 1) using the dimeric $Co_2(CNXyl)_8$ which contains two bridging isocyanide ligands and 2) by reducing cobaltocene with potassium and then exposing the salt to excess xylyl isocyanide.[13] A similar chemistry has led to the isolation of $[Mn(CNAr)_5]^-$ and $[Ru(CNR_4)]^{2-}$ by Cooper *et al.*[14,15]

The xylyl isocyanide ligand appeared again in the more recent work from the Ellis lab in isolating the hexakis(vanadium isocyanide) complexes with the metal atom in +1, 0 and -1 oxidation states.[3] Prior to this report in 1998, hexakis aryl isocyanide complexes had only been isolated for Group 6-10 transition metals.[3] The Ellis group had been using

a vanadium(I-) naphthalene intermediate to form other complexes and realized that this very reactive complex could also be used to access homoleptic isocyanide vanadates(I-).[3] Capitalizing on this earlier result, the Ellis group investigated the viability of using metal isocyanide complexes in natural product synthesis as a catalyst for reductive carbon-carbon bond formation.[16] In 1999, they reported isolation of homoleptic metallates(I-) of xylyl isocyanide with tantalum and niobium, the other group 5 metals.[16] However, traditional synthetic techniques that worked with carbonyl and phosphine chemistry were not successful for xylyl isocyanide.[16] Attempts to react xylyl isocyanide directly with the hexacarbonylmetallate were unsuccessful in yielding the desired homoleptic metallate.[16]

As the investigation continued, researchers in the Ellis lab discovered that reacting the neutral hexacarbonyl vanadium with xylyl isocyanide formed the tetrasubstituted *trans*-$V(CO)_2(CNXyl)_4$.[16] They then prepared homoleptic complexes by first oxidizing the metal to a +1 oxidation state using Ag^+ followed by substitution of all six carbonyls with isocyanides.[16] Using this method, the Ellis group was able to isolate homoleptic heptaisocyanide niobium and tantalum complexes.[16] Similar chemistry with *p*-isocyanotoluene was unsuccessful in yielding hexakis(isocyano)metallates with Group 5 transition metals.[17]

Figure I.6. Line drawing of Xylyl Isocyanide.

This chapter introduces the chemistry of the first diisocyanobimetallate species. The novel complex anion contains two electron-rich vanadium(I-) pentacarbonyl units linked by 1,4-diisocyano-2,3,5,6-tetramethylbenzene, also named 1,4-diisocyanodurene, (**DID**). This investigation includes synthesis, structural and spectroscopic characterization, and properties of salts of the $[(CO)_5V(\mu\text{-}\mathbf{DID})V(CO)_5]^{2-}$ dianion, as well as those of its mononuclear analog, $[(CO)_5V(CNXyl)]^{-1}$. In addition, 1,1'-diisocyanoferrocene-bridged bis(pentacarbonyl)vanadate(I-) system is described.

I.2. Experimental

I.2.1. General Procedures

Unless specified otherwise, all operations were performed under an atmosphere of 99.5% argon further purified by passage through columns of activated BASF catalyst and molecular sieves. All connections involving the gas purification systems were made of glass, metal, or other materials impermeable to air. Solutions were transferred via stainless steel needles (cannulas) whenever possible. Standard Schlenk techniques were employed with a double manifold vacuum line. Both CH_3CN and CD_3CN were distilled over CaH_2. THF was distilled from Na/benzophenone. Heptane and pentane were distilled from Na/benzophenone dissolved in a minimum amount of diglyme. DMSO was distilled over P_2O_5. Following purification, all solvents, including deuterated, were stored under argon.

Solution infrared spectra were recorded on a Thermo Nicolet Avatar 360 FTIR spectrometer with samples sealed in 0.1 mm gas-tight NaCl cells. NMR samples were analyzed on Bruker DRX-400 and Bruker Avance 500 spectrometers. ^{1}H and ^{13}C

chemical shifts are given with reference to residual ^{1}H and ^{13}C solvent resonances relative to Me_4Si. UV-Vis spectra were recorded in CH_2Cl_2 or CH_3CN at 24 °C using a CARY 100 spectrophotometer.

Cyclic voltammetric (CV) experiments on 2×10^{-3} M solutions of **1.1a**, **1.1b**, **1.2,** and **1.3** in CH_3CN were conducted at room temperature using an EPSILON (Bioanalytical Systems INC., West Lafayette, IN) electrochemical workstation. The electrochemical cell was placed in an argon-filled Vacuum Atmospheres dry-box. Tetrabutylammonium hexafluorophosphate (0.1 M solution in CH_3CN) was used as a supporting electrolyte. Cyclic voltammograms were recorded at 22 ± 2 °C using a three component system consisting of a platinum working electrode, a platinum wire auxiliary electrode, and a glass encased non-aqueous silver/silver chloride reference electrode. The reference Ag/Ag^+ electrode was monitored with the ferrocenium/ferrocene couple. IR compensation was achieved before each CV run by measuring the uncompensated solution resistance followed by incremental compensation and circuit stability testing. Background cyclic voltammograms of the electrolyte solution were recorded before adding the analytes. The half-wave potentials ($E_{1/2}$) were determined as averages of the cathodic and anodic peak potentials of reversible couples and are referenced to the external FcH^+/FcH couple.[18]

Melting points are uncorrected and were determined for samples in capillary tubes sealed under argon. Elemental analyses were carried out by Desert Analytics, Tucson, Arizona.

Compounds $[Et_4N][V(CO)_6]$,[19] $[Cp_2Co][V(CO)_6]$,[20] $V(CO)_6$,[21] $[Cp_2Co][BF_4]$,[22] 1,4-CNC_6Me_4NC (1,4-diisocyano-2,3,5,6-tetramethylbenzene, **DID**),[23] CNXyl (Xyl = 2,6-

dimethylphenyl),[24] and CN_2Fc (1,1'-diisocyanoferrocene)[25] were prepared according to literature procedures. Other reagents were obtained from commercial sources and used as received.

I.2.2. Synthesis of $[Cp_2Co]_2[V_2(CO)_{10}(\mu\text{-DID})]$ (1.1a) from $V(CO)_6$.

A colorless solution of **DID** (0.0716 g, 0.3886 mmol), in 100 mL of heptane was added to a cold (-70°C) canary yellow solution of hexacarbonylvanadium(0) (0.1702 g, 0.7772 mmol) in 200 mL of heptane in the dark with stirring. The reaction mixture was stirred at -70°C for 2 hours while acquiring a pale tangerine color and then warmed to 0°C. FTIR of the solution/slurry in the ν_{CN} and ν_{CO} regions indicated essentially complete consumption of the starting materials. Then, an orange-brown solution of cobaltocene (0.1470 g, 0.7772 mmol) in 20 mL of CH_2Cl_2 was transferred to the reaction mixture in one portion at 0 °C and the mixture was vigorously stirred for 30 min. The resulting dark solid was filtered off, washed with CH_2Cl_2 (100 mL) and pentane (50 mL), recrystallized from CH_3CN/Et_2O, and dried at 10^{-2} torr to afford dark violet, nearly black, **1.1a** (0.3020 g, 0.3198 mmol) in a 73% yield. Compound **1.1a** decomposes without melting at 138˚C. Anal. Calcd. for $C_{42}H_{32}Co_2N_2O_{10}V_2$: C, 53.41; H, 3.42; N, 2.97. Found: C, 52.89; H, 3.60; N, 3.38. [Calcd. for $C_{42}H_{32}Co_2N_2O_{10}V_2 \cdot (CH_3CN)_{0.25}$: C, 53.47; H, 3.46; N, 3.30]. % Carbon was repeatedly 0.5-0.6% low upon reanalysis. IR (CH_3CN): ν_{CN} 2041 w br, ν_{CO} 1926 m br, 1847 s sh 1839 vs 1824 m sh cm^{-1}. ^1H NMR (500 MHz, CD_3CN, 25°C): δ 2.28, 2.30, 2.33, 2.35 (all s, 12H combined intensity, C*H*$_3$), 5.65 (s, 20H, C_5H_5) ppm. $^{13}C\{^1H\}$ NMR (125 MHz, CD_3CN, 25°C): δ 16.3, 16.4, 16.6,

16.7 (CH_3), 86.0 (C_5H_5) ppm. UV-vis (CH_3CN, λ_{max} ($\varepsilon \times 10^3$ M^{-1} cm^{-1}), 24 °C): 486 (3.23) nm.

I.2.3. Synthesis of $[Cp_2Co]_2[V_2(CO)_{10}(\mu\text{-DID})]$ (1.1a) from $[Cp_2Co][V(CO)_6]$.

A solution of $[Cp_2Co][V(CO)_6]$ (0.1573 g, 0.3855 mmol) and DMSO (0.2 mL, 2.8 mmol) in 80 mL of THF was irradiated using a Hanovia Hg 450 W immersion lamp for 4 hrs at 22 °C with stirring. Then, the red-orange reaction mixture was concentrated to about 20 mL under vacuum. 1,4-Diisocyano-durene (0.0355g, 0.1927 mmol) dissolved in 20mL of THF was added to the above concentrated solution. The mixture was stirred for 10 hrs, concentrated to about 10mL, and stirred for an additional 8 hr period. An oily black precipitate formed. Pentane (30mL) was added to the reaction flask and the mixture was vigorously stirred for 30 min. Then, 20 mL of toluene was added with stirring and the solution/slurry was allowed to settle. The solution was carefully removed by cannula and the residue was washed with toluene (2×20 mL). The resulting dark violet, nearly black solid was washed with 50mL of pentane and then triturated with an additional 50mL of pentane. Filtration followed by drying at 10^{-2} torr provided crude **1.1a** as a dark violet powder. Recrystallization of this solid from CH_3CN/Et_2O gave microcrystalline **1.1a** (0.0572g, 0.0606 mmol) in a 31% yield. The product was spectroscopically (FTIR, NMR) identical to *bona fide* **1.1a** described above.

I.2.4. Synthesis of $[Et_4N]_2[V_2(CO)_{10}(\mu\text{-DID})]$ (1.1b).

A yellow solution of $[Et_4N][V(CO)_6]$ (0.3466 g, 0.9924 mmol) and DMSO (0.4 mL, 5.6 mmol) in 80 mL of THF was irradiated using a Hanovia Hg 450 W immersion lamp for 4 hrs at 22 °C with stirring. 1,4-Diisocyano-durene (0.0914g, 0.4962 mmol)

dissolved in 20mL of THF was added to the above solution and the mixture was stirred for 15 hrs. Then, the reaction mixture was concentrated to about 20 mL and stirred for an additional 2 hr period. Pentane (30mL) was added to the reaction flask and the mixture was vigorously stirred for 30 min. An oily dark red precipitate formed, which was washed with toluene (2×20 mL). The toluene washings were carefully removed via cannula. After addition of 50 mL of pentane with stirring, the solution/slurry was filtered; the filter-cake was dissolved in THF. This THF solution was filtered; the filtrate was layered with 150 mL of pentane and stored at -35 °C for 3 hrs. The magenta precipitate was filtered off, washed with pentane (2×10 mL) and dried at 10^{-2} torr to provide **1.1b** (0.2523 g, 0.3052 mmol) in a 62% yield as a free-flowing magenta solid. Mp: 82-84 °C. IR (CH_3CN): ν_{CN} 2034 w, ν_{CO} 1911 m, 1857 s sh 1839 vs cm^{-1}. ^1H NMR (500 MHz, CD_3CN, 25°C): δ 1.20 (t, 24H, CH_2CH_3, $^3J_{H-H}$ = 7 Hz), 2.30, 2.32 (both s, 12H combined intensity, CH_3), 3.16 (q, 16H, CH_2CH_3, $^3J_{H-H}$ = 7 Hz) ppm. $^{13}C\{^1H\}$ NMR (125 MHz, CD_3CN, 25°C): δ 7.7 (CH_2CH_3), 16.4 (CH_3), 53.2 (CH_2CH_3) ppm. UV-vis (CH_3CN, λ_{max} ($\varepsilon\times10^3$ M^{-1} cm^{-1}), 24 °C): 486 (10.23) nm.

I.2.5. Cation metathesis 1.1b → 1.1a.

A mixture of cobaltocenium tetrafluoroborate (0.0818g, 0.2963mmol) and **1.1b** (0.1225g, 0.1482mmol) was dissolved in 80mL of CH_2Cl_2. The resulting solution was stirred at 22 °C for 48 hrs to form a dark violet precipitate. After addition of *less* than 100 mL of heptane, the solid was filtered off, washed with 50mL of heptane, and dried at 10^{-2} torr. Recrystallization from CH_3CN/Et_2O (20/150 mL) followed by drying of the product at 10^{-2} torr afforded a 53% yield of **1.1a** (0.0738g 0.0781 mmol), which was spectroscopically (FTIR, ^1H NMR) identical to *bona fide* **1.1a** described above.

I.2.6. Synthesis of $[Cp_2Co]_2[(OC)_5V(CNXyl)]$ (1.2).

A colorless solution of 2,6-dimethylphenyl isocyanide (0.1970 g, 1.5019 mmol), in 70 mL of heptane was added to a yellow-green solution of hexacarbonylvanadium(0) (0.3325 g, 1.5183 mmol) in 100 mL of heptane at room temperature. The reaction mixture rapidly acquired a mustard color. After stirring for 2 hrs, an orange-brown solution of cobaltocene (0.3234 g, 1.7100 mmol) was added to the reaction mixture at 22 °C to result in the formation of dark aqua-colored slurry. This mixture was stirred for 1 hr and then filtered. The filter-cake was washed with heptane (2×30 mL) and recrystallized from THF/Et_2O to afford microcrystalline dark turquoise (bluish green) **1.2** (0.5425 g, 1.0610 mmol) in two crops in a 71% combined yield. Mp: 104-106 °C (dec). Anal. Calcd. for $C_{18}H_{19}CoNO_5V$: C, 56.38; H, 3.75; N, 2.74. Found: C, 56.43; H, 4.01; N, 2.61. IR (CH_3CN): ν_{CN} 2053 w, ν_{CO} 1943 m, 1849 s sh, 1837 vs cm^{-1}. ^1H NMR (400 MHz, CD_3CN, 21 °C): δ 2.36 (s, 6H, C*H*$_3$), 5.35 (s, 10H, C_5H_5), 7.02 (t, 1H, *p*-H, $^3J_{H-H}$ = 8 Hz), 7.05 (d, 2H, *m*-H, $^3J_{H-H}$ = 8 Hz) ppm. $^{13}C\{^1H\}$ NMR (100 MHz, CD_3CN, 21°C): δ 19.1 (*C*H_3), 88.9 (C_5H_5), 126.7, 128.6, 134.4 (aromatic *C*) ppm. UV-vis (CH_3CN, λ_{max} ($\varepsilon\times10^3$ M^{-1} cm^{-1}), 24 °C): 483 (1.75) nm.

I.2.7. Synthesis of $[Et_4N]_2[V_2(CO)_{10}(\mu$-1,1'-diisocyanoferrocene)] (1.3).

A yellow solution of $[Et_4N][V(CO)_6]$ (0.4254g, 1.2180mmol) and DMSO (0.43mL, 6.09mmol) in 80 mL of THF was irradiated using a Hanovia Hg 450 W immersion lamp for 4 hrs at 22 °C with stirring. 1,1'-Diisocyanoferrocene (0.1437g, 0.6090mmol) dissolved in 20mL of THF was added to the above solution and the mixture was stirred for 15 hrs. Then, the reaction mixture was concentrated to about 20 mL and stirred for an

additional 2 hr period. Pentane (30mL) was added to the reaction flask and the mixture was vigorously stirred for 30 min. An oily dark red residue formed, which was washed with toluene (2×20 mL). The toluene washings were carefully removed via cannula. The oily residue was dissolved in 10mL of acetonitrile and layered with ether to recrystallize. After complete diffusion had occurred, the residual solvent was removed by cannula. Washing with ether produced a free flowing red-orange powder in 26% yield (0.1372g, 0.1561mmol). Mp: 82-96 °C. IR (THF): ν_{CN} 2043 w, ν_{CO} 1925 m, 1856 s sh 1840 vs cm^{-1}. ^{1}H NMR (500 MHz, CD_3CN, 25°C): δ 1.21 (br, 24H, CH_2CH_3), 3.18 (br, 16H, CH_2CH_3) ppm, 4.22, 4.51 (both t, C_5H_4, J_{H-H} = 2 Hz). $^{13}C\{^{1}H\}$ NMR (125 MHz, CD_3CN, 25°C): δ 8.08 (CH_2CH_3), 53.43 (CH_2CH_3) ppm, 67.81, 69.91, 70.18 (C_5H_4). UV-vis (CH_3CN, λ_{max} ($\varepsilon\times10^3$ M^{-1} cm^{-1}), 24 °C): 382 (1.93) nm.

I.2.8. X-Ray Crystallographic Characterization of 1.1a

A black needle-shaped crystal of **1.1a** of dimensions 0.46 x 0.16 x 0.10 mm exhibited, at 100(2) K, a tetragonal, space group $P4_2/n$ - C_{4h}^4 (No. 86)[26] with *a* = 23.719(1) Å, *b* =23.719(1) Å, *c* = 7.1617(8) Å, V = 4029.2(6) $Å^3$ and Z = 4 in $[Co(C_5H_5)_2]_2[(V(CO)_5)_2(C_6(CH_3)_4(CN)_2)]$ units {d_{calcd} = 1.557 g/cm^3; μ_a(MoKα) = 1.319 mm^{-1}}. A full hemisphere of diffracted intensities (1850 10-second frames with an ω scan width of 0.30°) was measured for a single-domain specimen using graphite-monochromated MoKα radiation (λ = 0.71073 Å) on a Bruker SMART APEX CCD Single Crystal Diffraction System.[27] X-rays were provided by a fine-focus sealed x-ray tube operated at 50kV and 30mA. Lattice constants were determined with the Bruker SAINT software package using peak

centers for 8659 reflections. A total of 41416 integrated reflection intensities having $2\theta(MoK\alpha) < 60.20°$ were produced using the Bruker program SAINT;[28] 5907 of these were unique and gave $R_{int} = 0.051$ with a coverage which was 99.6% complete. The intensity data were corrected empirically for variable absorption effects;[29] the relative transmission factors ranged from 0.746 to 1.000. The Bruker software package SHELXTL Version 6.10[30] was used to solve the structure using "direct methods" techniques. All stages of weighted full-matrix least-squares refinement were conducted using F_o^2 data with the SHELXTL software package. A total of 264 parameters were refined using no restraints, 5907 data and weights of $w = 1/ [\sigma^2(F^2) + (0.0734 P)^2 + 0.3571 P]$, where $P = [F_O^2 + 2F_C^2] / 3$. Final agreement factors at convergence are: R_1(unweighted, based on F) = 0.050 for 4501 independent absorption-corrected reflections having $2\theta(MoK\alpha) < 60.20°$ and $I>2\sigma(I)$; R_1 (unweighted, based on F) = 0.070 and wR_2(weighted, based on F^2) = 0.129 for all 5907 independent absorption-corrected reflections having $2\theta(MoK\alpha) < 60.20°$. The largest shift/s.u. was 0.002 in the final refinement cycle. The final difference map had maxima and minima of 1.25 and -0.28 $e^-/Å^3$, respectively. The one peak in the final difference Fourier with electron density > 0.71 $e^-/Å^3$ was within 0.80 Å of the Co atom.

The final structural model incorporated anisotropic thermal parameters for all nonhydrogen atoms and isotropic thermal parameters for all hydrogen atoms. The two crystallographically independent methyl groups in the dianion were included in the structural model as rigid groups (using idealized sp^3-hybridized geometry and a C-H bond length of 0.98 Å), which were allowed to rotate about their C-C bonds in least-

squares refinement cycles. The remaining hydrogen atoms were included in the structural model as idealized atoms (assuming sp^2-hybridization of the carbon atoms and a C-H bond length of 0.95 Å). The isotropic thermal parameters of all idealized hydrogen atoms were fixed at values 1.2 (non-methyl) or 1.5 (methyl) times the equivalent isotropic thermal parameter of the carbon atom to which they are covalently bonded.

A region of the unit cell containing disordered solvent molecules of crystallization (presumably acetonitrile) was modeled using the Squeeze option in PLATON.[31] The displacement ellipsoids are drawn at the 50% probability level.

Table I.2. Crystal data and structure refinement for $[Co(C_5H_5)_2]_2$ $[(V(CO)_5)_2(C_6(CH_3)_4(CN)_2)]$.

Empirical formula	$C_{21}H_{16}CoNO_5V$
Formula weight	472.22
Temperature	100(2) K
Wavelength	0.71073 Å
Crystal system	Tetragonal
Space group	$P4_2/n - C_{4h}^4$ (No. 86)
Unit cell dimensions	**a** = 23.719 (1) Å
	b = 23.719 (1) Å
	c = 7.1617(8) Å
Volume	4029.2(6) $Å^3$
Z	8 empirical formula units
Density (calculated)	1.557 Mg/m^3
Absorption coefficient	1.319 mm^{-1}
F(000)	1912
Crystal size	0.46 x 0.16 x 0.10 mm^3
Theta range for data collection	2.43º to 30.10°
Index ranges	$-33 \leq h \leq 33, -33 \leq k \leq 33, -10 \leq l \leq 9$
Reflections collected	41416
Independent reflections	5907 [R_{int} = 0.051]
Completeness to theta = 30.10°	99.6 %
Absorption correction	SADABS
Max. and min. transmission	1.000 and 0.746
Refinement method	Full-matrix least-squares on F^2
Data / restraints / parameters	5907 / 0 / 264
Goodness-of-fit on F^2	1.069
Final R indices [I>2sigma(I)]	R_1 = 0.050, wR_2 = 0.120
R indices (all data)	R_1 = 0.070, wR_2 = 0.129
Largest diff. peak and hole	1.25 and -0.28 $e^-/Å^3$

I.2.9. X-Ray Crystallographic Characterization of 1.3

Orange-brown crystals of solvated $[\{V(CO)_5(CNC_5H_4)\}_2Fe][N(C_2H_5)_4]_2$ are, at 100(2) K, monoclinic, space group $P2_1/n$ [an alternate setting for $P2_1/c - C_{2h}^5$ (No. 14)] (1) with a = 12.692(3), b = 22.076(5) Å, c = 32.705(7) Å, β = 90.185(6)°, V = 9163(4) $Å^3$ and Z = 8 formula units {d_{calcd} = 1.385 g/cm^3; μ_a(MoKα) = 0.827 mm^{-1}}. A full hemisphere of diffracted intensities (1850 40-second frames with a ω scan width of 0.30°) was measured for a single-domain specimen using graphite-monochromated MoKα radiation (λ= 0.71073 Å) on a Bruker SMART APEX CCD Single Crystal Diffraction System.[27] X-rays were provided by a fine-focus sealed x-ray tube operated at 50kV and 30mA. Lattice constants were determined with the Bruker SAINT software package using peak centers for 8529 reflections. A total of 74087 integrated reflection intensities having 2θ(MoKα)< 50.00º were produced using the Bruker program SAINT;[28] 16097 of these were unique and gave R_{int} = 0.092 with a coverage which was 99.9% complete. The data were corrected empirically for variable absorption effects using equivalent reflections; the relative transmission factors ranged from 0.828 to 1.000. The Bruker software package SHELXTL was used to solve the structure using "direct methods" techniques. All stages of weighted full-matrix least-squares refinement were conducted using F_o^2 data with the SHELXTL Version 6.10 software package.[30]

All hydrogen atoms for the anions and cations were included into the structural model as idealized atoms (assuming sp^2- or sp^3-hybridization of the carbon atoms and C-H bond lengths of 0.98 – 1.00 Å). Methyl groups for the cations were included in the structural model with idealized "staggered" orientations. Hydrogen atoms were not included for any of the solvent moieties. The isotropic thermal parameters of all included hydrogen atoms were fixed at values 1.2 (nonmethyl) or 1.5 (methyl) times the equivalent

isotropic thermal parameter of the carbon atom to which they are covalently bonded. Two of the four tetraethylammonium cations are disordered with two possible orientations for each of their ethyl arms. The disorder for both cations is virtually identical. The two orientations are mirror images of each other with common positions for the nitrogen and terminal carbon atoms of the ethyl arms. The first of these cations has a major orientation that is occupied 68% of the time and the second has a major orientation that is occupied 53% of the time. A region of the asymmetric unit contains disordered solvent molecules. This region contains at least one molecule of CH_2Cl_2 and probably a mixture of acetonitrile, THF and/or pentane. Difference Fourier peaks for this region were included in the structural model as isotropic carbon atoms and their occupancy factors were adjusted downward to give them reasonable thermal parameters and account for (presumed) partial occupancy. The final occupancy factors assigned to these solvent atoms were: C2s, 1.00; C3s, 0.50; C4s, 1.00; C5s, 1.00; C6s, 0.50; C7s, 0.70; C8s, 0.70; and C9s, 0.50. The second chlorine atom of the dichloromethane solvent molecule is disordered over two sites; the major site is occupied 85% of the time. A free variable representing the length of a C-C single bond was included in the refinement to restrain selected segments of the disordered cations and solvent atoms. The values of 32 N-C, C-C and C-Cl bond lengths and 27 tetrahedral angles in these disordered groups were restrained by requiring pairs of nonhydrogen atoms to have separations near idealized multiples of this free variable. This free variable refined to a final value of 1.577(2) Å.

The final structural model incorporated anisotropic thermal parameters for all nonhydrogen atoms of the anions and cations as well as the carbon and the full and

major-occupancy chlorine atoms of the dichloromethane solvent molecule of crystallization. Isotropic thermal parameters were used for the remaining solvent nonhydrogen atoms and all included hydrogen atoms. A total of 1129 parameters were refined using 59 restraints, 16097 data and weights of $w = 1/ [\sigma^2(F^2) + (0.1338\ P)^2]$, where $P = [F_O^2 + 2F_C^2] / 3$. Final agreement factors at convergence are: R_1(unweighted, based on F) = 0.132 and wR_2(weighted, based on F^2) = 0.233 for all 16097 independent absorption-corrected reflections having $2\theta(MoK\alpha) < 50.00^o$. Parallel refinement with SQUEEZED data (C2s to C9s removed) gave R1 = 0.079. The largest shift/s.u. was 0.000 in the final refinement cycle. The final difference Fourier had maxima and minima of 1.56 $e^-/Å^3$ and -1.50 $e^-/Å^3$, respectively. The top ten maxima (1.56 $e^-/Å^3$ to 0.88 $e^-/Å^3$) in the final difference Fourier were within 1.04 Å of a disordered solvent atom.

Table I.3. Crystal data and structure refinement for $[N(CH_2CH_3)_4]_2$ $[(V(CO)_5)(CNC_5H_4)_2Fe]$.

Empirical formula	$C_{41.50}H_{48}ClFeN_4O_{10}V_2$
Formula weight	956.02
Temperature	100(2) K
Wavelength	0.71073 Å
Crystal system	Monoclinic
Space group	P2(1)/n
Unit cell dimensions	**a** = 12.692(3) Å **b** = 22.076(5) Å **c** = 32.705(7) Å
Volume	9163(4) $Å^3$
Z	8 empirical formula unites
Density (calculated)	1.386 Mg/m^3
Absorption coefficient	0.828 mm^{-1}
F(000)	3952
Crystal size	0.42 x 0.18 x 0.04 mm^3
Theta range for data collection	1.84° to 20.82°
Index ranges	$-12 \leq h \leq 12$, $-22 \leq k \leq 22$, $-32 \leq l \leq 32$
Reflections collected	49106
Independent reflections	9583 [R(int) = 0.1739]
Completeness to theta = 20.82°	99.8 %
Absorption correction	Multi-scans
Max. and min. transmission	1.000 and 0.787
Refinement method	Full-matrix least-squares on F^2
Data / restraints / parameters	9583 / 55 / 896
Goodness-of-fit on F^2	1.000
Final R indices [I>2sigma(I)]	R1 = 0.0808, wR2 = 0.1560
R indices (all data)	R1 = 0.1901, wR2 = 0.1752
Largest diff. peak and hole	0.798 and -0.680 $e^-/Å^3$

I.3. Results and Discussion

Scheme I.1. Syntheses of 1.1a and 1.1b.

The synthesis of complexes **1.1a** and **1.1b** are summarized in Scheme I.1. Complex **1.1a** can be obtained by first oxidizing the tetraethylammonium salt of hexacarbonylvanadate(I-), forming the reactive 17-electron hexacarbonylvanadium(0). Hexacarbonylvanadium(0) reacts with half an equivalent of **DID** and the resulting intermediate is then reduced *in situ* with cobaltocene to afford the deep red-purple **1.1a** in 66% yield over two steps. Compound **1.1a** can also be formed by first accessing **1.1b**. This method removes the need to oxidize hexacarbonylvanadium(-I), but adds a cation metathesis step. The photolytically generated tetraethylammonium pentacarbonylvanadate(I-) dimethylsulfoxide adduct[11] was combined with 0.5 equivalents of **DID** to form the tetraethylammonium salt, **1.1b**. Cation metathesis with cobaltocenium tetrafluoroborate gave a 33% yield of **1.1a** in two steps. Attempts to synthesize **1.1a** by photolysis of cobaltocenium hexacarbonylvanadate(I-) repeatedly performed sluggishly providing a maximum 30% yield of the product. This third method involved the initial formation of cobaltocenium hexacarbonylvanadate(I-), which requires oxidizing tetraethylammonium hexacarbonylvanadate(I-) followed by reduction of hexacarbonylvanadium(0) with cobaltocene, thus proving to be an impractical route.

Purification of **1.1a** and **1.2** proved quite facile as the products were poorly soluble in dichloromethane, allowing all unreacted materials to be easily washed away followed by recrystallization of the isolated solid. Complex **1.3** was somewhat more difficult to purify, requiring repeated washings with toluene to extract excess DMSO from the photolysis reaction, followed by recrystallization in acetonitrile and ether to provide free flowing powder. Compound **1.1b** was more soluble than the other vanadate salts, but after repeated triturations with pentane and toluene, the oily residue was converted to solid at which point recrystallization provided analytically pure **1.1b**.

Table I.4. Select bond distances and angles for relevant bis(pentacarbonyl) diisocyanide complexes and respective ligands.

Complex	M-CN (Å)	C≡N (Å)	CN-C (Å)	C≡N-C (°)
1.1a	2.026(3)	1.174(3)	1.390(3)	177.9(3)
1.3	2.009(8)	1.18(1)	1.358(9)	175.6(7)
	2.012(7)	1.167(9)	1.382(8)	163.8(7)
	2.020(7)	1.171(9)	1.385(8)	177.0(7)
	2.023(7)	1.179(9)	1.373(8)	165.6(7)
DID[32]		1.163(1)	1.405(1)	178.3(1)
bis(pentacarbonylchromium)	1.977(1)	1.160(2)	1.388(2)	170.2(1)
1,1'-diisocyanoferrocene[39]	1.992(2)	1.154(2)	1.386(2)	174.9(2)

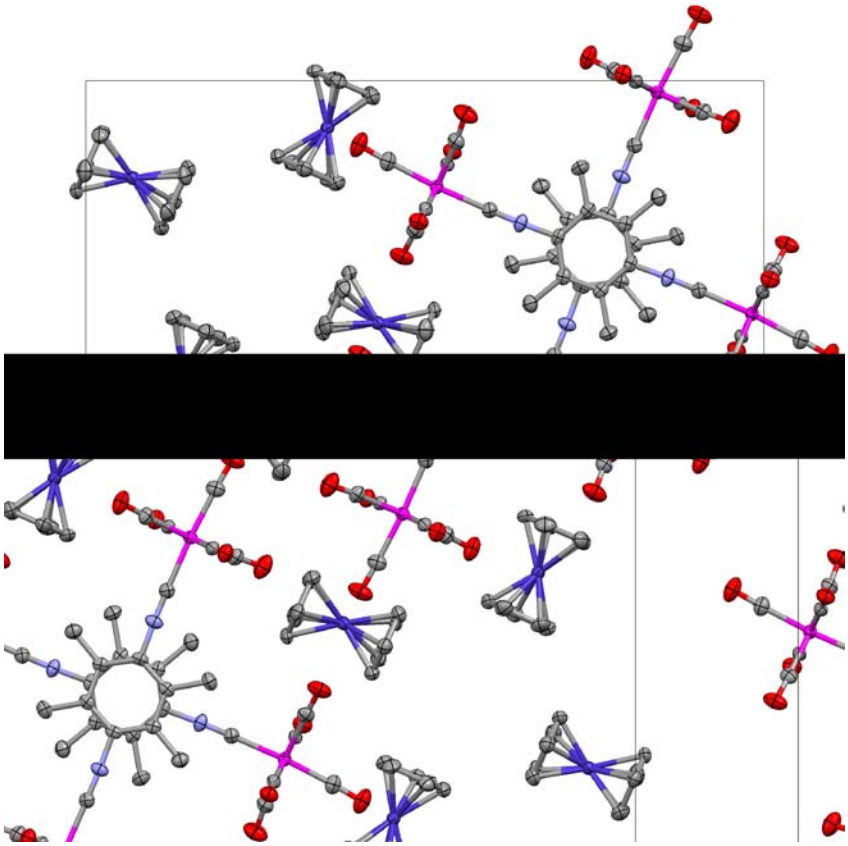

Figure I.7. Drawing of the tetragonal unit cell of 1.1a (view down c-axis, 50% thermal ellipsoids) emphasizing π-stacking and close interionic interactions. All H-atoms are omitted for clarity.

The single crystal X-ray analysis of **1.1a** revealed that only half of the V_2-dianion and one $[Cp_2Co]^+$ cation are crystallographically independent, as can be seen from the data in Table I.2. The packing diagram in Figure I.7 shows the aromatic portions of the dianions undergoing strong π-stacking interactions with intercentroid distances between the arene rings being 3.58Å. These non-covalent π-interactions[33] form columns of perfectly staggered $\{[V(CO)_5]_2(\mu\text{-}1,2\text{-}CNC_6Me_4NC)\}^{2-}$ dianions that are insulated from one another by layers of $[Cp_2Co]^+$ cations.

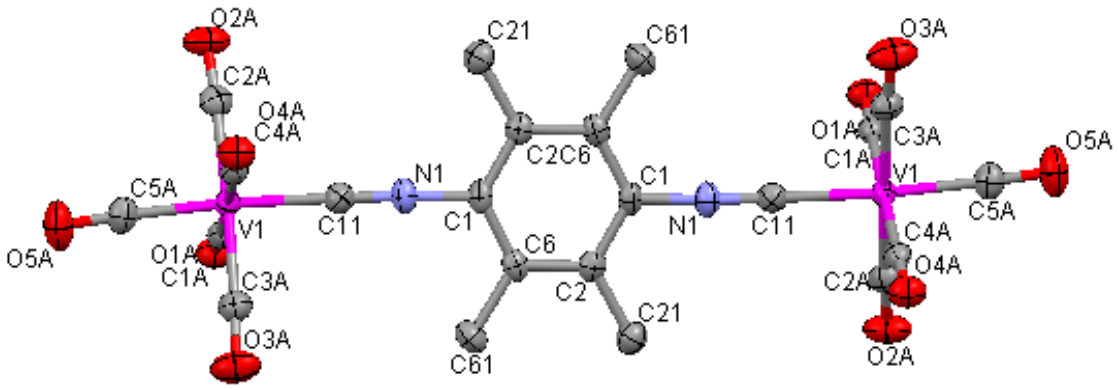

Figure I.8. Molecular structure of the dianion in 1.1a (50% thermal ellipsoids).

The molecular structure of the dianion within **1.1a** features nearly perfect octahedral V(I-) centers, as shown in Figure I.8. Table I.4 contains a summary of selected bond distances and angles for compounds relevant bis(pentacarbonyl)metal complexes and ligands. The C11-N1 distance is 0.010Å longer while the N1-C1 bond is 0.017Å shorter compared to corresponding parameters for **DID**.[32] These differences are statistically significant according to the 3σ criterion and can be attributed to V(dπ)→CNAr(pπ*) back-bonding interactions. Unlike observations of deviation of C-N-C bond angle in the tungsten(0) derivatives of **DIB**, the C1-N1-C11 angle in **1.1a** is 177.7(3)° versus 178.3(1)° for free **DID**.[5] The V(dπ)→diisocyanide(pπ*) interaction for **1.1a** is also manifested by the 77 cm^{-1} depression of ν_{CN} upon complexation of **DID** (ν_{CN} = 2118 cm^{-1} in CH_3CN) with the $[V(CO)_5]^-$ fragments. The *trans*-influence of the isocyanide ligand is also observed by the shorter V-C5A and longer C5A-O5A compared to all other V-C-O units within **1.1a**. This effect is attributed to the larger σ-donor/π-acceptor ratio of the isocyanide compared to a carbonyl ligand.[34] Also, the V-CO bonds *cis* to the V-CN bond in **1.1a** are comparable in length to the V-CO bonds in various salts of hexacarbonylvanadate(I-).[35]

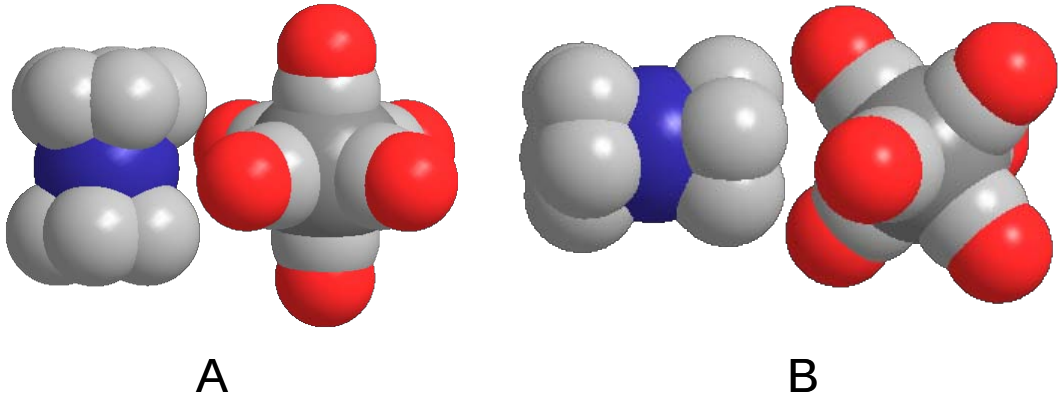

Figure I.9. Space-filling model of $Co(Cp)_2^+ | V(CO)_6^-$ contact ion interactions in side-double (A) and top-triple (B) arrangements.[36]

In the past, the charge transfer salt of cobaltocenium hexacarbonylvanadate(I-) was impossible to be thoroughly analyzed due to large disorder of $[V(CO)_6]^-$ in the crystal.[37] However, DFT calculations by Spears have suggested two stable geometries for the $Cp_2Co^+ | V(CO)_6^-$ contact ion pair (Figure I.9): one with two oxygen atoms lying in the cleft of the two Cp rings (Figure I.9A) and the other featuring two or three oxygen atoms contacting the top of the Cp ring (Figure I.9 B).[36] The cobaltocenium cations of **1.1a** exhibit Co-C bonds of 2.022(3)-2.037(3) Å and Co-Cp(centroid) distances of 1.63 Å, which are typical of many other cobaltocenium salts.[38] Each vanadium(I-) center in **1.1a** has four V···Co contact distances under 6.5 Å in the solid state as shown in Figure I.10: 5.38, 5.53, 5.73, and 6.48 Å. The shortest of these distances corresponds to a "side-double" interaction and compares remarkably well to contact distances predicted by Spears (5.4 Å and 6.1 Å for conformations A and B, respectively) for $[Cp_2Co][V(CO)_6]$.[36]

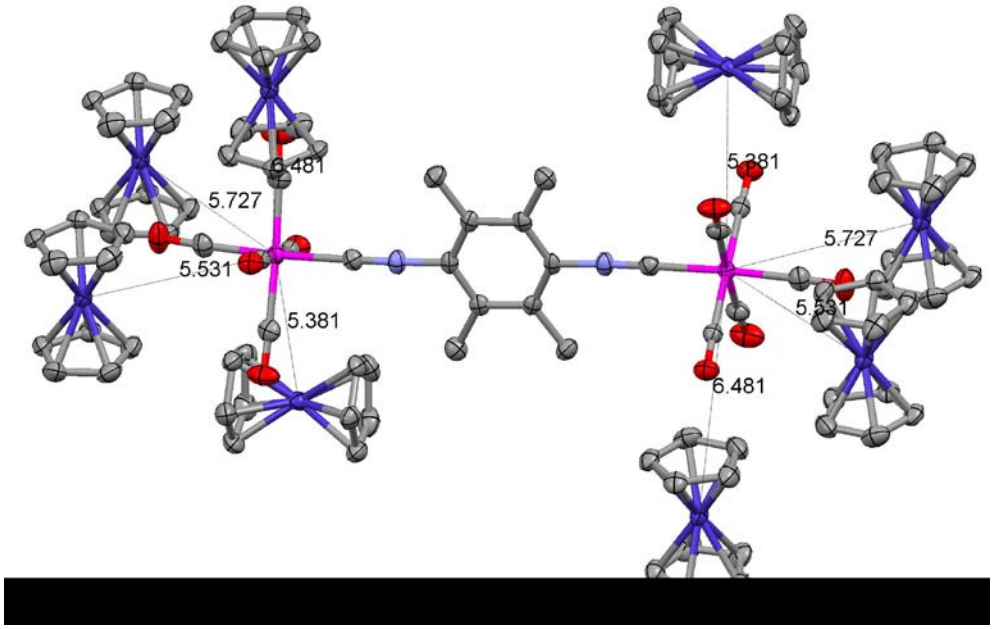

Figure I.10. Close V-Co contacts in 1.1a.

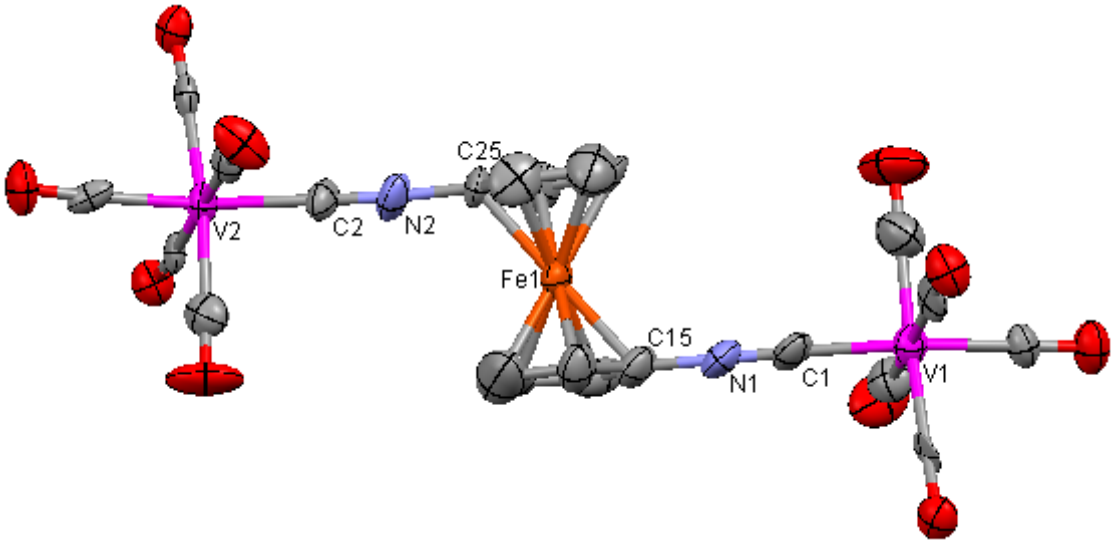

Figure I.11. Drawing of one of the dianions in the X-ray structure of complex 1.3 (50% thermal ellipsoids). Hydrogen atoms, counterions and solvent molecules are omitted for clarity.

The single crystal X-ray analysis of **1.3** revealed two crystallographically independent dianions, 4 tetraethylammonium cations and one solvent molecule in each unit cell. The $[N(CH_2CH_3)_4]^+$ cations and the solvent molecule exhibit significant

disorder and were resolved isotropically. Figure I.11 illustrates one of the dianions in the unit cell of **1.3**. Complex **1.3** features nearly perfect octahedral V(I-) centers, similar to **1.1a** and consistent with the analogous Cr(0) complex reported by Siemeling *et al*, shown in Figure I.12.[39]

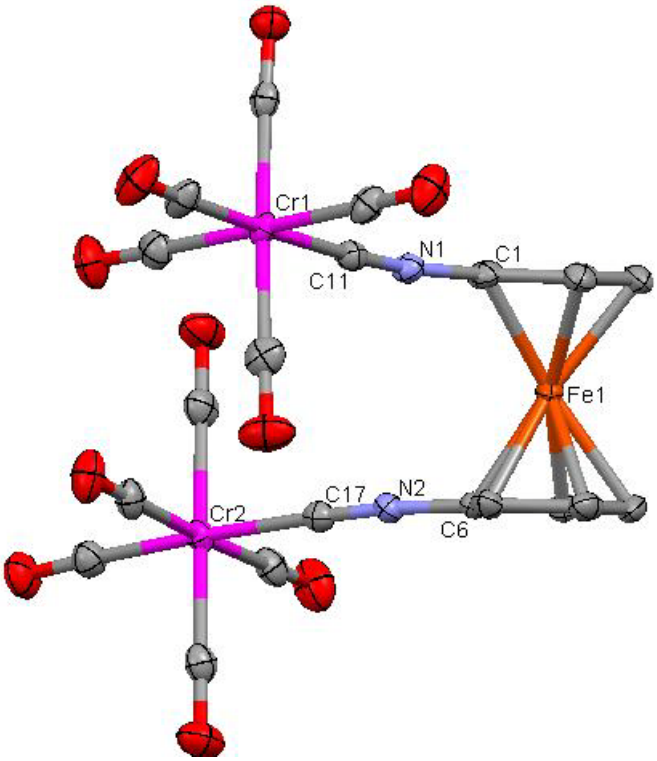

Figure I.12. X-ray crystal structure of bis(pentacarbonylchromium(0) 1,1'-diisocyanoferrocene (50% thermal ellipsoids).[39]

Several X-ray structures exist that incorporate 1,1'-diisocyanoferrocene into metal complexes.[40] The reported gold(I) complex of 1,1'-diisocyanoferrocene tends to exhibit a torsion angle between the two C≡N units of 0°.[40] In the case of the two examples using metal pentacarbonyls ($Cr(CO)_5$ and complex **1.3**), the torsion angle of the isocyanide units is non-zero. For the previously studied chromium complex, the torsion angle is approximately 54°, whereas in complex **1.3**, this angle is almost 180° in both crystallographically independent dianions.[39]

There are noticeable differences in bond lengths of complexes **1.1a**, **1.3**, and bis(pentacarbonylchromium) 1,1'-diisocyanoferrocene, as summarized in Table I.4. The bond length of the metal-carbon bond for the carbonyl located *trans* to the isocyanide is slightly longer in complex **1.3** compared to **1.1a**, however both of these are significantly larger than the chromium complex.[39] The C≡N bond is not significantly different in length between the three complexes, 1.175(4)Å for **1.1a**, 1.18(1)Å for **1.3**, and 1.160(2)Å for the chromium complex. Further comparisons between the three complexes are slightly hindered, however, due to the extensive disorder in the structure of complex **1.3**, which has led to large standard deviations in the structural parameters.

Table I.5. FTIR Data for complexes and ligands in CH_3CN. Data reported in cm^{-1}.

Complex	Ligand ν_{CN}	Complexed ν_{CN}	ν_{CO}
1.1a	2118	2041	1926 1847 1839
1.1b	2118	2034	1911 1857 1839
1.2	2108	2053	1943 1849 1837
1.3	2128	2043	1925 1856 1840

The FTIR spectra of **1.1a**, **1.1b**, **1.2** and **1.3** in ν_{CN} and ν_{CO} regions in acetonitrile are consistent with those reported for a few other $[(CO)_5V(CNR)]^-$ frameworks.[10] The ν_{CN} values for **DID**, xylyl isocyanide and 1,1'-diisocyanoferreocene are 2118 cm^{-1}, 2108 cm^{-1}, and 2128 cm^{-1}, respectively. The ν_{CN} value moves to lower energy for all three complexes: 2041 cm^{-1} for **1.1a**; 2034 cm^{-1} for **1.1b**; 2053 cm^{-1} for **1.2**; and 2043 cm^{-1} for **1.3**. These shifts in the isocyanide stretching frequencies are consistent with the isocyanide ligands behaving as π-acceptors, thus weakening the C≡N bond through

backbonding interactions with the electron-rich metal. The change in energies of the ν_{CO} bands for the complexes is consistent with substitution of only one carbonyl ligand at the metal center.[5,6,10] The FTIR data for the complexes **1.1a**, **1.1b**, **1.2** and **1.3** are summarized in Table I.5 and displayed in Figure I.13 - Figure I.16.

Interestingly, the ν_{CN} stretching bands for complexes **1.1a** and **1.3** are almost identical whereas the isocyanide stretching frequencies for complexes **1.1b** and **1.3** are 9 cm^{-1} different. The difference between complexes **1.1a** and **1.1b** is simply the counterion, which should not play a significant role in the energy of the isocyanide bond, unless interactions observed in the solid state (such as contact ion interactions and π-stacking aggregate formation) are conserved in the solution phase for compound **1.1a**. The comparisions of ν_{CN} values between complexes **1.1b** and **1.3** indicate less backbonding interactions when two electron-rich metal centers are bridged by 1,1'-diisocyanoferrocene.

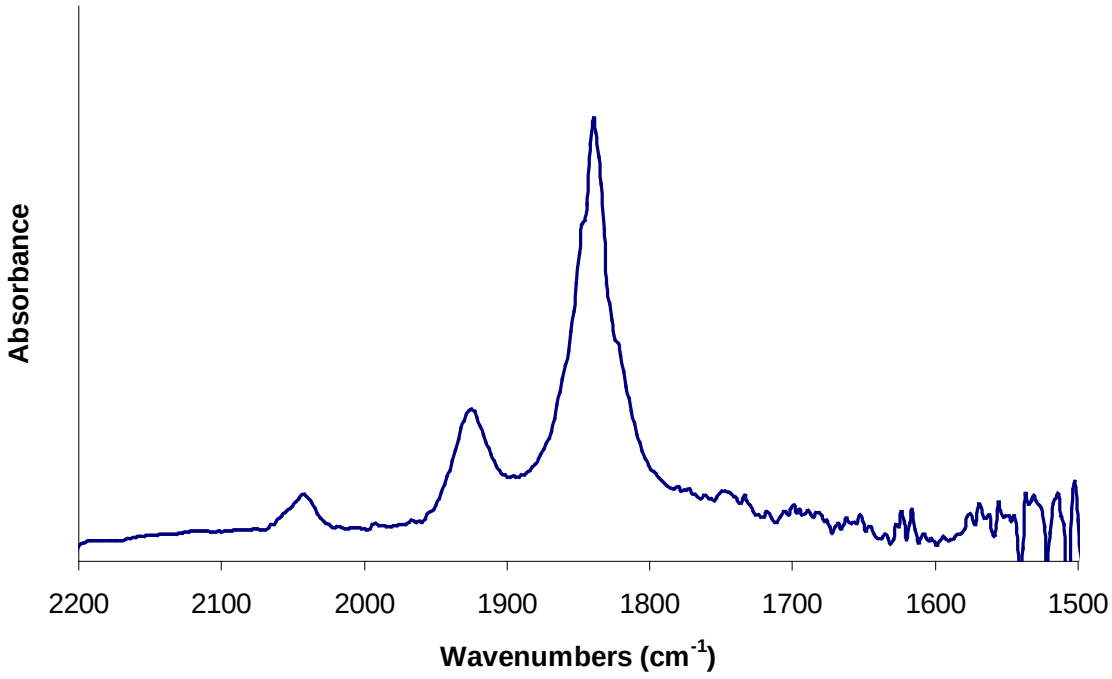

Figure I.13. FTIR Spectrum of 1.1a in CH_3CN.

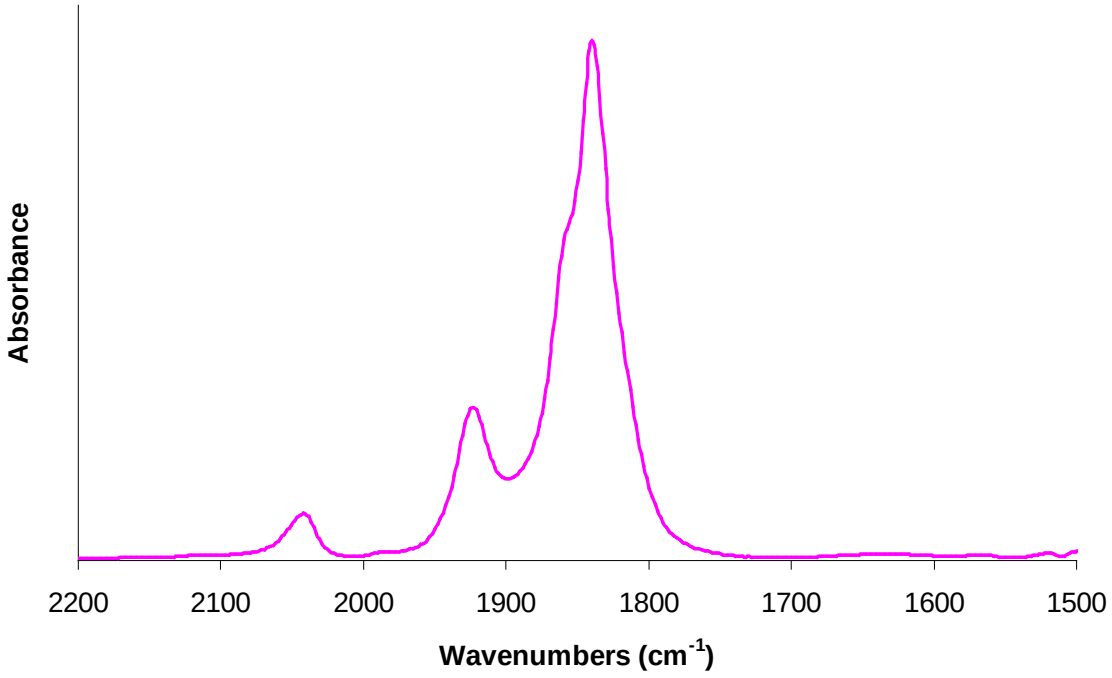

Figure I.14. FTIR Spectrum of 1.1b in CH_3CN.

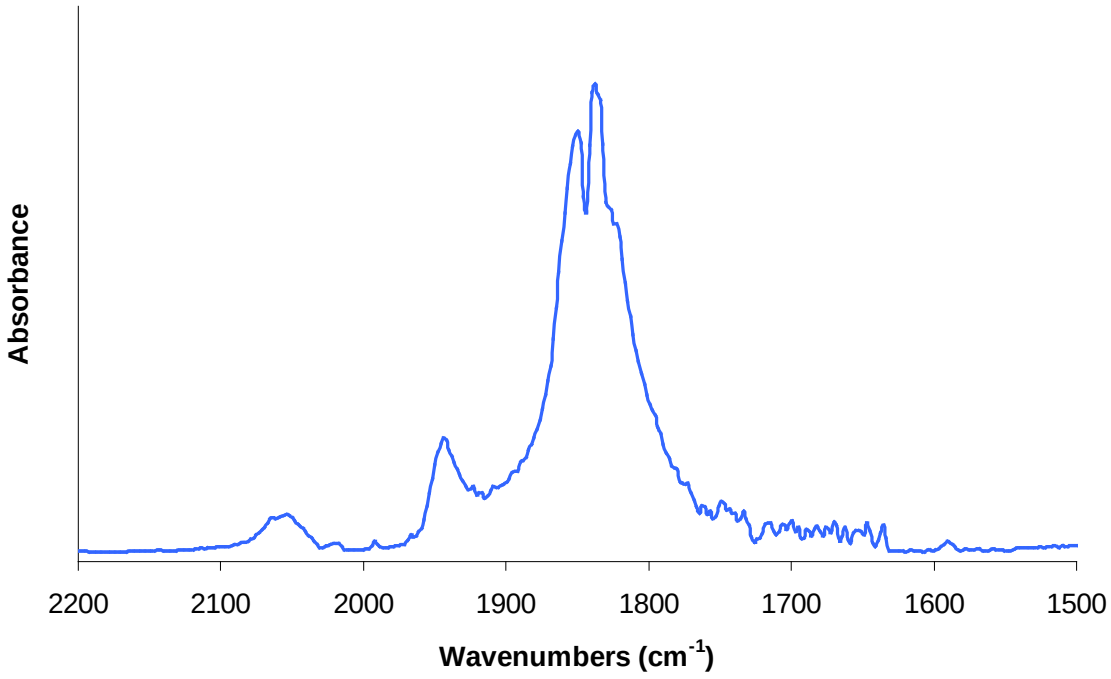

Figure I.15. FTIR Spectrum of 1.2 in CH_3CN.

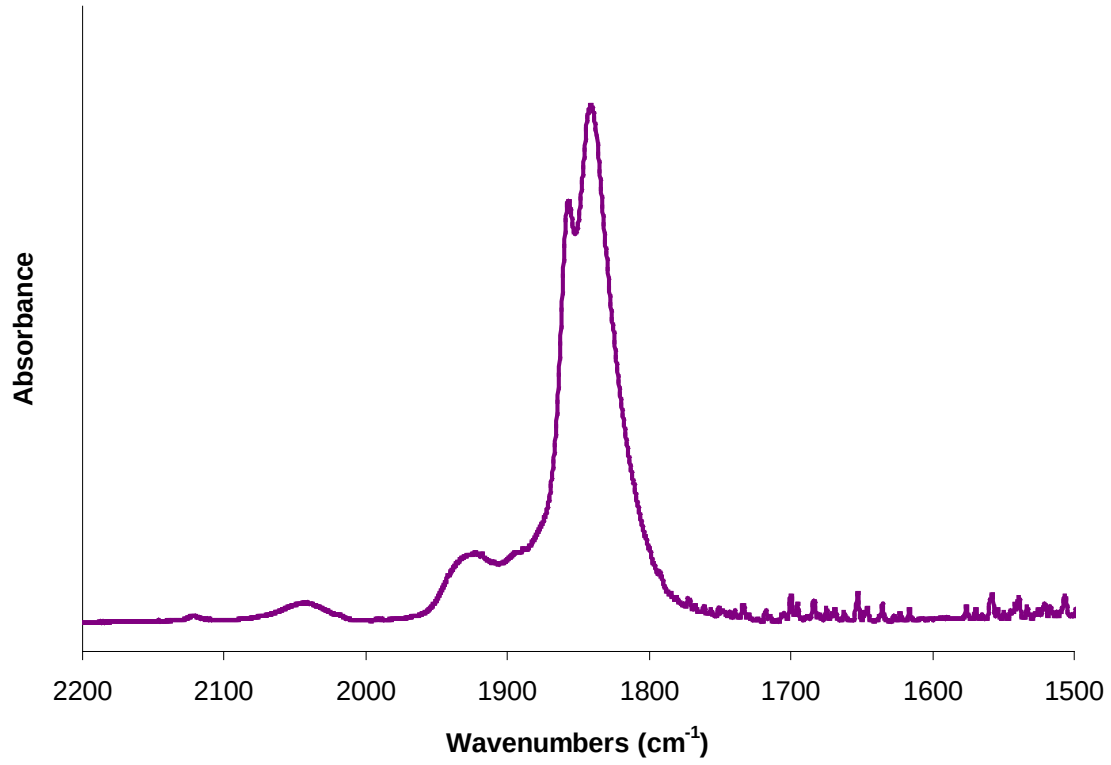

Figure I.16. FTIR Spectrum of 1.3 in CH_3CN.

The ^{1}H NMR spectrum of **1.1a** in air-free CD_3CN shows a singlet peak at 5.65 ppm due to the $[Cp_2Co]^+$ cations. There also are four closely spaced singlets from 2.28 – 2.35 ppm corresponding to the CH_3 substituents of the aromatic diisocyanide linker. These latter peaks can be grouped into two different levels of intensity and the combined integration of the 4 peaks corresponds to 12 protons when compared to the integration of the $[Cp_2Co]^+$ signal set at 20 hydrogens. If the above mentioned contact cation-anion interactions of complex **1.1a** seen in the solid state are preserved to some extent in solution, the CH_3 groups *ortho*- to the isocyanide linker would be inequivalent, thus giving rise to two methyl environments in the ^{1}H NMR. The presence of dimers formed via π-stacking interactions of the dianions of **1.1a** would produce the two additional methyl signals. The cobaltocenium cations may provide additional stabilization for dimeric adducts with possible contact ion interactions of these counterions with both units of the dimer, as seen in Figure I.7.

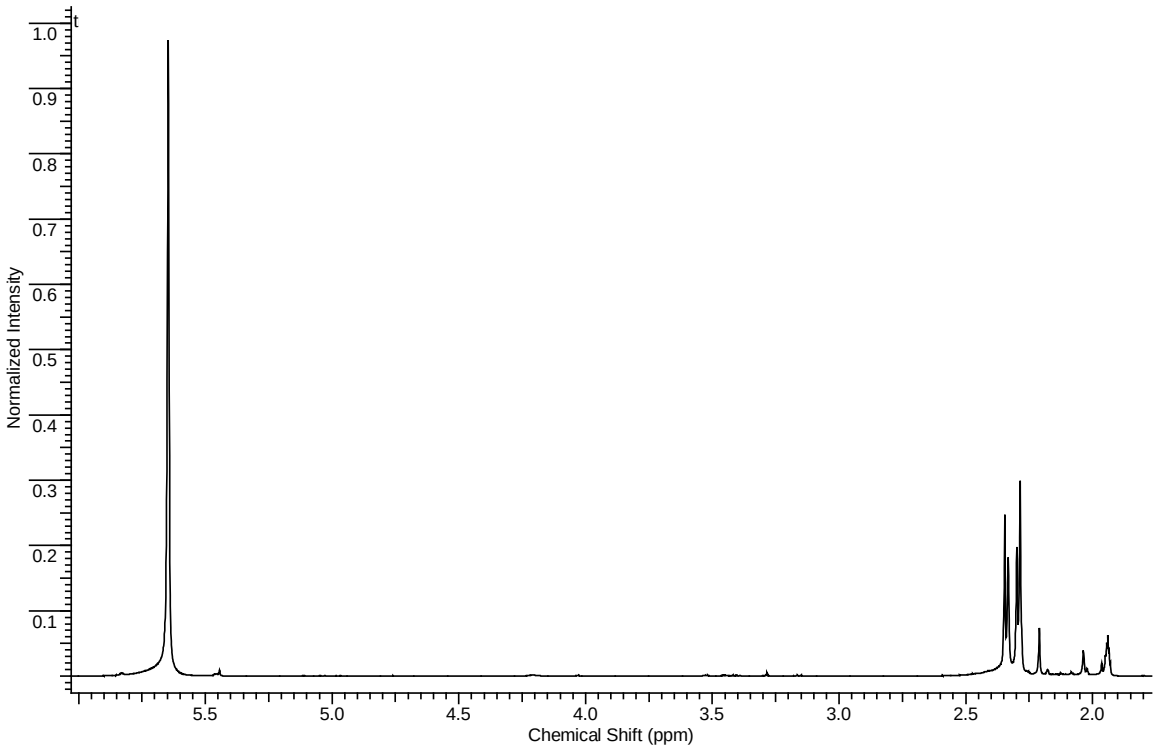

Figure I.17. ^{1}H NMR of 1.1a in CD_3CN at 25°C.

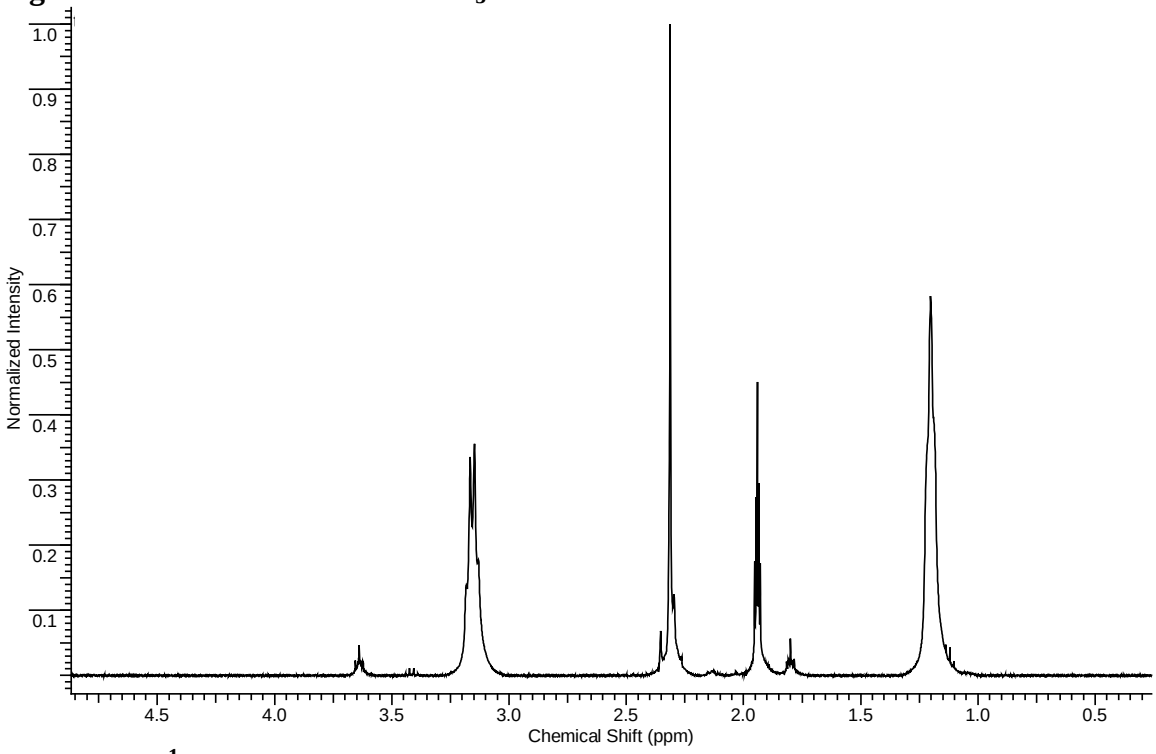

Figure I.18. ^{1}H NMR of 1.1b in CD_3CN at 25°C.

To test the ^{1}H NMR assignments in **1.1a** and the question of preservation of solid state contact ion interactions in the solution state, the spectrum of **1.1b** was also considered. In this material, the presence of the tetraethylammonium cation should remove the tight ion association seen in **1.1a**. Even though dimerization of the dianion through π-stacking interactions may still exist, the dimer would not contain any additional stabilization through cation-anion interactions. As such, only two ^{1}H NMR resonances were observed in the spectrum of **1.1b**, integrating for 12 H's versus the $[NEt_4]^+$ signals. ^{1}H NMR spectra of **1.1a** and **1.1b** are presented in Figure I.17 and Figure I.18.

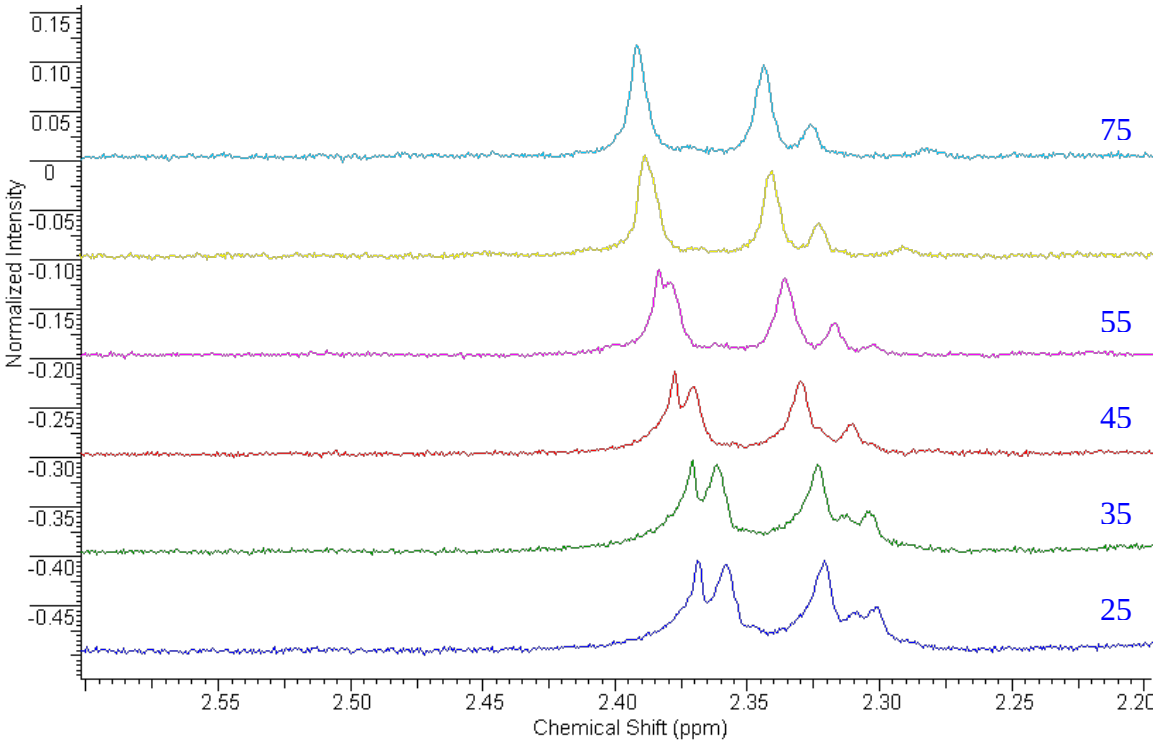

Figure I.19. Variable Temperature ^{1}H NMR Study of 1.1a from 25°C to 75°C.

The above rationalization of the ^{1}H NMR patterns for **1.1a** and **1.1b** are speculative at this stage and other explanations may, in principle, be possible. For example, partial decomposition of the complex due to introduction of air and/or moisture during the

process of sealing NMR samples and/or less than optimal quality of the NMR solvent with respect to the lack of O_2 and water might have led to the dissociation of one or both isocyanide carbon-vanadium bonds. The limited thermal stability of the complex in solution at ambient temperature may pose a problem as well. The mononuclear species $[(CO)_5V(\eta^1\text{-}\mathbf{DID})]^-$ alone would give rise to two sets of methyl resonances of equal intensity in ^1H NMR. While reasonable care was taken to completely exclude air and moisture from the NMR solvent and during the NMR tube sealing process, a more rigorous consideration of the above potential issues is certainly warranted.

Because of thermal, hydrolytic, and/or oxidative stability concerns, variable temperature and 2-D NMR experiments involving solutions of **1.1a** and **1.1b** were attempted. Figure I.19 shows changes in the four methyl resonances observed for **1.1a** upon increasing the temperature from room (22°C) to 75°C. Upon increasing the temperature, the cobaltocenium resonance shifted gradually upfield from 5.48 ppm to 4.59 ppm and the peak broadened significantly. Upon cooling the sample, the peak associated with the protons of the cation remained quite broad and the resonance peak position remained at 4.59 ppm. The four methyl peaks at room temperature occur, as mentioned previously, at 2.28, 2.30, 2.33 and 2.35. The peaks at 2.28 and 2.33 are approximately 1/3 of the intensity of the peaks at 2.30 and 2.35. Upon heating the sample, the peaks at 2.28 and 2.33 appeared to merge into the larger peaks and all peaks exhibited at downfield shift of about 0.04 ppm. Upon cooling of the sample, the peaks representing the methyl resonances returned to their original positions and shape.

Two dimensional experiments were performed to possibly resolve the methyl peaks to either one molecule or aggregates of π-stacked molecules. A NOESY experiment

proved inconclusive due to the close proximity of the resonances to one another. The gap between the two large peaks is approximately 16 Hz, while the gap between the large peak and its closest small peak is only 4 Hz. These distances are under the threshold of resonance energy for pulsing at a particular frequency in an NOE based experiment and therefore all four peaks are affected by the pulse and so no details could be elucidated. Likewise, an HMBC experiment was attempted, and again due to the close proximity of the resonances, it was quite difficult to determine any long range coupling to determine if the four methyl peaks were related to a single molecule with four different magnetic environments or the result of aggregates.

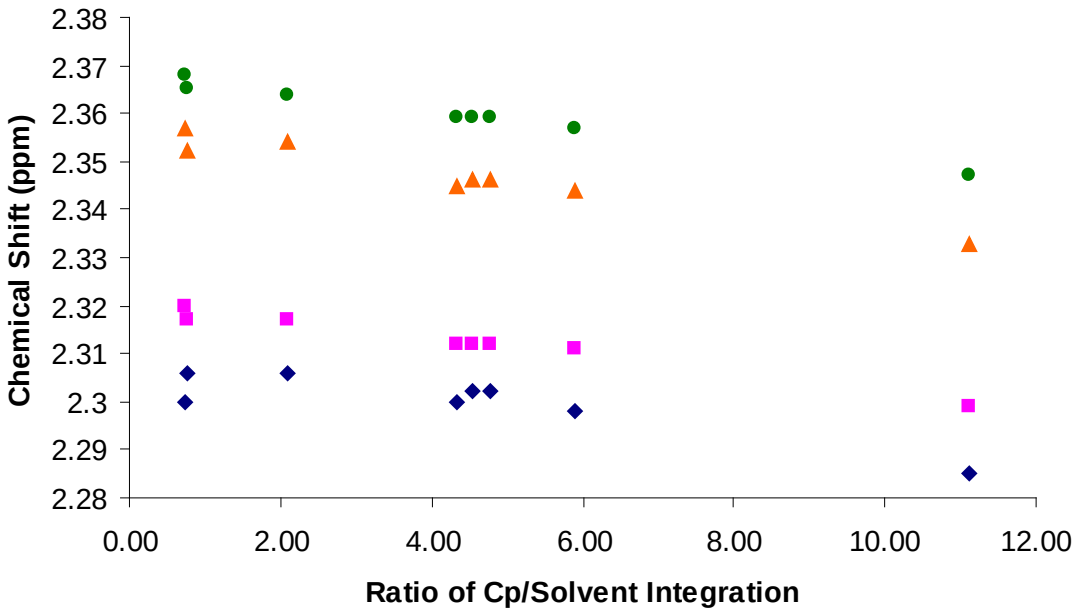

Figure I.20. Plot of Changing Concentration versus Chemical Shift for Complex 1.1a in CD_3CN.

A final experiment was performed to investigate the impact of concentration on the observed NMR resonances, as summarized in Figure I.20. Based on the previous experiments, it appeared the ratio of the tall peak to short peak varied slightly. Using the

integration values of the cobaltocenium protons versus residual solvent protons, a concentration ratio was deduced for several samples. The ratio of intensity of the peaks associated with the methyl protons was then analyzed. No apparent trend was observed, the ratio of the intensity of the peak at 2.28 ppm versus 2.30 ppm showed no distinct change. However, the chemical shifts of the four peaks did vary based on concentration, by as much as 20Hz. As the concentration of **1.1a** in solution was increased, the methyl peaks all shifted upfield. Dynamic processes, such as molecular aggregation, can influence the outcome seen in the NMR spectra of the sample. As more molecules of **1.1a** enter the solution more aggregates may form, causing the peak position to gradually shift. If any of the peaks associated with methyl protons were due to the presence of impurity or oxidation products, the change in chemical shift would not have varied with concentration. Because complex **1.1b** does not contain the cobaltocenium cations to participate in contact ion interactions, there are only two resonances associated with the methyl protons. However, a similar variable concentration analysis was performed with **1.1b**. The same concentration dependent upfield shift of the methyl proton resonances was observed for the two methyl peaks in the spectrum of **1.1b**, indicating that aggregate formation is not dependent on the contact ion interaction.

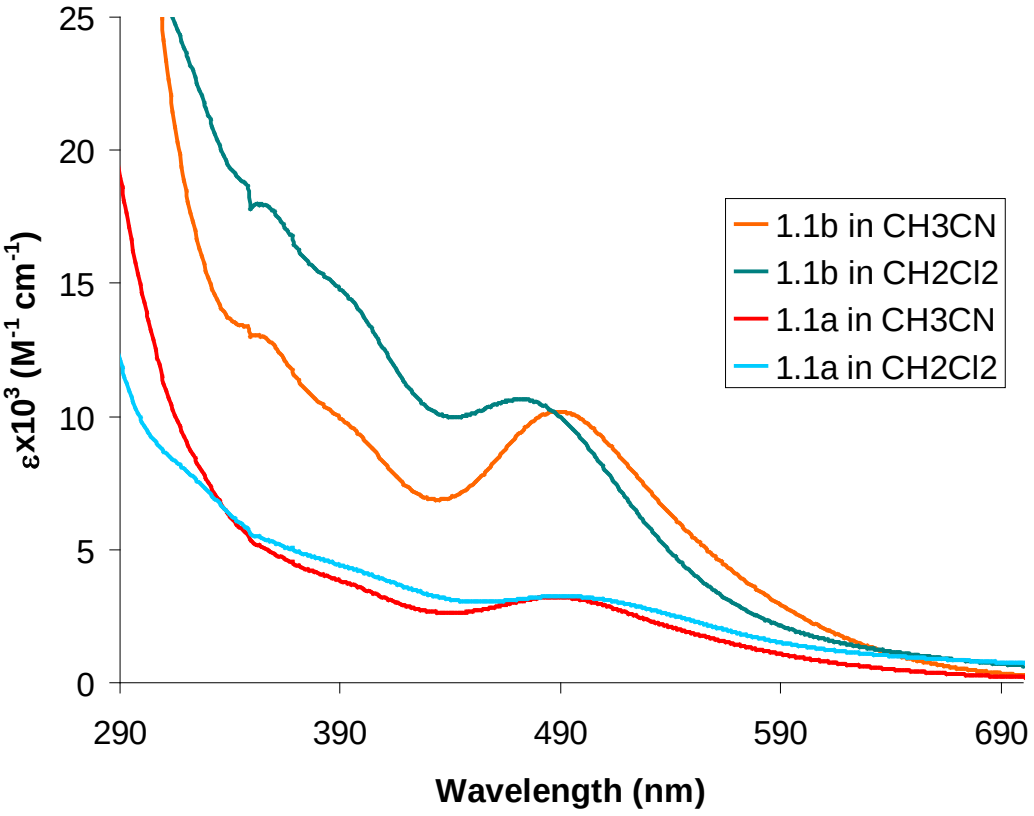

Figure I.21. UV-Vis spectra of 1.1a and 1.1b in CH_3CN and CH_2Cl_2.

Figure I.21 depicts the electronic spectra of complexes **1.1a** and **1.1b** in two solvents, polar acetonitrile and nonpolar dichloromethane. Complex **1.1b** exhibits an intense metal to ligand charge transfer band (MLCT) in acetonitrile at 489 nm. This peak is 6577 cm^{-1} less energetic than the corresponding band observed for the zero valent $[(CO)_5W]_2(\mu\text{-}CNC_6H_4NC)$ complex reported by Bennett.[6] Upon changing the solvent to dichloromethane, the MLCT band shifts by 736 cm^{-1} to higher energy. Similar solvent effects are not observed for complex **1.1a**, where the MLCT band occurs at 486 nm. This observed solvatochromic effect suggests limited solvent accessibility of the dianion in **1.1a** compared to **1.1b**, indicating some aggregation of the ions present in **1.1a** in the solution phase.

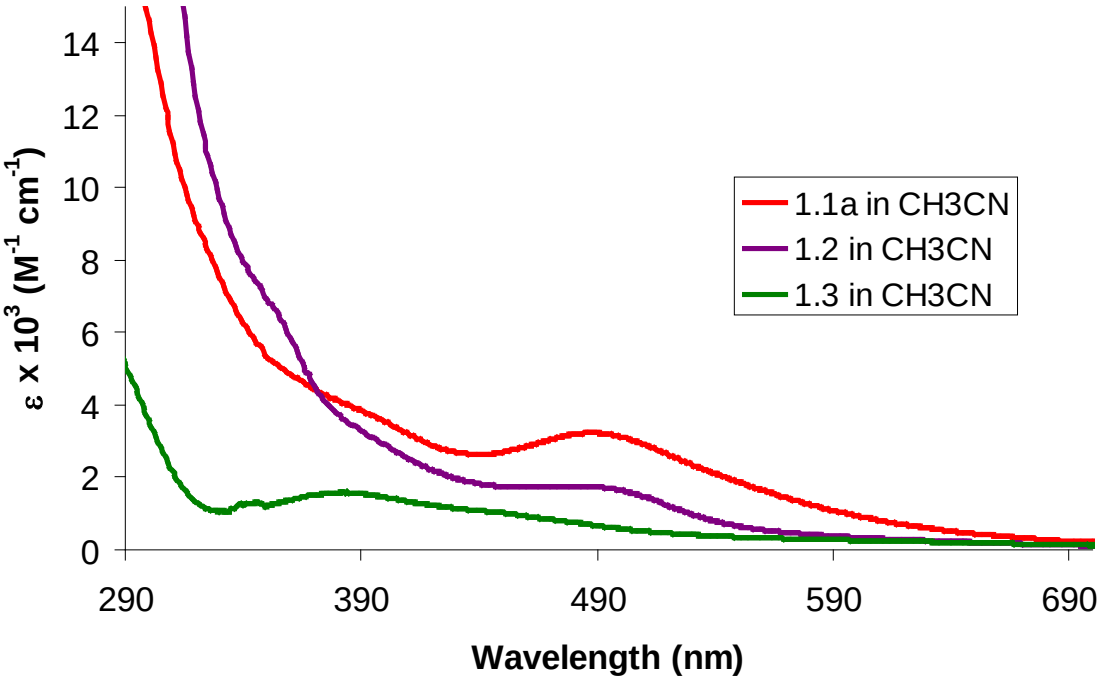

Figure I.22. UV-Vis spectra of 1.1a, 1.2 and 1.3 in CH_3CN.

Figure I.22 shows a comparison of the UV-visible spectrum of the bimetallic **1.1a** and monometallic **1.2**. Electronic communication between two metal centers through a connecting molecular bridge can often be investigated by comparing the MLCT bands of monometallic versus bimetallic complexes of the same ligand. For example, in 2006, Barybin *et al.* report the energy change upon binucleation of an aromatic bridging diisocyanoazulene system.[43] They found that upon coordination of the isocyanide to W(0) centers, the energy shift from the monometallic complex to the bimetallic complex was 2042 cm^{-1}.[43] Likewise, the 1,4-diisocyanobenzene framework analyzed by Bennett and coworkers exhibited a ΔE of binucleation of approximately 1221 cm^{-1}.[6] Mononuclear $[(CO)_5V(\eta^1\text{-}\mathbf{DID})]^{-1}$ was not successfully synthesized in this work, which made such a comparison with **1.1a** or **1.1b** not possible. However, a related complex, $[(CO)_5V(CNXyl)]^{-1}$, **1.2**, was accessed allowing for comparison of the MLCT band of **1.1a**/**1.1b** and a mononuclear (pentacarbonyl)vanadate(I-) of an isocyanoarene. Xylyl

isocyanide was chosen as it is a close analog to half of **DID**. Upon examination of the absorbance spectra of **1.1a** and **1.2**, it appears that there is little change in λ_{max}. This may indicate limited charge transport between the two vanadium metal centers through the **DID** bridge

Figure I.22 also shows the electronic spectrum of complex **1.3** in acetonitrile. Unlike the other three complexes, the most intense band in its spectrum has a significantly smaller ε value and the peak presumed to represent the MLCT occurs at a much higher energy (λ_{max} = 382 nm). The isocyanoferrocene motif has a higher σ-donor/π-acceptor ratio,[41] it is quite reasonable that the MLCT to diisocyanoferrocene is less facile than that to **DID**.

Figure I.23. Cyclic voltammogram of 1.1a in 0.1M [$^{n}Bu_4N$][PF_6] in CH_3CN at 100 mV/s, 22°C versus $FcH/Fc^{+}H$.

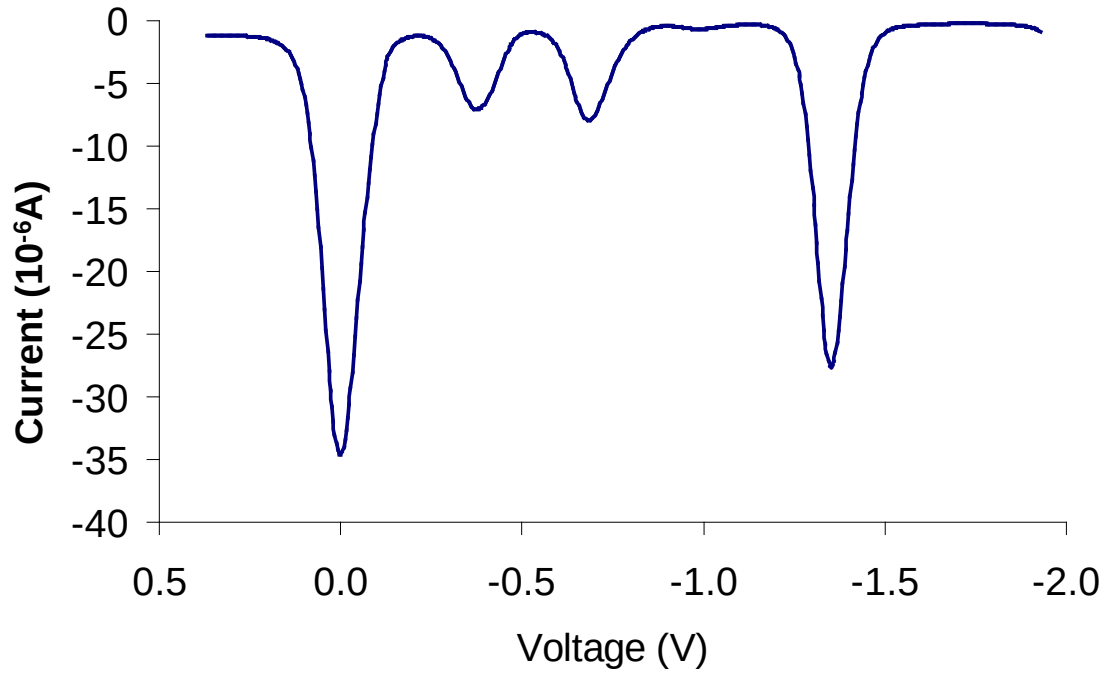

Figure I.24. Differential pulse voltammogram of 1.1a in 0.1M [^{n}Bu$_4$N][PF$_6$] in CH$_3$CN at 100 mV/s, 22°C versus FcH/Fc$^+$H.

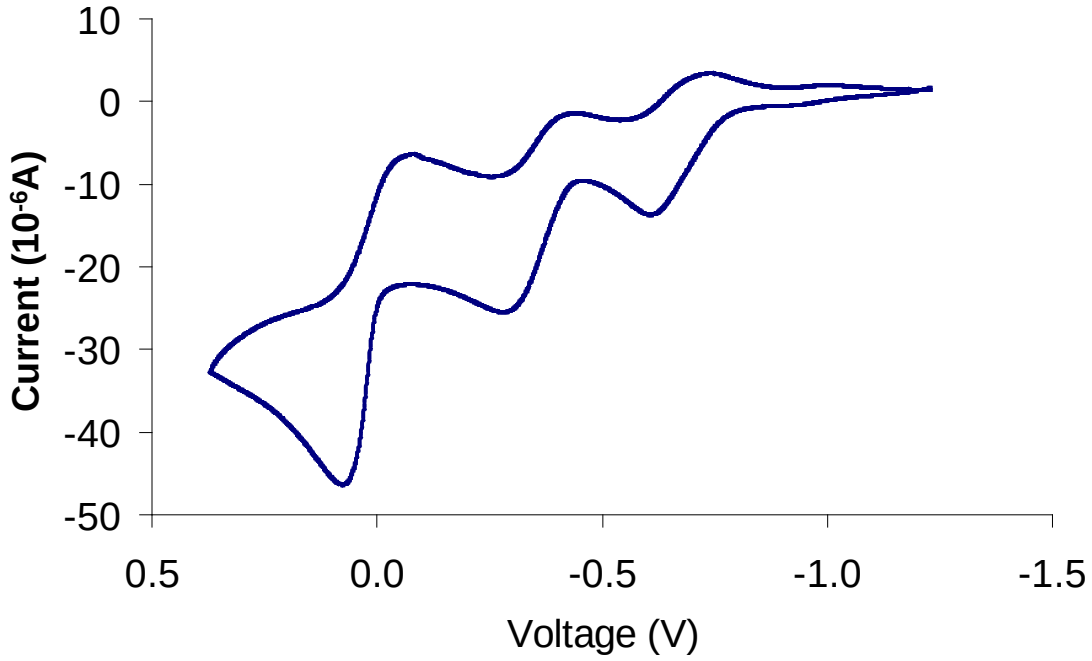

Figure I.25. Cyclic voltammogram of 1.1b in 0.1M [^{n}Bu$_4$N][PF$_6$] in CH$_3$CN at 100 mV/s, 22°C versus FcH/Fc$^+$H.

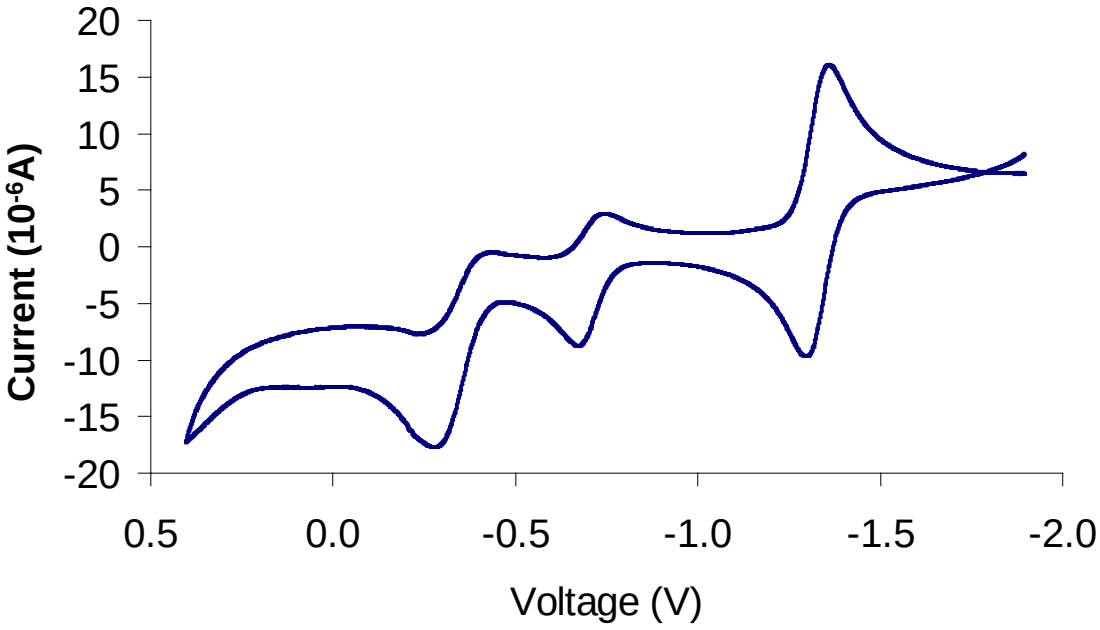

Figure I.26. Cyclic voltammogram of 1.2 in 0.1M [^{n}Bu$_4$N][PF$_6$] in CH$_3$CN at 100 mV/s, 22°C versus FcH/Fc^{+}H.

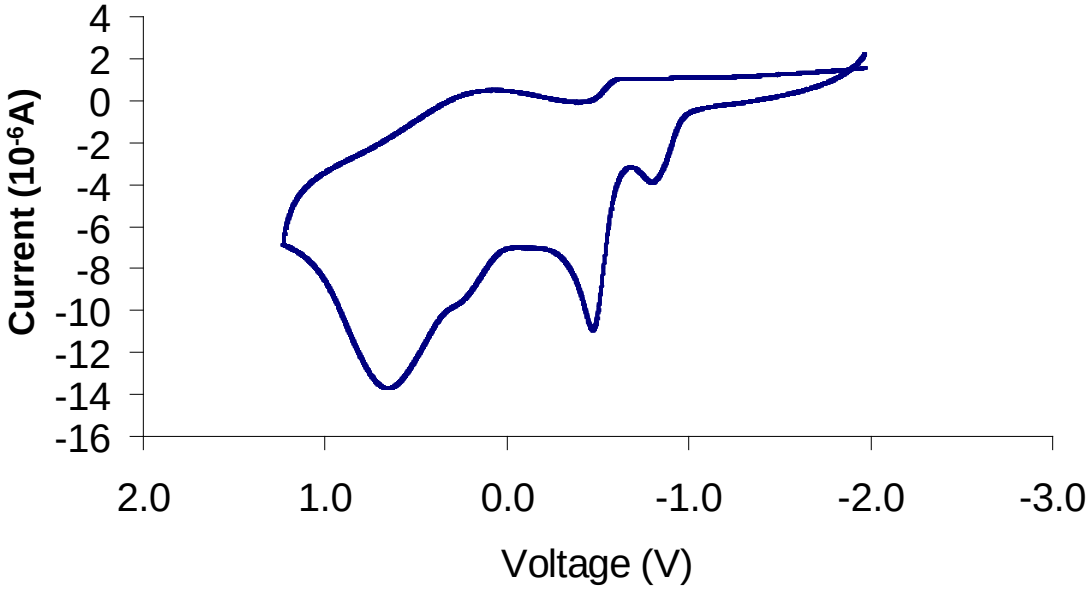

Figure I.27. Cyclic voltammogram of 1.3 in 0.1M [^{n}Bu$_4$N][PF$_6$] in CH$_3$CN at 100 mV/s, 22°C versus FcH/Fc^{+}H.

Table I.6. Electrochemical data for complexes 1.1a, 1.1b, 1.2, and $[Co(Cp)_2][V(CO)_6]^-$.

Compound	E_1	E_2	E_3
1.1a	-1.3230	-0.6655 ^{Q}	-0.3640 ^{Q}
1.1a (dpv)	-1.3520	-0.6840	-0.3760
1.1b		-0.6760 ^{Q}	-0.3545 ^{Q}
1.2	-1.3270	-0.7060 ^{Q}	-0.3570 ^{Q}
$[Co(Cp)_2][V(CO)_6]$	-1.323		-0.353 ^{Q}

E_1 corresponds to the half-wave potential for $Co^{+2} \rightarrow Co^{+3}$. E_2 corresponds to the half-wave potential for $V^{-1} \rightarrow V^0$. E_3 corresponds to the half-wave potential for $V^0 \rightarrow V^{+1}$. All reported transitions are reversible unless indicated. ^{Q} indicates quasi-reversible transitions. All data collected in 0.1M $[^nBu_4N][PF_6]$ in CH_3CN at 22°C and values are referenced to the FcH/Fc^+H couple.

Table I.7. Electrochemical data for complexes 1.1a, 1.1b, 1.2, 1.3, and 1,1'-diisocyanoferrocene.

Compound	E_1	E_2	E_3	E_4
1.1a	-1.325	-0.644	-0.329	
1.1b		-0.684	-0.335	
1.2	-1.336	-0.709	-0.320	
1.3		-0.846	-0.516	0.588
1,1'-diisocyanoferrocene				0.569

E_1 corresponds to the cathodic potential for $Co^{+2} \rightarrow Co^{+3}$. E_2 corresponds to the cathodic potential for $V^{-1} \rightarrow V^0$. E_3 corresponds to the cathodic potential for $V^0 \rightarrow V^{+1}$. E_4 corresponds to the cathodic potential for $Fe^{+2} \rightarrow Fe^{+3}$. All data collected in 0.1M $[^nBu_4N][PF_6]$ in CH_3CN at 22°C and values are referenced to the FcH/Fc^+H couple.

Figure I.23 through Figure I.27 show the cyclic voltammograms of complexes **1.1a, 1.1b, 1.2** and **1.3**. Table I.6 provides the numerical results of the electrochemical analysis

of these complexes along with previously unreported values for cobaltocenium hexacarbonylvanadate(I-). Table I.7 provides the cathodic potential values for all relevant compounds. For complexes **1.1a, 1.2**, and $[Co(Cp)_2][V(CO)_6]$, the most anodic potential corresponds to the fully reversible Cp_2Co/Cp_2Co^+ couple (average $\Delta(E_a\text{-}E_c)$ = 59mV, $i_p/i_c \approx 1$), providing a convenient internal electrochemical reference for the electrochemical behavior of the anions. For consistency, however, all data were referenced to the Cp_2Fe/Cp_2Fe^+ couple.

Complex **1.1a** exhibits two partially reversible red-ox events. These two events could either be due to the presence of simultaneous oxidation/reduction of both vanadium centers, corresponding to a V(-I)/V(0) transition and a V(0)/V(I) transition respectively, or could be attributed to a mixed valence species in which one vanadium center is oxidized, V(I-)/V(0), at the first potential and the second vanadium center is oxidized at the second potential. The latter scenario would indicate a high level of coupling between the two metal centers through the **DID** bridge. To determine the reason behind the appearance of two oxidation events for the bisvanadate(I-) dianion, complex **1.2** was analyzed electrochemically. Complex **1.2** exhibits two similar redox events, indicating that the observed transition in complex **1.1a** must be due to two processes, one for the conversion of V(-I) to V(0) and the second for the conversion of V(0) to V(I). It is interesting to note that the V(0) to V(I) transition for **1.1a** occurs at approximately the same potential as the V(-I) to V(0) transition in $[Cp_2Co][V(CO)_6]$. Complex **1.1b** also exhibits these two redox waves at very similar potentials.

Differential pulse voltammetry (DPV) was conducted to facilitate examination of the cyclic voltammetry data obtained for **1.1a**. One equivalent of ferrocene per one

equivalent of cobalticenium cation was added to the solution of **1.1a** as an internal reference. For **1.1a**, CV (Figure I.23) and DPV (Figure I.24) peak currents of the vanadium-based couples are notably smaller than those of the Co^{II}/Co^{III} couple. This observation nicely parallels the above structural and spectroscopic findings for **1.1a** as tight ion association and/or π-stacking aggregation of the anions of **1.1a** may, to some extent, mask the electroactive vanadium centers.

The cathodic potentials for all complexes are reported in Table I.7 for consistency. The reduction potential of **1.3** is significantly more negative than those for **1.1a, 1.1b,** or **1.2**. This is consistent with the previously mentioned increased σ-donor character of the ferrocene-based bridge compared to the benzene-based linker. Indeed, electron density on the vanadium centers bridged by 1,1'-diisocyanoferrocene should be greater than that in the case of the diisocyanoarene-bridged species, resulting in a more facile oxidation of the vanadium centers in the diisocyanoferrocene-linked complex.

I.4. Conclusions and Future Work

The first examples of diisocyanobimetallates were isolated and characterized by NMR, FTIR, X-ray crystallography, electronic spectroscopy and cyclic voltammetry. These species may be thought of as elementary units for assembling larger extremely electron-rich metal-organic frameworks that could function as electron reservoirs. Strong contact ion association and π-stacking aggregation of the bimetallic dianions were documented in complex **1.1a** in the solid state. These interactions may be preserved, to some extent, in solution, as well. The diisocyanoarene-bridged bisvanadate(I-) was accessed through multiple approaches, starting directly from the 18-electron $[V(CO)_6]^-$

complex and employing photolysis, or from the neutral 17-electron $V(CO)_6$ complex via the neutral electronically unsaturated divanadium(0) intermediate.

Further studies aimed at understanding inter-ionic association and π-aggregation of $\{[(OC)_5V]_2(\mu\text{-}CNC_6Me_4NC)\}^{2-}$ containing salts in solution, as well as work toward other diisocyanoarene-linked metallates (e.g., diisocyanoazulenes and diisocyanobiazulenes) still need to be conducted. In addition, assembly of 2D and 3D metal organic frameworks involving subvalent transition metal ions and diisocyanoarene linkers may now be possible.

I.5. References

1. Malatesta, Lamberto. *Progress in Inorganic Chemistry*. **1959**, *1*, 283.

2. Mitchell, Paul R.; Parish, Richard V. *Journal of Chemical Education*, **1969**, *46*, 811.

3. Ellis, John E. *Organometallics*, **2003**, *22*, 3322.

4. Barybin, Mikhail V.; Young, Victor G., Jr.; Ellis, John E. *Journal of the American Chemical Society*. **2000**, *122*, 4678.

5. Rommel, Jeffrey S.; Weinrach, Jeffrey B.; Grubisha, Desiree S.; Bennett, Dennis W. *Inorganic Chemistry*. **1988**, *27*, 2945.

6. Grubisha, Desiree S.; Rommel, Jeffrey S.; Lane, Thomas M.; Tysoe, Wilfred T.; Bennett, Dennis W. *Inorganic Chemistry*. **1992**, *31*, 5022.

7. Hanack, M.; Knecht, S.; Polley, R.; Subramanian, L. R. *Synthetic Metals*. **1996**, *80*, 183.

8. Hanack, Michael; Hees, Michael; Witke, Elisabeth. *New Journal of Chemistry*. **1998**, 169.

9. Holliday, Bradley J.; Farrell, Joshua R.; Mirkin, Chad A.; Lam, Kin-Chung; Rheingold, Arnold L. *Journal of the American Chemical Society*. **1999**, *121*, 6316.

10. Ellis, John E.; Fjare, Kristi L. *Organometallics*, **1982**, *1*, 898.

11. Ihmels, Klaus; Rehder, Dieter. *Organometallics*, **1985**, *4*, 1340.

12. Warnock, Garry F.; Cooper, N. John. *Organometallics*, **1989**, *8*, 1826.

13. Leach, Patricia A.; Geib, Steven J.; Corella, Joseph A.; Warnock, Garry F.; Cooper, N. John. *Journal of the American Chemical Society*, **1994**, *116*, 8566.

14. Corella, Joseph A., II; Thompson, Robert L.; Cooper, N. John. *Angewandte Chemie, International Edition*. **1992**, *31*, 83.

15. Utz, Tracy L.; Leach, Patricia A.; Geib, Steven J.; Cooper, N. John. *Chemical Communications*. **1997**, 847.

16. Barybin, Mikhail V.; Young, Victor G., Jr.; Ellis, John E. *Journal of the American Chemical Society*. **1999**, *121*, 9237.

17. Barybin, Mikhail V.; Young, Victor G., Jr.; Ellis, John E. *Journal of the American Chemical Society*. **2000**, *122*, 4678.

18. Connelly, Neil G.; Geiger, William E. *Chemical Reviews*. **1996,** *96*, 877.

19. Barybin, Mikhail V.; Pomije, Marie K.; Ellis, John E. *Inorganica Chimica Acta*. **1998**, *269*, 58.

20. Calderazzo, Fausto; Pampaloni, Guido; Zanazzi, Pier F. *Chemische Berichte*. **1986,** *119*, 2796.

21. Liu, Xin; Ellis, John E.; Miller, Trent D.; Ghalasi, Pransana; Miller, Joel S. *Inorganic Syntheses*. **2004,** 96.

22. Cotton, F. Albert; Daniels, Lee M.; Wilkinson, Chad C. *Acta Crystallographica, Section E*. **2001,** *57*, m529.

23. Swanson, Sally A.; McClain, Richard; Lovejoy, Katherine S.; Alamdari, Neda B.; Hamilton, Jeremy S.; Scott, J. Campbell. *Langmuir*. **2005,** *21*, 5034.

24. Ugi, I.; Fetzer, U.; Eholzer, U.; Knupfer, H.; Offermann, K. *Angewandte Chemie, International Edition English*. **1965,** *4*, 472.

25. van Leusen, Daan; Hessen, Bart. *Organometallics*. **2001**, *20*, 224.

26. International Tables for Crystallography, Vol. A, 4th ed., Kluwer: Boston (1996).

27. Data Collection: SMART Software Reference Manual (1998). Bruker-AXS, 5465 E. Cheryl Parkway, Madison, WI 53711-5373, USA.

28. Data Reduction: SAINT Software Reference Manual (1998). Bruker-AXS, 5465 E. Cheryl Parkway, Madison, WI 53711-5373, USA.

29. Sheldrick, G. M (2002). SADABS. Program for Empirical Absorption Correction of Area Detector Data. University of Göttingen, Germany.

30. (a) G. M. Sheldrick (2000). SHELXTL Version 6.10 Reference Manual. Bruker-AXS, 5465 E. Cheryl Parkway, Madison, WI 53711-5373 USA. (b) *International Tables for Crystallography, Vol. C*, Tables 6.1.1.4, 4.2.6.8, and 4.2.4.2, Kluwer: Boston (1995).

31. Van der Sluis, P.; Spek, A. L. *Acta Crystallographica, Section A*. **1990,** *46*, 194.

32. Zeller, Matthias; Hunter, Allen D.; Perrine, Cynthia L. *Acta Crystallographica, Section E*. **2003**, *59*, o1655.

33. Sinnokrot, Mutasem Omar; Sherrill, C. David. *Journal of the American Chemical Society*. **2004**, *126*, 7690.

34. Treichel, Paul M. *Advances in Organometallic Chemistry*, **1973**, *11*, 21-86.

35. Robinson, Randall E.; Holovics, Thomas C.; Deplazes, Stephan F.; Powell, Douglas R.; Lushington, Gerald H.; Thompson, Ward H.; Barybin, Mikhail V. *Organometallics*. **2005**, *24*, 2386.

36. a) Spears, Kenneth G.; Shang, Hairong. *Journal of Physical Chemistry, A*. **2000**, *104*, 2668. b) Marin, Timothy W.; Homoelle, Bradley J.; Spears, Kenneth G. *Journal of Physical Chemistry, A*. **2002**, *106*, 1152. c) Sando, Gerald M.; Spears, Kenneth G. *Journal of Physical Chemistry, A*. **2004**, *108*, 1290.

37. Bockman, T. M.; Kochi, Jay K. *Journal of the American Chemical Society*. **1989**, *111*, 4669.

38. Examples include: a) Migliori, Jesse M.; Reiff, William M.; Arif, Atta M.; Miller, Joel S. *Inorganic Chemistry*. **2004**, *43*, 6875. b) Andrews, Christopher G.; Macdonald, Charles L. B. *Acta Crystallographica, Section E*. **2005**, *E61*, m2103.

39. Siemeling, Ulrich; Rother, Dag; Bruhn, Clemens; Fink, Heinrich; Weidner, Tobias; Traeger, Frank; Rothenberger, Alexander; Fenske, Dieter; Priebe, Andreas; Maurer, Joerg; Winter, Rainer. *Journal of the American Chemical Society*. **2005**, *127*, 1102.

40. Examples include: Siemeling, Ulrich; Rother, Dag; Bruhn, Clemens. *Chemical Communications*. **2007**, 4227; Siemeling, Ulrich; Rother, Dag; Bruhn, Clemens, *Organometallics*. **2008**, *27*, 6419; Deplazes, Stephan F. Ligand design, coordination and electrochemistry of nonbenzenoid aryl isocyanides. University of Kansas, 2007. UMI, Ann Arbor MI, #3295011.

41. Nesmeyanov, A. N.; Perevalova, E. G.; Gubin, S. P.; Grandberg, I. I.; Kozlovskii, A. G. *Tetrahedron Letters*. **1966**, *22*, 2381.

42. El-Shihi, Taha; Siglmueller, Franz; Herrmann, Rudolf; Fernanda, M.; Carvalho, N. N.; Pombeiro, Armando J. L. *Journal of Organometallic Chemistry*. **1987**, *335*, 239-247.

43. Holovics, Thomas C.; Robinson, Randall E.; Weintrob, Edward C.; Toriyama, Masaharu; Lushington, Gerald H.; Barybin, Mikhail V. *Journal of the American Chemical Society*. **2006**, *128*, 2300.

CHAPTER II

II. Synthesis and Coordination Chemistry of Novel Linear Isocyanobiazulenes

II.1. Introduction

Figure II.1. The structures and atom numbering for azulene and naphthalene.

Azulene, shown in Figure II.1, is a nonalternant, aromatic hydrocarbon with molecular formula $C_{10}H_8$. Azulene is dark blue in color and has a dipole moment of approximately 1 Debye. The highly colored nature of azulene is attributed to the electron correlation phenomenon stemming from the loss of mirror symmetry (disregarding the signs of individual atomic contributions in the molecular orbitals (MOs)) between the highest occupied molecular orbital (**HOMO**) and the lowest unoccupied molecular orbital (**LUMO**), especially when compared to the benzenoid $C_{10}H_8$ isomer, naphthalene. This loss of symmetry, shown in Figure II.2 (adapted from Liu, 2002)[1], results in a dramatic lowering of the energy of the first excitation of azulene compared to that of naphthalene.

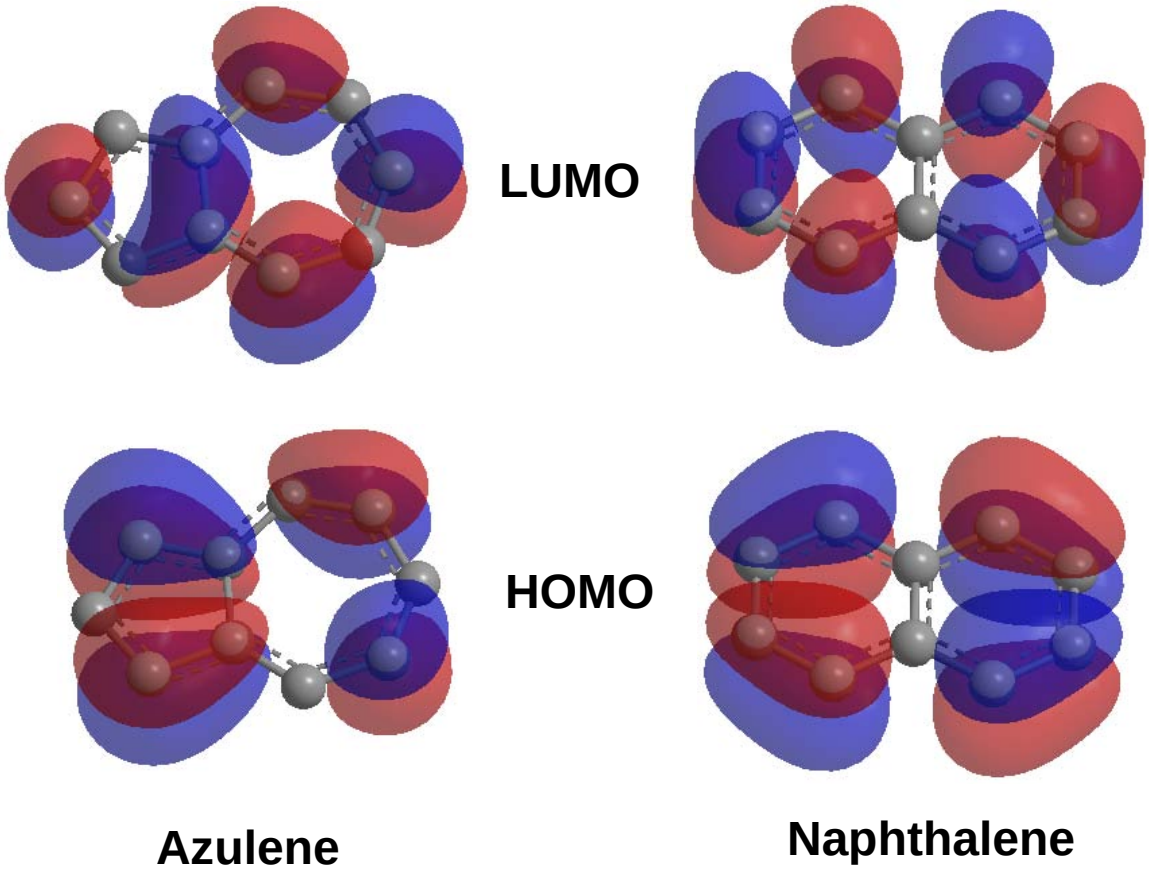

Figure II.2. Extended Huckel models of the HOMO and LUMO of azulene and naphthalene.

Recently, the Barybin group has established a new class of aryl isocyanides, isocyanoazulenes, and studied electron delocalization between electron-rich metal centers and the azulenic framework mediated by the isocyanide junction.[2] The chemistry of the homo- and heterobimetallic adducts of the rigid linear π-linker 2,6-diisocyanoazulene has opened new directions in the design of materials with advanced electronic and/or optoelectronic properties.[3] This nonbenzenoid diisocyanide functions as an effective structural and electronic bridge in low-valent transition metal molecular systems, as well as a convenient substrate for fabricating self-assembled monolayers (SAMs) of the 2,6-azulenic motif fitted with conducting "alligator clips" on a Au(111) surface.[4] One can also imagine extending the above 2,6-azulenic bridge by employing 2,6-polyazulenic

motifs in constructing new charge transport devices at the nanoscale as schematically represented in Figure II.3. To this date, the chemistry of all biazulenes has been very scarcely explored, primarily due to significant synthetic challenges in accessing such species.

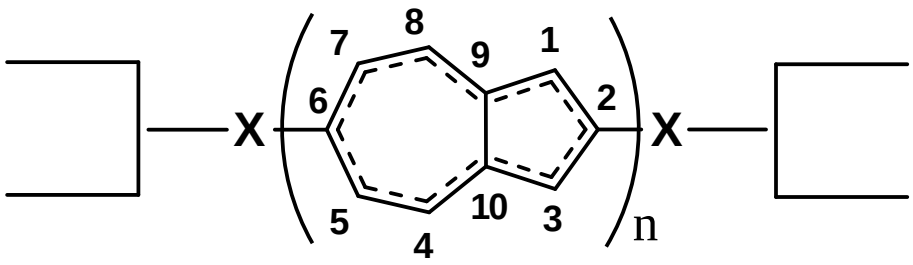

Figure II.3. Schematic representation of 2,6-coupled mono-(n=1) and biazulenic (n=2) charge transport linkers; X = junction unit.

Figure II.4. The three possible *linear* diisocyano-biazulenes.

There are three possible ways to link two azulene units linearly through the 2- and 6- positions, as illustrated in Figure II.4. The three different frameworks offer different advantages and disadvantages, both synthetically and in terms of electronic properties. The 6,6'-biazulene is predicted to have the greatest interplanar angle between the two azulene units at approximately 50° in the gas phase by DFT.[5] The 2,2'-biazulene is predicted to have an interplanar twist of less than 5°, while the less symmetrical 2,6'-biazulene offers a predicted interplanar angle of approximately 30°. The above interplanar angles are primarily governed by steric interactions of the hydrogen atoms as indicated in Figure II.4. Interestingly, two of the combinations offer a predicted interplanar angle that is less than that in the biphenyl motif (approximately 45°). The smaller interplanar angle between the two aromatic rings provides better orbital overlap and enhanced conjugation within the π-bridge, which is important for effective charge delocalization mediated by the organic bridge.

Scheme II.1. Synthetic scheme for the synthesis of 6,6'-biazulene.[5]

Despite the significant progress in the synthesis of functionalized monoazulenes, functionalized biazulenes are extremely difficult to access. Most reports on the synthesis

of biazulenes have made use of metal-catalyzed reactions of halogenated azulenes. One exception is the synthesis of 6,6'-biazulene by Hanke and Jutz in 1980, shown in Scheme II.1.[5] This synthesis is a modification of the synthesis of azulene reported by Hafner.[7] The reaction sequences make use of a ring opening reaction of pyridine or 4,4'-bipyridine, followed by coupling of the resulting pentafulvene with cyclopentadiene.[5,7] Interestingly, the yield of azulene reported by Hafner is 60% while the reported yield of the biazulene is only 30%.[5,7]

Scheme II.2. Synthesis of tetraethyl 2,2'-diamino-1,1',3,3'-tetraethoxycarbonyl-6,6'-biazulene.[9]

Further functionalization of the generated 6,6'-biazulene at the desired 2-position would prove quite challenging. In fact, there is no known pathway for aminating azulene itself at the 2-position. The best way to obtain 2-aminoazulene is by first forming 2-amino-1,3-diethoxycarbonylazulene and then decarboxylating the product to remove the ester functionalities.[8] As such, other methods for obtaining 6,6'-biazulene with functional groups already in place are necessary. In 2002, Sugihara *et al.* reported the

synthesis of 2,2'-diamino-1,1',3,3'-tetraethoxycarbonyl-6,6'-biazulene in a two step reaction of 17% total yield using a Suzuki-Miyuara coupling reaction, as shown in Scheme II.2.[9]

Scheme II.3. Synthesis of 2,2'-biazulene via Ullmann coupling, where R=H or CO_2Et and X=Cl or I.[10]

The synthesis of symmetric 2,2'-biazulene was first reported in 1982 by Morita and Takase using activated copper in an Ullmann aryl coupling reaction.[10] The Ullmann reaction requires high temperatures (ranging from 200 – 250°C) and is relatively unresponsive to a variety of haloazulenes with yields ranging from 10 – 80% depending on the starting azulene and whether a homo- or cross-coupled product is desired.[10] Specifically, 2,2'-biazulene and 1,1'-3,3'-tetraethoxycarbonyl-2,2'-biazulene were formed in 54 and 83% yield, respectively.[10]

Scheme II.4. Synthesis of 2-azulenylboronate.[11]

In their 2002 paper, Sugihara *et al.* used a nickel catalyzed coupling reaction of haloazulenes to form 2,2'-biazulene in 42% yield from 2-iodoazulene, 28% yield from 2-chloroazulene.[9] In 2004, Ito and coworkers reported the formation of a 2-azulenylboronate in 53% yield from 2-iodoazulene using palladium(II) 1,1'-

bis(diphenylphosphino)ferrocene with 5 mol% loading, shown in Scheme II.4.[11] The formed organoboronate is a desired reagent for use in Suzuki-Miyuara coupling reactions. The 2-azulenylboronate was also isolated from a lithiation reaction of 2-iodoazulene followed by immediate reaction with the borolane reagent.[11] Using the boronate, 2,2'-biazulene was formed in 40% yield using a tris(dibenzylideneacetone)dipalladium(0) catalyst.[11] One potential use of this reaction sequence is in the synthesis of cross-coupled 2,6'-biazulene.

The first report of 2,6'-biazulene that appeared in the literature was also in the 1982 Morita/Takase paper.[10] Again, the synthesis used activated copper in an Ullmann coupling reaction at 250°C in a sealed evacuated container.[10] The reaction was not specific for 2,6'-biazulene, producing 1,1',3,3'-tetraethoxycarbonyl-2,2'-biazulene in 21% yield and 1,1',3,3'-tetraethoxycarbonyl-2,6'-biazulene in 7% yield.[10] This inefficient process also has the same limitations as the functionalization of 6,6'-biazulene in that installing a desired functional group at the 2'-position has not been possible.

Scheme II.5. Synthesis of a functionalized 2,6'-biazulene.[9]

Cross-coupled 2,6'-biazulene was described in 2002 using a Stille reaction with an organotin reagent as an azulene metallating agent.[12] 1',3'-Diethoxycarbonyl-2,6'-biazulene was formed in a 35% yield in two steps, from 1,3-diethoxycarbonyl-6-bromoazulene and 2-bromoazulene using palladium catalysts in each step.[12] Again, this

material would provide significant challenges in functionalization of the 2'-position, thus limiting its usefulness in accessing functionalized biazulenes. Starting with 1,3'-diethoxycarbonyl-2-amino-6-bromoazulene would not be possible, as the stannylation reaction does not work well with primary amines.[13] In 2004, Ito and coworkers attempted to use the previously mentioned 2-azulenylboronate in a cross-coupling with 1,3-diethoxycarbonyl-2-amino-6-bromoazulene under standard Suzuki-Miyaura conditions to form 2-amino-1,3-bisethoxycarbonyl-6,2'-biazulene shown in Scheme II.5.[9]

Azulenes, in general, exhibit interesting electronic absorption spectra. In the absorbance spectra of azulene and functionalized azulenes, multiple peaks with detailed fine structure related to different vibrational states may be observed, especially in non-polar hydrocarbon solvents. Azulenes usually exhibit two distinct bands in the visible region (HOMO $\rightarrow$ LUMO and HOMO $\rightarrow$ LUMO+1 transitions) and two to three distinct bands in the ultra-violet region of the electromagnetic spectrum.

For azulene absorption in the visible region, the λ_{max} value occurs at 580 nm in cyclohexane and 575 nm in dichloromethane.[10,14] For the homo-coupled 2,2'-biazulene, this band shifts to 592 nm in chloroform and 580 nm in dichloromethane.[10,14] The slight bathochromic shift observed in dichloromethane solutions is accompanied by an increase in the molar absorptivity constant: log ε = 2.49 for azulene and 3.04 for 2,2'-biazulene.[14] For 6,6'-biazulene, the λ_{max} shifts to 592 nm in dichloromethane with a log ε value of 2.88.[14]

Table II.1. HOMO → LUMO transitions in the visible region for Azulene and Biazulenes in indicated solvents. [1,10,14]

Compound	λ_{max} (nm)	log ε	Solvent
Azulene	575	2.49	Methylene Chloride
Azulene	580	2.56	Cyclohexane
2,2-biazulene-1,3-diethoxycarboxylate	513	3.02	Cyclohexane
2,2'-biazulene	592	3.06	Chloroform
2,2'-biazulene	590	2.70	Dimethoxyethane
2,2'-biazulene radical anion	610	4.50	Dimethoxyethane
6,6'-biazulene	592	2.88	CH_2Cl_2
2,6'-biazulene	595	2.95	Chloroform
2,6'-biazulene-1,1'-3,3'-tetraethoxycarboxylate	504	3.08	Chloroform
1,1'-biazulene	612	2.80	Isooctane
1,1'-biazulene-3,3'-diethoxycarboxylate	575	2.33	Isooctane
1,2'-biazulene	579	2.96	Isooctane

The effect of substitution of azulene on the electronic absorption characteristics has been well addressed in a recent paper by Liu.[1] It was noted that when the substitution involves an electron donating group at the 1 or 3-position of azulene, a red shift in the HOMO → LUMO transition occurs.[1] Likewise, a blue shift occurs when a conjugated and/or electron withdrawing substituent is placed at the 1- or 3- position of azulene.[1] An analogous examination of the HOMO and LUMO of azulene (in Figure II.2) suggests that adding an aromatic fragment at the 2-position of azulene would result in stabilization of the LUMO, thereby resulting in a lower energy HOMO-LUMO gap manifested as a bathochromic shift in the absorption spectra of both 2,2'-biazulene and 6,6'-biazulene.

Addition of ethoxycarbonyl groups to the azulene framework, as expected, has a significant impact on the absorbance spectrum. 1,3-Diethoxycarbonyl-azulene is a deep red-colored compound, compared to deep blue azulene. In cyclohexane, λ_{max} shifts from

580 nm for azulene to 514 nm for 1,3-diethoxycarbonyl azulene.[10] This blue shift is also consistent with the observations by Liu, as the presence of the conjugated/electron withdrawing ester functionality would stabilize the HOMO, thereby widening the HOMO-LUMO gap compared to azulene itself.[1] Similarly, installation of the same ethyl ester functionality at the 1,1',3 and 3'-positions of 2,2'-biazulene results in a shift of λ_{max} from 592 nm (biazulene) to 513 nm (substituted biazulene).[10] Table II.1 contains a summary of the relevant spectral data.

Table II.2. ^{1}H NMR chemical shift (ppm) data for azulene and selected biazulenes in $CDCl_3$.[10,14,15]

Ring Position	Azulene	2,2'-biazulene	6,6'-biazulene
1/1'/3,3'	7.38	7.86	7.45
2/2'	7.90		7.96
4/4'/8/8'	8.31	8.28	8.43
5/5'/7/7'	7.12	7.13	7.40
6/6'	7.52	7.50	

In 1982, Morita and Takase made comparisons between the ^{1}H NMR patterns for substituted azulenes and their related biazulenes to assess the degree of coplanarity of the azulenic rings in biazulenes. The relevant data are compiled in Table II.2.[10] Although no crystal structures have been reported for the biazulenes to date, the analysis and explanations of their spectra are quite exemplary. For 2,2'-biazulene, the resonances for protons at 1,1', 3 and 3' positions shift from 7.40 ppm for azulene to 7.86 ppm for 2,2'-biazulene.[10] This pronounced downfield shift is consistent with deshielding stemming from the "ring-current effect" of the adjacent aromatic ring, similar to that observed for benzenoid compounds, as illustrated in Figure II.5.[16] The other three inequivalent protons of 2,2'-biazulene exhibit a shift of no more than 0.05 ppm.[10] The ^{1}H NMR chemical shift values for 5,5',7 and 7'-positions shift from 7.12 ppm for azulene to 7.40

ppm for 6,6'-biazulene, while the other three inequivalent protons exhibit chemical shift changes of less that 0.07 ppm.[10,15] Again, the protons located in the "halo" of the ring current are deshielded, resulting in a substantial downfield shift of the proton resonances for the biazulenic systems.

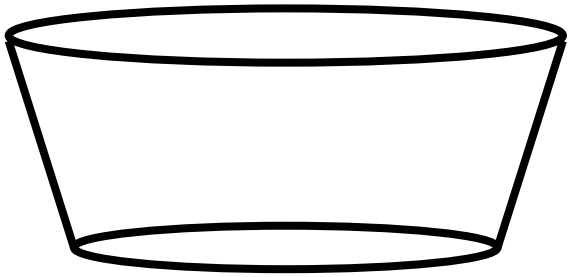

Figure II.5. Representation of the ring current effect on a hydrogen atom of 6,6'-biazulene.

Table II.3. Electrochemical reduction and oxidation potentials of azulene and biazulenes. Reduction potentials were obtained in DMF at 25°C. Oxidation potentials were obtained in 1:1 CH_3NO_2:CH_2Cl_2. All acquisitions used Ag/AgCl reference electrode in CH_3CN.[17,18]

Compound	E_1^C	E_2^C	E_1^A	E_2^A
Azulene	-1.54		0.96	
1,1'-biazulene	-1.75	-1.47	0.74	1.09
2,2'-biazulene	-1.74	-1.15		
4,4'-biazulene	-1.54	-1.30		
5,5'-biazulene	-1.69	-1.42		
6,6'-biazulene	-1.32	-1.09		
4,6'-biazulene	-1.4	-1.20		

Electrochemical behavior of several biazulenic systems has been studied in detail. In 1984, Hunig and coworkers reported the reduction half-wave potentials for a few biazulenes, including 2,2'-biazulene and 6,6'-biazulene.[17,18] They found that, although azulene exhibits a single, 1-electron reversible reduction, biazulenes appear to exhibit two stepwise single electron reversible reduction events, as illustrated in Scheme II.6.[17,18] Table II.3 summarizes representative electrochemical data.

Scheme II.6. Oxidation and Reduction processes for 2,2'-biazulene.

From Table II.3, it appears that for all biazulenes, the first one electron reduction is more facile than that of azulene, likely due to the distribution of a single charge over two ring systems. For 6,6'-biazulene and 4,6'-biazulene, the second reduction process is also more facile than for azulene itself, while the second reduction for 4,4'-biazulene is at the same potential for the single electron reduction of azulene. On average, the difference between the two stepwise reduction processes is 200mV, with the second single electron reduction occurring at a more negative potential than that for the reduction of azulene.

When attempting to rationalize the reported data, it is necessary to once again consider the shapes and energies of the HOMO and LUMO of azulene itself, shown in Figure II.2. The least negative reduction potential represents introduction of a single electron into the LUMO of the azulene framework. The atomic contributions to the LUMO of a biazulene should be greatest at even-numbered positions. Therefore, for

biazulenes coupled through carbon atoms at even positions, conjugation between the two rings would be enhanced, whereas for biazulenes coupled through odd numbered carbon atoms, the best orbital overlap would occur in either the HOMO or the LUMO + 1. As such, introducing an electron into the system of an "even-linked" biazulene would provide a stronger degree of conjugation involving both rings and result in a less negative potential. This provides a reasonable explanation for the observed reduction potentials of -1.15 V and -1.09 V as the first reduction steps for 2,2'-biazulene and 6,6'-biazulene, respectively.[17,18]

Figure II.6. Illustration of the location of negative charge in radical anion and dianion of 2,2'-biazulene.

The introduction of the second electron into various biazulenes also shows some interesting features. The least negative potential associated with introducing a second electron occurs for 6,6'-biazulene while the most negative potential occurs for 1,1'-biazulene and 2,2'-biazulene. Upon the formation of the radical anion, the lone electron is most likely to reside in the cyclopentadienide-like five-membered ring as shown in Figure II.6. The second added electron would therefore most likely be delocalized within the other five-membered ring of the biazulene framework. In the case of 6,6'-biazulene, the five-membered rings are as far apart as they can possibly be in any biazulenic system and formation of a closed shell dianion can be envisioned upon the two-electron reduction of this system. In the case of 1,1'- and 2,2'-biazulenes, the five-membered rings are adjoined and no closed-shell structure could be drawn upon the 2-e^- reduction of

either of these biazulenes. Thus the dianions of 1,1'- and 2,2'-biazulenes may be expected to be the least stable among all of the biazulenic dianions.

Table II.4. EPR data for azulene and biazulene radical anions generated (a) via reduction with potassium in DME or (b) electrolytically in DMF with $[N(^nPr)_4][ClO_4]$; reported as absolute values in gauss.[19,20]

Position	$a_{1,1'}^H$	$a_{2,2'}^H$	$a_{3,3'}^H$	$a_{4,4'}^H$	$a_{5,5'}^H$	$a_{6,6'}^H$	$a_{7,7'}^H$	$a_{8,8'}^H$
Azulene[a]	0.27	3.98	0.27	6.13	1.21	8.73	1.21	6.12
2,2'-biazulene[a]	0.48		0.48	4.05	1.23	5.27	1.23	4.05
5,5'-biazulene[a]	0.05	2.09	0.15	1.51		4.38	0.54	3.15
6,6'-biazulene[a]	0.50	3.14	0.50	6.32	0.82		0.82	1.51
Azulene[b]	0.27	3.95	0.27	6.22	1.34	8.83	1.34	6.22
1,1'-biazulene[b]		4.09	0.36	5.90	1.12	8.64	1.12	5.90
2,2'-biazulene[b]	0.49		0.49	4.11	1.25	5.35	1.25	4.11

Electron paramagnetic resonance (EPR) is another tool researchers have used to evaluate the extent of orbital overlap in polyaryl systems. Table II.4 summarizes the reported hyperfine coupling constants (a_H) involving various protons on azulene and biazulene systems in gauss.[19,20] These data were collected using both electrolytic and alkali metal reductions to generate the corresponding radical anions. For the azulene radical anion, the largest a_H values occur at positions 2, 4, 6 and 8. This is certainly consistent with the relative contributions of the corresponding carbon atoms to the LUMO of azulene (see Figure II.2).

Upon homo-coupling of azulene to form symmetric biazulenes, deviations of the a_H values for the corresponding radical anions from the analogous a_H values documented for

azulene may arise from additional electronic and steric interactions present in the biazulenes. If the hyperfine coupling constants determined for the biazulene radical anions are similar to those observed for the azulene radical anion, the biazulenic system is likely to be not coplanar and there should be little overlap between the π-systems of the individual azulene rings. This has indeed been observed in the case of the hyperfine coupling constants for 1,1'-biazulene radical anion. The values of a_H indicate that the unpaired electron is localized within one half of the dimeric anion and the exchange between the two halves of the molecule is slow on the experimental time scale. This is consistent with the predicted lack of planarity between the two azulene units in this biazulenic system.

Given the observations documented for 1,1'-biazulene radical anion, other homo-coupled azulenes through odd-numbered carbon atoms may be expected to exhibit a similar lack of conjugation, especially when compared to homo-coupled biazulenes featuring junctions at the even-numbered carbon atoms. In fact, considering the a_H values of 5,5'-biazulene radical anion versus those of 6,6'-biazulene radical anion, the above phenomenon becomes apparent. Because both biazulene radical anions feature connections at the 7-membered ring, they should exhibit roughly similar steric interactions. If a_H values were strictly dependent on coplanarity of the azulenic moeities, then the coupling constants for 5,5'-biazulene and 6,6'-biazulene radical anions would have been similar in magnitude. The actual measurements show that the a_H values for 5,5'-biazulene radical anion are approximately a factor of 2 smaller in magnitude compared to those of azulene itself and quite different from those observed for 6,6'-biazulene radical anion. The a_H values indicate that in 5,5'-biazulene radical anion, the

density of a single electron distributed evenly over the π-system of the azulene radical anion is now distributed evenly between the two rings of 5,5'-biazulene radical anion, consistent with improved planarity compared to 1,1'-biazulene radical anion.

Finally, in the case of 2,2'-biazulene, the extent of conjugation between the two azulenic π-systems is expected to be the best connectivity position and coplanarity of the two azulenyl rings. This is demonstrated by a_H values for the 2,2'-biazulene radical anion that are comparable in magnitude to azulene radical anion.

In this chapter, synthesis, characterization and coordination chemistry of 2,2'-diisocyano-1,1',3,3'-tetraethoxycarbonyl-6,6'-biazulene (**2.1c**) and 6-isocyano-2,2'-biazulene (**2.2c**) are reported. The first X-ray crystal structures of biazulenes and electronic properties of the novel biazulenic systems, pictured in Figure II.7, are described as well.

Figure II.7. 2,2'-Diisocyano-1,11,3,3'-tetraethxoycarbonyl-6,6'-biazulene (2.1c) and 6-isocyano-2,2'-biazulene(2.2c).

II.2. Experimental

II.2.1. General Procedures

Unless specified otherwise, all operations were performed under an atmosphere of 99.5% argon further purified by passage through columns of activated BASF catalyst and molecular sieves. All connections involving the gas purification systems were made of glass, metal, or other materials impermeable to air. Solutions were transferred via

stainless steel needles (cannulas) whenever possible. Standard Schlenk techniques were employed with a double manifold vacuum line. CH_2Cl_2, NEt_3, and N^iPr_2H were distilled over CaH_2. THF was distilled from Na/benzophenone. Pentane was distilled from Na/benzophenone dissolved in a minimum amount of diglyme. DMSO was stored over molecular sieves and made oxygen free by bubbling with argon for 1 hour prior to use. Following purification, all distilled solvents were stored under argon.

Solution infrared spectra were recorded on Shimadzu FTIR-8400S or on PerkinElmer Spectrum 100 FTIR spectrometers with samples sealed in 0.1 mm gas-tight NaCl cells. NMR samples were analyzed using Bruker DRX-400 and Bruker Avance 500 spectrometers. ^1H and ^{13}C chemical shifts are given with reference to residual ^1H and ^{13}C solvent resonances relative to Me_4Si. UV-Vis spectra were recorded in CH_2Cl_2 at 24 °C using a CARY 100 spectrophotometer.

Cyclic voltammetric (CV) experiments on 2×10^{-3} M solutions of selected compounds in CH_2Cl_2 were conducted at room temperature using an EPSILON (Bioanalytical Systems INC., West Lafayette, IN) electrochemical workstation. The electrochemical cell was placed in an argon-filled Vacuum Atmospheres dry-box. Tetrabutylammonium hexafluorophosphate (0.1 M solution in CH_3CN) was used as a supporting electrolyte. Cyclic voltammograms were recorded at 22 ± 2 °C using a three component system consisting of a platinum working electrode, a platinum wire auxiliary electrode, and a glass encased non-aqueous silver/silver chloride reference electrode. The reference Ag/Ag^+ electrode was monitored with the ferrocenium/ferrocene couple. IR compensation was achieved before each CV run by measuring the uncompensated solution resistance followed by incremental compensation and circuit stability testing.

Background cyclic voltammograms of the electrolyte solution were recorded before adding the analytes. The half-wave potentials ($E_{1/2}$) were determined as averages of the cathodic and anodic peak potentials of reversible couples and are referenced to the external FcH^+/FcH couple.[21]

Melting points are uncorrected and were determined for samples in sealed under argon capillary tubes. Elemental analyses were carried out by Chemisar/Guelph Chemical Laboratories Ltd, Ontario, Canada.

Compounds 2-amino-6-bromo-1,3-diethoxycarbonylazulene,[3] 2,2'-biazulene,[10] bisnaphthalenechromium(0),[22] bis(dicyclohexylphosphinomethyl)gold(I) chloride[23], acetic formic anhydride[24] and $[W(CO)_5THF]$[25] were prepared according to literature procedures. Other reagents were obtained from commercial sources and used as received.

II.2.2. Synthesis of 2,2'-diamino-1,1',3,3'-tetraethoxycarbonyl-6,6'-biazulene (2.1a).

This synthesis was adapted from Sugihara *et al.*[9] Palladium(II) diphenylphosphinoferrocene chloride monodichloromethane (0.226g, 0.277mmol), bis(pinacolato)diboron (0.176g, 0.692mmol), potassium acetate (0.814g, 8.303 mmol), and 2-amino-6-bromo-1,3-diethoxycarbonylazulene (1.013g, 2.768mmol) were placed in a 250mL single arm round bottom flask (SARB). To this mixture, 50mL of O_2-free DMSO was added at room temperature. The resulting orange-yellow solution was refluxed under argon for 5 hrs. The reaction was cooled to room temperature and 150mL of deionized H_2O was added to the flask. The mixture was filtered and the collected rust-

colored solid was washed with deionized H_2O (3×100 mL), followed by $CHCl_3$ (2×50 mL). The solid was dried under vacuum for 3 hours to provide 0.590 g (74%) of brick red **2.1a**. The $CHCl_3$ washings were combined, washed with 50mL of H_2O and dried over $MgSO_4$. The resulting solution was filtered and concentrated on a rotary evaporator and recrystallized with pentane to give an additional 0.199 g (25%) of **2.1a**, an essentially quantitative total yield. Mp: dec. 220°C. MS (ES+, m/z) calc. for $C_{32}H_{33}N_2O_8$: 573.2; found: 573.2. ^{1}H NMR ($CDCl_3$, 400MHz, 25°C): δ 1.48 (t, 3H, C*H*$_3$, $^3J_{HH}$ = 8Hz), 4.47 (q, 2H, C*H*$_2$, $^3J_{HH}$ = 8Hz), 7.78 (d, 1H, $H^{5,5',7,7'}$, $^3J_{HH}$ = 16Hz), 7.85 (s, br, 1H, N*H*$_2$), 9.17 (d, 1H, $H^{4,4',8,8'}$, $^3J_{HH}$ = 16Hz) ppm.

II.2.3. Synthesis of 2,2'-bisformamido-1,1',3,3'-tetraethoxycarboonyl-6,6'-biazulene (2.1b).

Without protection from air, **2.1a** (0.789g, 1.379mmol) was combined with 50mL of commercial CH_2Cl_2 to form a deep red solution. Acetic-formic anhydride (3.3 mL, 41 mmol) and formic acid (6.2mL, 0.17 mol) were added to the solution of **2.1a**. The reaction mixture was heated at 50°C for 2 hrs. The red/brown solution was cooled to room temperature and quenched with 100 mL of 10% aq. Na_2CO_3. The resulting mixture was filtered and the solid was washed with deionized H_2O (3×100 mL), 100% ethanol (2×20 mL), and diethyl ether (2×20 mL). The solid was dried in vacuo to provide 0.366g (42%) of chestnut-colored **2.1b**. An additional 0.346g (40%) of **2.1b** was obtained by removing ethanol and ether from the filtrate in vacuo and extracting the residue with CH_2Cl_2 (3×50 mL), drying over Na_2SO_4, concentrating on a rotary evaporator and recrystallizing by adding pentane. The total yield of **2.1b** was 82%. Mp: 254-256°C. HRMS (ES+, m/z) calc. for $C_{34}H_{33}N_2O_{10}$: 629.2135, found: 629.2139. ^{1}H NMR ($CDCl_3$,

400MHz, 22°C): δ 1.50 (t, 6H, C*H*$_3$, $^3J_{HH}$ = 8Hz), 4.53 (q, 4H, C*H*$_2$, $^3J_{HH}$ = 8Hz), 7.97 (d, 2H, $H^{5,5',7,7'}$, $^3J_{HH}$ = 8Hz), 8.71 (s, br, 1H, N*H*), 9.50 (d, 2H, $H^{4,4',8,8'}$, $^3J_{HH}$ = 8Hz), 10.42 (s, br, 1H, C*H*O) ppm.

II.2.4. Synthesis of 2,2'-diisocyano-1,1',3,3'-tetraethoxycarbonyl-6,6'-biazulene (2.1c).

0.358 g of **2.1b** (0.570 mmol) was dissolved in 20 mL of CH_2Cl_2 to form a red/brown solution in a 250 mL SARB flask. The solution was cooled to 0°C with an ice bath. A solution of triphosgene (0.423 g, 1.43 mmol) and triethylamine (0.8 mL, 5.7 mmol) in 10 mL of CH_2Cl_2 was prepared in a 100mL SARB flask and then transferred to the solution of **2.1b**. The reaction mixture was slowly warmed to room temperature with stirring for 3 hrs. Monitoring the reaction progress by TLC revealed incomplete conversion. An additional solution of triphosgene (0.450 g, 1.52 mmol) and triethylamine (0.8 mL, 5.7 mmol) in 10 mL CH_2Cl_2 was added to the reaction flask. After 1 hr of stirring, the purple solution was quenched with 80 mL of 10% aq. Na_2CO_3 and filtered. The collected solid was washed with CH_2Cl_2 (3×50 mL). The organic washings and filtrate were combined. The aqueous layer was extracted with additional CH_2Cl_2 (2×50 mL). The organic fractions were washed with 100mL of deionized H_2O, dried over Na_2SO_4, and concentrated on a rotary evaporator. The crude product was purified by column chromatography on silica. The hexanes:ethyl acetate (2:1) eluent provided a pink band containing 0.048 g of lavender colored **2.1c**. The hexanes:ethyl acetate (1:1) mixture eluted a red band containing 0.072 g of **2.1c**. Ethyl acetate provided a pink band containing 0.036 g of **2.1c**. Finally $CHCl_3$ pushed off a lavender band containing 0.027 g of **2.1c**. The cumulative yield of **2.1c** was 0.183 g (54%) obtained by

crystallization of the combined solutions at 0°C for 24hrs. Mp: dec 225°C. Anal. Calcd for $C_{34}H_{28}N_2O_8$: C: 68.91; H: 4.76; N: 4.73. Found: C: 68.62; H: 4.86; N: 4.96. FTIR (CH_2Cl_2): ν_{CN} = 2127 cm^{-1}. ^1H NMR (CD_2Cl_2, 400MHz, 22°C): δ 1.54 (t, 3H, C*H*$_3$, $^3J_{HH}$ = 8Hz), 4.55 (q, 2H, C*H*$_2$, $^3J_{HH}$ = 8Hz), 8.03 (d, 1H, $H^{5,5',7,7'}$, $^3J_{HH}$ = 10Hz), 9.93 (d, 1H, $H^{4,4',8,8'}$, $^3J_{HH}$ = 10Hz) ppm. ^{13}C NMR ($CDCl_3$, 125.7MHz, 22°C): δ 14.2 (*C*H_3), 61.3 (*C*H_2), 113.7, 131.9, 132.4, 140.2, 140.6, 156.5 (aromatic C), 163.1 (*C*O_2R), 178.6 (*C*NR) ppm. UV-Vis (CH_2Cl_2) λ_{max} (log ε): 531 nm (3.39), 390 nm (4.48), 341 nm (4.65), 247 nm (4.62).

II.2.5. Synthesis of mono- and dinuclear tungsten pentacarbonyl complexes of 2,2'-diisocyano-1,1',3,3'-tetraethoxycarbonyl-6,6'-biazulene, $[W(CO)_5]$·2.1c and $[W(CO)_5]_2$·2.1c.

$[W(CO)_5THF]$ was generated according to a literature procedure from 0.066 g $W(CO)_6$ (0.187 mmol) in 80 mL of THF.[25] Diisocyanide **2.1c** (0.221 g, 0.373 mmol) was dissolved in 30 mL of THF. The orange $[W(CO)_5THF]$ solution was slowly transferred to the lavender solution of **2.1c** over 30 minutes. The reaction mixture was stirred for 18hrs at room temperature. Then, all THF was removed in vacuo. The solid residue was dissolved in CH_2Cl_2 on air and chromatographed on silica gel to give a deep red band corresponding to the dinuclear adduct. Ethyl acetate (10%) in CH_2Cl_2 was used to push off an orange-red band of the mononuclear complex. Both materials were recrystallized from CH_2Cl_2/pentane to give 0.047 g (41%) of fuchsia **$[W(CO)_5]_2$·2.1c** and 0.064 g (37%) of scarlet **$[W(CO)_5]$·2.1c**.

$[W(CO)_5]$·2.1c: Mp:137-139°C dec. IR (CH_2Cl_2): ν_{CO} 1952 vs, 2044 m cm^{-1}; ν_{CN} 2136 s br. ^1H NMR (500mHz, CD_2Cl_2, 19°C): δ 1.49 (t, 3H, C*H*$_3$, $^3J_{HH}$ = 7Hz), 1.50 (t, 3H, C*H*$_3$, $^3J_{HH}$ = 7Hz), 4.50 (q, 2H, C*H*$_2$, $^3J_{HH}$ = 7Hz), 4.56 (q, 2H, C*H*$_2$, $^3J_{HH}$ = 7Hz), 8.05

(d, 2H, $H^{5,7}$, $^3J_{HH}$ = 11Hz), 8.06 (d, 2H, $H^{5,7}$, $^3J_{HH}$ = 11.5Hz), 9.88 (d, 2H, $H^{4,8}$, $^3J_{HH}$ = 11Hz), 9.90 (d, 2H, $H^{4,8}$, $^3J_{HH}$ = 11.5Hz) ppm. ^{13}C NMR (500MHz, CD_2Cl_2, 19°C): δ 14.57, 15.09 (*C*H_3), 61.63, 61.72 (*C*H_2), 114.13, 114.40, 132.29, 132,80, 133.13, 133.49, 140.13, 140.73, 140.84, 141.45, 156.74, 157.25 (aromatic C), 163.52, 164.89 (*C*O_2), 179.10 (*C*N), 194.61 (*C*O *cis*), 197.04 (*C*O *trans*) ppm. UV-Vis (CH_2Cl_2) λ_{max} (log ε): 485 nm (4.46).

$[W(CO)_5]_2$·2.1c: Mp: 186-188°C. Anal. Calcd for $C_{44}H_{28}N_2O_{18}W_2$: C: 42.61; H: 2.28; N: 2.26. Found: C: 43.01; H: 2.10; N: 2.04. FTIR (CH_2Cl_2): ν_{CO} 1954 vs, 2041 m cm^{-1}; ν_{CN} 2139 s cm^{-1}. ^{1}H NMR (500mHz, CD_2Cl_2, 19°C): δ 1.51 (t, 3H, C*H*$_3$, $^3J_{HH}$ = 7Hz), 4.57 (q, 2H, C*H*$_2$, $^3J_{HH}$ = 7 Hz), 8.08 (d, 1H, $H^{5,5',7,7'}$, $^3J_{HH}$ = 11Hz), 9.92 (d, 1H, $H^{4,4',8,8'}$, $^3J_{HH}$ = 11Hz) ppm. ^{13}C NMR (125MHz, CD_2Cl_2, 19°C): δ 15.09 (*C*H_3), 61.62 (*C*O_2), 114.24, 132.76, 133.48, 140.12, 141.43, 156.82 (aromatic C), 164.78 (*C*NR), 193.3 (W*C*O, *cis*), 195.72 (W*C*O, *trans*) ppm. UV-Vis (CH_2Cl_2) λ_{max} (log ε): 496 nm (4.41).

II.2.6. Synthesis of 6-amino-2,2'-biazulene (2.2a).

2,2-biazulene (1.047 g, 4.122 mmol) and 4-amino-4H-1,2,4-triazole (1.039 g, 12.37 mmol) were dissolved in 15 mL of O_2-free DMSO in a 250mL SARB. Potassium tertbutoxide (2.770 g, 24.37 mmol) was dissolved in 30 mL of O_2-free DMSO in a 100mL SARB. The colorless KO^{t}Bu solution was transferred to the green biazulene-containing solution and the resulting mixture immediately turned dark blue, then purple. After 5hrs of stirring at room temperature, the reaction mixture was transferred to a 500mL Erlenmeyer flask containing 400 mL of water. The resulting red mixture was filtered. The solid was washed with deionized H_2O (3×100 mL) and dried in vacuo for 3

hrs to give 0.904 g (82%) of orange/rust-colored **2.2a**. Mp: 152-155°C dec. HRMS (ES+, m/z) calc. for $C_{20}H_{16}N$: 270.1283, found: 270.1271. ^{1}H NMR (400MHz, Acetone-d^6, 21°C): δ 6.51 (s br, 2H, NH_2), 6.54 (d, 2H, $H^{5,7}$, $^{3}J_{HH}$ = 11Hz), 7.12 (t, 2H, $H^{5',7'}$, $^{3}J_{HH}$ = 9.5Hz), 7.41(t, 1H, $H^{6'}$, $^{3}J_{HH}$ = 9.5Hz), 7.50 (s, 2H, $H^{1,3}$), 7.74 (s, 2H, $H^{1',3'}$), 7.92 (d, 2H, $H^{4,8}$, $^{3}J_{HH}$ = 11Hz), 8.21 (d, 2H, $H^{4',8'}$, $^{3}J_{HH}$ = 9.5Hz) ppm. ^{13}C NMR (125MHz, Acetone-d^6, 19°C): δ 111.4, 111.5, 116.0, 118.0, 119.5, 124.5, 129.8, 135.0, 125.5, 135.6, 137.7, 138.8, 141.5, 142.8, 149.4, 160.4 (aromatic *C*) ppm.

II.2.7. Synthesis of 6-formamido-2,2'-biazulene (2.2b).

Acetic anhydride (9.13 mL, 97.6 mmol) and formic acid (11.0 mL, 0.292 mol) were combined in a vial without protection from air. The solution was heated at 65°C for 3 hrs with vigorous stirring and then cooled to room temperature. Compound **2.2a** (0.525 g, 1.952 mmol) was dissolved in 50mL of THF in a 250 mL SARB flask to afford a red/brown solution. The cooled mixed anhydride mixture was transferred to this solution and the reaction mixture was stirred for 18hrs at room temperature. The reaction was quenched with 50 mL of 10% aq. Na_2CO_3. The mixture was filtered and the filtercake was washed with deionized H_2O (3×100 mL). The collected solid was dried in vacuo to give 0.560 g (98%) of dark green-brown **2.2b**. Mp: 295°C dec. ^{1}H NMR (400MHz, DMSO-d^6, 23°C): δ 7.20 (t, 2H, $H^{5',7'}$, $^{3}J_{HH}$ = 9.5Hz), 7.41 (d, 2H, $H^{5,7}$, $^{3}J_{HH}$ = 10Hz), 7.55 (t, 1H, $H^{6'}$, $^{3}J_{HH}$ = 9.5Hz), 7.82 (s, 2H, $H^{1',3'}$), 7.84 (s br, 1H, N*H*), 7.87 (s, 2H, $H^{1,3}$), 8.25 (d, 2H, $H^{4,8}$, $^{3}J_{HH}$ = 10Hz), 8.33 (d, 2H, $H^{4',8'}$, $^{3}J_{HH}$ = 9.5Hz), 10.69 (s br, 1H, C*H*O) ppm.

II.2.8. Synthesis of 6-isocyano-2,2'-biazulene (2.2c).

A green-brown solution of **2.2b** (0.105 g, 0.354 mmol) and triethylamine (0.5 mL, 3.5 mmol) in 30mL of THF in a 250 mL SARB flask was frozen with liquid N_2. A solution of triphosgene (0.116 g, 0.389 mmol) in 15mL of THF was slowly transferred to the flask containing the frozen solution of **2.2b**. The liquid nitrogen bath was removed and the reaction mixture was allowed to thaw to room temperature. Stirring was initiated once possible and the mixture was stirred for 6 hrs. Then, 40 mL of 10% aq. Na_2CO_3 was added to quench the reaction. The mixture was stirred an additional 1 hr. THF was removed in vacuo. The mixture was filtered and the collected solid was washed with deionized H_2O (2×100 mL) and then with CH_2Cl_2 (3×50 mL). The organic washings were combined and washed with 50mL of deionized H_2O, dried over Na_2SO_4 and all solvent was removed on a rotary evaporator. The remaining residue was washed with 3× 50 mL of THF. The THF washings were combined, dried over Na_2SO_4, and the solvent was removed by rotary evaporation. The 0.062 g of the recovered filtercake was identified as unreacted **2.2b**. The material from the organic washings was dissolved in pentane, filtered and allowed to slowly evaporate to provide 0.043 g (44%) pine green **2.2c**. Mp: 220°C dec. Elemental analysis calc (found) of $C_{21}H_{13}N$: C: 90.29 (90.56); H: 4.69 (4.90); N: 5.01 (4.84). IR (CH_2Cl_2): ν_{CN} 2114 cm^{-1}. ^1H NMR (500MHz, CD_2Cl_2, 19°C):δ 7.12 (br m, 2H, $H^{5,5',7,7'}$), 7.48 (br t, 1H, $H^{6'}$), 7.80, 7.89 (br s, 2H, $H^{1,1',3,3'}$), 8.16, 8.26 (br d, 2H, $H^{4,4',8,8'}$) ppm. UV-Vis (CH_2Cl_2) λ_{max} (log ε): 559 nm (3.12), 598 nm (3.09).

II.2.9. Preliminary Small Scale Synthesis of Neutral and Cationic Hexakis(6-isocyano-2,2'-biazulene)chromium ($Cr(2.2c)_6$).

Bisnaphthalenechromium(0) (0.021 g, 0.068 mmol) was dissolved in 20 mL of THF in a 250 mL SARB flask and cooled to -78°C. Compound **2.2c** (0.115 g, 0.412 mmol) was dissolved in 20 mL of THF in a 100 mL SARB flask. The solution of **2.2c** was transferred to the chromium complex. The reaction mixture was slowly warmed to room temperature and stirred for 20 hrs. The solution turned dark green and solid was present. An FTIR spectrum of the reaction mixture revealed a broad stretch at 1956 cm^{-1} with no evidence of residual **2.2c**. The reaction mixture was filtered through a medium frit and washed with THF (2×10 mL) and then pentane (2×10 mL). Solvent was removed from the filtrate in vacuo and both the filtercake and the filtrate residue were dried to give 33 mg of dark green neutral Cr(**2.2c**)$_6$ (28%).

16.7 mg of neutral Cr(**2.2c**)$_6$ (0.0097 mmol) and $AgSbF_6$ (7 mg, 0.020 mmol) were dissolved in 20 mL of CH_2Cl_2 in a 100 mL SARB flask. The reaction mixture immediately turned red. Upon stirring overnight, FTIR spectra revealed a new isocyanide stretching vibration at 2050 cm^{-1}, indicating formation of [Cr(**2.2c**)$_6$][SbF_6] . Solvent was removed in vacuo to provide a dark green/black solid that was not further isolated.

II.2.10. X-Ray Crystallographic Characterization of $C_{34}H_{28}N_2O_8$, 2.1c.

Purple crystals of $C_{34}H_{28}N_2O_8$ are, at 100(2) K, tetragonal, space group $P\bar{4}n2$ – D_{2d}^{8} (No. 118)[26] with **a** = 17.6562(4) Å, **b** = 17.6562(4) Å, **c** = 4.5121(1) Å, V = 1406.61(5) $Å^3$ and Z = 2 molecules {d_{calcd} = 1.399 g/cm^3; $\mu_a(CuK\alpha)$ = 0.832 mm^{-1}}. A full hemisphere of diffracted intensities (3377 10- or 30-second frames with a phi or ω scan width of 0.50°) was measured for a single-domain specimen using monochromatic

CuKα radiation (λ= 1.54178 Å) on a Bruker X8 Proteum Single Crystal Diffraction System equipped with a Platinum 135 CCD area detector. X-rays were provided by a Bruker MicroStar-H rotating anode generator operated at 45kV and 60mA. The incident x-rays were focused using doubly diffracting Helios multilayer x-ray optics. Lattice constants were determined with the Bruker SAINT software package using peak centers for 4806 reflections. A total of 6995 integrated reflection intensities having 2θ(CuKα)< 131.13° were produced using the Bruker program SAINT[28]; 3279 of these were unique and gave R_{int} = 0.031 with a coverage which was 98.6% complete. The data were corrected empirically for variable absorption effects using equivalent reflections; the relative transmission factors ranged from 0.901 to 1.000. The Bruker software package SHELXTL was used to solve the structure using "direct methods" techniques. All stages of weighted full-matrix least-squares refinement were conducted using F_o^2 data with the SHELXTL Version 6.10 software package.[29]

The methyl group was incorporated into the structural model as a rigid group (using idealized sp^3-hybridized geometry and a C-H bond length of 0.98 Å) that was allowed to rotate about its C-C bond during least-squares refinement cycles. The remaining hydrogen atoms were included in the structural model as idealized atoms (assuming sp^2- or sp^3-hybridization of the carbon atoms and C-H bond lengths of 0.95 or 0.99 Å). The isotropic thermal parameters of all hydrogen atoms were fixed at values 1.2 (nonmethyl) or 1.5 (methyl) times the equivalent isotropic thermal parameter of the carbon atom to which they are covalently bonded.

The final structural model incorporated anisotropic thermal parameters for all nonhydrogen atoms and isotropic thermal parameters for all hydrogen atoms. A total of

103 parameters were refined using no restraints, 1186 data and weights of $w = 1/ [\sigma^2(F^2) + (0.0457\ P)^2 + 0.3397\ P]$, where $P = [F_O^2 + 2F_C^2] / 3$. Final agreement factors at convergence are: R_1(unweighted, based on F) = 0.030 for 1139 independent absorption-corrected "observed" reflections having $2\theta(CuK\alpha) < 131.13°$ and $I > 2\sigma(I)$; R_1(unweighted, based on F) = 0.031 and wR_2(weighted, based on F^2) = 0.079 for all 1186 independent absorption-corrected reflections having $2\theta(CuK\alpha) < 131.13°$. The largest shift/s.u. was 0.000 in the final refinement cycle. The final difference map had maxima and minima of 0.14 and -0.13 $e^-/Å^3$, respectively.

Table II.5. Crystal data and structure refinement for $C_{34}H_{28}N_2O_8$, 2.1c.

Empirical formula	$C_{34}H_{28}N_2O_8$	
Formula weight	592.59	
Temperature	100(2) K	
Wavelength	1.54178 Å	
Crystal system	Tetragonal	
Space group	P4n2 – D_{2d}^8	
Unit cell dimensions	**a** = 17.6562(4) Å	**α** = 90.000°
	b = 17.6562(4) Å	**β** = 90.000°
	c = 4.5121(1) Å	**γ** = 90.000°
Volume	1406.61(5) $Å^3$	
Z	2	
Density (calculated)	1.399 Mg/m^3	
Absorption coefficient	0.832 mm^{-1}	
F(000)	606	
Theta range for data collection	3.54° to 65.56°	
Index ranges	$-20 \leq h \leq 14$, $-18 \leq k \leq 20$, $-4 \leq l \leq 5$	
Reflections collected	6995	
Independent reflections	3279	
Completeness to theta = 65.56°	98.6%	
Absorption correction	Multi-scan	
Refinement method	Full-matrix least-squares on F^2	
Data / restraints / parameters	1186 / 0 / 103	
Goodness-of-fit on F^2	1.087	
Final R indices [I>2sigma(I)]	R_1 = 0.030 and wR_2 = 0.079	
R indices (all data)	R_1 = 0.031 and wR_2 = 0.081	
Largest diff. peak and hole	014 and -0.13 $e^-/Å^3$	

II.2.11. X-Ray Crystallographic Characterization of 1,1',3,3'-tetraethoxycarbonyl-2,2'-biazulene.

Red/burgundy crystals for polymorph I of $C_{32}H_{30}O_8$ are, at 100(2) K, monoclinic,

space group C2/c – C_{2h}^6 (No. 15)[26] with **a** = 15.840(3) Å, **b** = 12.149(2) Å, **c** = 13.889(3) Å, **β** = 100.836(3)°, V = 2625(1) $Å^3$ and Z = 4 dimeric molecules {d_{calcd} = 1.373 g/cm^3; μ_a(MoKα) = 0.099 mm^{-1}}. A full hemisphere of diffracted intensities (1850 40-second frames with a ω scan width of 0.30°) was measured for a single-domain specimen using graphite-monochromated MoKα radiation (λ= 0.71073 Å) on a Bruker SMART APEX CCD Single Crystal Diffraction System.[27] X-rays were provided by a fine-focus sealed x-ray tube operated at 50kV and 35mA. Lattice constants were determined with the Bruker SAINT software package using peak centers for 3290 reflections. A total of 8724 integrated reflection intensities having 2θ((MoKα)< 51.99° were produced using the Bruker program SAINT;[28] 2555 of these were unique and gave R_{int} = 0.067 with a coverage which was 98.6% complete. The Bruker software package SHELXTL was used to solve the structure using "direct methods" techniques. All stages of weighted full-matrix least-squares refinement were conducted using F_o^2 data with the SHELXTL Version 6.10 software package.[29]

The final structural model incorporated anisotropic thermal parameters for all nonhydrogen atoms and isotropic thermal parameters for all hydrogen atoms. All hydrogen atoms were located in a difference Fourier and included in the structural model as independent isotropic atoms whose parameters were allowed to vary in least-squares refinement cycles. A total of 241 parameters were refined using no restraints, 2555 data and weights of $w = 1/ [\sigma^2(F^2) + (0.0380\ P)^2 + 1.899\ P]$, where $P = [F_O^2 + 2F_C^2] / 3$. Final agreement factors at convergence are: R_1(unweighted, based on F) = 0.052 for 2013 independent "observed" reflections having 2θ(MoKα)< 51.99° and I>2σ(I); R_1(unweighted, based on F) = 0.069 and wR_2(weighted, based on F^2) = 0.108 for all 2555

independent reflections having 2θ(MoKα)< 51.99°. The largest shift/s.u. was 0.000 in the final refinement cycle. The final difference map had maxima and minima of 0.24 and -0.19 $e^-/Å^3$, respectively. The asymmetric unit for Polymorph I of $C_{32}H_{30}O_8$ contains half of a dimeric $C_{32}H_{30}O_8$ molecule. The molecule utilizes the crystallographic C_2 axis at (½, y, ¼) in the unit cell. All displacement ellipsoids are drawn at the 50% probability level.

Table II.6. Crystal data and structure refinement for $C_{32}H_{30}O_8$.

Empirical formula	$C_{32}H_{30}O_8$	
Formula weight	542.56	
Temperature	100(2) K	
Wavelength	0.71073 Å	
Crystal system	Monoclinic	
Space group	C2/c – C_{2h}^6 (No. 15)	
Unit cell dimensions	**a** = 15.840(3) Å	**α** = 90.000°
	b = 12.149(2) Å	**β** = 100.836(3)°
	c = 13.889(3) Å	**γ** = 90.000°
Volume	2625.1(9) $Å^3$	
Z	4	
Density (calculated)	1.373 Mg/m^3	
Absorption coefficient	0.099 mm^{-1}	
F(000)	1144	
Crystal size	0.28 x 0.14 x 0.12 mm^3	
Theta range for data collection	5.60° to 26.00°	
Index ranges	$-19 \le h \le 19$, $-14 \le k \le 14$, $-17 \le l \le 17$	
Reflections collected	8724	
Independent reflections	2555 [R_{int} = 0.067]	
Completeness to theta = 26.00°	98.6 %	
Absorption correction	None	
Refinement method	Full-matrix least-squares on F^2	
Data / restraints / parameters	2555 / 0 / 241	
Goodness-of-fit on F^2	1.101	
Final R indices [I>2sigma(I)]	R_1 = 0.052, wR_2 = 0.103	
R indices (all data)	R_1 = 0.069, wR_2 = 0.108	
Largest diff. peak and hole	0.24 and -0.19 $e^-/Å^3$	

II.2.12. X-Ray Crystallographic Characterization of 2,2'-biazulene.

Black crystals of $C_{20}H_{14}$ are, at 100(2) K, triclinic, space group $P\bar{1} - C_i^1$ (No. 2)[26] with **a** = 5.918(1) Å, **b** = 7.783(2) Å, **c** = 14.072(3) Å, α = 86.371(4)°, β = 86.451(4)°, γ = 88.463(4)°,V = 645.2(2) $Å^3$ and Z = 2 dimeric molecules {d_{calcd} = 1.309 g/cm^3; μ_a(MoKα) = 0.074 mm^{-1}}. A full hemisphere of diffracted intensities (1850 40-second frames with a ω scan width of 0.30°) was measured for a single-domain specimen using graphite-monochromated MoKα radiation (λ= 0.71073 Å) on a Bruker SMART APEX CCD Single Crystal Diffraction System.[27] X-rays were provided by a fine-focus sealed x-ray tube operated at 50kV and 35mA. Lattice constants were determined with the Bruker SAINT software package using peak centers for 1261 reflections. A total of 5797 integrated reflection intensities having 2θ((MoKα)< 52.00° were produced using the Bruker program SAINT;[28] 2539 of these were unique and gave R_{int} = 0.050 with a coverage which was 99.9% complete. The Bruker software package SHELXTL was used to solve the structure using "direct methods" techniques. All stages of weighted full-matrix least-squares refinement were conducted using F_o^2 data with the SHELXTL Version 6.10 software package.[29]

The final structural model incorporated anisotropic thermal parameters for all nonhydrogen atoms and isotropic thermal parameters for all hydrogen atoms. All hydrogen atoms were located in a difference Fourier and included in the structural model as independent isotropic atoms whose parameters were allowed to vary in least-squares refinement cycles. A total of 237 parameters were refined using no restraints, 2539 data and weights of $w = 1/ [\sigma^2(F^2) + (0.0537\ P)^2]$, where $P = [F_O^2 + 2F_C^2] / 3$. Final agreement factors at convergence are: R_1(unweighted, based on F) = 0.065 for 1898 independent

"observed" reflections having $2\theta(MoK\alpha) < 52.00°$ and $I > 2\sigma(I)$; R_1(unweighted, based on F) = 0.093 and wR_2(weighted, based on F^2) = 0.135 for all 2539 independent reflections having $2\theta(MoK\alpha) < 52.00°$. The largest shift/s.u. was 0.000 in the final refinement cycle. The final difference map had maxima and minima of 0.30 and -0.20 $e^-/Å^3$, respectively. The asymmetric unit for $C_{20}H_{14}$ contains two crystallographically-independent $C_{10}H_7$ half molecules. Each half molecule is situated near a crystallographic inversion center in the unit cell. All displacement ellipsoids are drawn at the 50% probability level.

Table II.7. Crystal data and structure refinement for $C_{20}H_{14}$.

Empirical formula	$C_{20}H_{14}$	
Formula weight	254.31	
Temperature	100(2) K	
Wavelength	0.71073 Å	
Crystal system	Triclinic	
Space group	$P\bar{1} - C_i^1$ (No. 2)	
Unit cell dimensions	**a** = 5.918(1) Å	α = 86.371(4)°
	b = 7.783(2) Å	β = 86.451(4)°
	c = 14.072(3) Å	γ = 88.463(4)°
Volume	645.5(2) $Å^3$	
Z	2	
Density (calculated)	1.309 Mg/m^3	
Absorption coefficient	0.074 mm^{-1}	
F(000)	268	
Crystal size	0.24 x 0.08 x 0.03 mm^3	
Theta range for data collection	2.62° to 26.00°	
Index ranges	$-7 \le h \le 7$, $-9 \le k \le 9$, $-17 \le l \le 17$	
Reflections collected	5797	
Independent reflections	2539 [R_{int} = 0.050]	
Completeness to theta = 26.00°	99.9 %	
Absorption correction	Multi-scan	
Max. and min. transmission	1.000 and 0.937	
Refinement method	Full-matrix least-squares on F^2	
Data / restraints / parameters	2539 / 0 / 237	
Goodness-of-fit on F^2	1.107	
Final R indices [I>2sigma(I)]	R_1 = 0.065, wR_2 = 0.125	
R indices (all data)	R1 = 0.093, wR_2 = 0.135	
Largest diff. peak and hole	0.30 and -0.20 $e^-/Å^3$	

II.2.13. Cyclic Voltammetry and Differential Pulse Voltammetry Studies of 2.1c, $[W(CO)_5]_2$·2.1c and 2.2c.

Cyclic voltammetry (CV) experiments were conducted on $2x10^{-3}$M solutions of **2.1c**, **$[W(CO)_5]_2$·2.1c** and **2.2c** in CH_2Cl_2 at room temperature using an Epsilon (Bioanalytical Systems Inc., West Lafayette, IN) electrochemical workstation. The electrochemical cell was placed in an argon filled Vacuum Atmospheres Corp. dry box. Tetrabutylammonium hexafluorophosphate purified by recrystallization (0.1M solution in CH_2Cl_2) was used as a supporting electrolyte. Cyclic voltammograms were recorded at 22°C ± 2°C using a three component system consisting of a platinum (Pt) working electrode, Pt wire auxiliary electrode, and a glass encased non-aqueous silver/silver chloride (Ag/Ag^+) electrode. The reference Ag/Ag^+ electrode was monitored using a ferrocene/ferrocenium (FcH/Fc^+H) couple. Data were referenced to an external FcH/Fc^+H couple.

II.3. Results and Discussion

Sugihara *et al.* published a synthesis of 2,2'-diamino-1,1',3,3'-tetraethoxycarbonyl-6,6'-biazulene **2.1a** in two steps from 2-amino-6-bromo-1,3-diethyoxycarbonylazulene in a 19% combined yield.[9] The reaction required the use of palladium(II) diphenylphosphinoferrocene (Pd(dppf)) and bis(triphenylphosphine)palladium(II). Each reaction step required column chromatography to purify the products. Initial attempts to reproduce this synthesis as published revealed the presence of insoluble red material at the base of the chromatography column after the first reaction step. This material was

removed from the column via spatula and NMR revealed that it was in fact compound **2.1a**, the product of the next step!

Based on this discovery, a modified synthetic procedure was developed that allowed for isolation of **2.1a** in one step using only the Pd(dppf) catalyst of the same loading (10 mol% vs. 2-amino-6-bromo-1,3-diethoxycarbonylazulene) as used by Sugihara *et al.*[9] The modified workup required no column chromatography. Instead the poor solubility of **2.1a** allowed for collection of the crude product by filtration and washing the filtercake with water and chloroform. All characterization of **2.1a** produced via this one-step synthesis was identical to that reported previously but the yield increased dramatically to an essentially quantitative conversion.[9]

Formylation of **2.1a** to form **2.1b** proceeded similar to that developed for monoazulenic compounds in the Barybin group using acetic formic anhydride with an excess of formic acid. Limited solubility of **2.1b** enabled purification of this substance by simple filtration and repeated washings of the crude product to provide a roughly 80% yield.

Dehydration of **2.1b** proved to be more challenging than those established for various formamidoazulenes containing only one azulenic nucleus. Attempts to dehydrate **2.1b** with phosphorus oxychloride ($POCl_3$) produced less than 10% yield of the corresponding isocyanide and was poorly reproducible. The use of triphosgene as a dehydrating agent allowed for isolation of **2.1c** in 54% yield after purification by column chromatography. Similar to many other isocyanoazulenes synthesized in the Barybin group, **2.1c** has good stability toward air and moisture. The dehydration reaction was

easily monitored by both TLC and FTIR, as diisocyanide **2.1c** exhibits a characteristic ν_{CN} band at 2127 cm^{-1}.

Complexation of **2.1c** with one-half an equivalent of $[W(CO)_5THF]$, generated photolytically *in situ*, provided facile access to both mononuclear **$[W(CO)_5]$·2.1c** and dinuclear **$[W(CO)_5]_2$·2.1c** adducts in reasonable yields. The reaction was monitored for progress by FTIR in both the ν_{CO} and ν_{CN} regions.

A 2001 report described various attempts at performing vicarious nucleophilic substitution to install an amine group at the 6-position of the azulenic framework.[30] 4-Amino-1,2,4-triazole (triazole), methoxyamine hydrochloride (methoxyamine) and trimethyl hydrazinium iodide (TMHI) were all used as potential nucleophiles activated by potassium *tert*butoxide (^{t}BuOK) in either dimethylsulfoxide (DMSO) or dimethylformamide (DMF).[30] The best yield of 6-aminoazulene was accomplished using 3 equivalents of the triazole with 6 equivalents of ^{t}BuOK, while installation of an amine at the 6-position of the 1,3-diethoxycarbonylazulene derivative was most efficient when 1 equivalent of TMHI was employed with 3 equivalents of ^{t}BuOK.[30]

The initial target in derivatizing the 2,2'-biazulenic framework with the isocyanide substitutents was linear 6,6'-diisocyano-2,2'-biazulene, both with ethyl ester groups at the 1,1',3, and 3'-positions and without such ester substitution. Attempts to aminate 1,1',3,3'-tetraethoxycarbonyl-2,2'-biazulene ($2BiAzE_4$) with 2 equivalents of TMHI and 6 equivalents of ^{t}BuOK were unsuccessful and caused loss of all starting material. Using only 1 equivalent of TMHI and 3 equivalents of ^{t}BuOK proved also unsuccessful and consumed the starting material. Efforts to employ both triazole and methoxyamine were

also disappointing and produced no desired product at the sacrifice of all starting material.

Due to the lack of success in aminating $2BiAzE_4$, attention was turned to 2,2'-biazulene (2BiAz). TMHI, triazole and methoxyamine were all considered in attempts to form 6,6'-diamino-2,2'-biazulene. However, the only product that formed was **2.2a**, regardless of number of equivalents of aminating agent or ^{t}BuOK used in the reaction scheme. Concentration and reaction time were also varied in an attempt to access the diaminobiazulene. The procedure described herein makes use of 3 equivalents of triazole with 6 equivalents of ^{t}BuOK in DMSO in an inert atmosphere to afford **2.2a** in 82% yield after filtration and washing. Limited solubility of the substituted biazulene made purification by filtration possible and convenient. Thus the remarkably regioselective monoamination of 2,2'-biazulene was accomplished in a high yield instead of the initially sought symmetric diaminated derivative. It is likely that installation of one amino group at carbon atom #6 of the parent 2,2'-biazulene scaffold deactivates nucleophilic substitution at the other end of the molecule (carbon atom #6').

Ostrowski *et al.* reported 6-aminoazulene was unstable to acidic conditions.[30] Prior to the 2001 work, it was believed that aminoazulenes in general were unstable and most frequently aminoazulenes were converted to acetamides for indirect characterization. A standard method for acetylation of an amine makes use of acetic acid, indicating that our previously used formylation techniques may also be useful for formylating **2.2a**. In fact, **2.2b** was generated using acetic formic anhydride (*in situ* formation) with a $\geq$ 100 fold excess of formic acid. Compound **2.2b** was isolated by filtration and purified by washing with water to provide a quantitative yield upon thorough drying.

Standard methods of dehydration of a formamide group to generate an isocyanide functionality rely on relatively harsh reagents such as phosgene or $POCl_3$ in the presence of a base, typically an amine. Initial attempts at dehydration of **2.2b** were made with 1 equivalent of $POCl_3$ in diisopropylamine. Reactions were run at reduced (-78°C, 0°C) and elevated (40°C, 65°C, 80°C) temperatures. No reaction was observed at reduced temperatures until the flask was warmed to approximately room temperature. At elevated temperatures, the reaction appeared to progress, but upon isolation and purification each reaction attempt provided less than 5% yield of **2.2c**. Reactions were attempted in air and inert atmospheres in a variety of solvents at varying concentrations, all to no avail. In a typical reaction, approximately 50% of the starting formamide **2.2b** was recovered.

Dehydration attempts using triphosgene with triethylamine produced similar results regardless of varying temperature or atmosphere, providing less than 5% yield of the desired isocyanide product and half of the unreacted starting material. The dehydration yield was improved to 20% by incorporating tetraethylammonium bromide in the reaction mixture, also providing almost quantitative amounts of the remaining unreacted starting material. Purification of the product was possible by both washing with pentane or by column chromatography on silica in CH_2Cl_2. The key problem with the chromatographic purification is the loss of valuable unreacted starting material on the column. The dehydration yield was increased further to 44% by freezing the solution of **2.2b** and triethylamine in THF followed by addition of a THF solution of triphosgene. During the gradual warming to room temperature, the reaction was monitored for completion by TLC and IR.

Scheme II.7. Formation of homoleptic neutral and cationic chromium complexes of 2.2c.

Scheme II.7 depicts the reaction sequence for formation of neutral and cationic homoleptic complexes of compound **2.2c** with chromium. Compound **2.2c** was treated with bisnaphthalenechromium(0) to generate hexakis(6-isocyano-2,2'-biazulene)chromium(0) in mediocre yield. This reaction was performed only once and is yet to be optimized. The complex was then treated with silver hexafluoroantimonate to generate hexakis(6-isocyano-2,2'-biazulene)chromium(I) hexafluoroantimonate, a low spin d^5 paramagnetic molecule. FTIR was used to follow both reactions, traces of which are shown in Figure II.14, by examining the energy of the isocyanide stretching vibration for both neutral and cationic octahedral complexes compared to the free ligand.

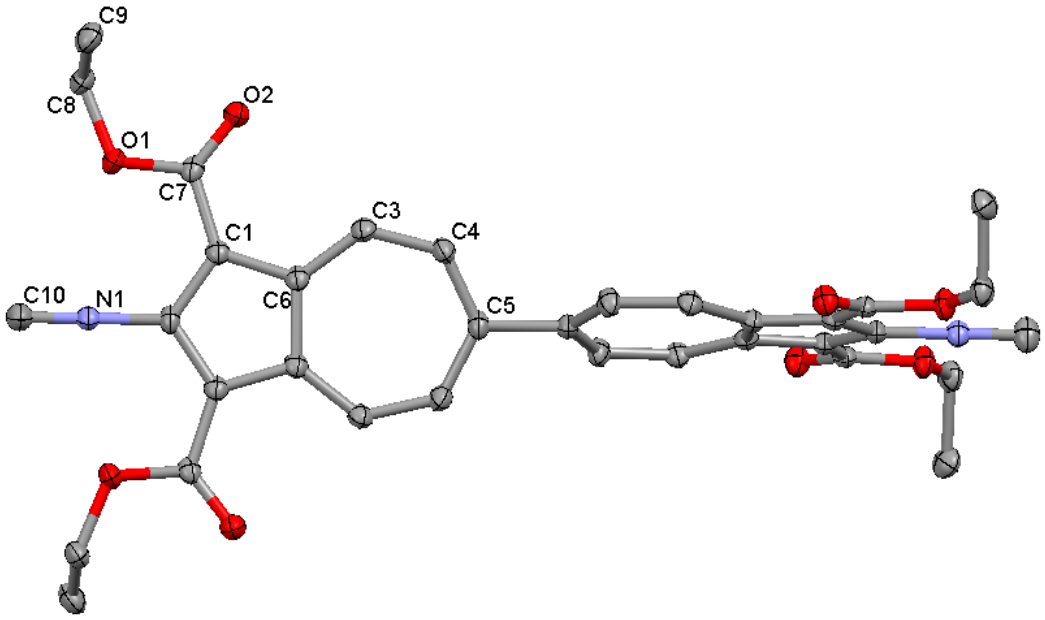

Figure II.8. X-ray structure of 2.1c (50% thermal ellipsoids). Hydrogen atoms are omitted for clarity.

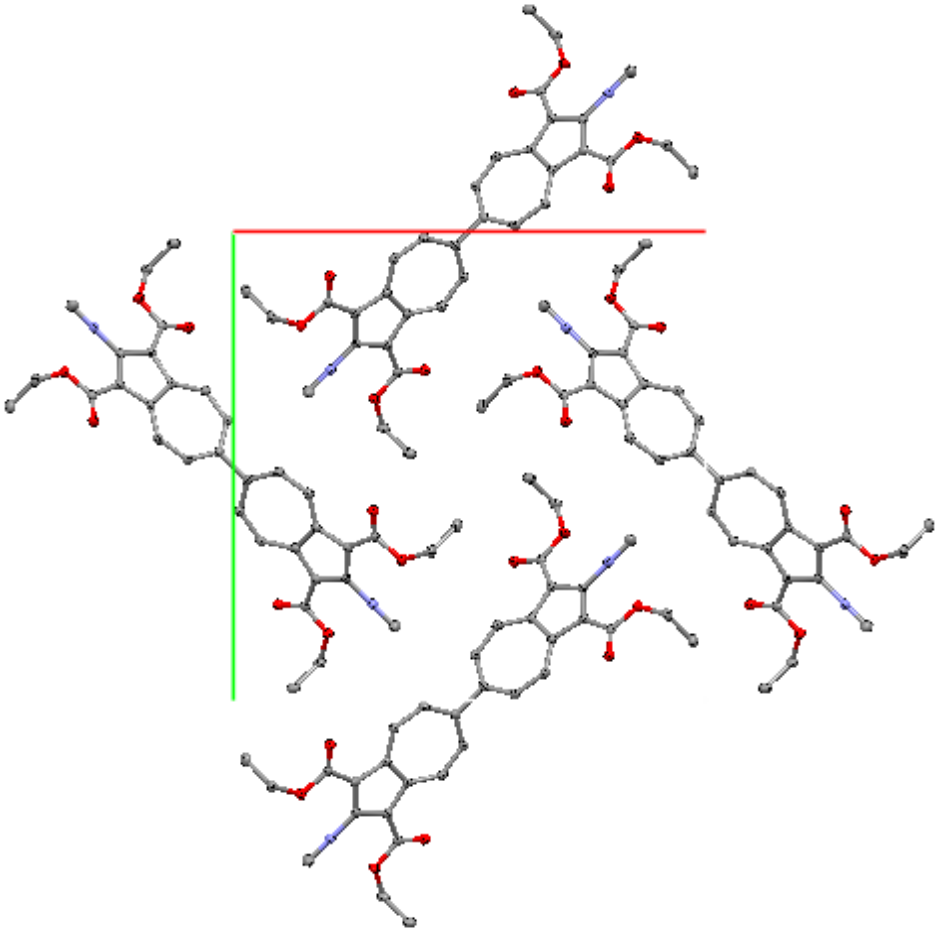

Figure II.9. Packing diagram of 2.1c viewed along the c axis. Hydrogen atoms are omitted for clarity.

Compound **2.1c** was crystallized from CH_2Cl_2 and revealed a highly symmetric structure shown in Figure II.8. This structure is the first example of a diisocyanobiazulene, and in fact, appears to be the first crystallographically characterized biazulene. The azulene rings deviate from coplanarity by 67°, 12° less planar than predicted by theoretical calculations in the gas phase. This slight difference between the solid state structure and calculated structures may be simply due to crystal packing constraints. Only one quarter of the molecule of **2.1c** is crystallographically independent.

Table II.8. C···O distances for selected azulenic complexes featuring weak hydrogen bonding interactions between the ester arms and the carbon atom at position 4 of the azulene ring.

Compound	O···C (Å)
2.1c	2.925(2)
1,1',3,3'-tetraethoxycarbonyl-2,2'-biazulene	2.929(2) 2.947(3)
Bis(pentacarbonylchromium) 2,6-diisocyano-1,3-diethoxycarbonylazulene[3]	2.914(4) 2.945(4)
Pentacarbonylchromium 2,6-diisocyano-1,3-diethoxycarbonylazulene[3]	2.909(4) 2.930(4)
Bis(pentacarbonyltungsten) 2,6-diisocyano-1,3-diethoxycarbonylazulene[3]	2.913(8) 2.951(7)

Each ethyl ester group of **2.1c** lies in the same plane as the azulenic moiety to which it is attached. This orientation of the 1,3-ester substituents with respect to the azulenic ring may be encouraged by a weak hydrogen bonding interaction between the carboxylate oxygen atom and the hydrogen at position 4 of the azulene ring, with a distance between C3 and O2 in Figure II.8 of 2.925Å. Such an orientation of the 1,3-ester groups in the solid state was documented for many other azulenic derivatives synthesized by the Barybin group, as summarized by the data in Table II.8. The only exceptions involve molecules that feature H-bonding of the ethoxycarbonyl unit with a substituent at position #2, such as formamide or thiol.[3,31] Overall the molecule of **2.1c** is approximately 1.7nm long, the isocyanide units feature a typical C≡N bond length of 1.16Å.

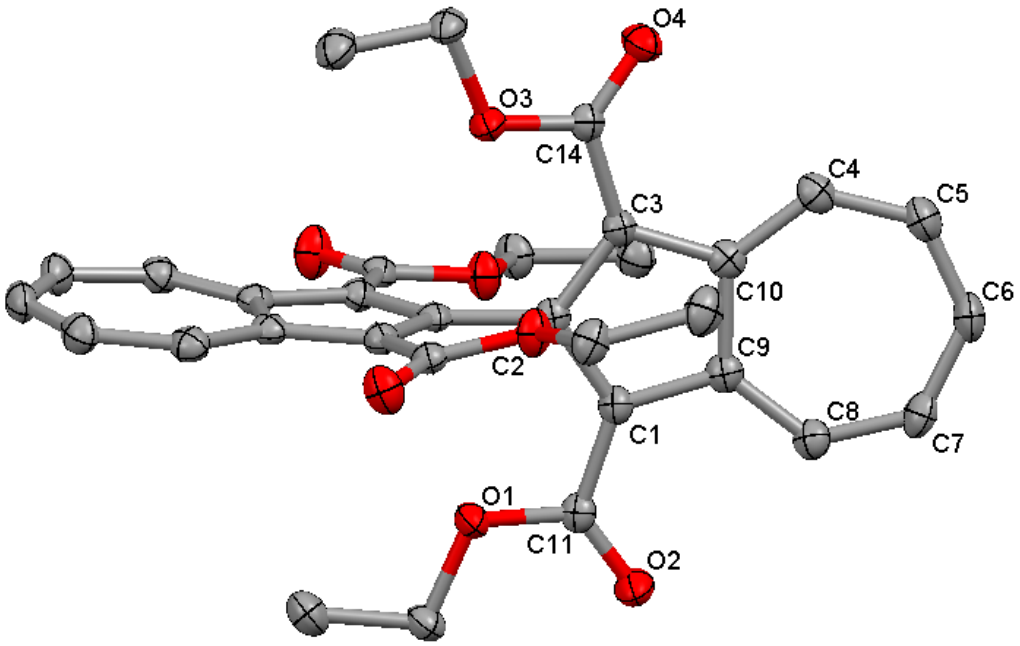

Figure II.10. X-ray structure of 1,1',3,3'-tetraethoxycarbonyl-2,2'-biazulene (50% thermal ellipsoids). Hydrogen atoms are omitted for clarity.

The X-ray crystal structure of 1,1',3,3'-tetraethoxycarbnyl-2,2'-biazulene, shown in Figure II.10, reveals the two azulenic rings in essentially perpendicular orientation with respect to each other. The ester groups are once again oriented in the same plane as the corresponding azulenic rings with the distance between the carboxylate units oxygen atoms and the hydrogen atoms at position 4/8 of 2.92Å. One half of the molecule is crystallographically independent. The overall length of the molecule is 1.19 nm.

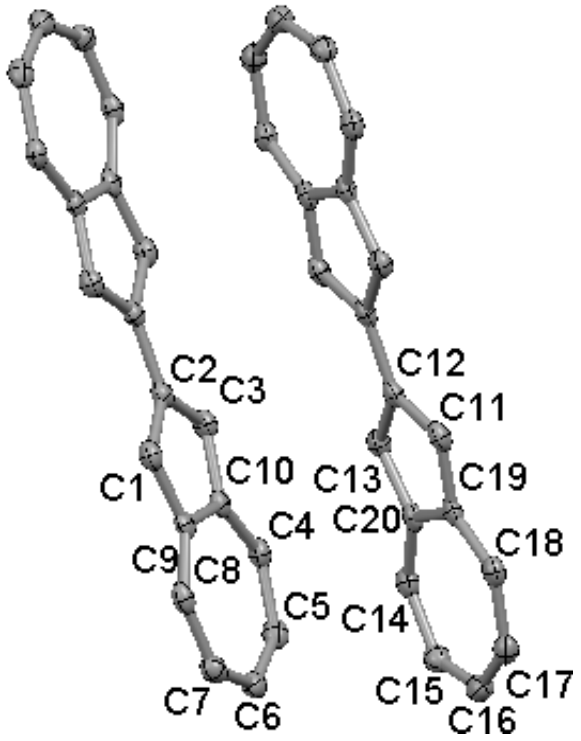

Figure II.11. X-ray crystal structure of 2,2'-biazulene (50% thermal ellipsoids). Hydrogen atoms are omitted for clarity. Both crystallographically independent biazulene molecules are shown.

The X-ray structure of 2,2'-biazulene was also acquired and is shown in Figure II.11. The compound crystallized with 2 independent molecules in the unit cell. Both independent biazulenes feature an interplanar angle of approximately 1° and a molecular length of 1.18 nm. The observed essentially planar structure of 2,2'-biazulene is consistent with the one predicted theoretically. It is also in accord with the electronic spectra and electrochemical properties of the compound recorded in solution. No notable intermolecular interactions, such as π-stacking, are observed in the structure.

Table II.9. IR data for select isocyanoazulenes and their complexes. [a] in CH_2Cl_2; [b] in Nujol; [c] in $CHCl_3$; [d] in THF.[2,3,4,32]

Compound	ν_{CN} (cm^{-1})	ν_{CO} (cm^{-1})
^{2}CNAz [a 2]	2118	
Cr(^{2}CNAz)$_6$ [b 2]	1954	
Cr(^{2}CNAz)$_6^+$ [a 2]	2062, 2047	
^{2}CNAzE$_2$ [a 4]	2127	
2.1c [a]	2127	
[W(CO)$_5$]·2.1c [a]	2136	2044, 1952
[W(CO)$_5$]$_2$·2.1c [a]	2139	2041, 1954
^{2}CNAzNC^6 [a 3]	2125, 2116	
W(CO)$_5$^{2}CNAzNC^6 [a 3]	2135, 2114	2043, 1955

Compound	ν_{CN} (cm^{-1})	ν_{CO} (cm^{-1})
$^{2}CNAzNC^{6}W(CO)_5$ [a 3]	2124	2031, 1961
$W(CO)_5{}^{2}CNAzNC^{6}W(CO)_5$ [a 3]	2136, 2123	2048, 2028, 1968, 1962
$^{6}CNAz$ [a 32]	2111	
$Cr(^{6}CNAz)_6$ [b 32]	1950	
$Cr(^{6}CNAz)_6{}^{+}$ [a 32]	2053	
$^{6}CNAzE_2$ [c 4]	2115	
2.2c [a]	2114	
Cr(2.2c)$_6$ [d]	1958	
Cr(2.2c)$_6{}^{+}$ [a]	2053	

The stretching frequency of the isocyanide functional group is extremely sensitive to the nature of bonding in which it is engaged. The ν_{CN} data for several relevant

previously studied isocyanoazulenes as well as for those reported in this Dissertation are compiled in Table II.9.[2,3,4,32] Compound **2.1c** exhibits the isocyanide stretching frequency identical to that of 2-isocyano-1,3-diethoxycarbonylazulene (^{2}CNAzE$_2$), which essentially constitutes a half of the molecule **2.1c**.

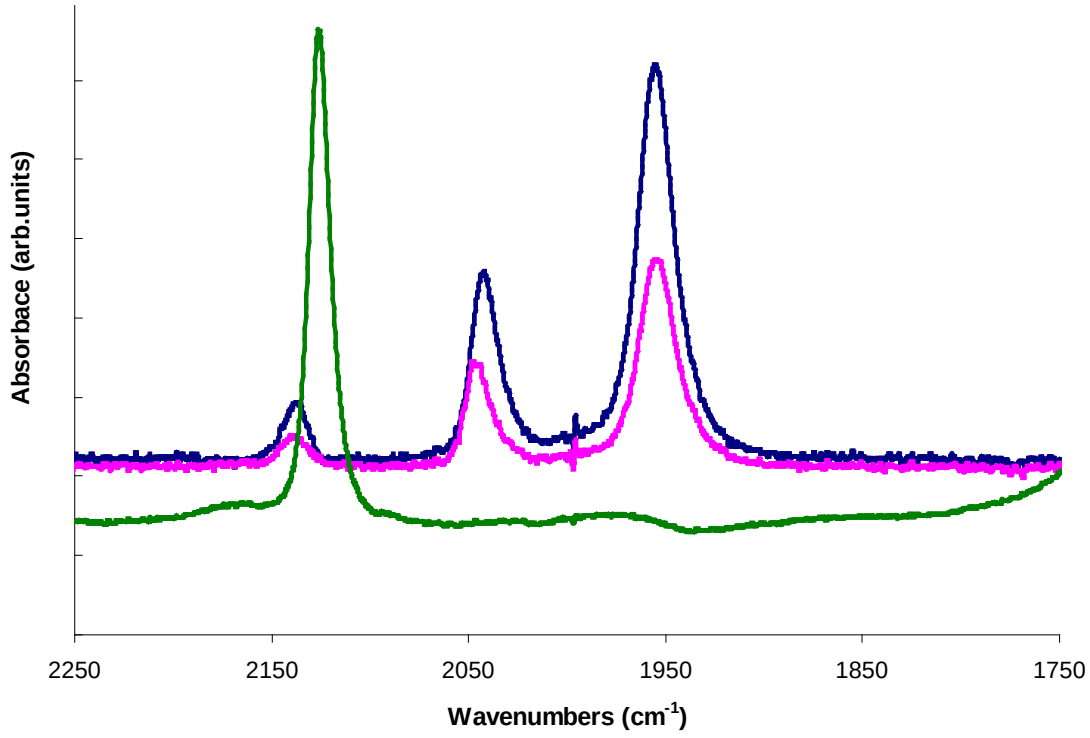

Figure II.12. FTIR traces for 2.1c (green), [W(CO)$_5$]·2.1c (pink), and [W(CO)$_5$]$_2$·2.1c (blue) in CH_2Cl_2.

Tungsten pentacarbonyl complexes of **2.1c** can be compared to the related W(CO)$_5$ complexes of ^{2}CNAzNC^6.[3] Figure II.12 illustrates the spectra of the two tungsten complexes as well as free **2.1c** for comparison. The monometallic adduct **W(CO)$_5$·2.1c** exhibits a broad ν_{CN} band with the maximum at 2136 cm^{-1} that likely contains the band associated with both bound and free isocyanide units. The slight increase in bond energy is consistent with that observed for ^{2}CNAzNC^6, where the tungsten bound isocyanide exhibits a stretching frequency of 2135 cm^{-1} for the isocyanide at the 2-position.[3] This

change in energy for the bond stretching was attributed to an increase in the σ-character of the isocyanide bond with the metal center, likely due to the electron withdrawing nature of the $W(CO)_5$ unit.[3]

Figure II.13. Resonance structures of 2.2c.

Isocyanides attached at the 6-position of the azulene framework exhibit stretching frequencies at approximately 10 cm^{-1} lower in energy than the isocyanides at the 2-position of azulene. This can be seen in comparing ^{2}CNAz vs. ^{6}CNAz, ^{2}CNAzE_2 vs. ^{6}CNAzE_2, each isocyanide of ^{2}CNAzNC^6 and **2.1c** vs. **2.2c**.[2,3,4] The change in bond energy in these four comparisons must be attributed to the slight dipole of the azulene ring system. Proximity of the isocyanide functionality to the partially positive 7-membered ring fragment results in a slight weakening of the C≡N, likely due to a resonance structure involving a double bond between the isocyanide and the 7-membered ring, as shown in Figure II.13.

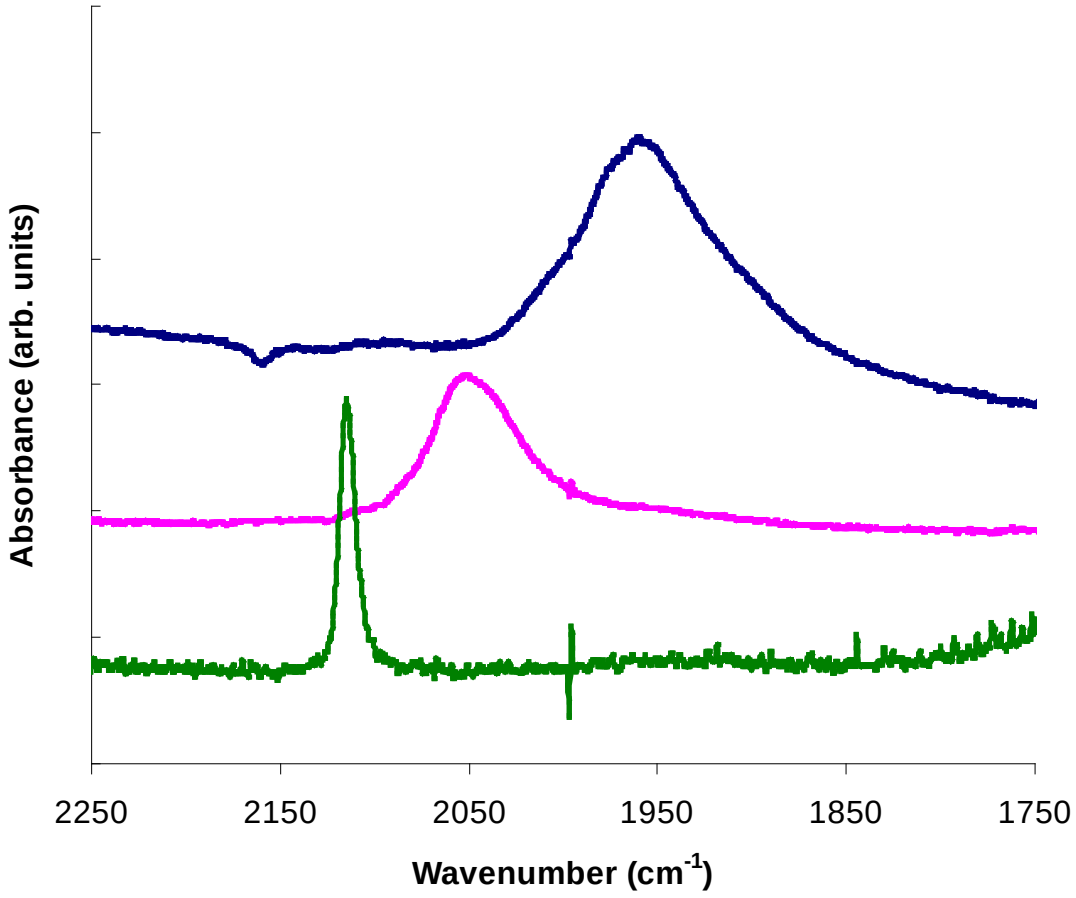

Figure II.14. FTIR spectra of 2.2c (green), $Cr(2.2c)_6$ (blue), and $[Cr(2.2c)_6]^+$ (pink) in CH_2Cl_2.

Complexation of **2.2c** with electron rich Cr(0) decreased the energy of the isocyanide stretching frequency by over 160 cm^{-1}, as illustrated in Figure II.14. This decrease can be attributed to increased π-backbonding interactions of the isocyanide with Cr(0), which causes the isocyanide to exhibit more double bond character, weakening the isocyanide bond. This same shift in energy is observed in complexation of ^{6}CNAz and ^{2}CNAz with Cr(0).[2] Likewise, oxidation of **$Cr(2.2c)_6$** to **$[Cr(2.2c)_6]^+$** returned some of the triple bond character to the isocyanide, as evidenced by the 50 cm^{-1} increase in energy of the isocyanide stretch.[2]

Table II.10. ^{1}H NMR data of azulene versus substituted and unsubstituted biazulenes. [a] in $CDCl_3$; [b] in CD_2Cl_2; [c] in d^6-acetone; [d] in d^6-DMSO.[5,10]

Ring Position	1/1'/3/3'	2/2'	4/4'/8/8'	5/5'/7/7'	6/6'	CH_2	CH_3
2,2'-biazulene[a 10]	7.86		8.28	7.13	7.50		
6,6'-biazulene[a 5]	7.45	7.96	8.43	7.40			
2.1a[a]			9.17	7.78		4.47	1.48
2.1b[a]			9.50	7.97		4.53	1.50
2.1c[b]			9.93	8.03		4.55	1.54
$W(CO)_5$2.1c[b]			9.88/9.90	8.05/8.06		4.50/4.56	1.49/1.50
$[W(CO)_5]_2$·2.1c[b]			9.92	8.08		4.57	1.51
2.2a[c]	7.50/7.74		7.92/8.21	6.54/7.12	7.41		
2.2b[d]	7.82/7.84		8.25/8.33	7.20/7.41	7.55		
2.2c[b]	7.80/7.89		8.16/8.26	7.12	7.48		

^{1}H NMR proved very useful in detecting changes in substitution of azulene based compounds. Table II.10 shows downfield shifts for all protons on changing from **2.1a** to **2.1b** and from **2.1b** to **2.1c**.[5,10] Upon converting from diamine **2.1a** to bisformamide **2.1b**, $H^{4,8,4',8'}$ exhibits a 30 ppm downfield shift while $H^{5,7,5',7'}$ shows a 20 ppm shift. Even the ethoxycarbonyl groups demonstrate a slight deshielding effect upon modification within the molecule upon conversion from an electron donating amine to an electron withdrawing formamide. The expansion of the deshielding effect into the ethyl ester arms indicates the extended conjugation of the π-system of the biazulene framework.

The limited solubility of **2.2a**, **2.2b** and **2.2c** made collection of ^{1}H NMR data for these species more challenging. Due to the variety of solvents used, comparison of chemical shifts must account for possible deviations due solely to solvent conditions rather than molecular effects. However, substitution with an amine at the 6-position of 2,2'-biazulene resulted in an upfield shift for all protons in **2.2a**, consistent with the introduction of an electron donating substituent. Formylation of the amine group resulted

in a downfield shift of all azulenic protons, due to the electron withdrawing nature of the formamides. Dehydration of the formamide to generate isocyanide **2.2c** resulted in an upfield shift of protons compared to the formamide, with the exception of the singlet associated with $H^{1,3,1',3'}$.

Table II.11. UV-vis data for various 2- and 6-substituted isocyanoazulenes in CH_2Cl_2. [a] in pentane.[2,3]

Compound	λ_{max} (nm)	Energy of transition (cm^{-1})
Azulene	575	17,391
^{2}CNAz	560	17,857
^{2}CNAzE_2	522	19,157
6,6'-biazulene	592	16,891
2.1c	531	18,832
^{6}CNAz [a]	585	17,094
^{6}CNAzE_2	543	18,416
2,2'-biazulene	592	16,891
2.2c	559	17,889
^{2}CNAzNC^{6}	535	18,691
W(CO)$_5$^{2}CNAzNC^{6}	466	21,459
^{2}CNAzNC^{6}W(CO)$_5$	466	21,459
W(CO)$_5$^{2}CNAzNC^{6}W(CO)$_5$	515	19,417
W(CO)$_5$2.1c	485	20,618
[W(CO)$_5$]$_2$·2.1c	496	20,161

Table II.11 contains electronic spectral data in the visible region for various isocyanoazulenes as well as unsubstituted azulene and biazulenes for comparison purposes.[2,3] Compound **2.1c** can best be compared to ^{2}CNAzE$_2$, as this molecule makes up half of the framework of **2.1c**. Upon conjoining two ^{2}CNAzE$_2$ units, the energy of the lowest energy electronic transition drops by about 300 cm^{-1}. Compound **2.2c** can best be compared to ^{6}CNAz, which may be viewed as one half of the framework of **2.2c**. Upon addition of the second azulene unit to the ^{6}CNAz framework at the 2-position, the lowest energy electronic transition exhibits a 800 cm^{-1} shift to higher energy.[2] The data indicates that there are very different processes occurring upon coupling azulenes at the 6,6'-position and the 2,2'-position. Figure II.15 illustrates the HOMO and LUMO of 6,6'-biazulene and 2,2'-biazulene obtained using an Extended Huckel molecular orbital calculation. It is quite clear from this drawing that the HOMO/LUMO gap of 6,6'-biazulene may be smaller than that for 2,2'-biazulene based simply the complimentary nature of the two frontier molecular orbitals, similar to the argument used by Liu when discussing azulene versus naphthalene.[1] The coincident shape and location of orbital contributions on the same atoms in the HOMO and LUMO of 2,2'-biazulene are likely responsible for the energy increase upon coupling of azulene. Likewise, the lack of such similarity in the frontier MO's of 6,6'-biazulene account for the energy gain observed for **2.1c** versus ^{2}CNAzE$_2$.

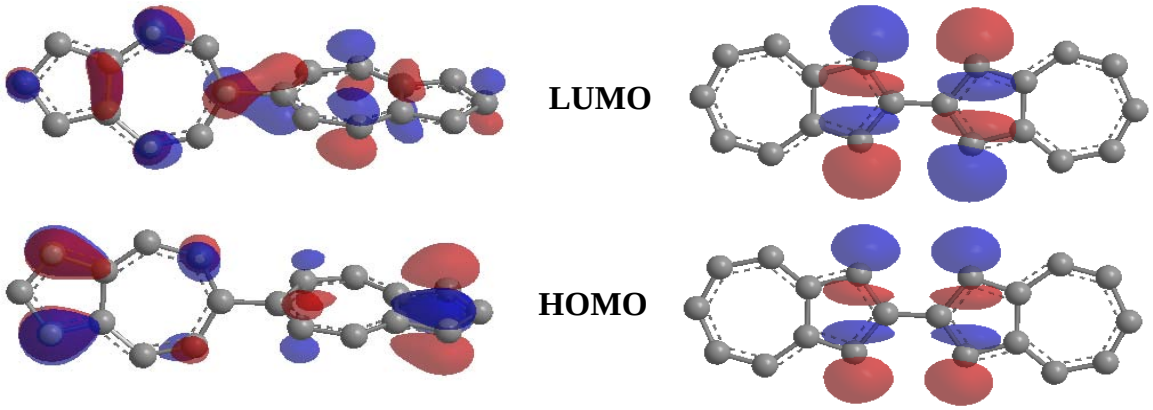

Figure II.15. Extended Huckel Frontier Molecular Orbital approximations for 6,6'-biazulene and 2,2'-biazulene.

Another apparent trend in the UV-vis data is that addition of an isocyanide to the azulene framework results in an energy increase in the lowest energy electronic transition. This feature is observed in the comparison of azulene to both ^{2}CNAz and ^{6}CNAz as well as the comparison of **2.1c** to 6,6'-biazulene and **2.2c** to 2,2'-biazulene.[2] The most reasonable explanation for this is that both the HOMO and LUMO contain features located on the isocyanide, regardless of the position of isocyanide substitution, resulting in a larger HOMO-LUMO energy gap.

Complexation of **2.1c** with $W(CO)_5$ units resulted in the appearance of a metal to ligand charge transfer electronic transition (MLCT). Previous reports of complexation of $W(CO)_5$ with isocyanide azulenes involved 2,6-diisocyano-1,3-diethoxycarbonylazulene (^{2}CNAzNC^{6}).[3] As mentioned previously, a large energy gain (almost 2000 cm^{-1}) was observed upon complexation of $W(CO)_5$ with the second isocyanide junction of ^{2}CNAzNC^{6}.[3] A similar study with **2.1c** resulted in only a small energy gain, merely 500 cm^{-1}) upon binucleation to involve the second isocyanide junction. This is again consistent with the observed deviation from coplanarity of the two azulene rings, shown in Figure II.8.

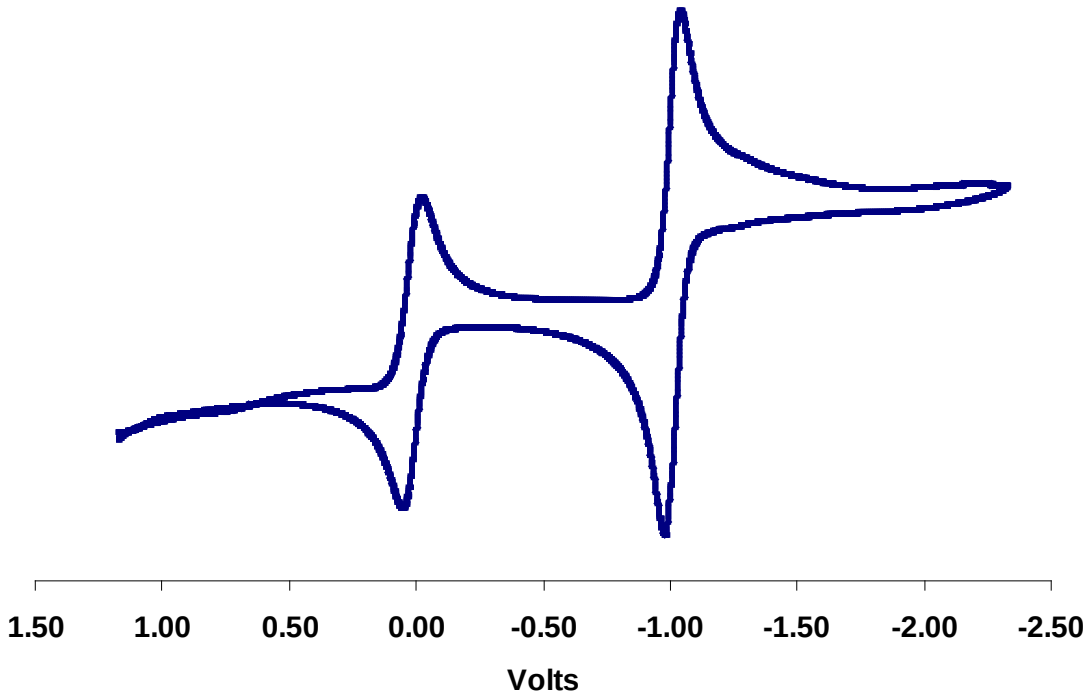

Figure II.16. Cyclic voltammogram of 2.1c with internal ferrocene/ferrocenium reference in CH_2Cl_2.

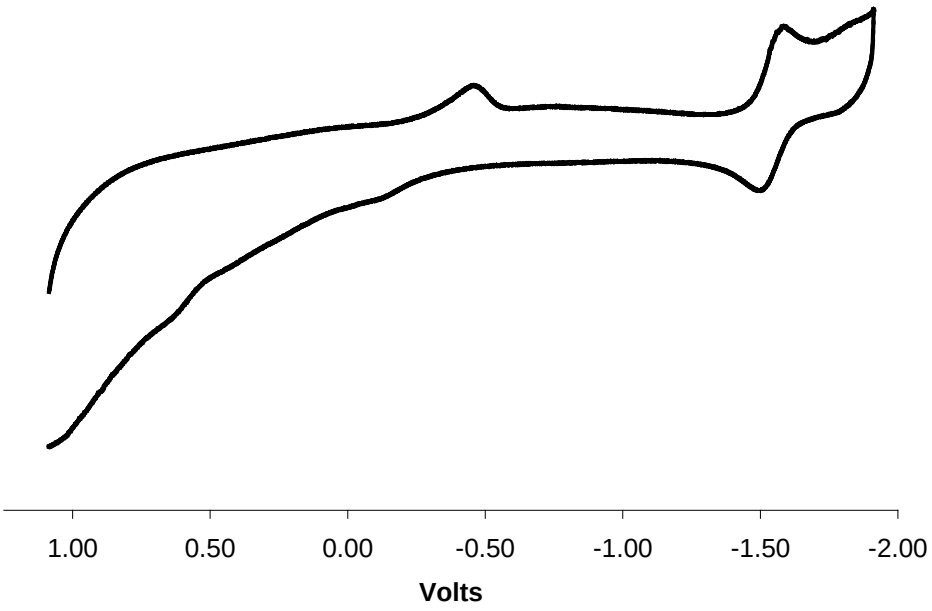

Figure II.17. Cyclic voltammogram of 2.2c in CH_2Cl_2 versus FcH/Fc^+H at 100mV/s scan rate.

Compound **2.1c** and its dinuclear $W(CO)_5$ complex exhibit a reversible 2-electron reduction at a single potential of -1.02 V and -1.01 V, respectively, versus ferrocene/ferrocenium in CH_2Cl_2 at 100mV/s scan rate, as shown for **2.1c** in Figure II.16. This two-electron reduction occurs at a significantly lower potential than that of azulene itself. A two-electron reduction of compound **2.1c** allows for the formation of a diamagnetic dianion by pairing the two electrons into the LUMO of **2.1c**. The formation of a closed shell dianion is consistent with the observation of an appreciably reduced reduction potential for compound **2.1c**.

The electrochemistry of **2.2c** is more complex than that of **2.1c**. Two reduction processes were observed for **2.2c** in CH_2Cl_2 versus ferrocene/ferrocenium at 100mV/s. The addition of an isocyanide to the 6-position of 2,2'-biazulene appears to have resulted in a more positive reduction potential by about 20mV, which is similar to that observed

for 6-isocyanoazulene.[2] The second reduction is irreversible under the conditions employed. Previous electrochemical studies have reported a second reduction potential for 2,2'-biazulene, which occurred at 30-50 mV more positive potential.[17] Based on the previously reported data (corrected for solvent and referencing methods)[21], the two redox potentials for 2,2'-biazulene would occur at -1.63 V (reversible) and -1.28 V (irreversible).[17] These results indicate that isocyanide group facilitates addition of electrons into the 2,2'-biazulenic framework. Unlike 2,2'-biazulene, **2.2c** did not exhibit a detectable oxidation wave, similar to 6-isocyanoazulene.[2] Table II.12 summarizes the electrochemical data.

Table II.12. Oxidation and Reduction potentials of 2.1c, 2.2c and $[W(CO)_5]_2$·2.1c as well as literature data for select comparable compounds in CH_2Cl_2 versus FcH/Fc^+H. [a] irreversible; [b] corrected for solvent (+0.01 V) and reference (+0.61 V).[17,21,33]

Compound	$E_{1/2,red1}$	$E_{1/2,red2}$	$E_{1/2,ox}$
Azulene	-2.16		0.54
2,2'-biazulene [b]	-1.63	-1.28[a]	0.49[a]
^{2}CNAz	-1.86[a]		0.92[a]
^{6}CNAz	-1.75		
2.1c	-1.02		
$[W(CO)_5]_2$·2.1c	-1.01		
2.2c	-1.54	-0.38[a]	

II.4. Conclusions and Future Work

The synthesis and characterization of 2,2'-diisocyano-1,1',3,3'-tetraethoxycarbonyl-6,6'-biazulene, the firsts diisocyanobiazulene, was accomplished in a

good yield. This novel linear nonbenzenoid aryl isocyanide is quite stable toward ambient environment and was fully characterized, including by single crystal X-ray crystallography. The synthesis of the corresponding intermediate diamine was improved dramatically compared to the previously published procedure and now involves a single-step Suzuki coupling transformation. Complexation of **2.1c** with tungsten pentacarbonyl units provided both dinuclear and mononuclear adducts, which were both stable to ambient atmosphere and column chromatography on silica.

6-Isocyano-2,2'-biazulene was synthesized and characterized in a reasonable yield. The established methodology allowed for selective installation of just one isocyanide on the 2,2'-biazulene framework. X-ray crystallographic characterization of the starting 2,2'-biazulene and its tetraethoxycarbonyl precursor was also accomplished. Preliminary results of complexation of **2.2c** with Cr(0) indicate potential utility of this biazulenic framework in coordination chemistry with electron-rich metal centers.

Future plans for **2.1c** should include studies into chemical reduction of this compound to isolate the corresponding dianion, which should be diamagnetic and feature two azulenic rings that are significantly more coplanar compared to the parent neutral 6,6'-biazulene system. The proposed dianion presents many potential opportunities for complexation through not only its isocyanide termini, but also through involvement of its cyclopentadienide-like rings to form η^5-motifs. Further exploration into the coordination chemistry of **2.1c** is also planned, including potential use as a porous metal-organic framework (MOF).

Coordination chemistry of compound **2.2c** needs to be extensively investigated as well as the electronic structure of **2.2c** and its metal complexes. Installation of the second isocyanide group or another metal ligating junction group also needs to be developed.

II.5. References

1. Liu, Robert S.H. *Journal of Chemical Education*. **2002**, *79*, 183.

2. Robinson, Randall E.; Holovics, Thomas C.; Deplazes, Stephan F.; Powell, Douglas R.; Lushington, Gerald H.; Thompson, Ward H.; Barybin, Mikhail V. *Organometallics*. **2005**, *24*, 2386.

3. Holovics, Thomas C.; Robinson, Randall E.; Weintrob, Edward C.; Toriyama, Masaharu; Lushington, Gerald H.; Barybin, Mikhail V. *Journal of the American Chemical Society*. **2006**, *128*, 2300.

4. DuBose, David L.; Robinson, Randall E.; Holovics, Thomas C.; Moody, David R.; Weintrob, Edward C.; Berrie, Cindy L.; Barybin, Mikhail V. *Langmuir*. **2006**, *22*, 4599.

5. Barybin, Mikhail V.; Thompson, Ward H. *Unpublished work.*

6. Hanke, Manfred; Jutz, Christian. *Synthesis*. **1980**, 31.

7. Hafner, Klaus; Meinhardt, Klaus Peter. *Organic Syntheses*. **1984**, *62*, 134.

8. Nozoe, T.; Matsumura, S.; Murase, Y.; Seto, S. *Chemistry and Industry>* **1955**, 1257.

9. Kurotobi, Kei; Tabata, Hiroshi; Miyauchi, Masato; Murafuji, Toshihiro; Sugihara, Yoshikazu. *Synthesis*. **2002**, 1013.

10. Morita, Tadayoshi; Takase, Kahei. *Bulletin of the Chemical Society of Japan*. **1982**, *55*, 1144.

11. Ito, Shunji; Terazono, Tomomi; Kubo, Takahiro; Okujima, Tetsuo; Morita, Noboru; Murafuji, Toshihiro; Sugihara, Yoshikazu; Fujimori, Kunihide; Kawakami, Jun; Tajiri, Akio. *Tetrahedron*. **2004**, *60*, 5357.

12. Okujima, Tetsuo; Ito, Shunji; Morita, Noboru. *Tetrahedron Letters*. **2002**, *43*, 1261.

13. Farina, Vittorio; Krishnamurthy, Venkat; Scott, William J. *The Stille Reaction*. John Wiley and Sons, **1998**.

14. Huenig, Siegfried; Ort, Burkhard. *Liebigs Annalen der Chemie*. **1984**, 1905.

15. Spectral Data from obtained from SDBSWeb : http://riodb01.ibase.aist.go.jp/sdbs/ (National Institute of Advanced Industrial Science and Technology, 02/13/2009)

16. Silverstein, Robert M.; Webster, Francis X. *Spectrophotometric Identification of Organic Compounds*. **1998**. John Wiley and Sons, Hoboken, NJ.

17. Huenig, Siegfried; Ort, Burkhard. *Liebigs Annalen der Chemie*. **1984**, 1959.

18. Huenig, Siegfried; Ort, Burkhard; Hanke, M.; Jutz, C.; Morita, T.; Takase, K.; Fukazawa, Y.; Aoyagi, M.; Ito, S. *Liebigs Annalen der Chemie*. **1984**, 1952.

19. Ikegami, Yusaku; Seto, Shuichi. *Bulletin of the Chemical Society of Japan*. **1970**, *43*, 2409.

20. Gerson, Fabian; Lopez, Javier; Metzger, Andre; Jutz, Christian. *Helvitica Chimica Acta*. **1980**, *63*, 2135.

21. Connelly, Neil G.; Geiger, William E. *Chemical Reviews*. **1996,** *96*, 877.

22. Pomije, Marie K.; Kurth, Chris J.; Ellis, John E.; Barybin, Mikhail V. *Organometallics*. **1997**, *16*, 3582-3587.

23. Irwin, Michael J.; Rendina, Louis M.; Vittal, Jagadese J.; Puddephatt, Richard J. *Chemical Communications* (Cambridge). **1996**, 1281-1282.

24. Krimen, Lewis I. *Organic Syntheses*. **1970,** *50*, 1.

25. Herrmann, W. A.; Zybill, C. In *Synthetic Methods of Organometallic and Inorganic Chemistry* (Herrmann/Brauer); Herrmann, W. A., Salzer, A., Eds.; Thieme: Stuttgart, **1996**. *1*, pp 117−119.

26. International Tables for Crystallography, Vol. A, 4th ed., Kluwer: Boston (1996).

27. Data Collection: SMART Software Reference Manual (1998). Bruker-AXS, 5465 E. Cheryl Parkway, Madison, WI 53711-5373 USA.

28. Data Reduction: SAINT Software Reference Manual (1998). Bruker-AXS, 6300 Enterprise Dr., Madison, WI 53719-1173, USA.

29. G. M. Sheldrick (2000). SHELXTL Version 6.10 Reference Manual. Bruker-AXS, 5465 E. Cheryl Parkway, Madison, WI 53711-5373 USA.

30. Makosza, M.; Osinski, P. W.; Ostrowski, S. *Polish Journal of Chemistry*. **2001**, *75*, 275.

31. Vorushilov, Alexander; Barybin, Mikhail V. *Unpublished work.*

32. Robinson, Randall E.; Holovics, Thomas C.; Deplazes, Stephan F.; Lushington, Gerald H.; Powell, Douglas R.; Barybin, Mikhail V. *Journal of the American Chemical Society*. **2003**, *125*, 4432.

33. Deplazes, Stephan F. Ligand design, coordination and electrochemistry of nonbenzenoid aryl isocyanides. University of Kansas, 2007. UMI, Ann Arbor MI, #3295011.

CHAPTER III

III. Novel Self-Assembled Monolayers of Isocyanoarenes and Polyisocyanoarenes on Gold(111) Surfaces

III.1. Introduction

Organized assembly of organic molecules on the surface of a metal film has arisen as a possible method for the controlled development of molecular devices, particularly as related to the fields of molecular wires, memory cells, and light harvesting materials.[1,2,3] Some issues in fabricating self-assembled monolayers (SAMs) using organic molecules rely on the ability to determine the orientation of the molecule on the surface, the concentration or coverage of molecules on the surface of the metal film, and the stability of the surfaces to ambient environments. The latter characteristic encompasses stability to air, light and moisture, and is most relevant to the ability to develop, and, perhaps, mass-produce molecular devices.

Many techniques are available for studying monolayers, especially related to determining the orientation of the molecule with respect to the surface and confirming that only a single layer of molecules covers the surface rather than multiple layers. Infrared spectroscopy that involves reflectance of radiation is a primary technique used in the study of isocyanide based monolayers. The isocyanide functional group exhibits a stretching band (ν_{CN}) in a region that is silent for many other oscillators, and the energy of the isocyanide stretching frequency is relatively well defined based on the mode of coordination of the :C≡N- fragment to the metal surface. For example, the isocyanide stretching frequency typically shifts to a higher energy when the carbon atom uses its lone pair to coordinate to a metal center incapable of back-bonding. This σ-interaction results in a strengthening of the carbon-nitrogen triple bond, as the lone electron pair is somewhat antibonding with respect to the CN bond. On the other hand, the ν_{CN} may shift

to a lower energy compared to that of the free ligand when the isocyanide coordination involves $d\pi \rightarrow p\pi^*$ backbonding. The selection rules for reflectance IR are somewhat different than that governing standard transmittance IR spectroscopy. Although the former method still requires a change in the instantaneous dipole moment of the unit upon excitation, reflectance IR only measures the component of the dipole moment change that is perpendicular to the surface being studied. Therefore, IR-active oscillations that are oriented parallel to the surface will produce no bands in a surface reflectance spectrum. Conversely, IR-active vibrations that are perfectly perpendicular to the metal surface will exhibit intense peaks in reflectance spectra. Finally, an IR-active oscillation that occurs at some angle between 0° and 90° with respect to the surface will exhibit a band, the intensity of which depends on the magnitude of the above angle.

Ellipsometry is another important technique used to characterize monolayers on metal surfaces. Ellipsometry measures the change in polarized light as it reflects or transmits from a metal surface, thereby allowing for changes in the height of the surface to be determined. This method provides information regarding the formation of a monolayer versus a multi-layer, as well as some insight as to the orientation of the coordinated molecules with respect to the surface.

Scheme III.1. Possible binding modes of isocyanides to metal atoms, clusters, and/or surfaces.[4]

Isocyanides are well known to coordinate to metal atoms or ions in a variety of oxidation states. As such, organic isocyanides make interesting candidates for studies of their SAMs on metal surfaces. Scheme III.1 illustrates possible binding modes of isocyanides to metal atoms, clusters, or surfaces.[5] Four of these potential binding modes involve an "end-on" coordination through the terminal carbon atom, but only two of these four maintain the triple bond character of the isocyanide junction. Therefore, infrared spectroscopy can be useful in differentiating, at least to some extent, the types of binding of the isocyanide functionality to a metal surface.

Reports on interactions of organic isocyanides with metal films first appeared in the literature in the 1980's. Acetonitrile and its isomer, methyl isocyanide, were adsorbed on a Ni(111) surface.[6,7] While both molecules appeared to chemisorb to the metal surface irreversibly, it was unclear as to whether the binding occurred through the terminal atom (either N or C) or via a bridging arrangement involving both the C and N atoms.[6,7] In addition, methyl isocyanide adsorbed on the nickel surface isomerized to acetonitrile over time.[6,7] Decomposition of the formed layers was accomplished at temperatures above 75°C.[6,7] The monolayer formation required O_2-free preparations, analysis, and storage, thereby limiting the potential usefulness from an application perspective.[6,7] A similar study was performed in 1983 using acetonitrile and methyl isocyanide adsorbed to a rhodium(111) surface that resulted in similar observations.[8]

In 1985, methyl isocyanide and carbon monoxide were adsorbed on a silver (311) surface at low temperatures and analyzed for binding modes using high resolution energy loss (HREEL) spectroscopy and electron simulated desorption ion angular distribution (ESDIAD) measurements.[9] Both carbon monoxide and methyl isocyanide can coordinate

to metals through σ- and π-interactions.[9] By using carbon monoxide and methyl isocyanide, attempts were made to force monolayer interactions with the metal surface via π-binding as illustrated in Figure III.1.[9] In fact, at low ligand coverage (or surface concentration), the coordination mode that involves the "lying-down" arrangement was strongly suggested, while at higher coverage, the weaker "end-on" σ-interactions were observed.[9]

Figure III.1. Example of σ and π bonding of methyl isocyaide to a Ag(311) surface.[9]

Significant progress was made in the 1990's by Angelici and coworkers in understanding binding of isocyanides to powdered gold.[10,11,12,13] The primary method of analysis in these experiments was diffuse reflectance infrared Fourier transform spectroscopy (DRIFTS). The radiation used in this technique is reflected, refracted and diffracted at the interface of the metal surface and the monolayer. This phenomenon provides detailed information about IR-active vibrational modes with components perpendicular to the surface being studied. Table III.1 contains ν_{CN} IR data for several different isocyanides (1) in the solution phase, (2) coordinated to gold powder and (3) within a gold(I) chloride complex.[11] The variation in the energy of the ν_{CN} bands make

DRIFTS an excellent tool for monitoring binding of isocyanides to metal surfaces. As the isocyanide functionality binds to a gold(0) surface, the isocyanide stretching frequency shifts to higher energy, thereby indicating a strengthening of the C≡N bond due to σ-bonding interactions of the carbon atoms lone pair with the metal. Likewise, when an isocyanide is coordinated to Au(I), the energy of the isocyanide stretching vibration increases due to the donating character of the isocyanide to the positively charged metal center. As expected, the energy of the bands for isocyanides bound to a gold surface are intermediate between the free isocyanide (lower energy) and the gold(I) complex (higher energy). These data also indicate that the isocyanides bind to the gold powder in a mostly terminal, head-on arrangement, similar to that observed in high coverage with Ag(311) surfaces described above.[9,11]

Table III.1. ν_{CN} frequencies of various isocyanides studied on gold powder.[11]

Compound	Solution CNR ν_{CN} (cm^{-1})	Adsorbed on Au ν_{CN} (cm^{-1})	Solution ClAu(CNR) ν_{CN} (cm^{-1})
phenyl isocyanide	2129	2190	2225
4-isocyanonitrobenzene	2127	2187	2220
^{t}butyl isocyanide	2138	2207	2238
^{n}butyl isocyanide	2151	2223	2254
ethyl isocyanoacetate	2163	2232	2261

Similar investigations were performed with aromatic molecules containing more than one isocyanide (polyisocyanides) on gold powder.[10,13] For instance, 1,4-

diisocyanobenzene (**DIB**) was combined with gold powder and analyzed by DRIFTS.[10] The solution isocyanide stretch for **DIB** occurs at 2128 cm^{-1} while those for **DIB** adsorbed on gold powder occur at 2180 and 2121 cm^{-1}. This indicates that one of the isocyanide units is bound to the gold, while the other isocyanide functionality remains unbound, or free.[10] Because of the selection rules governing reflectance IR, the intensity of the unbound isocyanide also helps assess the orientation of the molecule relative to the gold surface. In the case of gold-bound **DIB**, the molecule appears to orient more or less perpendicular to the surface in an "end-on" fashion through the terminal carbon atom.

Figure III.2. Bidentate and tridentate isocyanides used in monolayer studies on gold powder.[13]

Yet another set of investigations of isocyanides on gold powder involved bidentate and tridentate isocyanides with the potential to bind to the surface with all isocyanide units.[13] Figure III.2 illustrates four polydentate compounds that were adsorbed on gold powder.[13] The study included characterization of the monolayers, determination of relative binding affinities, and competition studies.[13] Based on DRIFTS data, each isocyanide unit appeared to bind to the gold powder surface in an "end-on" fashion for all potentially polydentate isocyanides considered.[13] Competition studies indicated the importance of the chelate effect in isocyanide gold interactions as the coordinated monoisocyanides were more easily displaced than the polydentate isocyanide ligands.[13]

Kubiak *et al*. investigated the formation of monolayers of *p*-diisocyanobenzene, 4,4'-diisocyanobiphenyl, and 4,4'-*p*-diisocyanoterphenyl on Au(111) surfaces.[14] Along with the reflection IR studies, optical ellipsometry was used to characterize the formed monolayers. Because ellipsometry measures the change in polarized light as it reflects or transmits from a metal surface, changes in the height of the surface can be determined. This technique provides information regarding the formation of a monolayer versus a multi-layer as well as allows for assessment of the orientation of the adsorbed molecules with respect to the metal surface. Similar to the observations by Angelici *et al.* for the gold powder systems, Kubiak and coworkers found that only one isocyanide unit of the above *p*-diisocyanide ligands binds to the metal surface because geometric constraints prohibit the binding of both isocyanide groups at the same time.[14] The authors also determined, based on the reflectance IR data that the isocyanide junctions bind in the terminal "end-on" fashion using σ-bonding interactions with the Au(111) surface.[14] The ellipsometric measurements yielded monolayer thicknesses consistent with η^1 "end-on" binding of the diisocyanoarene ligands as well.[14]

DIB was further used to anchor ruthenium phthalocyanine (RuPc) motifs to a Au(111) surface.[15] In analyzing the polarization modulation-infrared reflection-adsorption spectroscopy (PM-IRRAS) data, a peak at 2272 cm^{-1} was observed alongside peaks at 2176 and 2122 cm^{-1}.[15] The latter two bands represent the surface bound and free isocyanides, respectively.[15] Three potential sources for this unusual feature at 2272 cm^{-1} were suggested: a) a low coverage "lying-down" configuration of the isocyanide on the surface; b) nitrile impurities from isomerization; or c) aggregated **DIB** molecules.[15] However, metal-promoted oxidation of the coordinated isocyanide unit to form the

corresponding isocyanate, O=C=NR, is likely to be the actual cause for the observation of the band at 2272 cm^{-1} (*vida infra*). The gold/**DIB** monolayer was then exposed to a solution of RuPc to form the desired Au-bridge-metal complex arrangement, evidenced by the disappearance of the IR band at 2122 cm^{-1} and growth of a new peak at 2155 cm^{-1}.[15] Ellipsometric data for the metal capped monolayer indicated the experimental thickness of 15Å, which is consistent with the IR observations.[15]

Chen and coworkers initiated a study in 1999 to examine electron transport through the **DIB** framework at metal junctions.[16] A specially designed templating method was used to generate two Au(111) layers or Pd(111) layers at each isocyanide "alligator clip" of **DIB**.[16] A Semiconductor Parameter Analyzer was used to determine the *I/V* characteristics of the gold-gold or palladium-palladium junctioned diisocyanide bridges.[16] Thermal emission was determined to be the primary mechanism of conduction for monolayers formed by chemisorption of isocyanides onto metal surfaces, whereas electron hopping and thermal electron emission were involved when the metal isocyanide junction was formed via evaporation methods.[16] Palladium isocyanide junctions presented lower barriers to conduction than gold isocyanide junctions in this study.[16]

Figure III.3. Phenyl, biphenyl and terphenyl frameworks used in the conductivity studies comparing thiols and isocyanides: R = -SH or -N≡C.[2]

Table III.2. Values for the energy gap between the Fermi level and the HOMO of mono- and disubstituted polyphenyl thiols and isocyanides.[2]

Number of R groups (Figure III.3)	Number of Phenyl Rings	$E_f - E_H$ (eV, ±0.1) Thiol	$E_f - E_H$ (eV, ±0.1) Isocyanide
1	1	1.45	0.53
1	2	1.35	0.64
1	3	1.15	0.92
2	1	0.98	0.38
2	2	0.98	0.53
2	3	1.07	0.67

At approximately the same time, Kubiak and coworkers were comparing benzene-based isocyanides to benzene-based thiols in terms of conduction properties of their

SAMs using scanning tunneling microscopy (STM) to determine the *I/V* properties of the molecules adsorbed on gold surfaces.[2] Organic thiols have been extensively studied as potential components in the design of molecular wires. In order to truly understand the characteristics of SAMs of isocyanides, comparisons between thiols and isocyanides were investigated.[2] The *I/V* characteristics of phenyl, biphenyl and terphenyl mono- and diisocyanides versus mono- and dithiols (shown in Figure III.3) revealed that the conductance gap increased with increasing the number of phenyl rings for the isocyanides while the reverse was true for the thiols.[2] Using the *I/V* data, the energy gap between the Fermi level and the HOMO of the systems were compared for all molecules studied.[2] For the thiols, as the number of the phenyl rings increased, the energy gap between the Fermi level and the HOMO became smaller. This observation is consistent with the concept that extension of the π-system reduces the HOMO-LUMO gap and elevates the energy of the HOMO.[2] For isocyanides, the reverse trend was observed suggesting that as the number of the phenyl rings increase, the energy gap between the Fermi level and the HOMO widened.[2] This phenomenon was attributed to the ability of the isocyanide's π-orbitals to interact with the π-system of the phenyl rings, causing not only the highest occupied π orbitals associated with phenyl rings to increase in energy but also the π framework associated with isocyanides increase in energy.[2] As a consequence, aryl isocyanides containing phenyl rings were better electron donors than acceptors and therefore isocyanides with more phenyl rings exhibited a larger barrier to conductance.[2] However, the determined energy gap between the Fermi level and HOMO were smaller for all isocyanides compared to thiols, indicating that, in general, isocyanides present a smaller barrier to conduction than thiols (Table III.2).[2]

Figure III.4. Diisocyanides used in the binding modes study on Au(111) surfaces by Kubiak and coworkers.[4]

Kubiak *et al.* performed additional studies to better understand and determine the binding mode of SAMs of isocyanides on Au(111) surfaces using advancing water contact angle, reflection absorption infrared (RAIR) spectroscopy, and ellipsometry.[4] The diisocyanides studied are shown in Figure III.4.[4] The two alkyl diisocyanides exhibited only one isocyanide stretch in the RAIR spectra while the benzene-based diisocyanides all showed two stretching bands attributed to the isocyanide groups: one associated with the gold bound isocyanide and the other associated with the free isocyanide.[4] Ellipsometric data were consistent with the formation of single monolayers, with the alkyl diisocyanide values being lower than theoretical calculations based on the longest chain arrangement. The ellipsometric data also indicated the orientation of benzene-based diisocyanides being approximately perpendicular to the surface.[4] All of the above observations suggested η^1 binding through the terminal carbon atom to only one gold atom on the Au(111) surface, thus supporting the conclusions previously drawn by Angelici.[4,10,11]

Figure III.5. Benzenoid aryl diisocyanide polyphenyl complexes studied by Swanson and coworkers.[17]

Additional information regarding the binding modes of isocyanides on both gold and palladium surfaces were reported by Swanson *et al.* in 2005.[17] Ellipsometry, PM-IRRAS, and grazing angle attenuated total reflectance (GATR) spectroscopy were used to assist in determining the orientation of symmetrical benzene-based diisocyanides, with the variation being not only the number of phenyl rings, but also the incorporation of methyl substituents at positions *ortho* to the isocyanides, as shown in Figure III.5.[17] When the diisocyanides were bound to Au(111) or Pd(111) surfaces, the reflectance spectra indicated both metal bound (broad peaks at 1980-2000 cm^{-1} for Pd, 2170-2180 cm^{-1} for Au) and free (2110-2120 cm^{-1}) isocyanide oscillators, as well as an additional peak at approximately 2270 cm^{-1}.[17] The observed IR data were compared to those of the free ligands and some related metal complexes of the isocyanides. The binding mode of isocyanides to the Pd surface was consistent with a bent terminal η^1 coordination, involving $d\pi \rightarrow p\pi^*$ backbonding interactions that weaken the isocyanide bond, similar to what has been documented for many low-valent metal-isocyanide complexes.[17] In

addition, the possibility of μ_3-η^1 coordination of the isocyanides to the Pd surface was proposed as a complete binding motif. The coordination of the isocyanide ligands to the gold surface conformed to previous observations of terminal η^1 binding that involves only a σ-component.[17] The peak at *ca.* 2270 cm^{-1} had been previously mentioned by Palacin and coworkers and was attributed to either a low coverage μ_2-η^2 binding mode or the formation of π-stacked aggregates.[17] However, this peak was observed for both Pd and Au SAMs, and ellipsometric data were not consistent with aggregate formation.[17] The intensity of the peak at *ca.* 2270 cm^{-1} was amplified upon illumination or heating of the SAM in air.[17] Based on the analysis of the comparative data, the band at 2270 cm^{-1} was ultimately attributed to the formation of isocyanate produced by photooxidation of the free isocyanide end of the molecules without altering the bound isocyanide.[17] However, such a conclusion appears to be erroneous, especially in light of the careful study of isocyanide adsorption reported by Allara *et al.* in 2005.[5]

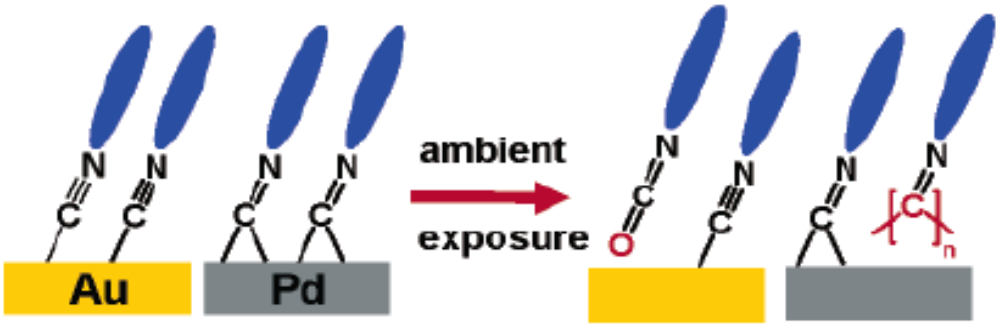

Scheme III.2. Cartoon illustrating the stability of organic isocyanides as SAMs to ambient conditions.[5]

Allara and coworkers, in an attempt to gain insight into the stability of isocyanide monolayers to ambient exposure, used 4,4'-di(phenylene-ethynylene)benzene isocyanide on Pd(111) and Au(111) surfaces.[5] Monolayers were formed in inert conditions and transferred to instruments for analysis with minimal exposure to ambient atmosphere.[5]

The IR spectrum of the freshly prepared SAM featured the expected broad stretch for isocyanide bound to gold at approximately 2170 cm^{-1}, spectrum A in Figure III.6.[5] Upon ambient exposure for a brief (60-second) period, the ν_{CN} peak decreased slightly in intensity and a new peak at approximately 2270 cm^{-1} was observed, as in spectrum B of Figure III.6.[5] The same observation was made after exposure of a freshly prepared SAM on Au to O_3 for only 30 seconds, spectrum C in Figure III.6.[5] Because only one isocyanide was available in the ligand chosen, the results indicated formation of isocyanate from the isocyanide bound to the gold surface, as illustrated in Scheme III.2.[5] Notably, oxidation of phenylacetylene on Au(111) to phenyl acetic acid and phenyl oxirane were reported in 2007, thus demonstrating another example of gold-promoted oxidation of the unsaturated substrate adsorbed to the metal surface.[18] Interestingly, the IR spectra of the aryl isocyanide SAMs on Pd before and after exposure to ambient conditions revealed new bands at 1600 cm^{-1} and 2210 cm^{-1} with a band at 1980 cm^{-1} gradually disappearing.[5] The two new peaks were consistent with formation of a poly(imine) species from the organic isocyanide bound to the surface, as shown in Scheme III.2.[5]

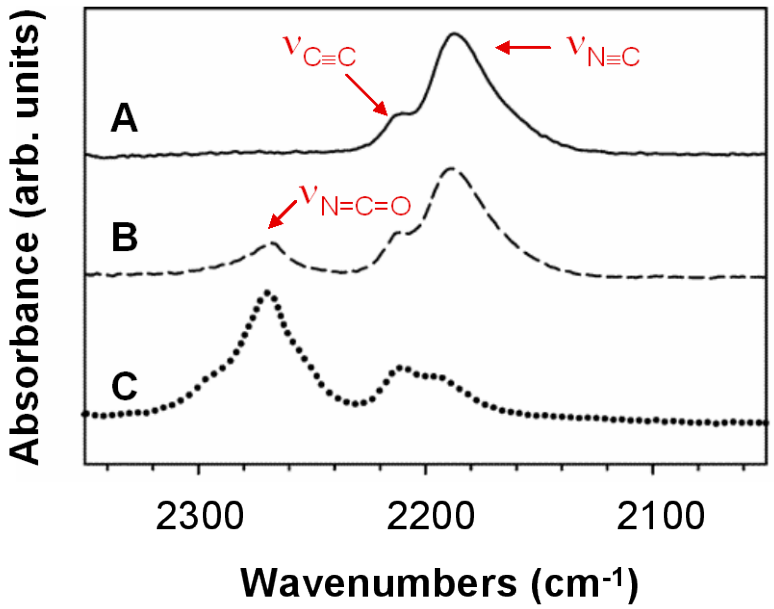

Figure III.6. IR spectra of SAM of 4,4'-di(phenylene-ethynylene)benzene on Au(111). Spectrum A = freshly prepared SAM under N_2; B = SAM upon exposure to air for 60 sec.; C = SAM upon exposure to O_3 for 30 sec. adapted from ref. 5

Table III.3. Solution and surface IR data for selected isocyanoazulenes.[19]

Compound	ν_{CN} CH_2Cl_2 (cm^{-1})	ν_{CN} Au(111) (cm^{-1})
2-isocyanoazulene	2127	2174
6-isocyanoazulene	2117	2176
2-isocyano-1,3-diethoxycarbonylazulene	2127	2169
6-isocyano-1,3-diethoxycarbonylazulene	2115	2178
2,6-diisocyano-1,3-diethoxycarbonylazulene	2116, 2125	2117, 2163
pentacarbonylchromium-2,6-diisocyano-1,3-diethoxycarbonylazulene (2-bound isomer)	2115, 2135	2120, 2171
pentacarbonylchromium-2,6-diisocyano-1,3-diethoxycarbonylazulene (6-bound isomer)	2125	2132, 2174

Recently, Barybin, Berrie and coworkers have reported on the first SAMs of azulenic compounds.[19] In this study, the isocyanide "alligator clips" were employed to anchor the azulenic motifs to a gold(111) surface. Isocyanoazulenes constitute a new class of aromatic isocyanides and many of these species exhibit remarkable air and thermal stability compared to benzenoid aryl and alkyl isocyanides.[20,21] Barybin and coworkers also demonstrated stepwise regioselective installation and complexation of two isocyanide junctions at the linear 2,6-azulenic moiety.[21] Table III.3 summarizes the ν_{CN} data relevant to the interaction of various isocyanoazulenes with Au(111) surfaces.[19] These IR data clearly demonstrate coordination of the isocyanoazulenes to the Au(111) surface in the expected terminal upright η^1 fashion.[19] Interestingly, no peaks were detected in the 2250 - 2300 cm^{-1} region (ν_{CNO}), even though all synthetic manipulations as well as subsequent spectroscopic analyses of the films were performed in air, often after allowing the SAM samples to be exposed to the ambient laboratory atmosphere for several days.[19] Thus, the isocyanoazulene films on gold have a significant advantage over those of benzenoid aryl isocyanides in terms of the film stability to ambient environment.[19]

Figure III.7. Pentacarbonylchromium complexes of the linear 2,6-diisocyanoazulene motif.

The above work by Barybin and coworkers demonstrated the ability to link two different metals (electron reservoirs) through the linear 2,6-diisocyanoazulene framework.[19] Coordination of the chromium pentacarbonyl units to one of the isocyanide junctions of the diisocyanoazulene scaffold provided an excellent spectroscopic handle for assessing the orientation of the diisocyanoazulene molecules adsorbed to the gold surface. The two monometallic isomers are drawn in Figure III.7. For the 2,6-diisocyanoazulene molecule capped with $(OC)_5Cr$ unit at either isocyanide, the ν_{CO} bands occur at approximately 2040 cm^{-1} and at 1960 cm^{-1} in solution.[19] The peak at 2040 cm^{-1} corresponds to the A_1 stretching mode of the carbonyl ligands, with the carbonyl oscillator positioned *trans* to the isocyanide junction providing the major contribution to this band.[19] The band at 1960 cm^{-1} is produced by the E stretching mode of the carbonyl ligands, with the carbonyl ligands *cis* to the isocyanide unit contributing the most to this vibration.[19] Upon binding of either of the monometallic diisocyanoazulene complexes to

the gold(111) surface, the relative intensity of the ν_{CO} band at 2040 cm^{-1} increased while that of the band at 1960 cm^{-1} decreased quite dramatically.[19] This indicates, by the surface IR selection rules, that the carbonyl located *trans* to the isocyanide junctions is in an almost perpendicular orientation with respect to the metal surface while the *cis* carbonyl ligands are nearly parallel to the surface.[19] Given that the (isocyanide)-Cr-(*trans*-CO) angle is essentially 180° in the octahedrally coordinated Cr(0) unit, one can conclude that the terminal upright η^1 coordination of the other ("free") isocyanide junction of the diisocyanoazulene motif to the gold surface is clearly realized.

Scheme III.3. Assembly of conductive molecular surfaces.

Of considerable interest to the field of molecular electronics is the ability to selectively bind an organic bridge to a surface in an organized fashion such that the unbound end of the molecule allows for conductivity from the metal surface to the opposite end of the molecule. A general design of such a framework is shown in Scheme III.3 and involves conductive junction groups, or "alligator clips", connecting a highly conjugated organic bridge to a metal surface. A second metal or electron reservoir could be attached at the second junction group to complete the circuit. Development of successful molecular surface scaffolds using aryl isocyanide motifs is attractive, but presents several challenges. The first difficulty relates to the poor environmental stability of most previously studied isocyanoarene SAMs, particularly with respect to

metal-promoted oxidation of isocyanides to isocyanates at the gold(111) surface.[5] A second obstacle is associated with the need to keep the HOMO-LUMO energy gap of the organic bridge relatively small to reduce the barrier to conduction of isocyanoarenes, as demonstrated by Kubiak *et al.* in the case of diisocyanobiphenyl.[2] This chapter addresses formation and properties of the self-assembled monolayer films of the first isocyanobiazulenes described in Chapter II (compounds **3.1** and **3.2**) on gold. In addition, efforts towards improving the environmental stability of conventional benzenoid aryl isocyanide SAMs on gold by "stitching" individual adsorbed benzenoid isocyanide units together (compound **3.3**) are presented (Figure III.8).

Figure III.8. Three molecules investigated as SAMs on Au(111) surfaces.

III.2. Experimental

III.2.1. General Procedures

Solvents used for the formation of SAMs were all reagent grade or higher purity and required no further purification. Gold-coated mica substrates with 1500Å of Au(111) covering 2.0 cm x 1.6 cm were purchased from Molecular Imaging Corp. These substrates were soaked in dichloromethane, acetone and methanol for 2 hours in each solvent, then rinsed thoroughly with hot methanol and dried under a stream of nitrogen immediately before use. Monolayer films were obtained by immersing freshly cleaned metal substrate (gold on mica) into a *ca.* 2mM solution of 2,2'-diisocyano-1,1',3,3'-tetraethoxycarbonyl-6,6'-biazulene (**3.1**), 6-isocyano-2,2'-biazulene (**3.2**), or 8,16,24,32-tetraisocyano[2.2.2.2]metacyclophane (**3.3**). The syntheses of compounds **3.1** and **3.2** are described in Chapter 2 of this Dissertation (pages 73 and 76). Tetraisocyanide **3.3** was synthesized according to the literature.[22] After *ca.* 24-48 hour exposure of the gold films to solutions of the isocyanides, the samples were removed from the solutions, rinsed thoroughly with CH_2Cl_2 and dried in a flow of N_2 gas.

The grazing angle incidence reflection-absorption Fourier transform infrared spectroscopy data were collected on a nitrogen purged Thermo Nicolet 670 FTIR spectrometer with a VeeMax grazing angle accessory set at an angle of 70°. A freshly cleaned bare gold on mica substrate was used to collect the background spectrum before each experiment. Ten thousand scans were collected for each background/sample pair from 600 cm^{-1} to 4000 cm^{-1} at a 4 cm^{-1} resolution. Solution FTIR data were also collected on a Thermo Nicolet 670 FTIR spectrometer employing 32 scans from 600 to 4000 cm^{-1} at a 1 cm^{-1} resolution.

Film thicknesses were determined using an Auto EL III ellipsometer (Rudolph Research). All measurements were made with a HeNe laser at a wavelength of 632.8 nm

and an incident angle of 70°. The optical constants for the gold films were determined for each sample individually from measurements on the freshly cleaned bare gold sample. A refractive index of 1.45 was assumed for the organic thin films studied.[23] Measurements for bare substrates and SAMs were taken at a minimum of four different spots on each sample. The reported thicknesses are averages of the measurements over each of those spots along with the standard deviation of the measurement.

Density functional theory (DFT) electronic structure calculations on **3.3** were performed by Dr. Kumar Vanka and Prof. Ward H. Thompson using the Gaussian 03 program[24] with the B3LYP functional[25] and 3-21G* and 6-31+G* basis sets.

III.3. Results and Discussion

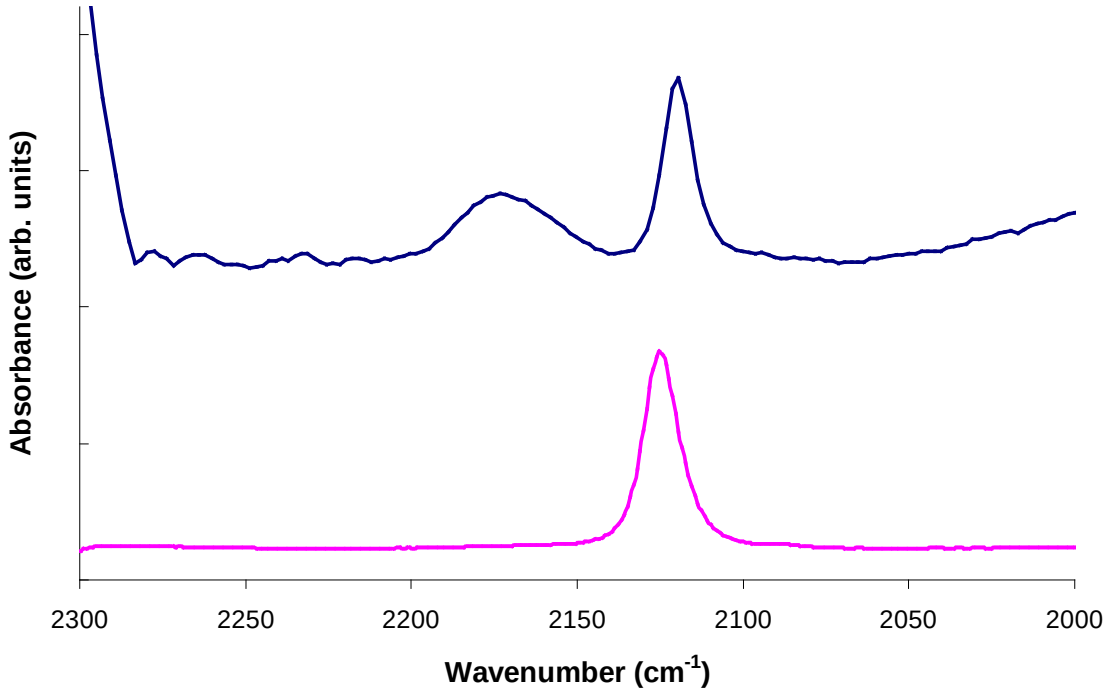

Figure III.9. IR spectra of 3.1 adsorbed to Au(111) (blue) or in CH_2Cl_2 solution (pink).

Immersion of a Au(111) surface into a 2mM solution of **3.1** in CH_2Cl_2 for 24 hours under ambient conditions produced a film, the surface IR spectrum of which is shown in blue in Figure III.9. The FTIR spectrum of **3.1** in a dichloromethane solution is shown in pink in the same Figure for comparative purposes. The IR pattern for the sample of **3.1** adsorbed on gold(111) features two ν_{CN} bands: the broad band at 2173 cm^{-1} corresponds to the isocyanide group bound to gold and the relatively sharp peak at 2119 cm^{-1} is due to the "free" isocyanide oscillator that does not interact with the metal surface. Notably, the ν_{CN} value for the diisocyanobiazulene **3.1** in CH_2Cl_2 is 2125 cm^{-1}. The lack of significant absorption at *ca.* 2270 cm^{-1} in this surface IR spectrum suggests reasonable oxidative stability of **3.1** adsorbed to gold in an ambient environment. The IR band describing vibration of the gold-bound isocyanide group of **3.1** has energy and $W_{1/2}$ values that are very similar to the corresponding parameters document by Barybin *et al.* for both 2-isocyanoazulene and 2-isocyano-1,3-diethoxycarbonylazulene.[19] The latter isocyanoazulene derivative may be viewed as one half of diisocyanobiazulene **3.1**. The observed *ca.* 50 cm^{-1} shift in ν_{CN} from free isocyanide to gold-bound isocyanides for **3.1** is consistent with terminal upright η^1 coordination of **3.1** through the isocyanide carbon atom.

The theoretical thickness of the monolayer of **3.1** on gold, assuming perfectly upright coordination, can be conveniently calculated given the X-ray crystal structure of **3.1** reported in Chapter II of this Thesis (Figure II.8). This theoretical monolayer height is 19.1Å, including an approximated gold-carbon bond distance of 2.04Å. The experimental thickness determined by fixed-wavelength ellipsometry was determined to be 18(2)Å. Thus, the film of **3.1** on Au(111) clearly constitutes a monolayer and the ν_{CN}

of 2119 cm^{-1} in the IR spectrum of **3.1** does indeed correspond to the terminal ("free") isocyanide group of the chemisorbed diisocyanobiazulene and not to diisocyanoazulene molecules simply "trapped" physically within the film.

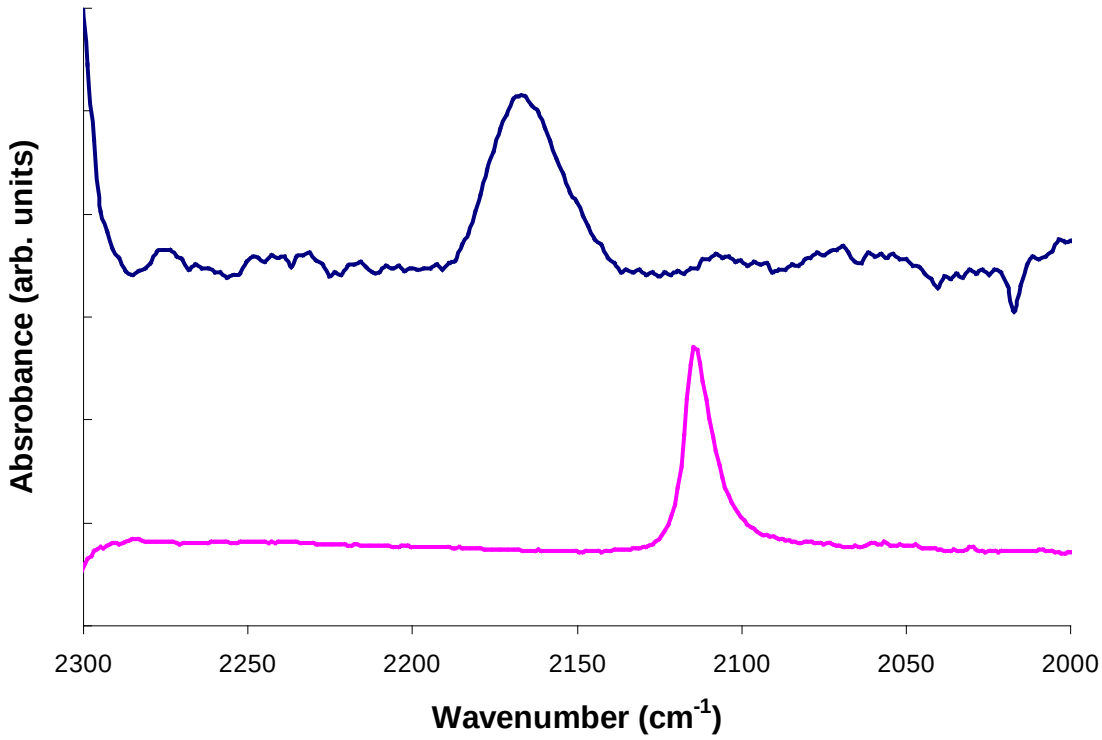

Figure III.10. Surface (blue) and solution (pink) IR spectra of 3.2 on Au(111) or in CH_2Cl_2.

Exposure of a Au(111) surface sample to a 2mM solution of **3.2** in CH_2Cl_2 for 48 hours afforded a film sample, the surface IR spectrum of which is shown in Figure III.10 (blue line). The IR spectrum of **3.2** is shown on the same Figure in pink. As expected, the isocyanide band shifted from 2114 cm^{-1} in the solution phase to 2167 cm^{-1} for the SAM. No "free" isocyanide stretching band could be detected in the surface IR spectrum. This observation nicely parallels that of Barybin and Berrie for the chemisorption of 6-isocyanoazulene on a gold(111) surface.[19] Thus, extending the 6-

isocyanoazulene motif by adding another azulenic unit in a linear fashion has no negative impact on the monolayer formation. Binding to the gold surface is consistent with terminal η^1 coordination as well.

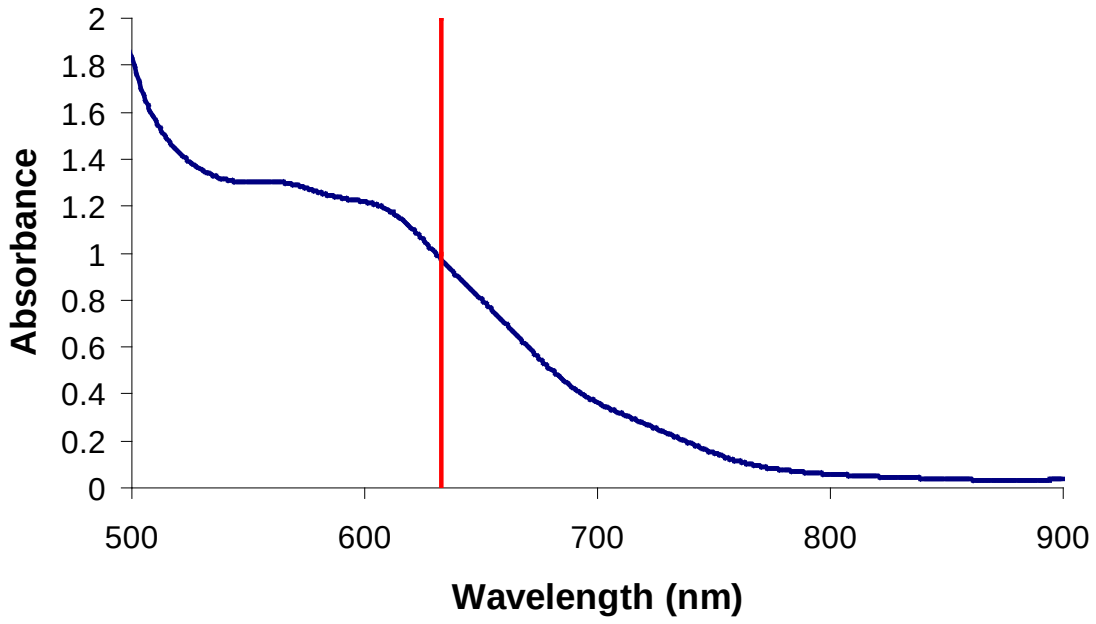

Figure III.11. Electronic absorbance spectrum of $1x10^{-4}$ M 3.2 in CH_2Cl_2 at 25°C.

Ellipsometric thickness measurements afforded a monolayer height of 27(2)Å, whereas the theoretical height of **3.2** based on the crystal structure shown in Figure II.11, a gold-carbon length of 2.04Å and an isocyanide-azulene length of 2.56Å was determined to be 17.45Å. A possible explanation of the notable discrepancy between the theoretical and measured film thickness is as follows. The fixed wavelength ellipsometer used to record these measurements employs a light source with $\lambda = 633$ nm. The vast majority of organic substances do not absorb at this wavelength. However, Figure III.11 illustrates that compound **3.2** absorbs light at 633 nm (indicated by the red line) to an appreciable extent. The absorption of light can alter the experimentally determined thickness values,

as the model used in the fixed wavelength ellipsometer assumes no absorption of light at 633 nm by the film.

The isocyanobiazulene SAMs on Au(111) appear to have the same remarkable stability in ambient conditions as those of 2,6-diisocyano-1,3-diethoxycarbonylazulene as compared to other aryl and alkyl isocyanides.[19] Given the exceptional stability of 2,6-diisocyano-1,3-diethoxycarbonylazulene SAMs in air, all procedures involving SAMs of **3.1** and **3.2** were performed in air as well.[19] IR spectra and ellipsometric thickness characteristics of SAMs of both **3.1** and **3.2** were unchanged, even after several days and even weeks of exposure to air. Thus, unlike SAMs of related 4,4'-diisocyanobiphenyl, a benzenoid congener of **3.1**, SAMs of isocyanobiazulene based substrates do not appear to oxidize readily to isocyanates on Au(111) surfaces. Notably, the films of **3.1** and **3.2** on Au(111) constitute the only biazulenic SAMs available to date.

Self-assembled monolayers of organic isocyanides on metal surfaces are often compared and contrasted with SAMs of organic thiols.[2,3,5,16,17,26] Reinhoudt *et al.* have demonstrated that [1.1.1.1]metacyclophane-based organic surfaces on metallic gold can be built by self-assembly of the corresponding cyclophane derivatized with four long-chain alkyl thiol anchors.[27,28] Kubiak,[4] Angelici[13] and McCarley[29] have demonstrated that alkyl di- and triisocyanides with reasonably flexible hydrocarbon substituents adsorb to metallic gold via all of their isocyanide junctions, at least at low coverage. As previously stated, aryl isocyanide based SAMs, including 2,6-dimethyl substituted isocyanoarenes, have exhibited gold facilitated oxidation of the metal bound isocyanide functionality to form the isocyanate group ($\nu_{NCO} \approx 2270$ cm^{-1}).[5,17]

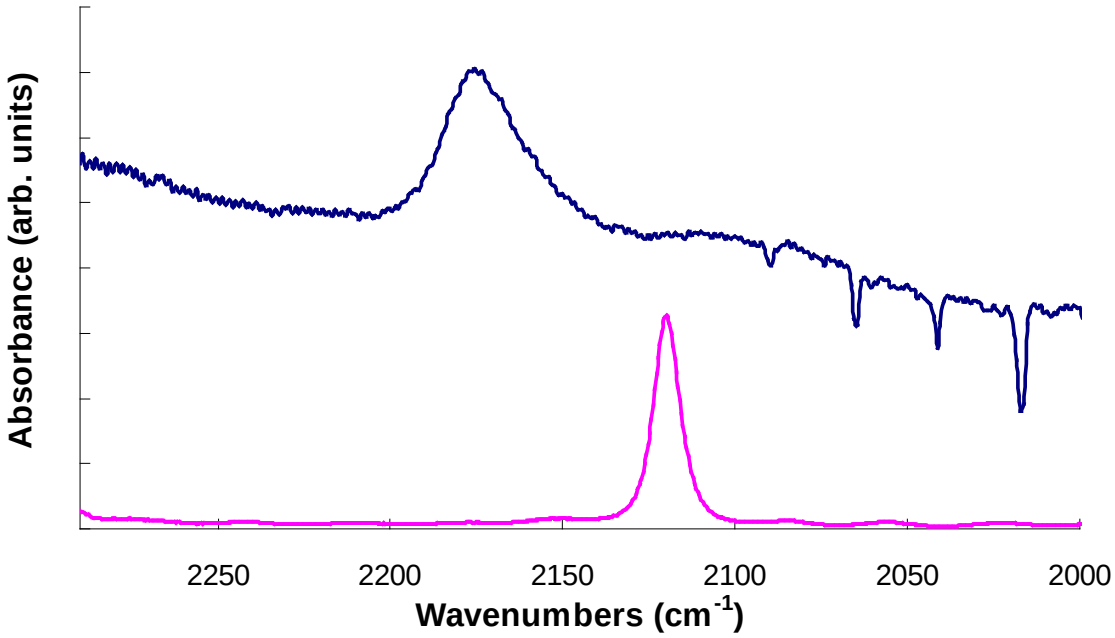

Figure III.12. Surface and solution IR spectra for 3.3 on Au(111) (blue) and in CH_2Cl_2 (pink).

Immersion of a freshly cleaned Au(111) film into a 2mM solution of **3.3** in CH_2Cl_2 at room temperature in ambient atmosphere resulted in the IR spectrum shown in Figure III.12 by a blue line, while the pink line represents the IR spectrum of the solution of **3.3**. The surface IR spectrum indicates that all four isocyanides of **3.3** have coordinated to the gold surface, with the frequency of the isocyanide stretching vibration increasing from 2119 cm^{-1} to 2175 cm^{-1} upon adsorption to gold(111), as no free isocyanide stretch is observed. The 56 cm^{-1} change in ν_{CN} is consistent with terminal upright coordination of the isocyanide groups and compares well with the ν_{CN} of other aryl isocyanides on gold. The collected ellipsometry data indicated an experimental thickness of 5.8(1)Å while a theoretical thickness, determined from a crystal structure of **3.3**[22] and approximate gold-carbon distance of 2.04Å, was calculated to be 6.4Å. Thus, both FTIR and ellipsometric thickness characteristics of **3.3** on gold(111) are indicative of upright coordination of the aryl isocyanide moieties of **3.3**, roughly perpendicular to the metal surface.

Figure III.13. Potential coordination of 3.3 in an η^1:η^1 fashion.

Previous investigations into complexation of **3.3** with metals led to predictions of binding through an η^4 coordination mode.[30] In their 2008 report, Barybin *et al.* discovered a solid state configuration of **3.3** complexed to four tungsten pentacarbonyl units in a μ_4-η^1:η^1:η^1:η^1 fashion.[22] Based on the reports by Kubiak and Angelici, coordination of **3.3** to a metal surface was anticipated to occur through a μ_2-η^1:η^1 mode, such as that illustrated in Figure III.13. When no free isocyanide vibrational stretch was observed, density functional theory electronic structure calculations were employed to assist with an explanation of the observed spectra.

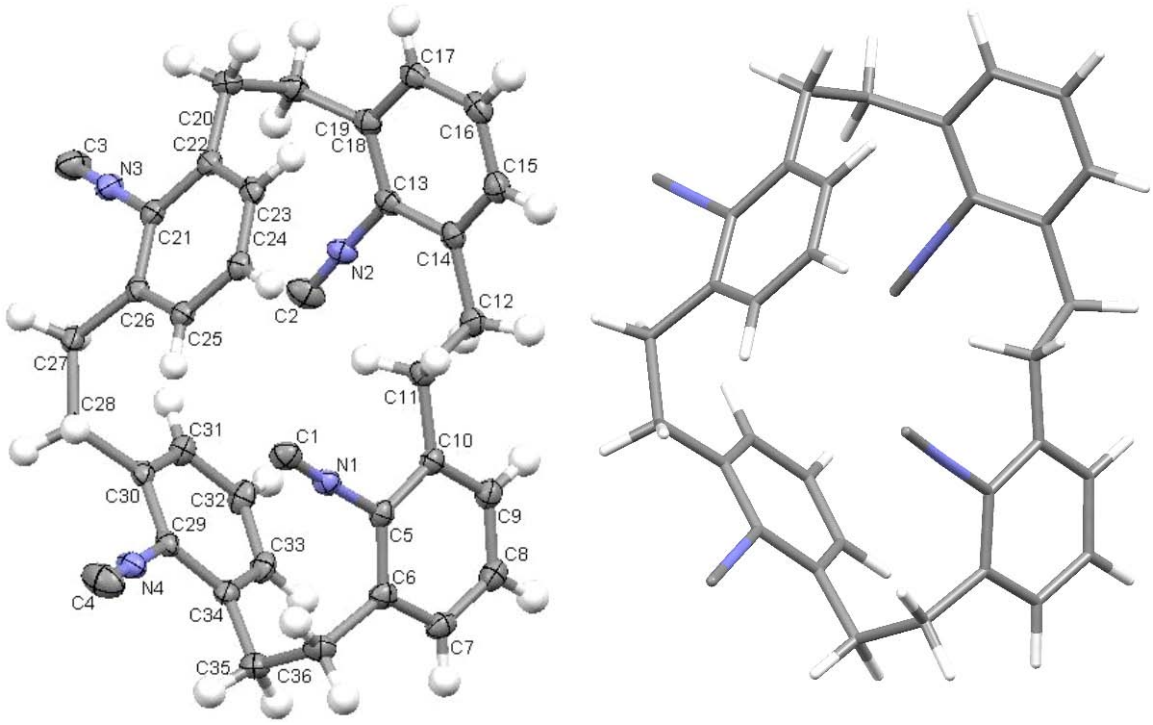

Figure III.14.Solid state structure of 3.3 and DFT-optimized structure of 3.3 (lowest energy conformation found in this study). [22]

Table III.4. Selected bond distances, angles and torsional angles for X-ray and DFT structures of 3.3.[22]

3.3 (X-ray)		**3.3** (DFT)[a]
	C-NC_6 [Å]	
1.157(2) 1.157(2) 1.156(2) 1.156(2)		1.179 1.179 1.178 1.178
	CN-C_6 [Å]	
1.407(2) 1.407(2) 1.405(2) 1.403(2)		1.391 1.390 1.390 1.390
	C-N-C [deg]	
179.6(2) 178.1(2) 177.4(2) 177.4(2)		179.3 179.1 177.7 176.7
	C-CH_2-CH_2-C [deg]	
173.3(1) 69.0(1) 58.4(1) 48.4(1)		165.6 66.0 62.7 54.9

[a] Lowest energy conformation found in this study.

In order to estimate the energy cost associated with accessing conformations of **3.3** that would be suitable for interacting with the gold(111) surface in an upright fashion using all four isocyanide anchors, a lowest energy conformation of compound **3.3** was found using DFT. Figure III.14 shows the solid state structure (50% ellipsoids) and the lowest energy conformation (DFT) of compound **3.3.**[22] Table III.4 provides a comparison of selected bond distances and angles for both the solid state structure and the DFT lowest energy conformation, indicating that crystal packing forces have little impact on geometry of **3.3** in the solid state.[22] The structural data indicate that the lowest energy conformation adopted by compound **3.3** is such that the four isocyanide junction groups are not in an ideal configuration for η^1: η^1: η^1: η^1 coordination.

Table III.5. Relative energies of ten hypothetical conformations of 3.3 coordinated to Au(111) in the η^1: η^1: η^1: η^1 fashion.

structure	d_x (Å)	d_y (Å)	α (deg)	β (deg)	ΔE (kcal/mol)
a	8.65	8.65	60	120	125.9
b	7.63	7.63	60	120	92.4
c	5.76	5.76	60	120	14.3
d	4.99	4.99	60	120	0.0
e	8.65	4.99	90	90	31.4
f	8.65	5.76	60	120	81.2
g	8.65	7.63	79.1	100.9	33.4
h	5.76	7.63	79.1	100.9	29.2
i	7.63	4.99	70.9	109.1	24.1
j	5.76	4.99	90	90	1.8

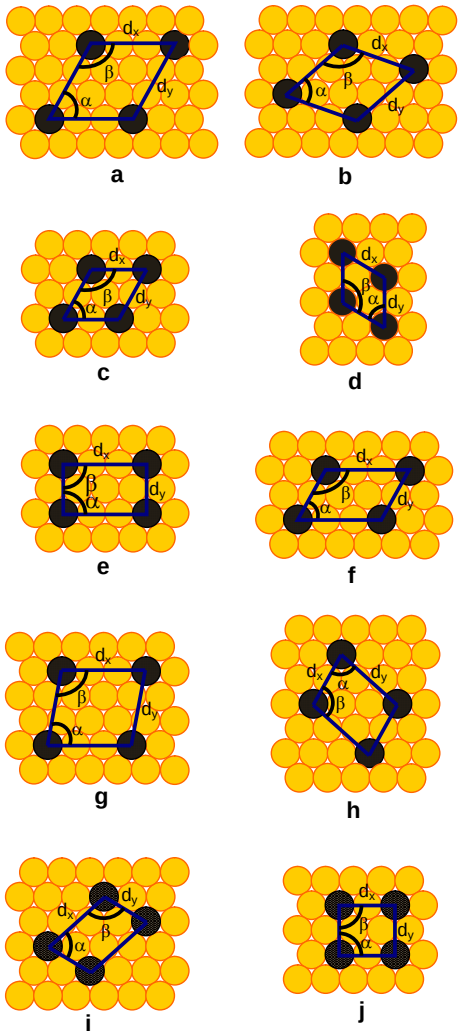

Figure III.15. Ten possible arrangements of 3.3 on a Au(111) surface through η^1: η^1: η^1: η^1 coordination.

Ten different scenarios were screened by DFT using the 3-21G* basis set. In the preliminary screening, the initial geometries of **3.3** were chosen to have four terminal isocyanide carbon atoms restrained to lie in a plane that would be parallel to a gold surface upon coordination of the tetraisocyanide. In addition, interatomic distances and angles between the terminal carbon atoms were fixed to match one of ten combinations of interatomic distances and angles involving four gold atoms on the (111) surface of the fcc Au lattice. These interatomic distances and angles, as well as the relative energy associated with each conformation are reported in Table III.5 and cartoons of these

geometric constraints are provided in Figure III.15. The data in Table III.5 reveal two conformations of compound **3.3**, structures d and j in Table III.5 and Figure III.15, that were energetically more favorable than the other eight geometries.

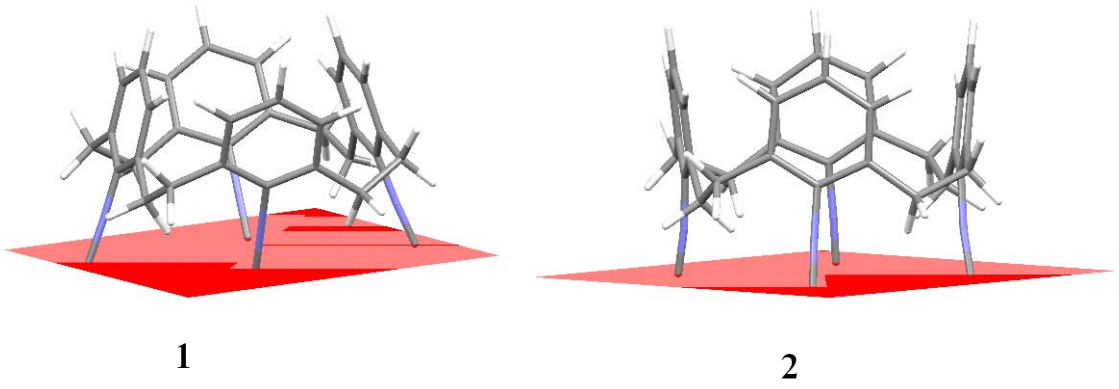

1 **2**

Figure III.16. Two lowest energy conformations of 3.3 on Au(111) surface.

The two lowest energy configurations, d and j, were selected for further consideration using the 6-31+G* basis set. At this higher level, the two structures, pictured in Figure III.16, were shown to be essentially isoenergetic, at a difference of 0.2 kcal/mol between the two conformations, with conformation 2 being lower in energy. The C-N-C units within both structures 1 (177.1° and 179.4°) and 2 (173.3° and 173.7°) are nearly linear, consistent with the experimental FTIR data for **3.3** adsorbed on gold. It is also important to note that the optimized constrained structures 1 and 2 in Figure III.16 are less than 8 kcal/mol destabilized compared to the DFT optimized structure of "free" **3.3** shown in Figure III.14. This energy could be easily offset by the formation of just one gold-isocyanide bond (*ca*. 20 kcal/mol). Thus, the adsorption of **3.3** to gold(111) via all four of its –NC anchors is clearly favorable energetically, however either conformation 1 or 2 in Figure III.16 could be possible. Conformation 1 would result in a greater degree of tilting of the isocyanoarene units with respect to the gold surface (14°-

and 16°) compared to comformation 2 (5° and1°). This suggests comformation 2 may be more likely at higher surface concentration, with more efficient packing; however additional theoretical and experimental work is needed.

The surface IR spectrum of **3.3** on Au(111), like those of **3.1** and **3.2**, showed no signs of photooxidation, unlike other benzene-based aryl isocyanides, despite the preparation and handling of the SAM of **3.3** being performed completely in air. The enhanced stability of this tetraisocyanide ligand may be attributed to a chelate effect, typically discussed in traditional coordination chemistry. The enhanced stability is not likely to be attributed to the methylene linkers of the cyclophane, as *ortho*-methyl substituted mono and diisocyanobiphenyl demonstrate photooxidation as do their non-methylated congeners.

III.4. Conclusions and Future Work

The work in this chapter was initiated to 1) assemble the first monolayers of biazulenic frameworks, 2) to improve on the stability of self-assembled monolayers of isocyanide substituted organic frameworks and 3) to attempt to reduce the barrier of conduction of SAMs of organic isocyanides.

2,2'-diisocyano-1,3,1',3'-tetraethoxycarbonyl-6,6'-biazulene and 6-isocyano-2,2'-biazulene were successful adsorbed onto Au(111) surfaces. The surface IR spectra of the SAMs of these molecules revealed a remarkable stability of isocyanobiazulenes to ambient conditions. Based on previously recorded electronic absorbance spectra, both of these biazulenic moieties should exhibit a significantly smaller HOMO-LUMO gap

compared to related isocyanobiphenyls, thereby improving electron transfer properties of molecules larger than a nanometer.

The first self-assembled monolayer of a tetraisocyanide was also achieved with this work. DFT electronic structure calculations supported the observation of binding of all four isocyanide junctions of the tetraisocyano[2.2.2.2]metacyclophane . The surface IR spectrum of the metacyclophane showed that this benzene-based polyaryl isocyanide did not photooxidize, and the SAM could be prepared in air.

Future studies on compound **3.1** include imaging and conductivity of the diisocyanobiazulene framework. Also, investigations into the ability of **3.1** to tether other metal centers to the gold surface need to be done. Imaging of SAMs of **3.3** could reveal more detail relating to the theoretical predictions regarding binding of the tetraisocyanide molecule. The presence of cavities in the monolayer of **3.3** could provide for potential uses of metacyclophanes in the field of molecular storage. Future work relating to compound **3.2** should include attempts at functionalizing the second azulene ring at the 6-position while the molecule is tethered to the gold surface, as this may eliminate some of the synthetic challenges that have been experienced to this point. Spectrophotometric ellipsometry using monolayers of **3.2** could provide interesting information about the impact of absorbed light on the models used in fixed-wavelength ellipsometry and should be pursued.

III.5. References

1. McCreery, Richard L. *Chemistry of Materials*. **2004**, *16*, 4477.
2. Hong, S.; Reifenberger, R.; Tian, W.; Datta, S.; Henderson, J.; Kubiak, C. P. *Superlattices and Microstructures*. **2000**, *28*, 289.

3. Chen, J.; Wang, W.; Klemic, J.; Reed, M. A.; Axelrod, B. W.; Kaschak, D. M.; Rawlett, A. M.; Price, D. W.; Dirk, S. M.; Tour, J. M.; Grubisha, D. S.; Bennett, D. W. *Annals of the New York Academy of Sciences*. **2002**, *960*, 69.

4. Henderson, Jason I.; Feng, Sue; Bein, Thomas; Kubiak, Clifford P. *Langmuir*. **2000**, *16*, 6183.

5. Stapleton, Joshua J.; Daniel, Thomas A.; Uppili, Sundarajan; Cabarcos, Orlando M.; Naciri, Jawad; Shashidhar, Ranganathan; Allara, David L. *Langmuir*. **2005**, *21*, 11061.

6. Friend, C. M.; Stein, Judith; Muetterties, E. L. *Journal of the American Chemical Society*. **1981**, *103*, 767.

7. Friend, C. M.; Muetterties, E. L.; Gland, John. *Journal of Physical Chemistry*. **1981**, *85*, 3256.

8. Semancik, Steve; Haller, Gary L.; Yates, John T., Jr. *Journal of Chemical Physics*. **1983**, *78*, 6970.

9. Ceyer, S. T.; Yates, J. T., Jr. *Journal of Physical Chemistry*. **1985**, *89*, 3842.

10. Robertson, Mitchell J.; Angelici, Robert J. *Langmuir*. **1994**, *10*, 1488.

11. Shih, Kuo-Chen; Angelici, Robert J. *Langmuir*. **1995**, *11*, 2539.

12. Ontko, Allyn C.; Angelici, Robert J. *Langmuir*. **1998**, *14*, 1684.

13. Ontko, Allyn C.; Angelici, Robert J. *Langmuir*. **1998**, *14*, 3071.

14. Henderson, Jason I.; Feng, Sue; Ferrence, Gregory M.; Bein, Thomas; Kubiak, Clifford P. *Inorganica Chimica Acta*. **1996**, *242*, 115.

15. Huc, Vincent; Bourgoin, Jean-Philippe; Bureau, Christophe; Valin, Francoise; Zalczer, Gilbert; Palacin, Serge. *Journal of Physical Chemistry, B*. **1999**, *103*, 10489.

16. Chen, J.; Calvet, L. C.; Reed, M. A.; Carr, D. W.; Grubisha, D. S.; Bennett, D. W. *Chemical Physics Letters*. **1999**, *313*, 741.

17. Swanson, Sally A.; McClain, Richard; Lovejoy, Katherine S.; Alamdari, Neda B.; Hamilton, Jeremy S.; Scott, J. Campbell. *Langmuir*. **2005**, *21*, 5034.

18. McDonagh, Andrew M.; Zareie, Hadi M.; Ford, Michael J.; Barton, Christopher S.; Ginic-Markovic, Milena; Matisons, Janis G. *Journal of the American Chemical Society*. **2007**, *129*, 3533.

19. DuBose, David L.; Robinson, Randall E.; Holovics, Thomas C.; Moody, David R.; Weintrob, Edward C.; Berrie, Cindy L.; Barybin, Mikhail V. *Langmuir*. **2006**, *22*, 4599.

20. Robinson, Randall E.; Holovics, Thomas C.; Deplazes, Stephan F.; Powell, Douglas R.; Lushington, Gerald H.; Thompson, Ward H.; Barybin, Mikhail V. *Organometallics*. **2005**, *24*, 2386.

21. Holovics, Thomas C.; Robinson, Randall E.; Weintrob, Edward C.; Toriyama, Masaharu; Lushington, Gerald H.; Barybin, Mikhail V. *Journal of the American Chemical Society*. **2006**, *128*, 2300.

22. Toriyama, Masaharu; Maher, Tiffany R.; Holovics, Thomas C.; Vanka, Kumar; Day, Victor W.; Berrie, Cindy L.; Thompson, Ward H.; Barybin, Mikhail V. *Inorganic Chemistry*. **2008**, *47*, 3284.

23. Huang, X.; Zhao, M. T.; Janiszewska, L.; Prasad, P. N. *Synthetic Metals*. **1988**, *24*, 245-253.

24. Gaussian 03, Revision C.02, M. J. Frisch, G. W. Trucks, H. B. Schlegel, G. E. Scuseria, M. A. Robb, J. R. Cheeseman, J. A. Montgomery, Jr., T. Vreven, K. N. Kudin, J. C. Burant, J. M. Millam, S. S. Iyengar, J. Tomasi, V. Barone, B. Mennucci, M. Cossi, G. Scalmani, N. Rega, G. A. Petersson, H. Nakatsuji, M. Hada, M. Ehara, K. Toyota, R. Fukuda, J. Hasegawa, M. Ishida, T. Nakajima, Y. Honda, O. Kitao, H. Nakai, M. Klene, X. Li, J. E. Knox, H. P. Hratchian, J. B. Cross, V. Bakken, C. Adamo, J. Jaramillo, R. Gomperts, R. E. Stratmann, O. Yazyev, A. J. Austin, R. Cammi, C. Pomelli, J. W. Ochterski, P. Y. Ayala, K. Morokuma, G. A. Voth, P. Salvador, J. J. Dannenberg, V. G. Zakrzewski, S. Dapprich, A. D. Daniels, M. C. Strain, O. Farkas, D. K. Malick, A. D. Rabuck, K. Raghavachari, J. B. Foresman, J. V. Ortiz, Q. Cui, A. G. Baboul, S. Clifford, J. Cioslowski, B. B. Stefanov, G. Liu, A. Liashenko, P. Piskorz, I. Komaromi, R. L. Martin, D. J. Fox, T. Keith, M. A. Al-Laham, C. Y. Peng, A. Nanayakkara, M. Challacombe, P. M. W. Gill, B. Johnson, W. Chen, M. W. Wong, C. Gonzalez, and J. A. Pople, Gaussian, Inc., Wallingford CT, 2004.

25. a) Miehlich, Burkhard; Savin, Andreas; Stoll, Hermann; Preuss, Heinzwerner. *Chemical Physics Letters*. **1989**, *157*, 200; b) Lee, Chengteh; Yang, Weitao; Parr, Rboert G. *Physical Review B*. **1988**, *37*, 785.

26. Seminario, J. M.; Zacarias, A. G.; Tour, J. M. *Journal of the American Chemical Society*. **1999**, *121*, 411.

27. Schierbaum, K. –D.; Weiss, T.; Thoden van Velzen, E. U.; Engbersen, J. F. J.; Reinhoudt, D. N.; Göpel, W. *Science*, **1994**, *265*, 1413.

28. Thoden van Velzen, E. U.; Engbersen, J. F. J.; Reinhoudt, D. N. *Journal of the American Chemical Society*, **1994**, *116*, 3597.

29. Lin, S.; McCarley, R. L. *Langmuir*, **1999**, *15*, 151.

30. Ito, Yoshihiko; Kobayashi, Kazuhiro; Saegusa, Takeo. *Journal of Organometallic Chemistry*. **1986**, *303*, 301.

Appendix 1

IV. Adventures in the Development of Novel Chemistry Labs for Foundations of Chemistry Honors

IV.1. Introduction

As part of the educational and outreach activities of Prof. Barybin's NSF Career grant, five new laboratory experiments were developed for the two semester sequence of Foundations of Chemistry – Honor's labs. The five laboratory exercises are described herein, including background information and the experimental design used to enable successful implementation of these new multi-week experiments. The new labs were incorporated into the Fall 2007 and Spring 2008 semesters for the first trial. In class comments and end of semester course evaluations were used to modify the experiments for the second trial in the Fall 2008 and Spring 2009 semesters.

IV.2. Chemistry and Art

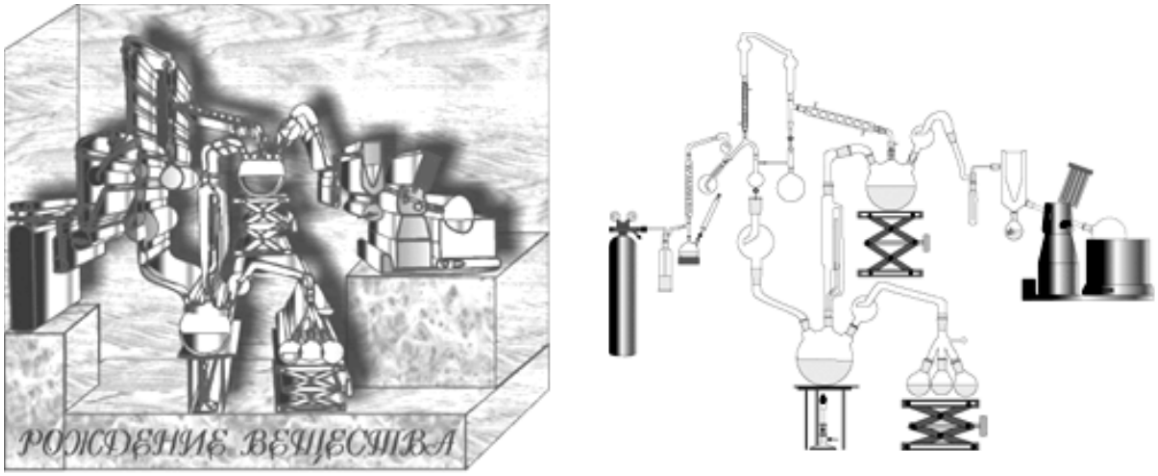

Figure IV.1. Representations of "Birth of a Substance" glassware sculpture by M. Tsivel.

The initial proposal for "Chemistry and Art" focused on introducing chemistry glassware and techniques from the perspective of art. The original plan was to use

ChemArt Deluxe software to aid the students in making their own "glass" sculptures from chemical equipment, with the sculptures obeying the intended use of the glassware. An example of such a sculpture, in Figure IV.1, is "Birth of a Substance" by M. Tsivel. The proposed experiment required students to first familiarize themselves with common glassware used in a synthetic chemistry lab, learn the proper function and usage of the glassware and then design an assembly of their own based on their knowledge of glassware.

Due to difficulties in transferring the large number of files to students and desiring a more hands-on approach, the experiment was modified for implementation into the lab setting. In the first year of the experiment, glassware obtained from a synthetic research lab was assembled at five different stations in the lab room. Station 1 consisted of items the students would find in the general chemistry lab: a beaker, an Erlenmeyer flask, a watch glass, a graduated cylinder, a stirring rod, a glass funnel, a test tube and a Bunsen burner. Station 2 was made up of glassware the students would see in an organic chemistry teaching lab: a ceramic Buchner funnel, a filter flask, a glass fritted funnel, a separatory funnel, and a Barrett distillation receiver. Station 3 consisted of a glass assembly used for Soxhlet extractions, shown in Figure IV.2. Station 4 was an example of a long-path distillation assembly, pictured in Figure IV.3. Station 5 contained a glassware assembly that showed a synthetic reaction setup with a mechanical stirrer, an addition funnel and a reflux condenser, demonstrated by Figure IV.4. Students were provided with various resources for identifying each piece of glassware.[1-4] Students were instructed to draw all glassware/assemblies in their lab notebooks, identify each individual piece of glassware and determine the proper usage for each piece of glassware.

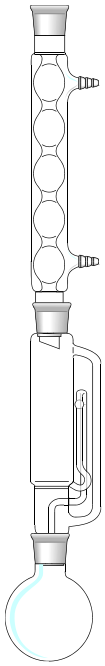

Figure IV.2. Example of a Soxhlet assembly used in Station 3 of Chemistry and Art.

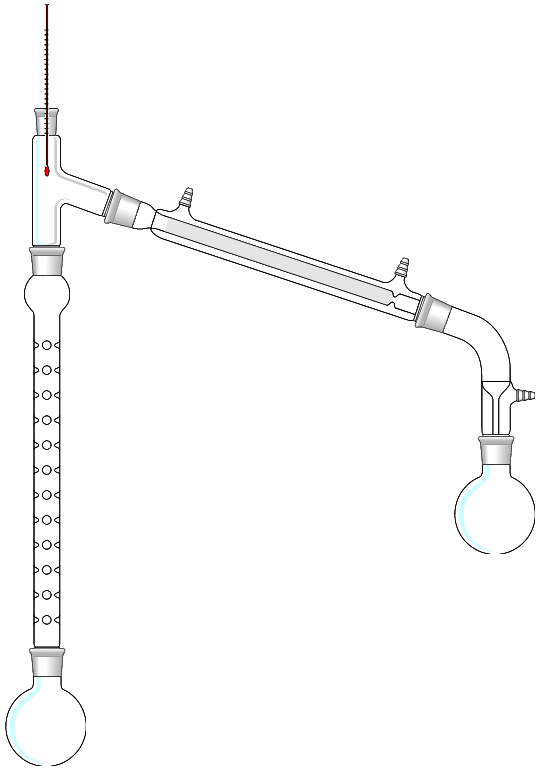

Figure IV.3. Representation of the long-path distillation assembly for station 4.

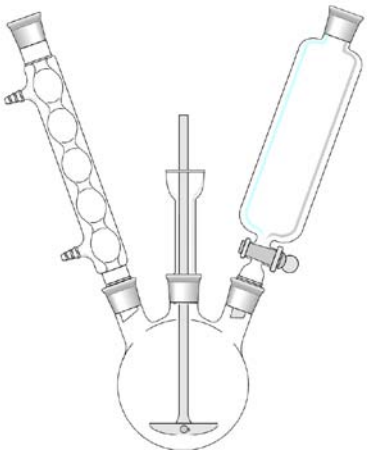

Figure IV.4. Synthetic reaction assembly demonstrated by station 5 of Chemistry and Art.

The following lab session, six new stations were assembled in which all the same glassware was used from the previous session, but the pieces were assembled incorrectly to create “sculptures”. The students were asked to identify the improperly used pieces. The students were also provided with clip-art files of different glassware that they could use to make their own “sculptures”. The clip-art was purchased from ChemSW. Pictures of the various sculptures are shown in Figure IV.5.

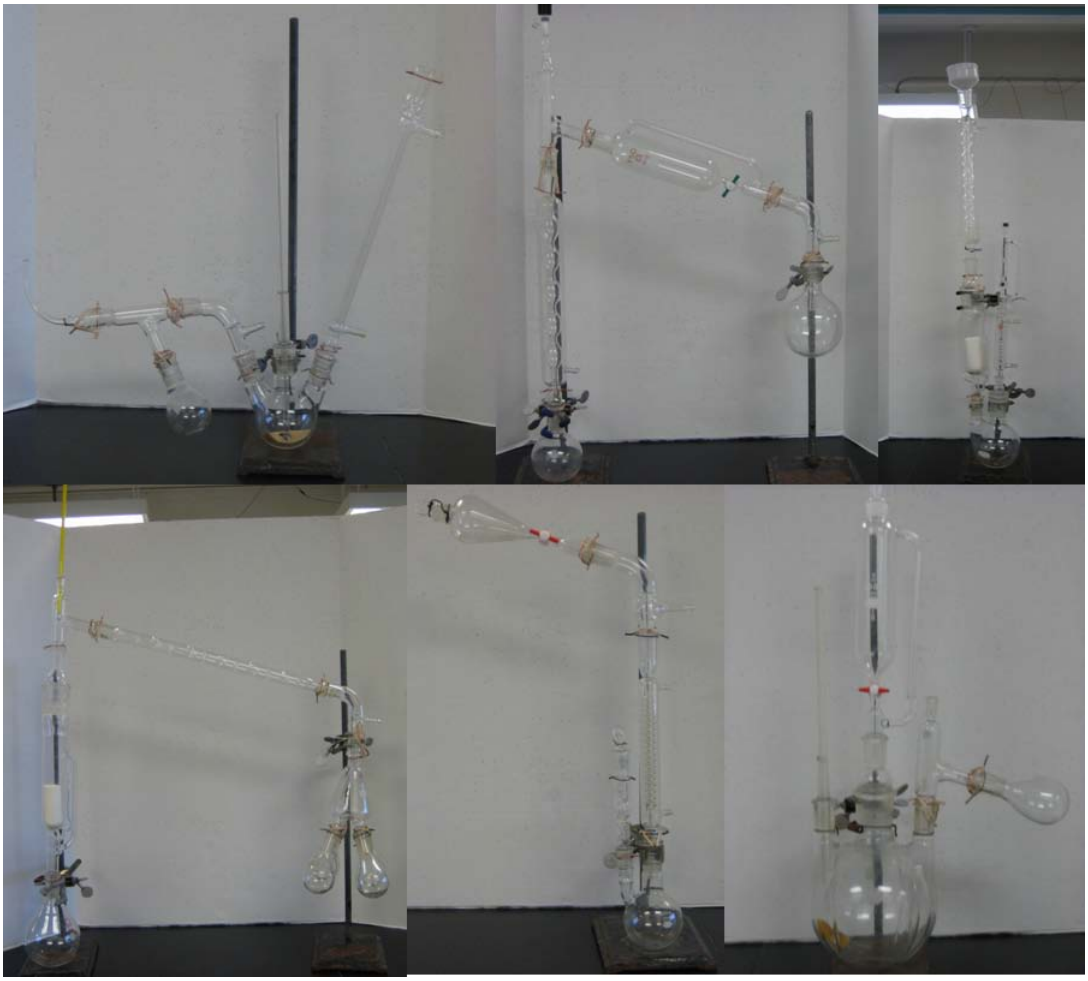

Figure IV.5. Six stations used in the second session of Chemistry and Art lab.

Although during the lab sessions, the students appeared to enjoy the process of drawing the assemblies and identifying glassware, the lab was not conducive to writing a formal report, and the students reported being frustrated with the process of writing a lab report and trying to make assemblies out of the clip-art. In end of semester course evaluations, students commented on a lack of cohesion between the glassware used in the assemblies and glassware used during the remainder of the semester.

During the Fall 2008 semester, modifications were made to correct some of the difficulties and address the comments students made. Because the lab occurs as the first lab session, the students were introduced to the various materials that would be available

to them for the remainder of the semester, both glassware and instrumentation. Students were asked to examine all three drawers they were assigned for the semester. For the glassware drawer, students were instructed to draw pictures of each different type of glassware and identify each piece as well as provide a general description of how the glassware is used, focusing primarily on the differences between each. Several stations were also assembled around the room to provide students with an opportunity to see glassware and instrumentation in the context of how the materials would be used during the semester. Station 1 consisted of a standard titration setup using a buret, a beaker, a pH probe and temperature probe (both connected to the Vernier lab box and interacting with LoggerPro on the computer), a stir plate and a stir bar. Station 2 had several volumetric pipets and a volumetric flask with a colored solution in the flask. The students were instructed as to the appropriate method of filling a volumetric flask and the technique of using a volumetric pipet to transfer a known volume of liquid. Station 3 had two different colored solution and an OceanOptics spectrophotometer connected to the OOBase software on the computer. Students could transfer solutions into cuvettes and measure the absorbance spectrum of the precalibrated instrument.

The second lab session during the Fall 2008 semester introduced "Art" into chemistry by allowing students to use various chemical drawing tools to view molecules from different angles, similar to works done by the artists in pictures shown in Figure IV.6, Figure IV.7, and Figure IV.8. Students were instructed to visit the Molecule of the Day website[7], select one of the molecules from the past week and then draw the molecule using both ChemBioDraw Ultra 11.0 and ChemBio3D Ultra 11.0.[9] The students were shown a variety of the imaging tools available in both computer programs, including the

various viewing modes in ChemBio3D. Once the students were familiarized with the computer programs, they were asked to design their own molecules and view the structures in both ChemBioDraw and ChemBio3D. Students made molecules that looked like flowers, turtles, snowflakes and many other creations.

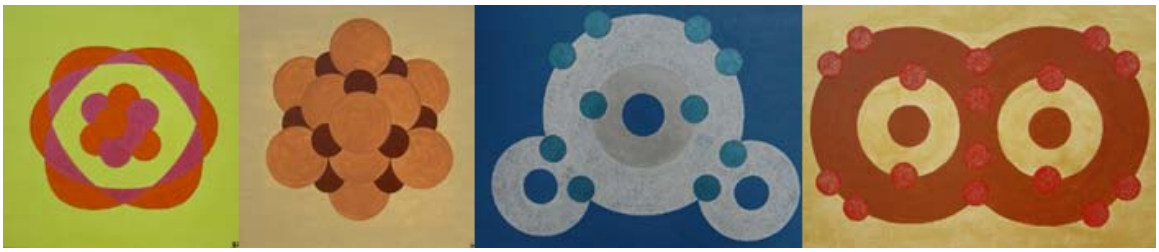

Figure IV.6. Examples of images used to stimulate students in the second session of Chemistry and Art 2008, from Sarah at artofchemistry.com.[5]

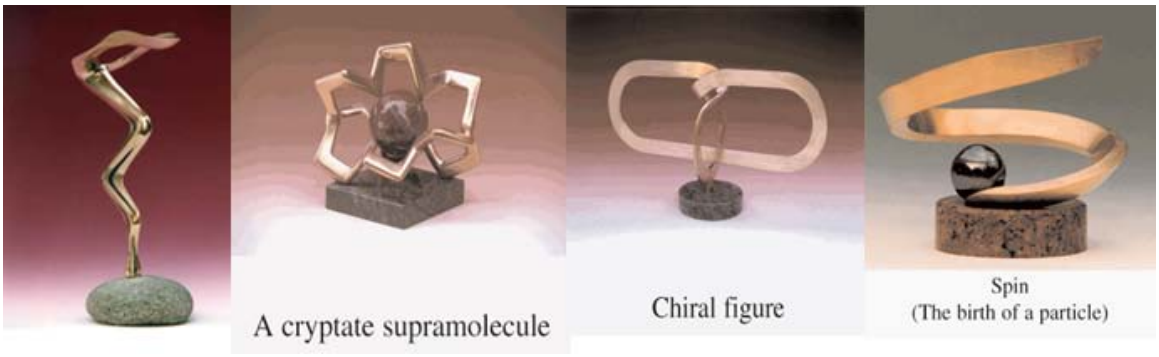

Figure IV.7. Examples of images used in the second session of Chemistry and Art, sculptures by Bela Vizi.[6]

Figure IV.8. Example of an image used in the second session of Chemistry and Art, sculpture by Robert Chambers.[7]

The student feedback during the lab sessions indicated a stronger enthusiasm for the modified experiments than previously observed for any of the general chemistry experiments. No formal report was required, as the process didn't allow for a formal write up that is typically required. Over the long term, students demonstrated a much better understanding of what tools were available to use during the remainder of the semester compared to classes previously taught.

IV.3. Tuning Colors Through Substitution

The proposed experiment titled "Tuning Colors through Substitution" was designed to compare colorless naphthalene and naphthalene derivatives to deep blue colored azulene and azulene derivatives. The azulene and naphthalene compounds were donated by the research lab of Prof. Misha Barybin. The purpose of the lab is to relate molecular orbitals (MOs), particularly Frontier MOs, to energy of light absorbed by colored molecules.

Figure IV.9. Numbering scheme of azulene.

Robert Liu reported in 2002 on the unique properties of colorful azulene and azulene derivatives in relation to the colorless isomer naphthalene.[10] The deep blue color of azulene has been attributed to the nonalternant aromatic nature of this molecule.[10] Comparing the highest occupied molecular orbital (HOMO) and the lowest unoccupied

molecular orbital (LUMO) of azulene versus naphthalene, see Figure IV.10, it can clearly be seen that the location of electron density of the HOMO is quite different from that of the LUMO in azulene where as the location of electron density of the HOMO and LUMO of naphthalene are identical. The coincident nature of orbital contributions between the HOMO and LUMO cause naphthalene to have a greater energy gap between these two orbitals, while azulene has an energy gap that falls in the visible region of the electromagnetic spectrum. Liu reported on color differences of substituted azulenes dependent upon the electron donating and withdrawing character of the substituent.[10] Figure IV.9 demonstrates the numbering scheme used for naming of azulene derivatives.

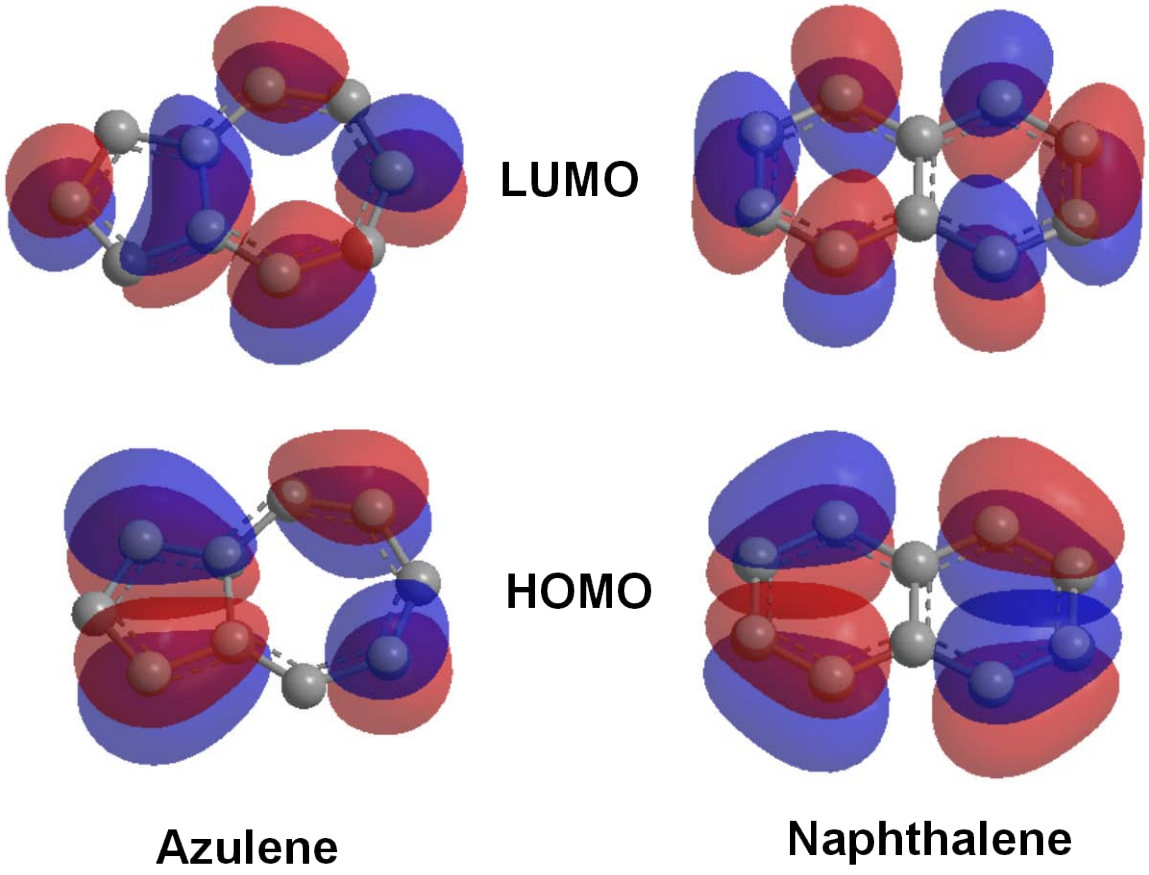

Figure IV.10. Extended Huckel models of the HOMO and LUMO of azulene and naphthalene from ChemBio3D software.[9]

To introduce the concepts and tools needed for this experiment, the lab was split into three sessions. The textbook used for the associated lecture course of Foundation of Chemistry – Honors covers molecular orbital theory fairly early, so the concepts are not entirely foreign to the students, and the three sessions were aligned with the lecture course to complement the text. For the first session, students were instructed to use ChemBioDraw and ChemBio3D to discover information about the molecular orbitals of several aromatic compounds, benzene, naphthalene, anthracene and azulene. The students drew each of the four molecules in ChemBioDraw and in ChemBio3D. In ChemBio3D, they used the Extended Huckel calculation tools to calculate molecular orbitals and then were able to view these surfaces in the program. The molecular orbital calculations included calculations of energy levels for each of the molecular orbitals. Students were asked to draw the HOMO and LUMO of each molecule and record the energy assigned to each of these MO levels. Students were then asked to calculate an energy difference between the HOMO and LUMO and convert the value to wavelength. Then students collected actual absorbance spectra of the 4 molecules in heptane using an Ocean Optics spectrophotometer. Students quickly recognized that the observed experimental data were inconsistent with the predicted quantitative data from the Huckel calculations.

Neither benzene nor naphthalene exhibited a peak in the visible region, while anthracene showed a peak at the edge of the visible region, around 360 nm. Azulene displayed absorbance peaks between 500 and 800 nm, with some interesting features in the region from 500 to 700 nm relating to vibrational transitions. Students were asked to compare the absobance spectra values to the predicted energy values. One observation

that revealed the limitations of the Huckel approach to molecular orbital calculations was that the predicted energy gap for naphthalene and azulene were identical, due to the fact that both these molecules have the same number of π-electrons. Students also observed that the molecular orbitals for all the benzene based molecules demonstrated electron density on the same atoms while azulene was characterized as shown in Figure IV.10. Instructions to students focused on explaining the limitations of the Huckel MO theory as a quantitative tool despite the reliable qualitative description of molecular orbitals.

The second and third lab sessions focused solely on the collection of absorbance spectra for azulene and naphthalene derivatives. In the second session, students investigated monosubstituted azulene and naphthalene compounds while in the third session they studied polysubstituted azulenes. In the Fall 2007 semester, all solutions were made in heptane and only heptane soluble compounds were used. In the Fall 2008 semester, ethanol was used as the solvent with cuvettes that tolerated polar solvents, to allow for more compounds to be used. After data collection during the second session, students were instructed to look for any trends in the data. With some guidance, students analyzed the data according to whether the HOMO or LUMO of azulene would be affected by the substituent (even or odd substitution position) and whether the wavelength of maximum absorbance moved to higher or lower energy. After reviewing the data, the students observed some very interesting trends and with a brief explanation from the Liu paper, could determine which substituents were electron donating and which were electron withdrawing. Through discussion, students agreed that destabilization of a molecular orbital would be caused by an electron donating substituent, while stabilization

of a molecular orbital would be caused by an electron withdrawing substituent. The students then deduced the following scenarios:

1. If the position of substitution is even, then the LUMO would change in energy.
    a. If the LUMO goes up in energy, the HOMO-LUMO gap would be larger and therefore the λ_{max} would be smaller. This would be caused by an electron donating substituent.
    b. If the LUMO goes down in energy, the HOMO-LUMO gap would be smaller and the λ_{max} would be larger. This would be caused by an electron withdrawing substituent
2. If the position of substitution is odd, then the HOMO energy would change.
    a. If the HOMO goes up in energy, the HOMO-LUMO gap would be smaller and λ_{max} would be larger, caused by an electron donating substituent.
    b. If the HOMO goes down in energy, the HOMO-LUMO gap would be larger and λ_{max} would be smaller, caused by an electron withdrawing substituent.

Using this analysis, students identified the different substituents as either electron donating or withdrawing and based on the magnitude of the change in the wavelength, the degree of this type of character. During the third session, students then used polysubstituted azulene derivatives to determine which substituents had the most impact and if the effect on the HOMO-LUMO energy gap was an additive type feature.

Student feedback during the lab sessions indicated that they really enjoyed the experiment. They reported having a better understanding of molecular orbital theory and the importance of this theory to chemists. In the end of semester evaluations, many students indicated that the Tuning Colors lab was their favorite because it overlapped so well with the course and they were able to visualize the concept and explain the concept more clearly at exam time. The students appeared to have gained a much stronger understanding of the relationship between wavelength and energy than observed by students in previous courses. A list of the compounds used and some of the data obtained are presented in Table IV.1.

Table IV.1. Naphthalene and azulene derivatives used during Tuning Colors through Substitution.

1-naphthanoic acid	2-(azulen-1-yl)acetic acid
2-methoxynaphthalene	1-isocyanatoazulene
2-formamidonaphthalene	2-(azulen-1-yl)acetonitrile
2-isocyanonaphthalene	methyl azulene-1-carboxylate
2-naphthanoic acid	1-formamidoazulene
2-bromonaphthalene	azulene-1-carbonyl azide
1-methylazulene	2-chloroazulene
azulene-1-carbaldehyde	2-aminoazulene
1-isocyanoazulene	4-formamidoazulene
1-chloroazulene	4-isocyanoazulene
1-nitroazulene	5-isocyanatoazulene
1-(azulen-1-yl)-trifluoroethanone	5-formamidoazulene
2-formamidoazulene	5-isocyanoazulene
2-methylazulene	5-nitroazulene
2-isocyanoazulene	5-azulenoic acid
6-isocyanoazulene	2-(azulen-6-yl)acetic acid
6-aminoazulene	6-formamidoazulene
1,3-diisocyanatoazulene	1,3-diethoxycarbonylazulene
1,3-dimethoxycarbonylazulene	1,3-di-tert-butylazulene
azulene-1,3-dicarbonyl azide	1,3,5-tribromoazulene
1,3-dimethylazulene	azulene-2,6-dicarbonyl azide

1,3-dichloroazulene	2,6-azulenoic diacid
1,1'-(azulene-1,3-diyl)bis(2,2,2-trifluoroethanone)	4,6,8-trimethylazulene
1,3-dibromoazulene	1,3-di-tert-butyl-5-nitroazulene
N-(1,3-di-tert-butylazulen-5-yl)formamide	1,3-diethoxycarbonyl-6-isocyanoazulene
1,3-di-tert-butyl-5-isocyanoazulene	2-amino-1,3-diazulenoic acid
1,3-diethoxycarbonyl-6-bromoazulene	2-isocyano-1,3-dimethylazulene
1,3-diethoxycarbonyl-2-aminoazulene	1-bromo-3-nitroazulene
1,3-diethoxycarbonyl-2-formamidoazulene	1-methyl-3-nitroazulene
1,3-diethoxycarbonyl-2-isocyanoazulene	4,6,8-trimethyl-1-nitroazulene
1,3-diethoxycarbonyl-2-chloroazulene	4,6,8-trimethyl-1-isocyanoazulene
1,2,3-triphenyl-6-aminoazulene	2,4,6,8-tetramethyl-1-nitroazulene
1,2,3-triphenyl-6-formamidoazulene	2,4,6,8-tetramethyl-1-isocyanoazulene
1,2,3-triphenyl-6-isocyanoazulene	

Table IV.2. Collected data for Tuning Colors through Substitution in Fall 2007 semester.

Compound	**Wavelength**	**Compound**	**Wavelength**
Azulene	580	4,6,8-trimethylazulene	548
5-azulenoic acid	565	1,3-di-tert-butyl-5-nitroazulene	619
azulene-1-carbaldehyde	542	2-aminoazulene	480
1-methylazulene	526	azulen-1-yl benzoate	609
methyl azulene-1-carboxylate	545	5-formamidoazulene	614
1,3-dimethoxycarbonyl-azulene	512	1-formamidoazulene	629
1,3-dimethoxycarbonyl-azulene	513	2-formamidoazulene	539
azulene-1-carbonyl azide	533	4-formamidoazulene	555
azulene-1,3-dicarbonyl azide	495	1,3-dibromoazulene	624
1-(azulen-1-yl)-trifluoroethanone	526	1,3-dichloroazulene	639
1,1'-(azulene-1,3-diyl)bis(2,2,2-trifluoroethanone)	481	1,3,5-tribromoazulene	652

Compound	Wavelength	Compound	Wavelength
1-chloroazulene	416	1-isocyanoazulene	588
1-isocyanatoazulene	412	1,3-di-tert-butyl-5-isocyanoazulene	646
4-isocyanoazulene	605	2-isocyanoazulene	563
1-nitroazulene	532	2-(azulen-1-yl)acetonitrile	584
1-(azulen-1-yl)-2-phenyldiazene	430	1,3-dimethylazulene	580
2-(azulen-1-yl)acetic acid	591	1-isocyano-2,4,6,8-tetramethylazulene	539
1,3-di-tert-butylazulene	631	N-(1,3-di-tert-butylazulen-6-yl)formamide	664
2-methylazulene	562	1,3-dimethoxycarbonyl-2-isocyanoazulene	536
1,3-dimethoxycarbonyl-2-chloroazulene	501	1,3-dimethoxycarbonyl-2-formamidoazulene	475
1,3-dimethoxycarbonyl-2-aminoazulene	426	2-isocyano-1,3-dimethylazulene	621
4,6,8-trimethyl-1-nitroazulene	514	2,4,6,8-tetramethyl-1-nitroazulene	513
4,6,8-trimethyl-1-isocyanoazulene	573	1,3-dimethoxycarbonyl-6-bromoazulene	514
1,2,3-triphenylazulen-6-amine	533	6-isocyano-1,2,3-triphenylazulene	544
N-(1,2,3-triphenylazulen-6-yl)formamide	633		

Figure IV.11. Solutions of azulene derivatives used in Tuning Colors through Substitution.

IV.4. Hydrogen Bonding Interaction – The "Almighty" Weak Bond

The proposed hydrogen bonding lab was designed to investigate the "odd-even effect" on melting points of polyamides. As demonstrated in Figure IV.12, polyamides with an even number of carbon atoms in the polymer backbone possess more potential for hydrogen bonding interactions than polyamides with an odd number of carbon atoms in the polymer backbone. The impact of hydrogen bonding should be observed in the melting points of the various polymers, to be observed during the lab.

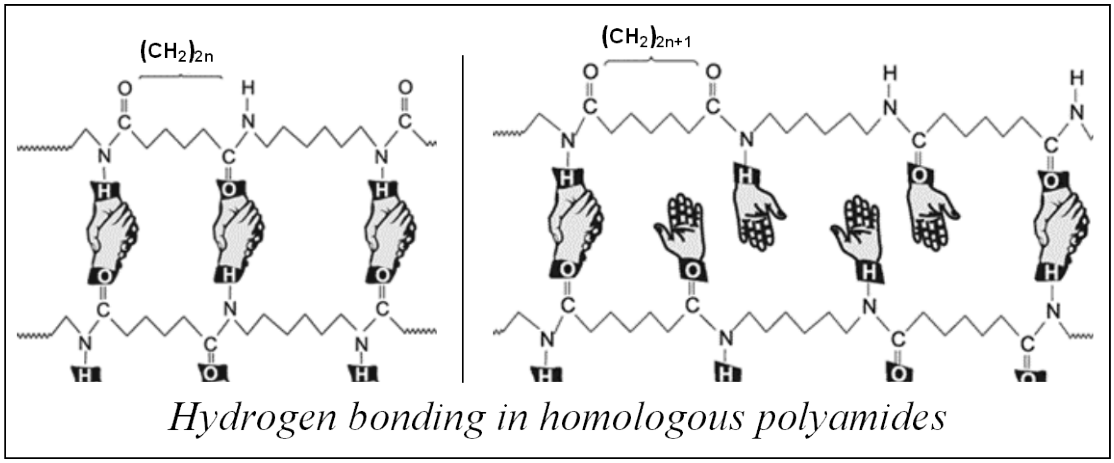

Figure IV.12. Example of potential hydrogen bonding interactions in polyamides of even carbon chain length and odd carbon chain length, courtesy of Prof. Barybin.

In Fall of 2007, implementation of a two session experiment relating to hydrogen bonding interactions was pursued. For the first lab session, students used various solvents, graduated cylinders and a Vernier temperature probe connected to LoggerPro software to determine changes in the combined volume and temperature upon addition of equal quantities of the various solvents. Students designed a data table, shown in Table IV.3, in which they recorded the final volume of the two solvents, the change in temperature from room temperature, and observations regarding miscibility.

Table IV.3. Data table used for collection of solvent mixing data.

Solvent	Isopropanol	Ethanol	Acetone	Dichloromethane	Heptane
Water					
Isopropanol	X				
Ethanol		X			
Acetone			X		
Dichloromethane				X	
Heptane					X

The second part of the first session of the hydrogen bonding experiment focused on determining melting points of various polyamides: nylon 6/9, nylon 6/10, nylon 6/12, nylon 4/6, nylon 6, nylon 11, and nylon 12. The resins were purchased from commercial

sources, flattened with a KBr pellet press and sliced into slivers using a razor blade prior to the lab period. During lab, students obtained a sliver and inserted it into a melting point capillary, then recorded the melting point on a Mel-Temp apparatus. Polymer formulas and literature data of melting points are presented in Table IV.4. Students were instructed to use ChemBioDraw to determine the potential for hydrogen bonding interactions of each polyamide.

Table IV.4. Melting point data for various polyamides.

Name	Formula	Melting point, °C	Even/Odd?
Nylon 4/6	$[HN(CH_2)_4NHCO(CH_2)_4CO]_n$	>300	Even
Nylon 6	$[HNCO(CH_2)_5]_n$	210-220	Odd
Nylon 6/6	$[HN(CH_2)_6NHCO(CH_2)_4CO]_n$	255-265	Even
Nylon 6/9	$[HN(CH_2)_6NHCO(CH_2)_7CO]_n$	207-215	Odd
Nylon 6/10	$[HN(CH_2)_6NHCO(CH_2)_8CO]_n$	220-227	Even
Nylon 6/12	$[HN(CH_2)_6NHCO(CH_2)_{10}CO]_n$	215-240	Even
Nylon 11	$[HNCO(CH_2)_{10}]_n$	189-192	Even
Nylon 12	$[HNCO(CH_2)_{11}]_n$	172-180	Odd

The second lab session for hydrogen bonding in Fall 2007 was adapted from Nyasulu and Macklin and focused on determining the pKa values of two isomeric organic acids, maleic and fumaric acid.[11] Maleic acid, under standard potentiometric titration conditions with sodium hydroxide, exhibits two distinct equivalence points and therefore two pKa values, while fumaric acid exhibits a very steep single equivalence point and only one discernable pKa value. Using ChemBioDraw and ChemBio3D, the students made models of both fumaric and maleic acid and tried to determine what types of intermolecular forces each compound could participate in. The class was split into groups of four students or less, so each group was given either fumaric or maleic acid to analyze. After predicting types of intermolecular forces involved with each molecule, the students acquired melting points for the assigned acid. The students made approximately

0.025M solutions of their assigned acid and titrated 25mL aliquots of the solution with 0.05M NaOH using pH probes connected to LoggerPro software to collect the data.

Lab reports indicated these lab exercises strongly influenced student understanding of intermolecular forces, particularly hydrogen-bonding interactions. Students reported during lab sessions that the melting point determination of the polyamides was quite difficult, as sometime the polyamides would discolor prior to melting.

In the Fall of 2008, the experiment was condensed to a one week session focused solely on the examination of fumaric and maleic acids. Due to the difficulty in preparing polyamide samples for melting point determination and the problems reported by students with this task, this part of the experiment was temporarily removed. Potential solutions to improve the polyamide experiment would be to allow each group of students to make an even polyamide and an odd polyamide and then determine the melting point of that polymer and share data. The synthesis would provide additional hands-on activities that was lacking from the first implementation of this experiment. Making the polymers in the class would also allow students to pull the strands more finely and could make acquiring melting point data less challenging.

IV.5. Green Chemistry – Solar Cells

The original proposal for a "green" chemistry experiment in the Foundations of Chemistry Honors lab was to expand the "Construction of Solar Energy Devices with Natural Dyes" by Prof. John Warner.[12] The primary goal of this experiment was to introduce the concepts of alternative energy resources and renewable feedstocks.

Another goal of the experiment was to stress the importance of environmental processes in scientific research.

The procedure described by Prof. Warner was sufficiently detailed to reproduce in the teaching lab.[12] The first semester of implementation of this experiment was the Spring of 2008. Students combined titanium oxide (P25) with trimesic acid in a mortar and pestle and ground with water until the solution was slightly thickened (approximately 5 minutes). Conductive glass (TEC 15, 25 x 25 mm squares) was purchased from Hartford Glass Company. Tape was used to mask out an area on the conductive side of the glass and a glass stirring rod was used to smoothly apply a thin, almost transparent, layer of the titanium oxide mixture, illustrated in Figure IV.13. The coated glass was dried in an oven for 30-60 minutes at 65°C.

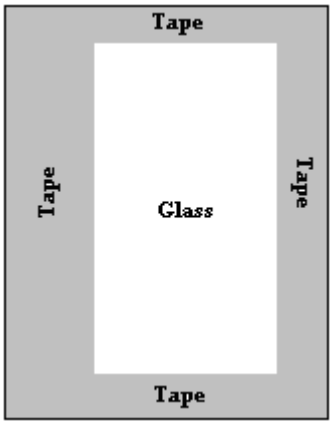

Figure IV.13. Diagram of tape mask on a piece of conductive glass.

An electrolyte solution was made in advance of the lab using 8.3g (0.5 M) of potassium iodide and 0.64 g (0.05 M) of iodine in water-free ethylene glycol in a 100 mL volumetric flask. Approximately 4 pieces of frozen blackberries were placed in a petri dish with 10 mL of water. The blackberries were crushed by hand to get a colored solution. The room temperature titanium oxide coated glass was placed coated side down

in the blackberry juice for 10 minutes. A second piece of conductive glass was annealed in the flame of a candle on the conductive side only (a Bunsen burner caused the glass to crack). The titanium electrode was removed from the berry juice, rinsed with water, rinsed with ethanol and then blotted dry with a KimWipe. A piece of parafilm was removed from the paper backing and placed gently over the titanium electrode. The shape of the titanium coating was transferred to the parafilm and the cavity was cut out of the parafilm. The parafilm was placed back on the titanium electrode and the parafilm paper backing was used to adhere the parafilm to the glass with out disrupting the coating, as shown in Figure IV.14. The parafilm made a well over the titanium oxide coating, allowing electrolyte solution to be placed into the well.

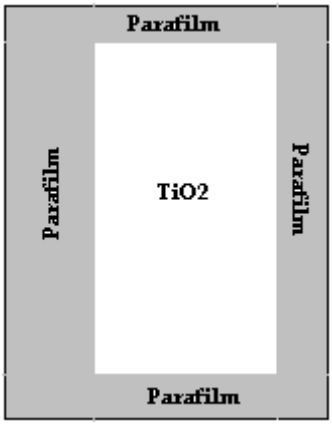

Figure IV.14. Diagram of the parafilm well over the titanium oxide coating on conductive glass.

To assemble the solar cell, students placed 3 drops of electrolyte solution into the well made by the parafilm. The carbon coated electrode was placed in an offset fashion on top of the titanium electrode, illustrated in Figure IV.15. The solar cell assembly was finished with two small binder clips on either side of the assembly to hold all components tightly together. A digital multimeter was used to measure voltage and current of the

assembly in the dark, on exposure to ambient light, and on exposure to sunlight. A light table was provided in case of a cloudy day.

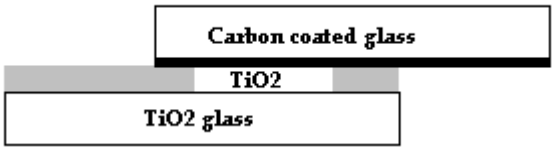

Figure IV.15. Diagram of the offset arrangement of two electrodes used in the construction of a solar cell.

The second session of the multi-session experiment provided students with an opportunity to test several other fruits as dyes for the solar cell. Students were provided with blackberries, blueberries, raspberries and strawberries, as well as the other materials needed to make the solar cells. Students were instructed to develop a hypothesis regarding their expectations and test the hypothesis. Several groups decided to also determine if combining fruits together increased the voltage that could be obtained from the solar cell.

During the second year of implementation, few modifications were made. First, the titanium oxide coated glass pieces were dried on a hot plate rather than a drying oven due to convenience of the hot plate. At the end of the first lab session, students were given an opportunity to decide what they would like to change in the following session to allow for more diverse hypotheses. Several groups wanted to compare the effects of different types of fruits on the output of the solar cell. One group decided to examine food coloring as the dye. Another suggested hypothesis was to vary the size of the titanium oxide region in a controlled fashion and observe the impact on the cell output. A fourth hypothesis was to use different colored light sources to see if that changed the resulting voltage and/or current.

Students were extremely enthusiastic about this experiment. Many of the students enrolled in the course are engineering majors. The comments relating to this experiment indicated that students enjoyed an experiment that related to current topics – particularly alternative energy and renewable resources, as well as an experiment that related to their own future career interests. The students enjoyed posing their own hypothesis and the ability to have an opportunity to be creative in the laboratory.

IV.6. Kinetics of Oscillating Reactions

The final multi-session experiment proposed was a semi-quantitative investigation of the kinetics of oscillating reaction. Oscillating reactions present an interesting discussion relating not only to kinetics, but also, chemical equilibrium, red-ox reactions and catalysis. The original proposal was designed to relate the study of oscillating reactions to oscillations in biological processes such as circadian rhythms, hormone levels, etc.

The first lab session was adapted from Copper and Koubek.[13] Students were asked to investigate the kinetics of a standard iodine clock reaction, using aqueous solutions of 0.06 M potassium iodide, 0.04 M hydrogen peroxide, 0.01 M sodium thiosulfate, a buffer of 1 M acetic acid and 1 M sodium acetate buffer, and a 2% starch solution, versus an acid catalyzed iodine clock reaction, using the above reagents, excluding the buffer and adding 0.50 M nitric acid. This procedure was chosen to allow students to develop skills in determining rate laws of a fairly simple reaction so that these skills could be applied to the oscillating reactions.

Table IV.5. Volumes of reagents used in the non-catalyzed iodine clock reaction.

Trial	KI (mL)	H_2O (mL)	H_2O_2 (mL)	Stock solution (mL)
1	25	30	20	25
2	25	20	30	25
3	25	0	50	25
4	15	10	50	25
5	10	15	50	25

Table IV.6. Volumes of reagents used in the acid-catalyzed iodine clock rection.

Trial	KI (mL)	H_2O (mL)	H_2O_2 (mL)	HNO_3 (mL)	Stock solution (mL)
6	25	0	20	30	25
7	25	10	20	20	25
8	25	20	20	10	25
9	25	25	20	5	25
10	25	30	20	0	25

Students were provided with Table IV.5 and Table IV.6 as the volumes of each reagent needed to acquire the appropriate kinetics data. Students generated their own stock solutions for the reaction. For non-catalyzed reactions, the stock solution was made from 25 mL of sodium thiosulfate, 25 mL of acetic acid/acetate buffer, 25 mL of starch solution diluted in a 250 mL volumetric flask. For the catalyzed reactions, the stock solution consisted of 25 mL of $Na_2S_2O_3$ and 25mL of starch solution diluted in a 250 mL

volumetric flask. All volume measurements of solutions containing sodium thiosulfate were performed with volumetric pipets. All other reagents were measured using graduated cylinders. Students combined the reagents in the order indicated in the table, with the stock solution last in the case of the non-catalyzed reaction and the stock solution and acid added simultaneously as the last reagent for the acid catalyzed reaction, then recorded the time it took for the solution to turn dark blue.

Detailed instructions were provided for the students to analyze the data so that students would be ready for working on the more complicated oscillating reactions. Method one instructions were as follows:

> Determine the rate order with respect to hydrogen peroxide for the non-catalyzed reaction by comparing Trials 1 and 2 in the following equation:
>
> $$\ln\left(\frac{time_2}{time_1}\right) = x\left\{\ln\left(\frac{[H_2O_2]_1}{[H_2O_2]_2}\right)\right\}$$
>
> where x provides the rate order. Similar comparisons for flask 1 and 3, or 2 and 3 will provide the order for hydrogen peroxide. Comparisons of flask 3, 4, and 5 provide the rate order for potassium iodide. Comparing flask 6-9 provide information relating to the acid catalyzed reactions.

Method two instructions made used of plotting the log of concentration of thiosulfate divided by time versus the log of the concentration of peroxide, iodide or nitric acid. By assuming that the amount of thiosulfate in each reaction determines the amount of excess I^- available to create the blue color, the rate order for all other reagents could be determined. The slope of the line provides the reaction order. Following the determination of the rate order using either method, students can determine the rate constant for the non-catalyzed reactions as well as the rate constant for the

iodide/peroxide only term of the combined rate law for the acid catalyzed reaction. Plotting the calculated rate constant for the iodide/peroxide term of the catalyzed reaction versus acid concentration provides a line, whose equation gives the rate constant for the acid term of catalyzed reaction (the slope) and the rate constant for the non-catalyzed reaction (y-intercept). The final rate laws for the non-catalyzed and catalyzed reactions are:

Non-catalyzed: $rate = 0.015[I^-][H_2O_2]$

Catalyzed: $rate = 0.003[I^-][H_2O_2] + 0.41[I^-][H_2O_2][H^+]$

At the end of the lab session, three oscillating reactions were demonstrated for the students. The three reactions were the Briggs-Rauscher (BR), the Belousov-Zhabotinsky (BZ) and a modified BZ (MBZ). The initial concentrations for the demonstrations and student experiments were taken from Shakashiri.[14] For the BR reaction, 3 aqueous solutions were prepared in 250mL volumetric flasks:

1) 4M hydrogen peroxide in water
2) 0.2M potassium iodate in 0.077M sulfuric acid
3) 0.15M malonic acid, 5mL of 2% starch solution and 0.02M manganese sulfate monohydrate.

Solutions 1 and 2 were combined and then solution C was added. The observed color oscillations are from orange to white/colorless to blue. For the BZ reaction, 4 aqueous solutions were used:

1) 0.23M potassium bromate in a 250mL volumetric flask
2) 0.31M malonic acid and 0.059M potassium bromide in a 250 mL volumetric flask

3) 0.019M cerium ammonium nitrate in 2.7M sulfuric acid in a 250mL volumetric flask
4) 1.25 mM ferroin in a 10mL volumetric flask

Solutions 1 and 2 were combined and stirred until colorless. Solution 3 and 4 were added. The oscillations cycled through red, blue, green and purple clear solutions. For the MBZ reaction, 3 aqueous solutions were made in 250mL volumetric flasks:

1) 0.13M potassium bromate in 4.5M sulfuric acid
2) 0.3M citric acid and 5.7×10^{-3} M potassium bromide
3) 0.025 M manganese sulfate monohydrate in 4.5M sulfuric acid

Solutions 1 and 2 were combined and stirred until colorless, approximately 30 minutes. Solution 3 was added. The solution becomes opaque and cycles through colorless and pink. Students observed the three different reactions and determined which one of the three reactions they wanted to study during the next two sessions.

Table IV.7. Volumes of reagents used in each oscillating reaction trial.

Trial	Solution 1 (mL)	Solution 2 (mL)	Solution 3 (mL)	Water (mL)
1	25	25	25	0
2	25	20	25	5
3	25	15	25	10
4	25	10	25	15
5	25	25	20	5
6	25	25	15	10
7	25	25	10	15
8	20	25	25	5
9	15	25	25	10
10	10	25	25	15

In the second lab session, each group of students made the above solutions for their chosen reactions. Students were instructed to run 10 trials for their reaction by combining the volumes indicated in Table IV.7. For the BZ reaction, an additional 10mL solution of 1.25mM ferroin should be added in each trial. Solutions were combined as mentioned for the demonstrations. For the BZ and MBZ reactions, students must wait until the combination of solution 1 and 2 are colorless before continuing with the reaction. Students observed the time for the reaction to being oscillating and then recorded the time of each color change for 5 to 10 minutes. Observations were used to

relate changes in initial concentration to variations in both the “initiation” time and the timing of the color cycles.

For the third lab session, students were provided with additional tools for analyzing their oscillating reaction, including pH probes, temperature probes, conductivity probes, and a UV-vis spectrophotometer. Students could decide which instrument or instruments they want to use to further examine the oscillating reaction kinetics.

In the second year of implementation of the oscillating reactions part of the kinetics experiments, the modified BZ reaction was removed due to the higher concentration of acid required for this reaction. There were significant problems caused by the formation of bromine gas in the modified BZ that were not observed in the other reactions.

At the end of the 2-semester Foundations of Chemistry lab course, both Honors and regular sections, a poster session is held for students to present results on a multiweek project. Students in the Honors course were allowed to choose to present on the solar cell experiment or the oscillating reactions laboratory. The poster session provided an opportunity for the students to present their unique hypotheses in either experiment to other chemistry students, graduate students and departmental faculty.

Students expressed slight frustrations with the oscillating reaction experiments, due to the large quantity of data that they collected. They struggled to determine the best way to process and assemble the data for interpretation. At the same time, students reported they enjoyed running the oscillating reactions themselves, as many had seen them in demonstration shows and were quite curious about the chemistry involved.

Students appeared to develop a strong fundamental knowledge base relating not only to kinetics, reflected in their exams in the lecture course, but also developed better understanding of chemical equilibria based on this experiment.

IV.7. References

1. Ockerman, Herbert W. *Illustrated Chemistry Laboratory Terminology*. CRC Press, Inc. **1991.**

2. Moore, James, A.; Dalrymple, David L. *Experimental Methods in Organic Chemistry*. W.B. Saunders Company. **1971**.

3. Harwood, Laurence M.; Moody, Christopher J.; Percy, Jonathan M. *Experimental Organic Chemistry*. Blackwell Science, Ltd. **1999**.

4. Aikens, David A.; Bailey, Ronald A.; Giachino, Gary G.; Moore, James A.; Tomkins, Reginald P.T. *Integrated Experimental Chemistry: Principles and Techniques*. Vol 1. Allyn and Bacon, Inc. **1978**.

5. Art of Chemistry – Homepage. http://www.artofchemistry.com/ (accessed March 27, 2009).

6. Chemical Mythology (Chemistry in Structures or Chemical Evolution) - Homepage. http://www.mi.sanu.ac.yu/vismath/visbook/vizi/index.html (accessed March 27, 2009).

7. Robert Chambers – Homepage. http://www.robertchambers.com/Index.html (accessed March 27, 2009).

8. Molecule of the Day - Homepage. http://scienceblogs.com/moleculeoftheday/ (accessed March 27, 2009).

9. CambridgeSoft – Homepage. http://chembiofinderbeta.cambridgesoft.com/ (accessed March 27, 2009)

10. Liu, Robert S. *Journal of Chemical Education*. **2002,** *79,* 183.

11. Nyasulu, Frazier W.; Macklin, John. *Journal of Chemical Education*. **2006**, *83*, 770.

12. Warner, John. In *Greener Approaches to Undergraduate Chemistry Experiments*; Kirchhoff, Mary; Ryan, Mary A., Eds. American Chemical Society: Washington, D.C. **2002**.

13. Copper, Christine L.; Koubek, Edward. *Journal of Chemical Education*. **1998**, *75*, 87.

14. Shakhashiri, B. Z. *Chemical Demonstrations: A Handbook for Teachers of Chemistry, vol. 2*; University of Wisconsin Press: Wisconsin, **1985**.

Appendix 2

V. Crystallographic Data for $C_{44}H_{35}Co_2N_3O_{10}V_2$, 1.1a

Table V.1. Atomic coordinates and equivalent isotropic displacement parameters for $C_{44}H_{35}Co_2N_3O_{10}V_2$, 1.1a. U(eq) is defined as one third of the trace of the orthogonalized U_{ij} tensor.

	x	y	z	U(eq)
V(1)	0.156539(18)	0.982566(17)	0.38525(6)	0.02540(14)
C(11)	0.19086(11)	0.90433(11)	0.3842(4)	0.0295(6)
N(11)	0.20981(10)	0.85863(9)	0.3824(3)	0.0314(5)
C(1)	0.23022(11)	0.80371(10)	0.3804(3)	0.0251(5)
C(2)	0.19119(11)	0.75953(11)	0.3808(3)	0.0252(5)
C(6)	0.28863(11)	0.79569(11)	0.3784(3)	0.0258(5)
C(21)	0.12834(11)	0.77082(13)	0.3831(4)	0.0359(6)
C(61)	0.32862(12)	0.84459(12)	0.3768(4)	0.0358(6)
C(1A)	0.22160(11)	1.01408(12)	0.2547(4)	0.0330(6)
O(1A)	0.25888(9)	1.03401(10)	0.1743(3)	0.0482(6)
C(2A)	0.12356(11)	0.96683(11)	0.1387(4)	0.0278(6)
O(2A)	0.10443(8)	0.95956(8)	-0.0059(3)	0.0375(4)
C(3A)	0.08947(11)	0.95387(12)	0.5131(4)	0.0337(6)
O(3A)	0.04908(10)	0.93967(11)	0.5881(3)	0.0536(6)
C(4A)	0.18898(11)	0.99847(11)	0.6317(4)	0.0293(6)
O(4A)	0.20751(8)	1.00916(8)	0.7749(3)	0.0380(5)
C(5A)	0.11913(13)	1.05427(12)	0.3886(4)	0.0357(6)
O(5A)	0.09453(11)	1.09720(10)	0.3946(3)	0.0531(6)
Co(1)	0.069278(15)	0.143466(15)	0.90673(5)	0.02900(14)
C(1B)	0.12102(12)	0.19395(13)	0.7565(5)	0.0447(7)
C(2B)	0.14591(12)	0.13998(14)	0.7809(5)	0.0441(7)
C(3B)	0.15135(11)	0.12995(12)	0.9753(5)	0.0394(7)
C(4B)	0.13043(12)	0.17768(12)	1.0713(4)	0.0367(6)
C(5B)	0.11156(12)	0.21703(12)	0.9359(5)	0.0380(7)
C(6B)	-0.00165(12)	0.13320(15)	0.7542(5)	0.0458(8)
C(7B)	-0.01396(11)	0.16236(12)	0.9215(4)	0.0356(7)
C(8B)	0.00144(11)	0.12714(12)	1.0722(4)	0.0355(6)
C(9B)	0.02350(12)	0.07689(12)	1.0000(5)	0.0416(7)
C(10B)	0.02150(13)	0.08002(13)	0.8047(5)	0.0466(8)

Table V.2. Bond lengths [Å] for $C_{44}H_{35}Co_2N_3O_{10}V_2$, 1.1a.

V(1)-C(5A)	1.919(3)	Co(1)-C(1B)	2.024(3)
V(1)-C(1A)	1.953(3)	Co(1)-C(7B)	2.027(3)
V(1)-C(3A)	1.958(3)	Co(1)-C(9B)	2.029(3)
V(1)-C(4A)	1.962(3)	Co(1)-C(2B)	2.031(3)
V(1)-C(2A)	1.967(3)	Co(1)-C(3B)	2.033(3)
V(1)-C(11)	2.026(3)	Co(1)-C(8B)	2.036(3)
C(11)-N(11)	1.174(3)	Co(1)-C(4B)	2.037(3)

N(11)-C(1)	1.390(3)	C(1B)-C(5B)	1.414(5)
C(1)-C(2)	1.398(4)	C(1B)-C(2B)	1.420(4)
C(1)-C(6)	1.399(4)	C(1B)-H(1B)	0.9500
C(2)-C(6)#1	1.394(3)	C(2B)-C(3B)	1.418(5)
C(2)-C(21)	1.515(4)	C(2B)-H(2B)	0.9500
C(6)-C(2)#1	1.395(3)	C(3B)-C(4B)	1.414(4)
C(6)-C(61)	1.498(4)	C(3B)-H(3B)	0.9500
C(21)-H(21A)	0.9801	C(4B)-C(5B)	1.418(4)
C(21)-H(21B)	0.9800	C(4B)-H(4B)	0.9500
C(21)-H(21C)	0.9799	C(5B)-H(5B)	0.9500
C(61)-H(61A)	0.9800	C(6B)-C(7B)	1.414(4)
C(61)-H(61B)	0.9799	C(6B)-C(10B)	1.422(5)
C(61)-H(61C)	0.9800	C(6B)-H(6B)	0.9500
C(1A)-O(1A)	1.156(3)	C(7B)-C(8B)	1.413(4)
C(2A)-O(2A)	1.144(3)	C(7B)-H(7B)	0.9500
C(3A)-O(3A)	1.149(3)	C(8B)-C(9B)	1.401(4)
C(4A)-O(4A)	1.144(3)	C(8B)-H(8B)	0.9500
C(5A)-O(5A)	1.174(4)	C(9B)-C(10B)	1.402(5)
Co(1)-C(10B)	2.021(3)	C(9B)-H(9B)	0.9500
Co(1)-C(6B)	2.021(3)	C(10B)-H(10B)	0.9500
Co(1)-C(5B)	2.023(3)		

Symmetry transformations used to generate equivalent atoms:
#1 -x+1/2, -y+3/2, z

Table V.3. Angles [°] for $C_{44}H_{35}Co_2N_3O_{10}V_2$, 1.1a.

C(5B)-Co(1)-C(9B)	154.46(14)	H(21A)-C(21)-H(21B)	109.5
C(1B)-Co(1)-C(9B)	163.65(14)	C(2)-C(21)-H(21C)	109.6
C(7B)-Co(1)-C(9B)	68.52(12)	H(21A)-C(21)-H(21C)	109.5
C(10B)-Co(1)-C(2B)	108.13(13)	H(21B)-C(21)-H(21C)	109.5
C(6B)-Co(1)-C(2B)	120.02(14)	C(6)-C(61)-H(61A)	109.5
C(5B)-Co(1)-C(2B)	68.73(12)	C(6)-C(61)-H(61B)	109.4
C(1B)-Co(1)-C(2B)	41.01(13)	H(61A)-C(61)-H(61B)	109.5
C(7B)-Co(1)-C(2B)	154.67(13)	C(6)-C(61)-H(61C)	109.5
C(9B)-Co(1)-C(2B)	126.40(13)	H(61A)-C(61)-H(61C)	109.5
C(10B)-Co(1)-C(3B)	120.46(12)	H(61B)-C(61)-H(61C)	109.5
C(6B)-Co(1)-C(3B)	155.33(13)	O(1A)-C(1A)-V(1)	177.7(2)
C(5B)-Co(1)-C(3B)	68.68(12)	O(2A)-C(2A)-V(1)	177.7(2)
C(1B)-Co(1)-C(3B)	68.97(13)	O(3A)-C(3A)-V(1)	176.7(3)
C(7B)-Co(1)-C(3B)	162.70(13)	O(4A)-C(4A)-V(1)	178.2(2)
C(9B)-Co(1)-C(3B)	108.07(12)	O(5A)-C(5A)-V(1)	177.4(3)
C(2B)-Co(1)-C(3B)	40.86(13)	C(10B)-Co(1)-C(6B)	41.21(14)
C(10B)-Co(1)-C(8B)	68.01(13)	C(10B)-Co(1)-C(5B)	163.24(14)
C(6B)-Co(1)-C(8B)	68.52(13)	C(6B)-Co(1)-C(5B)	124.91(13)
C(5B)-Co(1)-C(8B)	119.72(12)	C(10B)-Co(1)-C(1B)	126.03(15)
C(1B)-Co(1)-C(8B)	154.32(12)	C(6B)-Co(1)-C(1B)	106.78(14)

C(7B)-Co(1)-C(8B)	40.70(12)	C(5B)-Co(1)-C(1B)	40.91(13)
C(9B)-Co(1)-C(8B)	40.31(12)	C(10B)-Co(1)-C(7B)	68.73(12)
C(2B)-Co(1)-C(8B)	163.39(13)	C(6B)-Co(1)-C(7B)	40.89(12)
C(3B)-Co(1)-C(8B)	125.90(13)	C(5B)-Co(1)-C(7B)	106.66(12)
C(10B)-Co(1)-C(4B)	154.84(13)	C(1B)-Co(1)-C(7B)	119.17(12)
C(6B)-Co(1)-C(4B)	162.45(13)	C(10B)-Co(1)-C(9B)	40.49(14)
C(5B)-Co(1)-C(4B)	40.89(12)	C(6B)-Co(1)-C(9B)	68.82(14)
C(5B)-C(4B)-H(4B)	126.1	C(1B)-Co(1)-C(4B)	68.91(13)
Co(1)-C(4B)-H(4B)	126.9	C(7B)-Co(1)-C(4B)	125.11(12)
C(1B)-C(5B)-C(4B)	108.4(3)	C(9B)-Co(1)-C(4B)	120.03(13)
C(1B)-C(5B)-Co(1)	69.58(17)	C(2B)-Co(1)-C(4B)	68.63(13)
C(4B)-C(5B)-Co(1)	70.08(16)	C(3B)-Co(1)-C(4B)	40.67(12)
C(1B)-C(5B)-H(5B)	125.8	C(8B)-Co(1)-C(4B)	107.56(12)
C(4B)-C(5B)-H(5B)	125.8	C(5B)-C(1B)-C(2B)	107.6(3)
Co(1)-C(5B)-H(5B)	126.1	C(5B)-C(1B)-Co(1)	69.51(16)
C(7B)-C(6B)-C(10B)	107.3(3)	C(2B)-C(1B)-Co(1)	69.73(17)
C(7B)-C(6B)-Co(1)	69.80(16)	C(5B)-C(1B)-H(1B)	126.2
C(10B)-C(6B)-Co(1)	69.39(17)	C(2B)-C(1B)-H(1B)	126.2
C(7B)-C(6B)-H(6B)	126.3	Co(1)-C(1B)-H(1B)	126.2
C(10B)-C(6B)-H(6B)	126.3	C(3B)-C(2B)-C(1B)	108.0(3)
Co(1)-C(6B)-H(6B)	126.0	C(3B)-C(2B)-Co(1)	69.66(16)
C(8B)-C(7B)-C(6B)	107.8(3)	C(1B)-C(2B)-Co(1)	69.26(16)
C(8B)-C(7B)-Co(1)	69.97(15)	C(3B)-C(2B)-H(2B)	126.0
C(6B)-C(7B)-Co(1)	69.31(16)	C(1B)-C(2B)-H(2B)	126.0
C(6B)-C(10B)-H(10B)	125.9	Co(1)-C(2B)-H(2B)	126.7
Co(1)-C(10B)-H(10B)	126.2	C(4B)-C(3B)-C(2B)	108.1(3)
C(5A)-V(1)-C(1A)	91.84(12)	C(4B)-C(3B)-Co(1)	69.83(16)
C(5A)-V(1)-C(3A)	85.78(12)	C(2B)-C(3B)-Co(1)	69.48(16)
C(1A)-V(1)-C(3A)	177.53(12)	C(4B)-C(3B)-H(3B)	125.9
C(5A)-V(1)-C(4A)	89.98(11)	C(2B)-C(3B)-H(3B)	125.9
C(1A)-V(1)-C(4A)	92.71(11)	Co(1)-C(3B)-H(3B)	126.3
C(3A)-V(1)-C(4A)	87.98(11)	C(3B)-C(4B)-C(5B)	107.8(3)
C(5A)-V(1)-C(2A)	89.74(11)	C(3B)-C(4B)-Co(1)	69.50(16)
C(1A)-V(1)-C(2A)	87.54(11)	C(5B)-C(4B)-Co(1)	69.03(17)
C(3A)-V(1)-C(2A)	91.75(11)	C(3B)-C(4B)-H(4B)	126.1
C(4A)-V(1)-C(2A)	179.63(12)	C(8B)-C(7B)-H(7B)	126.1
C(5A)-V(1)-C(11)	176.10(12)	C(6B)-C(7B)-H(7B)	126.1
C(1A)-V(1)-C(11)	91.80(11)	Co(1)-C(7B)-H(7B)	126.2
C(3A)-V(1)-C(11)	90.56(11)	C(9B)-C(8B)-C(7B)	108.5(3)
C(4A)-V(1)-C(11)	91.25(11)	C(9B)-C(8B)-Co(1)	69.61(16)
C(2A)-V(1)-C(11)	89.01(10)	C(7B)-C(8B)-Co(1)	69.33(16)
N(11)-C(11)-V(1)	178.8(2)	C(9B)-C(8B)-H(8B)	125.7
C(11)-N(11)-C(1)	177.9(3)	C(7B)-C(8B)-H(8B)	125.7
N(11)-C(1)-C(2)	118.2(2)	Co(1)-C(8B)-H(8B)	126.9
N(11)-C(1)-C(6)	118.2(2)	C(8B)-C(9B)-C(10B)	108.1(3)
C(2)-C(1)-C(6)	123.6(2)	C(8B)-C(9B)-Co(1)	70.09(16)

C(6)#1-C(2)-C(1)	118.5(2)	C(10B)-C(9B)-Co(1)	69.42(17)
C(6)#1-C(2)-C(21)	120.3(2)	C(8B)-C(9B)-H(9B)	125.9
C(1)-C(2)-C(21)	121.3(2)	C(10B)-C(9B)-H(9B)	125.9
C(2)#1-C(6)-C(1)	117.9(2)	Co(1)-C(9B)-H(9B)	126.1
C(2)#1-C(6)-C(61)	120.7(2)	C(9B)-C(10B)-C(6B)	108.3(3)
C(1)-C(6)-C(61)	121.5(2)	C(9B)-C(10B)-Co(1)	70.09(17)
C(2)-C(21)-H(21A)	109.5	C(6B)-C(10B)-Co(1)	69.40(17)
C(2)-C(21)-H(21B)	109.3	C(9B)-C(10B)-H(10B)	125.9

Table V.4. Anisotropic displacement parameters ($Å^2$x 10^3) for $C_{44}H_{35}Co_2N_3O_{10}V_2$, 1.1a. The anisotropic displacement factor exponent takes the form: $-2\pi^2$ [$h^2 a^{2*}U_{11}$ + ... + 2 h k a* b* U_{12}]

	U_{11}	U_{22}	U_{33}	U_{23}	U_{13}	U_{12}
V(1)	27(1)	23(1)	26(1)	1(1)	0(1)	0(1)
C(11)	32(1)	30(1)	26(1)	0(1)	-2(1)	0(1)
N(11)	41(1)	28(1)	25(1)	0(1)	-2(1)	7(1)
C(1)	37(1)	23(1)	16(1)	-2(1)	-2(1)	7(1)
C(2)	31(1)	30(1)	14(1)	1(1)	-2(1)	7(1)
C(6)	35(1)	28(1)	15(1)	-2(1)	-1(1)	2(1)
C(21)	30(1)	42(2)	37(2)	1(1)	-3(1)	7(1)
C(61)	40(2)	34(2)	33(2)	-3(1)	0(1)	-2(1)
C(1A)	32(1)	39(2)	28(1)	2(1)	-7(1)	-2(1)
O(1A)	36(1)	73(2)	35(1)	7(1)	-3(1)	-19(1)
C(2A)	26(1)	26(1)	32(2)	2(1)	3(1)	0(1)
O(2A)	36(1)	44(1)	33(1)	-2(1)	-2(1)	-5(1)
C(3A)	35(2)	37(2)	29(1)	-2(1)	0(1)	-4(1)
O(3A)	49(1)	76(2)	36(1)	-3(1)	7(1)	-22(1)
C(4A)	27(1)	26(1)	34(2)	5(1)	5(1)	0(1)
O(4A)	39(1)	48(1)	27(1)	-1(1)	-3(1)	-4(1)
C(5A)	46(2)	34(2)	27(2)	2(1)	0(1)	4(1)
O(5A)	77(2)	41(1)	41(1)	3(1)	0(1)	23(1)
Co(1)	27(1)	27(1)	33(1)	2(1)	3(1)	5(1)
C(1B)	36(2)	48(2)	50(2)	15(2)	12(1)	1(1)
C(2B)	29(1)	50(2)	53(2)	-4(2)	12(1)	4(1)
C(3B)	27(1)	37(2)	53(2)	3(1)	-3(1)	6(1)
C(4B)	33(1)	37(2)	41(2)	1(1)	-4(1)	-2(1)
C(5B)	31(1)	27(1)	56(2)	5(1)	6(1)	0(1)
C(6B)	37(2)	63(2)	38(2)	0(2)	-8(1)	0(1)
C(7B)	22(1)	35(1)	50(2)	4(1)	4(1)	3(1)
C(8B)	29(1)	36(2)	41(2)	3(1)	7(1)	-5(1)
C(9B)	35(2)	30(1)	60(2)	7(1)	0(1)	-3(1)
C(10B)	39(2)	41(2)	59(2)	-19(2)	3(2)	-3(1)

Table V.5. Hydrogen coordinates and isotropic displacement parameters for $C_{44}H_{35}Co_2N_3O_{10}V_2$, 1.1a.

	x	y	z	U(eq)
H(21A)	0.1116	0.7576	0.2659	0.054
H(21B)	0.1218	0.8114	0.3963	0.054
H(21C)	0.1110	0.7509	0.4883	0.054
H(61A)	0.3466	0.8481	0.4994	0.054
H(61B)	0.3078	0.8792	0.3487	0.054
H(61C)	0.3575	0.8385	0.2811	0.054
H(1B)	0.1123	0.2114	0.6406	0.054
H(2B)	0.1570	0.1150	0.6839	0.053
H(3B)	0.1664	0.0969	1.0312	0.047
H(4B)	0.1292	0.1825	1.2029	0.044
H(5B)	0.0953	0.2528	0.9613	0.046
H(6B)	-0.0077	0.1466	0.6308	0.055
H(7B)	-0.0298	0.1991	0.9309	0.043
H(8B)	-0.0025	0.1360	1.2009	0.043
H(9B)	0.0374	0.0461	1.0710	0.050
H(10B)	0.0335	0.0515	0.7205	0.056

Table V.6. Torsion angles [°] for $C_{44}H_{35}Co_2N_3O_{10}V_2$, 1.1a.

C(5A)-V(1)-C(11)-N(11)	28(12)	C(2B)-C(1B)-C(5B)-Co(1)	-59.5(2)
C(1A)-V(1)-C(11)-N(11)	-131(12)	C(3B)-C(4B)-C(5B)-C(1B)	-0.3(3)
C(3A)-V(1)-C(11)-N(11)	49(12)	Co(1)-C(4B)-C(5B)-C(1B)	-59.2(2)
C(4A)-V(1)-C(11)-N(11)	137(12)	C(3B)-C(4B)-C(5B)-Co(1)	58.89(19)
C(2A)-V(1)-C(11)-N(11)	-43(12)	C(10B)-Co(1)-C(5B)-C(1B)	-44.2(5)
V(1)-C(11)-N(11)-C(1)	-22(17)	C(6B)-Co(1)-C(5B)-C(1B)	-74.4(2)
C(11)-N(11)-C(1)-C(2)	1(7)	C(7B)-Co(1)-C(5B)-C(1B)	-115.56(18)
C(11)-N(11)-C(1)-C(6)	-179(100)	C(9B)-Co(1)-C(5B)-C(1B)	169.5(2)
N(11)-C(1)-C(2)-C(6)#1	179.9(2)	C(2B)-Co(1)-C(5B)-C(1B)	38.07(18)
C(6)-C(1)-C(2)-C(6)#1	-0.2(3)	C(3B)-Co(1)-C(5B)-C(1B)	82.07(19)
N(11)-C(1)-C(2)-C(21)	0.1(3)	C(8B)-Co(1)-C(5B)-C(1B)	-157.80(17)
C(6)-C(1)-C(2)-C(21)	180.0(2)	C(4B)-Co(1)-C(5B)-C(1B)	119.6(2)
N(11)-C(1)-C(6)-C(2)#1	178.6(2)	C(10B)-Co(1)-C(5B)-C(4B)	-163.8(4)
C(2)-C(1)-C(6)-C(2)#1	-1.3(3)	C(6B)-Co(1)-C(5B)-C(4B)	165.97(18)
N(11)-C(1)-C(6)-C(61)	-0.5(3)	C(1B)-Co(1)-C(5B)-C(4B)	-119.6(2)
C(2)-C(1)-C(6)-C(61)	179.6(2)	C(7B)-Co(1)-C(5B)-C(4B)	124.85(18)
C(5A)-V(1)-C(1A)-O(1A)	-32(6)	C(9B)-Co(1)-C(5B)-C(4B)	49.9(3)
C(3A)-V(1)-C(1A)-O(1A)	-16(8)	C(2B)-Co(1)-C(5B)-C(4B)	-81.51(19)
C(4A)-V(1)-C(1A)-O(1A)	-122(6)	C(3B)-Co(1)-C(5B)-C(4B)	-37.51(18)
C(2A)-V(1)-C(1A)-O(1A)	58(6)	C(8B)-Co(1)-C(5B)-C(4B)	82.6(2)
C(11)-V(1)-C(1A)-O(1A)	147(6)	C(10B)-Co(1)-C(6B)-C(7B)	118.5(3)
C(5A)-V(1)-C(2A)-O(2A)	31(6)	C(5B)-Co(1)-C(6B)-C(7B)	-74.2(2)
C(1A)-V(1)-C(2A)-O(2A)	-60(6)	C(1B)-Co(1)-C(6B)-C(7B)	-115.44(19)

C(3A)-V(1)-C(2A)-O(2A)	117(6)	C(9B)-Co(1)-C(6B)-C(7B)	81.22(19)
C(4A)-V(1)-C(2A)-O(2A)	73(21)	C(2B)-Co(1)-C(6B)-C(7B)	-158.04(18)
C(11)-V(1)-C(2A)-O(2A)	-152(6)	C(3B)-Co(1)-C(6B)-C(7B)	168.6(3)
C(5A)-V(1)-C(3A)-O(3A)	-2(4)	C(8B)-Co(1)-C(6B)-C(7B)	37.81(17)
C(1A)-V(1)-C(3A)-O(3A)	-18(6)	C(4B)-Co(1)-C(6B)-C(7B)	-42.5(5)
C(4A)-V(1)-C(3A)-O(3A)	88(4)	C(5B)-Co(1)-C(6B)-C(10B)	167.26(19)
C(2A)-V(1)-C(3A)-O(3A)	-92(4)	C(1B)-Co(1)-C(6B)-C(10B)	126.0(2)
C(11)-V(1)-C(3A)-O(3A)	179(100)	C(7B)-Co(1)-C(6B)-C(10B)	-118.5(3)
C(5A)-V(1)-C(4A)-O(4A)	-14(8)	C(9B)-Co(1)-C(6B)-C(10B)	-37.30(19)
C(1A)-V(1)-C(4A)-O(4A)	77(8)	C(2B)-Co(1)-C(6B)-C(10B)	83.4(2)
C(3A)-V(1)-C(4A)-O(4A)	-100(8)	C(3B)-Co(1)-C(6B)-C(10B)	50.0(4)
C(2A)-V(1)-C(4A)-O(4A)	-56(23)	C(8B)-Co(1)-C(6B)-C(10B)	-80.7(2)
C(11)-V(1)-C(4A)-O(4A)	169(100)	C(4B)-Co(1)-C(6B)-C(10B)	-161.0(4)
C(1A)-V(1)-C(5A)-O(5A)	-177(100)	C(10B)-C(6B)-C(7B)-C(8B)	-0.2(3)
C(3A)-V(1)-C(5A)-O(5A)	3(6)	Co(1)-C(6B)-C(7B)-C(8B)	-59.64(19)
C(4A)-V(1)-C(5A)-O(5A)	-85(6)	C(10B)-C(6B)-C(7B)-Co(1)	59.5(2)
C(2A)-V(1)-C(5A)-O(5A)	95(6)	C(10B)-Co(1)-C(7B)-C(8B)	80.6(2)
C(11)-V(1)-C(5A)-O(5A)	24(7)	C(6B)-Co(1)-C(7B)-C(8B)	119.0(3)
C(10B)-Co(1)-C(1B)-C(5B)	165.61(17)	C(5B)-Co(1)-C(7B)-C(8B)	-116.47(18)
C(6B)-Co(1)-C(1B)-C(5B)	124.40(18)	C(1B)-Co(1)-C(7B)-C(8B)	-159.04(18)
C(7B)-Co(1)-C(1B)-C(5B)	81.8(2)	C(9B)-Co(1)-C(7B)-C(8B)	36.95(18)
C(9B)-Co(1)-C(1B)-C(5B)	-163.8(4)	C(2B)-Co(1)-C(7B)-C(8B)	168.2(3)
C(2B)-Co(1)-C(1B)-C(5B)	-118.9(3)	C(3B)-Co(1)-C(7B)-C(8B)	-44.8(5)
C(3B)-Co(1)-C(1B)-C(5B)	-81.32(19)	C(4B)-Co(1)-C(7B)-C(8B)	-75.4(2)
C(8B)-Co(1)-C(1B)-C(5B)	49.2(4)	C(10B)-Co(1)-C(7B)-C(6B)	-38.4(2)
C(4B)-Co(1)-C(1B)-C(5B)	-37.60(17)	C(5B)-Co(1)-C(7B)-C(6B)	124.5(2)
C(10B)-Co(1)-C(1B)-C(2B)	-75.5(2)	C(1B)-Co(1)-C(7B)-C(6B)	82.0(2)
C(6B)-Co(1)-C(1B)-C(2B)	-116.7(2)	C(9B)-Co(1)-C(7B)-C(6B)	-82.0(2)
C(5B)-Co(1)-C(1B)-C(2B)	118.9(3)	C(2B)-Co(1)-C(7B)-C(6B)	49.2(4)
C(7B)-Co(1)-C(1B)-C(2B)	-159.34(19)	C(3B)-Co(1)-C(7B)-C(6B)	-163.8(4)
C(9B)-Co(1)-C(1B)-C(2B)	-45.0(5)	C(8B)-Co(1)-C(7B)-C(6B)	-119.0(3)
C(3B)-Co(1)-C(1B)-C(2B)	37.56(19)	C(4B)-Co(1)-C(7B)-C(6B)	165.59(19)
C(8B)-Co(1)-C(1B)-C(2B)	168.1(3)	C(6B)-C(7B)-C(8B)-C(9B)	0.5(3)
C(4B)-Co(1)-C(1B)-C(2B)	81.3(2)	Co(1)-C(7B)-C(8B)-C(9B)	-58.73(19)
C(5B)-C(1B)-C(2B)-C(3B)	0.3(3)	C(6B)-C(7B)-C(8B)-Co(1)	59.23(19)
Co(1)-C(1B)-C(2B)-C(3B)	-59.1(2)	C(10B)-Co(1)-C(8B)-C(9B)	37.64(19)
C(5B)-C(1B)-C(2B)-Co(1)	59.4(2)	C(6B)-Co(1)-C(8B)-C(9B)	82.2(2)
C(10B)-Co(1)-C(2B)-C(3B)	-115.90(19)	C(5B)-Co(1)-C(8B)-C(9B)	-158.91(18)
C(6B)-Co(1)-C(2B)-C(3B)	-159.43(18)	C(1B)-Co(1)-C(8B)-C(9B)	166.3(3)
C(5B)-Co(1)-C(2B)-C(3B)	81.60(19)	C(7B)-Co(1)-C(8B)-C(9B)	120.1(3)
C(1B)-Co(1)-C(2B)-C(3B)	119.6(3)	C(2B)-Co(1)-C(8B)-C(9B)	-42.0(5)
C(7B)-Co(1)-C(2B)-C(3B)	165.7(3)	C(3B)-Co(1)-C(8B)-C(9B)	-74.9(2)
C(9B)-Co(1)-C(2B)-C(3B)	-74.7(2)	C(4B)-Co(1)-C(8B)-C(9B)	-116.00(19)
C(8B)-Co(1)-C(2B)-C(3B)	-42.2(5)	C(10B)-Co(1)-C(8B)-C(7B)	-82.5(2)
C(4B)-Co(1)-C(2B)-C(3B)	37.56(17)	C(6B)-Co(1)-C(8B)-C(7B)	-37.98(18)
C(10B)-Co(1)-C(2B)-C(1B)	124.5(2)	C(5B)-Co(1)-C(8B)-C(7B)	80.9(2)

C(6B)-Co(1)-C(2B)-C(1B)	81.0(2)	C(1B)-Co(1)-C(8B)-C(7B)	46.1(4)
C(5B)-Co(1)-C(2B)-C(1B)	-38.0(2)	C(9B)-Co(1)-C(8B)-C(7B)	-120.1(3)
C(7B)-Co(1)-C(2B)-C(1B)	46.1(4)	C(2B)-Co(1)-C(8B)-C(7B)	-162.2(4)
C(9B)-Co(1)-C(2B)-C(1B)	165.7(2)	C(3B)-Co(1)-C(8B)-C(7B)	165.00(17)
C(3B)-Co(1)-C(2B)-C(1B)	-119.6(3)	C(4B)-Co(1)-C(8B)-C(7B)	123.86(18)
C(8B)-Co(1)-C(2B)-C(1B)	-161.8(4)	C(7B)-C(8B)-C(9B)-C(10B)	-0.6(3)
C(4B)-Co(1)-C(2B)-C(1B)	-82.0(2)	Co(1)-C(8B)-C(9B)-C(10B)	-59.2(2)
C(1B)-C(2B)-C(3B)-C(4B)	-0.5(3)	C(7B)-C(8B)-C(9B)-Co(1)	58.56(19)
Co(1)-C(2B)-C(3B)-C(4B)	-59.35(19)	C(10B)-Co(1)-C(9B)-C(8B)	-119.3(3)
C(1B)-C(2B)-C(3B)-Co(1)	58.8(2)	C(6B)-Co(1)-C(9B)-C(8B)	-81.4(2)
C(10B)-Co(1)-C(3B)-C(4B)	-157.94(19)	C(5B)-Co(1)-C(9B)-C(8B)	46.4(3)
C(6B)-Co(1)-C(3B)-C(4B)	166.2(3)	C(1B)-Co(1)-C(9B)-C(8B)	-158.6(4)
C(5B)-Co(1)-C(3B)-C(4B)	37.71(18)	C(7B)-Co(1)-C(9B)-C(8B)	-37.30(18)
C(1B)-Co(1)-C(3B)-C(4B)	81.73(19)	C(2B)-Co(1)-C(9B)-C(8B)	166.25(19)
C(7B)-Co(1)-C(3B)-C(4B)	-39.7(5)	C(3B)-Co(1)-C(9B)-C(8B)	124.66(19)
C(9B)-Co(1)-C(3B)-C(4B)	-115.35(19)	C(4B)-Co(1)-C(9B)-C(8B)	81.8(2)
C(2B)-Co(1)-C(3B)-C(4B)	119.4(3)	C(6B)-Co(1)-C(9B)-C(10B)	37.94(18)
C(8B)-Co(1)-C(3B)-C(4B)	-74.3(2)	C(5B)-Co(1)-C(9B)-C(10B)	165.7(3)
C(10B)-Co(1)-C(3B)-C(2B)	82.6(2)	C(1B)-Co(1)-C(9B)-C(10B)	-39.3(5)
C(6B)-Co(1)-C(3B)-C(2B)	46.8(4)	C(7B)-Co(1)-C(9B)-C(10B)	81.99(19)
C(5B)-Co(1)-C(3B)-C(2B)	-81.71(19)	C(2B)-Co(1)-C(9B)-C(10B)	-74.5(2)
C(1B)-Co(1)-C(3B)-C(2B)	-37.69(19)	C(3B)-Co(1)-C(9B)-C(10B)	-116.05(19)
C(7B)-Co(1)-C(3B)-C(2B)	-159.1(4)	C(8B)-Co(1)-C(9B)-C(10B)	119.3(3)
C(9B)-Co(1)-C(3B)-C(2B)	125.24(19)	C(4B)-Co(1)-C(9B)-C(10B)	-158.91(17)
C(8B)-Co(1)-C(3B)-C(2B)	166.29(18)	C(8B)-C(9B)-C(10B)-C(6B)	0.5(3)
C(4B)-Co(1)-C(3B)-C(2B)	-119.4(3)	Co(1)-C(9B)-C(10B)-C(6B)	-59.1(2)
C(2B)-C(3B)-C(4B)-C(5B)	0.5(3)	C(8B)-C(9B)-C(10B)-Co(1)	59.63(19)
Co(1)-C(3B)-C(4B)-C(5B)	-58.60(19)	C(7B)-C(6B)-C(10B)-C(9B)	-0.2(3)
C(2B)-C(3B)-C(4B)-Co(1)	59.14(19)	Co(1)-C(6B)-C(10B)-C(9B)	59.5(2)
C(10B)-Co(1)-C(4B)-C(3B)	49.6(4)	C(7B)-C(6B)-C(10B)-Co(1)	-59.7(2)
C(6B)-Co(1)-C(4B)-C(3B)	-160.7(4)	C(6B)-Co(1)-C(10B)-C(9B)	-119.5(3)
C(5B)-Co(1)-C(4B)-C(3B)	-119.5(3)	C(5B)-Co(1)-C(10B)-C(9B)	-158.4(4)
C(1B)-Co(1)-C(4B)-C(3B)	-81.87(19)	C(1B)-Co(1)-C(10B)-C(9B)	167.27(17)
C(7B)-Co(1)-C(4B)-C(3B)	166.57(18)	C(7B)-Co(1)-C(10B)-C(9B)	-81.41(18)
C(9B)-Co(1)-C(4B)-C(3B)	82.9(2)	C(2B)-Co(1)-C(10B)-C(9B)	125.31(19)
C(2B)-Co(1)-C(4B)-C(3B)	-37.73(18)	C(3B)-Co(1)-C(10B)-C(9B)	82.3(2)
C(8B)-Co(1)-C(4B)-C(3B)	125.12(18)	C(8B)-Co(1)-C(10B)-C(9B)	-37.48(17)
C(10B)-Co(1)-C(4B)-C(5B)	169.1(3)	C(4B)-Co(1)-C(10B)-C(9B)	47.1(4)
C(6B)-Co(1)-C(4B)-C(5B)	-41.2(5)	C(5B)-Co(1)-C(10B)-C(6B)	-38.8(5)
C(1B)-Co(1)-C(4B)-C(5B)	37.61(17)	C(1B)-Co(1)-C(10B)-C(6B)	-73.2(2)
C(7B)-Co(1)-C(4B)-C(5B)	-73.9(2)	C(7B)-Co(1)-C(10B)-C(6B)	38.11(18)
C(9B)-Co(1)-C(4B)-C(5B)	-157.59(17)	C(9B)-Co(1)-C(10B)-C(6B)	119.5(3)
C(2B)-Co(1)-C(4B)-C(5B)	81.76(19)	C(2B)-Co(1)-C(10B)-C(6B)	-115.2(2)
C(3B)-Co(1)-C(4B)-C(5B)	119.5(3)	C(3B)-Co(1)-C(10B)-C(6B)	-158.21(19)
C(8B)-Co(1)-C(4B)-C(5B)	-115.40(18)	C(8B)-Co(1)-C(10B)-C(6B)	82.0(2)
C(2B)-C(1B)-C(5B)-C(4B)	0.0(3)	C(4B)-Co(1)-C(10B)-C(6B)	166.6(3)

Co(1)-C(1B)-C(5B)-C(4B) 59.53(19)

Symmetry transformations used to generate equivalent atoms:
#1 -x+1/2, -y+3/2, z

Appendix 3

VI. Crystallographic Data for $C_{38}H_{48}FeN_4O_{10}V_2$, 1.3

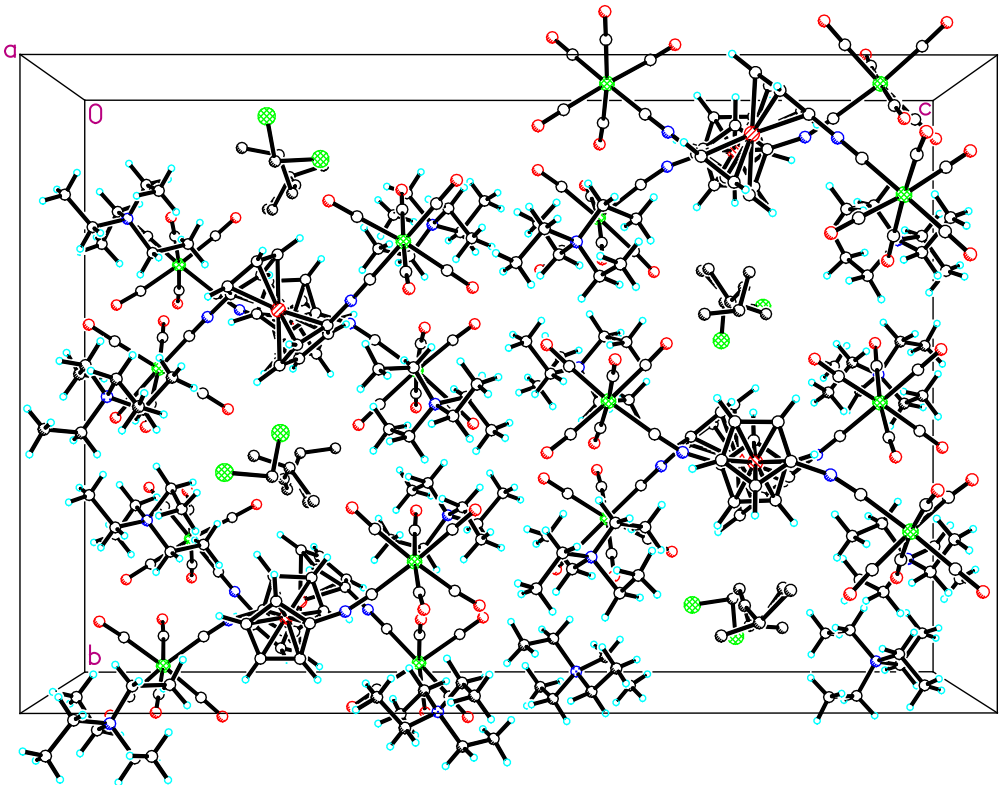

Figure VI.1. Packing diagram of $C_{38}H_{48}FeN_4O_{10}$, including solvent and counterions.

Table VI.1. Atomic coordinates (x 10^4) and equivalent isotropic displacement parameters ($Å^2$ x 10^3) for $C_{38}H_{48}FeN_4O_{10}V_2$, 1.3. U(eq) is defined as one third of the trace of the orthogonalized U_{ij} tensor.

	x	y	z	U(eq)
Fe(1)	355(1)	3805(1)	2465(1)	30(1)
V(1)	2534(1)	4741(1)	3943(1)	31(1)
V(2)	-1933(1)	2815(1)	1011(1)	29(1)
O(10)	3351(4)	5638(2)	4595(2)	49(1)
O(11)	4652(3)	4056(2)	4066(1)	39(1)
O(12)	1485(4)	3938(2)	4602(1)	50(1)
O(13)	368(4)	5372(3)	3908(2)	85(2)
O(14)	3373(4)	5659(3)	3305(2)	70(2)
O(20)	-2855(4)	1967(2)	356(1)	48(1)
O(21)	-4078(3)	3467(2)	883(1)	39(1)
O(22)	-871(4)	3561(2)	321(1)	44(1)
O(23)	127(4)	2054(3)	1024(2)	73(2)
O(24)	-2825(4)	1933(2)	1658(1)	53(1)
N(1)	1916(4)	3939(3)	3172(2)	45(2)
N(2)	-1243(4)	3638(3)	1771(2)	40(1)

C(1)	2129(5)	4221(3)	3462(2)	38(2)
C(2)	-1469(5)	3351(3)	1480(2)	35(2)
C(10)	3023(5)	5293(3)	4356(2)	37(2)
C(11)	3865(5)	4308(3)	4012(2)	31(1)
C(12)	1890(5)	4222(3)	4352(2)	39(2)
C(13)	1171(6)	5129(3)	3919(2)	51(2)
C(14)	3069(5)	5313(3)	3538(2)	44(2)
C(15)	1736(5)	3756(3)	2773(2)	34(2)
C(16)	1429(5)	3175(3)	2646(2)	42(2)
C(17)	1359(5)	3201(4)	2216(2)	53(2)
C(18)	1610(5)	3769(4)	2089(2)	56(2)
C(19)	1857(5)	4126(4)	2425(2)	45(2)
C(20)	-2479(5)	2284(3)	602(2)	35(2)
C(21)	-3270(5)	3242(3)	943(2)	31(2)
C(22)	-1259(5)	3306(3)	587(2)	34(2)
C(23)	-631(5)	2353(3)	1029(2)	44(2)
C(24)	-2499(5)	2275(3)	1425(2)	34(2)
C(25)	-1036(4)	3839(3)	2160(2)	31(1)
C(26)	-725(5)	4426(3)	2277(2)	37(2)
C(27)	-633(5)	4430(4)	2711(2)	49(2)
C(28)	-894(5)	3854(4)	2855(2)	49(2)
C(29)	-1140(5)	3478(3)	2522(2)	43(2)
Fe(2)	5334(1)	3778(1)	2473(1)	26(1)
V(3)	2936(1)	4713(1)	1034(1)	34(1)
V(4)	7641(1)	2751(1)	3881(1)	47(1)
O(40)	1656(4)	5544(2)	465(2)	49(1)
O(41)	3878(4)	3992(2)	303(2)	51(1)
O(42)	4698(4)	5682(3)	986(2)	84(2)
O(43)	2020(5)	5398(3)	1776(2)	72(2)
O(44)	976(4)	3879(2)	983(2)	48(1)
O(50)	8761(4)	1843(2)	4454(2)	51(1)
O(51)	6618(5)	3448(3)	4608(2)	70(2)
O(52)	5781(4)	1847(3)	3830(2)	78(2)
O(53)	8588(6)	2154(3)	3116(2)	98(2)
O(54)	9637(6)	3543(3)	3971(2)	94(2)
N(31)	4242(4)	3873(3)	1646(2)	44(2)
N(32)	6391(5)	3654(3)	3293(2)	57(2)
C(31)	3766(5)	4179(3)	1419(2)	40(2)
C(32)	6868(6)	3324(4)	3509(2)	53(2)
C(40)	2136(5)	5231(3)	678(2)	37(2)
C(41)	3551(6)	4263(3)	571(2)	41(2)
C(42)	4068(6)	5307(4)	1005(2)	54(2)
C(43)	2369(6)	5129(3)	1505(2)	46(2)
C(44)	1731(5)	4174(3)	1010(2)	36(2)
C(45)	4758(5)	3507(3)	1927(2)	35(2)
C(46)	5864(5)	3410(3)	1940(2)	35(2)

C(47)	6050(5)	3013(3)	2266(2)	38(2)
C(48)	5097(6)	2869(3)	2455(2)	42(2)
C(49)	4268(5)	3176(3)	2245(2)	38(2)
C(50)	8341(6)	2186(3)	4239(2)	43(2)
C(51)	7001(7)	3186(4)	4337(3)	56(2)
C(52)	6466(6)	2195(3)	3848(3)	53(2)
C(53)	8227(7)	2385(4)	3403(3)	66(2)
C(54)	8888(7)	3264(4)	3928(2)	63(2)
C(55)	5910(5)	4037(3)	3026(2)	36(2)
C(56)	4805(5)	4159(3)	3003(2)	40(2)
C(57)	4646(5)	4560(3)	2678(2)	41(2)
C(58)	5633(5)	4683(3)	2498(2)	42(2)
C(59)	6416(5)	4359(3)	2713(2)	35(2)
N(6)	3421(4)	2216(2)	707(1)	35(1)
C(61)	3854(6)	1670(3)	943(3)	39(3)
C(62)	4942(6)	1823(4)	1142(3)	75(3)
C(63)	2363(5)	2053(4)	532(3)	34(2)
C(64)	1778(6)	2580(3)	315(2)	51(2)
C(65)	4227(7)	2388(4)	367(2)	38(3)
C(66)	4433(6)	1862(3)	73(2)	50(2)
C(67)	3376(7)	2785(3)	987(2)	30(2)
C(68)	2603(8)	2608(5)	1348(2)	108(4)
C(61')	4465(11)	2398(6)	915(7)	92(12)
C(62')	4942(6)	1823(4)	1142(3)	75(3)
C(63')	2880(11)	2763(6)	494(6)	77(10)
C(64')	1778(6)	2580(3)	315(2)	51(2)
C(65')	3589(12)	1685(6)	407(4)	36(5)
C(66')	4433(6)	1862(3)	73(2)	50(2)
C(67')	2642(13)	2005(6)	1059(4)	63(8)
C(68')	2603(8)	2608(5)	1348(2)	108(4)
N(7)	2464(4)	7279(2)	873(2)	35(1)
C(71)	2338(9)	7815(5)	1132(4)	42(4)
C(72)	1439(7)	7721(4)	1469(2)	70(3)
C(73)	1436(10)	7049(5)	682(4)	45(4)
C(74)	901(6)	7566(3)	416(2)	55(2)
C(75)	3297(10)	7374(5)	562(4)	40(3)
C(76)	3540(6)	6827(3)	285(2)	46(2)
C(77)	2891(9)	6730(6)	1170(4)	49(4)
C(78)	3968(7)	7050(6)	1344(3)	151(7)
C(71')	1673(11)	7135(5)	1205(4)	38(4)
C(72')	1439(7)	7721(4)	1469(2)	70(3)
C(73')	1962(8)	7792(6)	598(4)	33(3)
C(74')	901(6)	7566(3)	416(2)	55(2)
C(75')	2680(9)	6763(6)	630(4)	42(4)
C(76')	3540(6)	6827(3)	285(2)	46(2)
C(77')	3440(10)	7585(6)	1063(4)	42(4)

C(78')	3968(7)	7050(6)	1344(3)	151(7)
N(8)	7939(4)	5190(2)	761(2)	33(1)
C(81)	8962(6)	4920(3)	921(2)	49(2)
C(82)	9588(6)	5345(4)	1187(2)	55(2)
C(83)	8134(5)	5755(3)	499(2)	43(2)
C(84)	8928(6)	5696(3)	168(2)	50(2)
C(85)	7213(5)	5390(3)	1102(2)	43(2)
C(86)	6882(6)	4886(4)	1390(2)	56(2)
C(87)	7430(6)	4697(3)	499(2)	43(2)
C(88)	6324(6)	4828(3)	361(2)	51(2)
N(9)	7059(4)	5309(2)	4210(2)	31(1)
C(91)	6226(6)	5195(3)	4535(2)	49(2)
C(92)	5976(6)	5729(3)	4809(2)	49(2)
C(93)	8115(5)	5491(3)	4411(2)	43(2)
C(94)	8619(6)	5001(4)	4666(2)	58(2)
C(95)	6732(6)	5821(3)	3928(2)	45(2)
C(96)	5738(6)	5714(4)	3694(2)	58(2)
C(97)	7180(6)	4728(3)	3981(2)	50(2)
C(98)	7970(6)	4761(4)	3625(2)	54(2)
Cl(1)	7621(4)	5765(2)	2577(2)	215(3)
Cl(2)	8999(4)	6361(2)	2046(1)	153(2)
Cl(2')	9716(11)	6081(11)	2534(9)	153(10)
C(1S)	8371(9)	6434(5)	2516(3)	143(6)
C(2S)	10824(5)	6077(3)	2974(2)	43(2)
C(3S)	11579(16)	6151(8)	2591(6)	151(11)
C(4S)	12156(5)	6761(3)	2460(2)	45(2)
C(5S)	13462(6)	6560(5)	2467(3)	92(3)
C(6S)	14692(9)	6355(6)	2574(5)	67(5)
C(7S)	15200(11)	6906(6)	2797(4)	58(5)
C(8S)	15446(9)	6885(5)	2863(3)	22(3)
C(9S)	14742(16)	6158(8)	2181(5)	85(6)

Table VI.2. Bond lengths [Å] for $C_{38}H_{48}FeN_4O_{10}V_2$, 1.3.

Fe(1)-C(18)	2.017(7)	O(44)-C(44)	1.162(7)
Fe(1)-C(17)	2.019(7)	O(50)-C(50)	1.161(8)
Fe(1)-C(15)	2.020(6)	O(51)-C(51)	1.166(9)
Fe(1)-C(25)	2.027(6)	O(52)-C(52)	1.161(9)
Fe(1)-C(27)	2.032(7)	O(53)-C(53)	1.162(10)
Fe(1)-C(16)	2.032(7)	O(54)-C(54)	1.140(9)
Fe(1)-C(26)	2.035(6)	N(31)-C(31)	1.171(8)
Fe(1)-C(19)	2.038(7)	N(31)-C(45)	1.385(8)
Fe(1)-C(29)	2.040(7)	N(32)-C(32)	1.181(9)
Fe(1)-C(28)	2.041(7)	N(32)-C(55)	1.359(9)
V(1)-C(10)	1.922(7)	C(45)-C(49)	1.417(9)
V(1)-C(13)	1.931(7)	C(45)-C(46)	1.420(9)

V(1)-C(12)	1.944(7)	C(46)-C(47)	1.401(9)
V(1)-C(14)	1.952(8)	C(47)-C(48)	1.397(9)
V(1)-C(11)	1.954(7)	C(48)-C(49)	1.426(9)
V(1)-C(1)	2.012(7)	C(55)-C(59)	1.402(9)
V(2)-C(20)	1.908(7)	C(55)-C(56)	1.429(9)
V(2)-C(24)	1.942(7)	C(56)-C(57)	1.397(9)
V(2)-C(23)	1.943(7)	C(57)-C(58)	1.413(9)
V(2)-C(21)	1.953(7)	C(58)-C(59)	1.410(9)
V(2)-C(22)	1.960(7)	N(6)-C(63)	1.503(7)
V(2)-C(2)	2.024(7)	N(6)-C(61)	1.531(7)
O(10)-C(10)	1.165(7)	N(6)-C(61')	1.540(9)
O(11)-C(11)	1.156(7)	N(6)-C(65')	1.543(9)
O(12)-C(12)	1.154(8)	N(6)-C(63')	1.553(9)
O(13)-C(13)	1.152(8)	N(6)-C(67)	1.555(7)
O(14)-C(14)	1.146(8)	N(6)-C(65)	1.561(7)
O(20)-C(20)	1.166(7)	N(6)-C(67')	1.589(9)
O(21)-C(21)	1.156(7)	C(61)-C(62)	1.562(8)
O(22)-C(22)	1.149(7)	C(63)-C(64)	1.551(8)
O(23)-C(23)	1.167(8)	C(65)-C(66)	1.531(8)
O(24)-C(24)	1.151(7)	C(67)-C(68)	1.587(8)
N(1)-C(1)	1.167(8)	N(7)-C(75')	1.416(14)
N(1)-C(15)	1.382(8)	N(7)-C(71)	1.464(12)
N(2)-C(2)	1.178(8)	N(7)-C(75)	1.483(13)
N(2)-C(25)	1.373(8)	N(7)-C(71')	1.515(13)
C(15)-C(16)	1.401(9)	N(7)-C(73)	1.533(12)
C(15)-C(19)	1.410(9)	N(7)-C(77')	1.540(13)
C(16)-C(17)	1.413(10)	N(7)-C(73')	1.580(13)
C(17)-C(18)	1.358(11)	N(7)-C(77)	1.644(14)
C(18)-C(19)	1.388(10)	C(71)-C(72)	1.603(9)
C(25)-C(26)	1.407(9)	C(73)-C(74)	1.585(9)
C(25)-C(29)	1.432(9)	C(75)-C(76)	1.543(9)
C(26)-C(27)	1.425(9)	C(77)-C(78)	1.640(9)
C(27)-C(28)	1.395(10)	N(8)-C(85)	1.515(8)
C(28)-C(29)	1.405(10)	N(8)-C(81)	1.520(8)
Fe(2)-C(45)	2.020(6)	N(8)-C(87)	1.526(8)
Fe(2)-C(55)	2.030(6)	N(8)-C(83)	1.532(8)
Fe(2)-C(48)	2.030(6)	C(81)-C(82)	1.506(10)
Fe(2)-C(59)	2.034(6)	C(83)-C(84)	1.489(9)
Fe(2)-C(58)	2.035(7)	C(85)-C(86)	1.520(9)
Fe(2)-C(47)	2.036(6)	C(87)-C(88)	1.501(9)
Fe(2)-C(49)	2.036(6)	N(9)-C(97)	1.493(8)
Fe(2)-C(46)	2.040(6)	N(9)-C(95)	1.516(8)
Fe(2)-C(56)	2.041(6)	N(9)-C(91)	1.524(8)
Fe(2)-C(57)	2.049(6)	N(9)-C(93)	1.545(8)
V(3)-C(40)	1.920(7)	C(91)-C(92)	1.514(9)
V(3)-C(43)	1.935(8)	C(93)-C(94)	1.509(9)

V(3)-C(44)	1.939(7)	C(95)-C(96)	1.492(9)
V(3)-C(42)	1.948(8)	C(97)-C(98)	1.540(9)
V(3)-C(41)	1.973(8)	Cl(1)-C(1S)	1.769(8)
V(3)-C(31)	2.020(7)	Cl(2)-C(1S)	1.741(9)
V(4)-C(53)	1.911(9)	Cl(2)-Cl(2')	1.94(2)
V(4)-C(50)	1.926(8)	Cl(2')-C(1S)	1.878(10)
V(4)-C(52)	1.934(8)	Cl(2')-C(2S)	2.01(2)
V(4)-C(54)	1.952(9)	C(2S)-C(3S)	1.589(10)
V(4)-C(51)	1.955(9)	C(3S)-C(4S)	1.593(10)
V(4)-C(32)	2.009(8)	C(4S)-C(5S)	1.715(8)
O(40)-C(40)	1.153(8)	C(5S)-C(6S)	1.661(9)
O(41)-C(41)	1.142(8)	C(6S)-C(9S)	1.359(19)
O(42)-C(42)	1.153(9)	C(6S)-C(7S)	1.558(10)
O(43)-C(43)	1.158(8)	C(6S)-C(8S)	1.781(17)

Table VI.3. Bond Angles [°] for $C_{38}H_{48}FeN_4O_{10}V_2$, 1.3.

C(18)-Fe(1)-C(17)	39.3(3)	C(40)-V(3)-C(41)	92.6(3)
C(18)-Fe(1)-C(15)	67.5(3)	C(43)-V(3)-C(41)	177.2(3)
C(17)-Fe(1)-C(15)	67.6(3)	C(44)-V(3)-C(41)	88.5(3)
C(18)-Fe(1)-C(25)	112.9(3)	C(42)-V(3)-C(41)	90.5(3)
C(17)-Fe(1)-C(25)	112.1(3)	C(40)-V(3)-C(31)	178.7(3)
C(15)-Fe(1)-C(25)	179.0(3)	C(43)-V(3)-C(31)	88.5(3)
C(18)-Fe(1)-C(27)	139.2(4)	C(44)-V(3)-C(31)	94.4(3)
C(17)-Fe(1)-C(27)	178.6(4)	C(42)-V(3)-C(31)	92.3(3)
C(15)-Fe(1)-C(27)	112.0(3)	C(41)-V(3)-C(31)	88.7(3)
C(25)-Fe(1)-C(27)	68.3(3)	C(53)-V(4)-C(50)	92.5(3)
C(18)-Fe(1)-C(16)	67.7(3)	C(53)-V(4)-C(52)	89.4(4)
C(17)-Fe(1)-C(16)	40.8(3)	C(50)-V(4)-C(52)	88.7(3)
C(15)-Fe(1)-C(16)	40.5(3)	C(53)-V(4)-C(54)	89.6(4)
C(25)-Fe(1)-C(16)	138.7(3)	C(50)-V(4)-C(54)	87.5(3)
C(27)-Fe(1)-C(16)	139.7(3)	C(52)-V(4)-C(54)	176.0(3)
C(18)-Fe(1)-C(26)	112.0(3)	C(53)-V(4)-C(51)	174.8(4)
C(17)-Fe(1)-C(26)	138.4(3)	C(50)-V(4)-C(51)	92.6(3)
C(15)-Fe(1)-C(26)	140.3(3)	C(52)-V(4)-C(51)	91.7(3)
C(25)-Fe(1)-C(26)	40.5(2)	C(54)-V(4)-C(51)	89.6(4)
C(27)-Fe(1)-C(26)	41.0(3)	C(53)-V(4)-C(32)	87.9(4)
C(16)-Fe(1)-C(26)	179.1(3)	C(50)-V(4)-C(32)	178.1(3)
C(18)-Fe(1)-C(19)	40.0(3)	C(52)-V(4)-C(32)	89.5(3)
C(17)-Fe(1)-C(19)	67.2(3)	C(54)-V(4)-C(32)	94.3(3)
C(15)-Fe(1)-C(19)	40.6(3)	C(51)-V(4)-C(32)	87.0(3)
C(25)-Fe(1)-C(19)	140.2(3)	C(31)-N(31)-C(45)	177.1(7)
C(27)-Fe(1)-C(19)	111.6(3)	C(32)-N(32)-C(55)	175.6(8)
C(16)-Fe(1)-C(19)	68.3(3)	N(31)-C(31)-V(3)	179.2(6)
C(26)-Fe(1)-C(19)	112.1(3)	N(32)-C(32)-V(4)	178.4(7)
C(18)-Fe(1)-C(29)	141.1(3)	O(40)-C(40)-V(3)	179.8(6)

C(17)-Fe(1)-C(29)	113.1(3)	O(41)-C(41)-V(3)	177.8(6)
C(15)-Fe(1)-C(29)	137.9(3)	O(42)-C(42)-V(3)	176.3(7)
C(25)-Fe(1)-C(29)	41.2(3)	O(43)-C(43)-V(3)	177.1(7)
C(27)-Fe(1)-C(29)	68.2(3)	O(44)-C(44)-V(3)	175.8(6)
C(16)-Fe(1)-C(29)	110.8(3)	N(31)-C(45)-C(49)	125.3(6)
C(26)-Fe(1)-C(29)	68.9(3)	N(31)-C(45)-C(46)	125.1(6)
C(19)-Fe(1)-C(29)	178.5(3)	C(49)-C(45)-C(46)	109.6(6)
C(18)-Fe(1)-C(28)	178.7(3)	N(31)-C(45)-Fe(2)	125.7(5)
C(17)-Fe(1)-C(28)	141.4(4)	C(49)-C(45)-Fe(2)	70.2(4)
C(15)-Fe(1)-C(28)	111.5(3)	C(46)-C(45)-Fe(2)	70.3(3)
C(25)-Fe(1)-C(28)	68.1(3)	C(47)-C(46)-C(45)	106.4(6)
C(27)-Fe(1)-C(28)	40.1(3)	C(47)-C(46)-Fe(2)	69.7(4)
C(16)-Fe(1)-C(28)	112.1(3)	C(45)-C(46)-Fe(2)	68.8(3)
C(26)-Fe(1)-C(28)	68.2(3)	C(48)-C(47)-C(46)	109.6(6)
C(19)-Fe(1)-C(28)	138.6(3)	C(48)-C(47)-Fe(2)	69.7(4)
C(29)-Fe(1)-C(28)	40.3(3)	C(46)-C(47)-Fe(2)	70.1(4)
C(10)-V(1)-C(13)	92.0(3)	C(47)-C(48)-C(49)	108.5(6)
C(10)-V(1)-C(12)	91.4(3)	C(47)-C(48)-Fe(2)	70.1(4)
C(13)-V(1)-C(12)	84.9(3)	C(49)-C(48)-Fe(2)	69.7(4)
C(10)-V(1)-C(14)	87.4(3)	C(45)-C(49)-C(48)	105.9(6)
C(13)-V(1)-C(14)	90.0(3)	C(45)-C(49)-Fe(2)	68.9(4)
C(12)-V(1)-C(14)	174.7(3)	C(48)-C(49)-Fe(2)	69.2(4)
C(10)-V(1)-C(11)	87.3(3)	O(50)-C(50)-V(4)	179.7(7)
C(13)-V(1)-C(11)	174.7(3)	O(51)-C(51)-V(4)	179.7(7)
C(12)-V(1)-C(11)	89.8(3)	O(52)-C(52)-V(4)	177.9(7)
C(14)-V(1)-C(11)	95.3(3)	O(53)-C(53)-V(4)	178.9(9)
C(10)-V(1)-C(1)	173.0(3)	O(54)-C(54)-V(4)	176.2(7)
C(13)-V(1)-C(1)	89.7(3)	N(32)-C(55)-C(59)	125.3(6)
C(12)-V(1)-C(1)	95.4(3)	N(32)-C(55)-C(56)	126.1(6)
C(14)-V(1)-C(1)	85.9(3)	C(59)-C(55)-C(56)	108.6(6)
C(11)-V(1)-C(1)	91.6(2)	N(32)-C(55)-Fe(2)	123.8(5)
C(20)-V(2)-C(24)	88.7(3)	C(59)-C(55)-Fe(2)	70.0(4)
C(20)-V(2)-C(23)	90.3(3)	C(56)-C(55)-Fe(2)	69.9(4)
C(24)-V(2)-C(23)	88.6(3)	C(57)-C(56)-C(55)	107.3(6)
C(20)-V(2)-C(21)	84.4(3)	C(57)-C(56)-Fe(2)	70.3(4)
C(24)-V(2)-C(21)	93.0(3)	C(55)-C(56)-Fe(2)	69.0(3)
C(23)-V(2)-C(21)	174.5(3)	C(56)-C(57)-C(58)	108.3(6)
C(20)-V(2)-C(22)	90.1(3)	C(56)-C(57)-Fe(2)	69.7(4)
C(24)-V(2)-C(22)	174.8(3)	C(58)-C(57)-Fe(2)	69.2(4)
C(23)-V(2)-C(22)	86.4(3)	C(59)-C(58)-C(57)	108.5(6)
C(21)-V(2)-C(22)	91.9(2)	C(59)-C(58)-Fe(2)	69.7(4)
C(20)-V(2)-C(2)	174.5(3)	C(57)-C(58)-Fe(2)	70.3(4)
C(24)-V(2)-C(2)	86.5(3)	C(55)-C(59)-C(58)	107.3(6)
C(23)-V(2)-C(2)	92.3(3)	C(55)-C(59)-Fe(2)	69.6(4)
C(21)-V(2)-C(2)	93.1(2)	C(58)-C(59)-Fe(2)	69.8(4)
C(22)-V(2)-C(2)	94.9(3)	C(63)-N(6)-C(61)	108.8(5)

C(1)-N(1)-C(15)	163.8(7)	C(63)-N(6)-C(61')	175.9(10)
C(2)-N(2)-C(25)	165.6(7)	C(61)-N(6)-C(61')	71.1(6)
N(1)-C(1)-V(1)	176.8(6)	C(63)-N(6)-C(65')	72.5(7)
N(2)-C(2)-V(2)	175.1(6)	C(61)-N(6)-C(65')	70.9(7)
O(10)-C(10)-V(1)	177.1(6)	C(61')-N(6)-C(65')	111.0(9)
O(11)-C(11)-V(1)	177.7(5)	C(63)-N(6)-C(63')	67.8(6)
O(12)-C(12)-V(1)	176.8(6)	C(61)-N(6)-C(63')	174.2(8)
O(13)-C(13)-V(1)	178.4(8)	C(61')-N(6)-C(63')	111.9(7)
O(14)-C(14)-V(1)	178.4(7)	C(65')-N(6)-C(63')	111.5(9)
N(1)-C(15)-C(16)	126.2(6)	C(63)-N(6)-C(67)	112.6(5)
N(1)-C(15)-C(19)	125.0(7)	C(61)-N(6)-C(67)	110.7(5)
C(16)-C(15)-C(19)	108.8(6)	C(61')-N(6)-C(67)	64.1(8)
N(1)-C(15)-Fe(1)	126.5(4)	C(65')-N(6)-C(67)	173.0(6)
C(16)-C(15)-Fe(1)	70.2(4)	C(63')-N(6)-C(67)	67.5(8)
C(19)-C(15)-Fe(1)	70.4(4)	C(63)-N(6)-C(65)	111.9(5)
C(15)-C(16)-C(17)	106.0(7)	C(61)-N(6)-C(65)	108.4(5)
C(15)-C(16)-Fe(1)	69.3(4)	C(61')-N(6)-C(65)	71.7(9)
C(17)-C(16)-Fe(1)	69.1(4)	C(65')-N(6)-C(65)	68.9(5)
C(18)-C(17)-C(16)	109.1(7)	C(63')-N(6)-C(65)	77.4(8)
C(18)-C(17)-Fe(1)	70.3(4)	C(67)-N(6)-C(65)	104.3(5)
C(16)-C(17)-Fe(1)	70.1(4)	C(63)-N(6)-C(67')	69.5(8)
C(17)-C(18)-C(19)	109.6(7)	C(61)-N(6)-C(67')	68.2(8)
C(17)-C(18)-Fe(1)	70.4(4)	C(61')-N(6)-C(67')	107.0(9)
C(19)-C(18)-Fe(1)	70.8(4)	C(65')-N(6)-C(67')	109.0(6)
C(18)-C(19)-C(15)	106.6(7)	C(63')-N(6)-C(67')	106.1(9)
C(18)-C(19)-Fe(1)	69.2(4)	C(67)-N(6)-C(67')	77.7(6)
C(15)-C(19)-Fe(1)	69.0(4)	C(65)-N(6)-C(67')	176.5(8)
O(20)-C(20)-V(2)	177.2(6)	N(6)-C(61)-C(62)	110.8(6)
O(21)-C(21)-V(2)	175.5(6)	N(6)-C(63)-C(64)	114.9(6)
O(22)-C(22)-V(2)	175.4(5)	C(66)-C(65)-N(6)	112.1(6)
O(23)-C(23)-V(2)	176.4(7)	N(6)-C(67)-C(68)	105.2(6)
O(24)-C(24)-V(2)	176.8(6)	C(75')-N(7)-C(71)	175.1(8)
N(2)-C(25)-C(26)	127.0(6)	C(75')-N(7)-C(75)	65.8(6)
N(2)-C(25)-C(29)	124.5(6)	C(71)-N(7)-C(75)	111.3(6)
C(26)-C(25)-C(29)	108.5(6)	C(75')-N(7)-C(71')	111.3(7)
N(2)-C(25)-Fe(1)	127.5(4)	C(71)-N(7)-C(71')	71.4(6)
C(26)-C(25)-Fe(1)	70.0(3)	C(75)-N(7)-C(71')	174.8(8)
C(29)-C(25)-Fe(1)	69.8(4)	C(75')-N(7)-C(73)	70.7(7)
C(25)-C(26)-C(27)	107.2(6)	C(71)-N(7)-C(73)	114.2(7)
C(25)-C(26)-Fe(1)	69.5(4)	C(75)-N(7)-C(73)	112.0(7)
C(27)-C(26)-Fe(1)	69.4(4)	C(71')-N(7)-C(73)	70.0(7)
C(28)-C(27)-C(26)	108.2(6)	C(75')-N(7)-C(77')	115.0(8)
C(28)-C(27)-Fe(1)	70.3(4)	C(71)-N(7)-C(77')	60.1(7)
C(26)-C(27)-Fe(1)	69.6(4)	C(75)-N(7)-C(77')	69.0(7)
C(27)-C(28)-C(29)	109.2(6)	C(71')-N(7)-C(77')	109.7(7)
C(27)-C(28)-Fe(1)	69.6(4)	C(73)-N(7)-C(77')	173.3(7)

C(29)-C(28)-Fe(1)	69.8(4)	C(75')-N(7)-C(73')	109.6(8)
C(28)-C(29)-C(25)	106.9(6)	C(71)-N(7)-C(73')	72.9(7)
C(28)-C(29)-Fe(1)	69.9(4)	C(75)-N(7)-C(73')	78.2(7)
C(25)-C(29)-Fe(1)	68.9(3)	C(71')-N(7)-C(73')	107.0(7)
C(45)-Fe(2)-C(55)	179.1(3)	C(73)-N(7)-C(73')	70.3(6)
C(45)-Fe(2)-C(48)	68.2(3)	C(77')-N(7)-C(73')	103.8(6)
C(55)-Fe(2)-C(48)	111.0(3)	C(75')-N(7)-C(77)	70.9(7)
C(45)-Fe(2)-C(59)	140.3(3)	C(71)-N(7)-C(77)	106.9(7)
C(55)-Fe(2)-C(59)	40.4(3)	C(75)-N(7)-C(77)	105.9(7)
C(48)-Fe(2)-C(59)	137.3(3)	C(71')-N(7)-C(77)	68.9(7)
C(45)-Fe(2)-C(58)	113.1(3)	C(73)-N(7)-C(77)	105.9(6)
C(55)-Fe(2)-C(58)	67.8(3)	C(77')-N(7)-C(77)	79.8(6)
C(48)-Fe(2)-C(58)	177.7(3)	C(73')-N(7)-C(77)	175.4(7)
C(59)-Fe(2)-C(58)	40.6(3)	N(7)-C(71)-C(72)	111.9(8)
C(45)-Fe(2)-C(47)	67.7(3)	N(7)-C(73)-C(74)	110.3(8)
C(55)-Fe(2)-C(47)	111.7(3)	N(7)-C(75)-C(76)	115.9(8)
C(48)-Fe(2)-C(47)	40.2(3)	C(78)-C(77)-N(7)	99.2(7)
C(59)-Fe(2)-C(47)	110.5(3)	C(85)-N(8)-C(81)	112.4(5)
C(58)-Fe(2)-C(47)	138.1(3)	C(85)-N(8)-C(87)	111.2(5)
C(45)-Fe(2)-C(49)	40.9(3)	C(81)-N(8)-C(87)	105.9(5)
C(55)-Fe(2)-C(49)	138.4(3)	C(85)-N(8)-C(83)	105.8(5)
C(48)-Fe(2)-C(49)	41.1(3)	C(81)-N(8)-C(83)	111.9(5)
C(59)-Fe(2)-C(49)	178.2(3)	C(87)-N(8)-C(83)	109.6(5)
C(58)-Fe(2)-C(49)	141.1(3)	C(82)-C(81)-N(8)	113.8(6)
C(47)-Fe(2)-C(49)	68.5(3)	C(84)-C(83)-N(8)	116.4(6)
C(45)-Fe(2)-C(46)	40.9(2)	N(8)-C(85)-C(86)	114.4(5)
C(55)-Fe(2)-C(46)	139.0(3)	C(88)-C(87)-N(8)	115.3(6)
C(48)-Fe(2)-C(46)	68.3(3)	C(97)-N(9)-C(95)	111.3(5)
C(59)-Fe(2)-C(46)	110.9(3)	C(97)-N(9)-C(91)	106.4(5)
C(58)-Fe(2)-C(46)	111.2(3)	C(95)-N(9)-C(91)	111.1(5)
C(47)-Fe(2)-C(46)	40.2(2)	C(97)-N(9)-C(93)	110.3(5)
C(49)-Fe(2)-C(46)	69.3(3)	C(95)-N(9)-C(93)	107.5(5)
C(45)-Fe(2)-C(56)	139.0(3)	C(91)-N(9)-C(93)	110.4(5)
C(55)-Fe(2)-C(56)	41.1(3)	C(92)-C(91)-N(9)	115.5(6)
C(48)-Fe(2)-C(56)	112.5(3)	C(94)-C(93)-N(9)	114.5(6)
C(59)-Fe(2)-C(56)	68.7(3)	C(96)-C(95)-N(9)	115.1(6)
C(58)-Fe(2)-C(56)	67.9(3)	N(9)-C(97)-C(98)	114.0(6)
C(47)-Fe(2)-C(56)	140.6(3)	C(1S)-Cl(2)-Cl(2')	61.1(6)
C(49)-Fe(2)-C(56)	111.1(3)	C(1S)-Cl(2')-Cl(2)	54.3(5)
C(46)-Fe(2)-C(56)	179.1(3)	C(1S)-Cl(2')-C(2S)	131.2(15)
C(45)-Fe(2)-C(57)	112.7(3)	Cl(2)-Cl(2')-C(2S)	156.6(13)
C(55)-Fe(2)-C(57)	67.9(3)	Cl(2)-C(1S)-Cl(1)	105.7(6)
C(48)-Fe(2)-C(57)	141.2(3)	Cl(2)-C(1S)-Cl(2')	64.6(9)
C(59)-Fe(2)-C(57)	68.3(3)	Cl(1)-C(1S)-Cl(2')	98.0(8)
C(58)-Fe(2)-C(57)	40.5(3)	C(3S)-C(2S)-Cl(2')	81.8(11)
C(47)-Fe(2)-C(57)	178.6(3)	C(2S)-C(3S)-C(4S)	125.3(11)

C(49)-Fe(2)-C(57)	112.8(3)	C(3S)-C(4S)-C(5S)	102.9(9)
C(46)-Fe(2)-C(57)	139.2(3)	C(6S)-C(5S)-C(4S)	168.6(9)
C(56)-Fe(2)-C(57)	40.0(3)	C(9S)-C(6S)-C(7S)	132.3(15)
C(40)-V(3)-C(43)	90.2(3)	C(9S)-C(6S)-C(5S)	86.3(11)
C(40)-V(3)-C(44)	85.7(3)	C(7S)-C(6S)-C(5S)	105.8(9)
C(43)-V(3)-C(44)	91.6(3)	C(9S)-C(6S)-C(8S)	133.3(14)
C(40)-V(3)-C(42)	87.7(3)	C(7S)-C(6S)-C(8S)	10.7(8)
C(43)-V(3)-C(42)	89.7(3)	C(5S)-C(6S)-C(8S)	115.8(9)
C(44)-V(3)-C(42)	173.3(3)		

Table VI.4. Anisotropic displacement parameters (Å2x 103) for $C_{38}H_{48}FeN_4O_{10}V_2$, 1.3. The anisotropic displacement factor exponent takes the form: $-2\pi^2 [h^2 a^{*2} U_{11} + ... + 2 h k a^* b^* U_{12}]$

	U_{11}	U_{22}	U_{33}	U_{23}	U_{13}	U_{12}
Fe(1)	23(1)	48(1)	20(1)	-1(1)	1(1)	3(1)
V(1)	30(1)	38(1)	25(1)	-1(1)	0(1)	2(1)
V(2)	29(1)	33(1)	24(1)	-1(1)	0(1)	1(1)
O(10)	63(3)	44(3)	39(3)	-3(2)	-1(2)	3(3)
O(11)	29(2)	41(3)	46(3)	1(2)	-3(2)	7(2)
O(12)	57(3)	53(3)	38(3)	8(3)	5(2)	-8(3)
O(13)	37(3)	83(4)	134(6)	6(4)	15(3)	21(3)
O(14)	66(4)	79(4)	65(4)	35(3)	-6(3)	-1(3)
O(20)	64(3)	46(3)	35(3)	-8(2)	-7(2)	-7(3)
O(21)	30(3)	47(3)	40(3)	5(2)	0(2)	6(2)
O(22)	50(3)	43(3)	39(3)	8(2)	10(2)	-5(2)
O(23)	41(3)	78(4)	100(5)	25(4)	20(3)	18(3)
O(24)	70(4)	50(3)	40(3)	12(3)	18(3)	12(3)
N(1)	27(3)	71(4)	36(3)	-14(3)	-8(3)	6(3)
N(2)	26(3)	54(4)	38(3)	-10(3)	-8(2)	5(3)
C(1)	25(3)	50(4)	39(4)	-1(3)	0(3)	6(3)
C(2)	27(3)	45(4)	32(4)	4(3)	-2(3)	3(3)
C(10)	41(4)	41(4)	27(4)	1(3)	0(3)	10(3)
C(11)	38(4)	33(4)	21(3)	-5(3)	1(3)	-9(3)
C(12)	38(4)	42(4)	36(4)	-5(3)	-3(3)	3(3)
C(13)	38(4)	53(5)	61(5)	0(4)	4(4)	9(4)
C(14)	37(4)	57(5)	38(4)	12(4)	-4(3)	8(3)
C(15)	23(3)	52(4)	28(4)	-1(3)	-1(3)	7(3)
C(16)	32(4)	48(5)	46(4)	-3(4)	-6(3)	11(3)
C(17)	27(4)	81(6)	50(5)	-36(5)	-4(3)	18(4)
C(18)	24(4)	107(7)	37(4)	5(5)	3(3)	10(4)
C(19)	24(3)	71(5)	40(4)	7(4)	2(3)	-3(3)
C(20)	38(4)	34(4)	31(4)	9(3)	0(3)	10(3)
C(21)	38(4)	34(4)	21(3)	0(3)	2(3)	-11(3)
C(22)	34(4)	33(4)	34(4)	-8(3)	-4(3)	5(3)
C(23)	34(4)	52(5)	46(4)	14(4)	4(3)	2(3)

C(24)	40(4)	34(4)	27(4)	2(3)	4(3)	10(3)
C(25)	18(3)	45(4)	30(4)	-7(3)	-4(3)	2(3)
C(26)	32(4)	39(4)	41(4)	0(3)	-6(3)	3(3)
C(27)	28(4)	69(5)	49(5)	-24(4)	-6(3)	10(4)
C(28)	31(4)	81(6)	33(4)	3(4)	5(3)	12(4)
C(29)	26(4)	47(4)	54(5)	7(4)	4(3)	3(3)
Fe(2)	23(1)	36(1)	20(1)	1(1)	-1(1)	1(1)
V(3)	32(1)	41(1)	29(1)	-1(1)	-6(1)	-2(1)
V(4)	54(1)	52(1)	35(1)	10(1)	-14(1)	-13(1)
O(40)	65(3)	38(3)	45(3)	8(2)	-11(3)	9(3)
O(41)	77(4)	41(3)	35(3)	-3(2)	9(3)	4(3)
O(42)	43(3)	62(4)	147(6)	-11(4)	8(4)	-13(3)
O(43)	84(4)	81(4)	52(4)	-25(3)	1(3)	10(3)
O(44)	43(3)	50(3)	50(3)	4(2)	-9(2)	-8(3)
O(50)	48(3)	53(3)	51(3)	7(3)	-5(3)	-3(3)
O(51)	113(5)	54(4)	41(3)	2(3)	-12(3)	5(3)
O(52)	45(3)	53(4)	136(6)	-4(4)	-2(4)	-4(3)
O(53)	109(6)	131(6)	55(4)	-24(4)	3(4)	-18(5)
O(54)	95(5)	103(5)	83(5)	41(4)	-46(4)	-55(4)
N(31)	38(3)	67(4)	27(3)	-2(3)	-8(3)	11(3)
N(32)	73(5)	61(4)	35(4)	-1(3)	-23(3)	2(4)
C(31)	30(4)	57(5)	33(4)	-4(3)	5(3)	4(3)
C(32)	65(5)	55(5)	38(4)	7(4)	-21(4)	-13(4)
C(40)	42(4)	33(4)	35(4)	-7(3)	3(3)	-7(3)
C(41)	51(4)	37(4)	35(4)	14(3)	-7(3)	-10(3)
C(42)	35(4)	58(5)	68(6)	-16(4)	-7(4)	-1(4)
C(43)	48(4)	51(5)	39(4)	-1(4)	-8(4)	-6(4)
C(44)	41(4)	43(4)	23(3)	1(3)	-9(3)	3(3)
C(45)	38(4)	43(4)	24(3)	-6(3)	-8(3)	7(3)
C(46)	33(4)	46(4)	26(3)	-7(3)	-1(3)	4(3)
C(47)	32(4)	36(4)	45(4)	-13(3)	-7(3)	8(3)
C(48)	49(4)	28(4)	48(4)	4(3)	-7(3)	3(3)
C(49)	30(4)	38(4)	45(4)	-14(3)	-7(3)	2(3)
C(50)	44(4)	55(5)	31(4)	1(4)	-2(3)	-9(4)
C(51)	82(6)	40(5)	47(5)	12(4)	-15(4)	-6(4)
C(52)	44(5)	46(5)	68(6)	5(4)	-8(4)	4(4)
C(53)	69(6)	84(7)	43(5)	-1(5)	-5(4)	-13(5)
C(54)	72(6)	75(6)	43(5)	20(4)	-25(4)	-22(5)
C(55)	41(4)	48(4)	19(3)	-5(3)	-6(3)	0(3)
C(56)	37(4)	55(5)	29(4)	-10(3)	7(3)	-5(3)
C(57)	32(4)	41(4)	50(4)	-14(3)	-4(3)	9(3)
C(58)	47(4)	37(4)	41(4)	5(3)	1(3)	-3(3)
C(59)	29(3)	40(4)	36(4)	-11(3)	2(3)	1(3)
N(6)	38(3)	33(3)	34(3)	-7(2)	3(2)	-3(2)
C(61)	37(6)	36(6)	43(6)	-6(5)	-9(5)	4(4)
C(62)	60(6)	89(7)	77(6)	-1(6)	-30(5)	10(5)

C(63)	22(5)	50(6)	29(5)	-6(5)	3(4)	-10(4)
C(64)	53(5)	53(5)	48(5)	-3(4)	-1(4)	11(4)
C(65)	30(5)	40(6)	45(6)	-6(5)	9(4)	0(4)
C(66)	47(4)	60(5)	44(4)	-19(4)	12(3)	1(4)
C(67)	39(5)	24(5)	27(5)	-13(4)	-4(4)	-10(4)
C(68)	106(8)	187(12)	31(5)	-30(6)	7(5)	70(8)
C(61')	54(18)	80(20)	150(30)	-40(20)	15(19)	-41(16)
C(62')	60(6)	89(7)	77(6)	-1(6)	-30(5)	10(5)
C(63')	130(30)	31(14)	70(20)	3(13)	31(19)	25(16)
C(64')	53(5)	53(5)	48(5)	-3(4)	-1(4)	11(4)
C(65')	38(12)	39(12)	30(12)	-19(9)	6(9)	-2(9)
C(66')	47(4)	60(5)	44(4)	-19(4)	12(3)	1(4)
C(67')	28(13)	80(20)	77(19)	33(16)	20(12)	12(12)
C(68')	106(8)	187(12)	31(5)	-30(6)	7(5)	70(8)
N(7)	33(3)	43(3)	29(3)	-6(3)	1(2)	-6(3)
C(71)	42(8)	33(7)	50(9)	-22(6)	-3(6)	4(6)
C(72)	103(7)	68(6)	41(5)	-4(4)	23(5)	32(5)
C(73)	33(7)	57(9)	45(8)	-24(7)	-15(6)	9(6)
C(74)	48(5)	67(5)	51(5)	-9(4)	-14(4)	10(4)
C(75)	37(7)	48(8)	35(7)	-8(6)	-4(6)	-7(6)
C(76)	52(5)	50(5)	37(4)	-8(3)	4(3)	13(4)
C(77)	59(9)	35(8)	54(9)	-1(7)	13(7)	8(7)
C(78)	57(7)	340(20)	54(6)	-42(9)	-30(5)	81(10)
C(71')	32(8)	55(10)	28(8)	9(7)	4(6)	-8(7)
C(72')	103(7)	68(6)	41(5)	-4(4)	23(5)	32(5)
C(73')	37(8)	35(8)	28(8)	-1(6)	2(6)	1(6)
C(74')	48(5)	67(5)	51(5)	-9(4)	-14(4)	10(4)
C(75')	33(8)	41(9)	53(10)	-5(7)	-10(7)	6(7)
C(76')	52(5)	50(5)	37(4)	-8(3)	4(3)	13(4)
C(77')	25(7)	71(11)	30(8)	-5(7)	0(6)	-24(7)
C(78')	57(7)	340(20)	54(6)	-42(9)	-30(5)	81(10)
N(8)	36(3)	31(3)	32(3)	2(2)	3(2)	6(2)
C(81)	46(4)	50(5)	51(5)	5(4)	-2(4)	20(4)
C(82)	45(5)	66(5)	55(5)	4(4)	-5(4)	16(4)
C(83)	43(4)	34(4)	52(5)	9(3)	-2(3)	1(3)
C(84)	50(4)	60(5)	40(4)	17(4)	-1(3)	-17(4)
C(85)	43(4)	48(4)	39(4)	3(3)	6(3)	15(3)
C(86)	62(5)	74(6)	31(4)	7(4)	13(4)	9(4)
C(87)	55(5)	34(4)	40(4)	4(3)	9(3)	-5(3)
C(88)	54(5)	58(5)	40(4)	2(4)	6(4)	-7(4)
N(9)	35(3)	28(3)	30(3)	-4(2)	4(2)	-7(2)
C(91)	45(4)	61(5)	40(4)	0(4)	8(3)	-6(4)
C(92)	43(4)	68(5)	37(4)	-11(4)	4(3)	-2(4)
C(93)	43(4)	45(4)	43(4)	-1(3)	6(3)	-1(3)
C(94)	54(5)	75(6)	47(5)	-8(4)	-3(4)	17(4)
C(95)	50(4)	43(4)	41(4)	6(3)	-1(3)	1(3)

C(96)	58(5)	61(5)	54(5)	-1(4)	-14(4)	-1(4)
C(97)	52(5)	50(5)	46(5)	-11(4)	3(4)	-4(4)
C(98)	55(5)	66(5)	42(4)	-16(4)	12(4)	-1(4)
Cl(1)	157(4)	113(3)	377(8)	-53(4)	28(5)	-17(3)
Cl(2)	174(5)	157(4)	129(4)	-34(3)	34(3)	-27(3)
C(1S)	115(10)	162(13)	153(12)	72(11)	33(9)	-45(10)

Table VI.5. Hydrogen coordinates (x 10^4) and isotropic displacement parameters ($Å^2$x 10^3) for $C_{38}H_{48}FeN_4O_{10}V_2$, 1.3.

	x	y	z	U(eq)
H(16)	1299	2815	2824	51
H(17)	1155	2857	2033	63
H(18)	1616	3908	1798	67
H(19)	2079	4561	2422	54
H(26)	-594	4776	2089	45
H(27)	-419	4784	2883	58
H(28)	-887	3727	3148	58
H(29)	-1353	3042	2534	51
H(46)	6403	3587	1752	42
H(47)	6759	2865	2355	45
H(48)	5010	2598	2698	50
H(49)	3498	3157	2306	45
H(56)	4249	3991	3187	48
H(57)	3952	4726	2586	49
H(58)	5757	4953	2257	50
H(59)	7189	4362	2656	42
H(61A)	3935	1323	755	46
H(61B)	3348	1553	1159	46
H(62A)	5199	1470	1295	113
H(62B)	4861	2166	1330	113
H(62C)	5448	1928	928	113
H(63A)	1912	1899	755	41
H(63B)	2459	1719	333	41
H(64A)	1102	2435	209	77
H(64B)	2209	2731	89	77
H(64C)	1655	2908	511	77
H(65A)	3953	2738	211	46
H(65B)	4900	2511	497	46
H(66A)	4944	1988	-134	75
H(66B)	3772	1744	-61	75
H(66C)	4715	1516	226	75
H(67A)	3102	3139	833	36
H(67B)	4085	2885	1094	36
H(68A)	2535	2951	1536	162
H(68B)	2887	2258	1496	162

H(68C)	1909	2506	1235	162
H(61C)	4338	2727	1115	110
H(61D)	4968	2548	708	110
H(62D)	5648	1919	1246	113
H(62E)	4986	1483	950	113
H(62F)	4485	1711	1372	113
H(63C)	3336	2913	271	93
H(63D)	2789	3095	695	93
H(64D)	1473	2926	169	77
H(64E)	1310	2461	538	77
H(64F)	1864	2240	126	77
H(65C)	2913	1583	272	43
H(65D)	3833	1324	560	43
H(66D)	4634	1499	-81	75
H(66E)	5057	2032	208	75
H(66F)	4131	2162	-114	75
H(67C)	2925	1652	1210	76
H(67D)	1937	1904	949	76
H(68D)	2134	2535	1580	162
H(68E)	2338	2952	1188	162
H(68F)	3313	2700	1449	162
H(71A)	2156	8168	959	50
H(71B)	3015	7904	1271	50
H(72A)	1410	8077	1648	106
H(72B)	1600	7361	1633	106
H(72C)	756	7667	1333	106
H(73A)	947	6919	900	54
H(73B)	1585	6694	506	54
H(74A)	241	7415	298	83
H(74B)	1379	7687	196	83
H(74C)	753	7917	591	83
H(75A)	3954	7492	705	48
H(75B)	3085	7718	387	48
H(76A)	4103	6934	94	69
H(76B)	2905	6715	131	69
H(76C)	3766	6483	453	69
H(77A)	2388	6636	1391	59
H(77B)	3045	6357	1013	59
H(78A)	4328	6771	1532	227
H(78B)	3785	7423	1490	227
H(78C)	4435	7147	1115	227
H(71C)	1956	6812	1384	46
H(71D)	1011	6987	1080	46
H(72D)	871	7634	1663	106
H(72E)	1223	8053	1288	106
H(72F)	2076	7838	1620	106

H(73C)	1841	8160	764	40
H(73D)	2451	7897	373	40
H(74D)	607	7877	236	83
H(74E)	406	7484	639	83
H(74F)	1021	7194	260	83
H(75C)	2012	6635	499	51
H(75D)	2902	6432	815	51
H(76D)	3574	6450	127	69
H(76E)	4228	6907	410	69
H(76F)	3350	7162	103	69
H(77C)	3236	7937	1233	51
H(77D)	3935	7722	849	51
H(78D)	4420	7233	1554	227
H(78E)	4390	6782	1171	227
H(78F)	3409	6815	1476	227
H(81A)	8796	4551	1080	59
H(81B)	9401	4797	686	59
H(82A)	10229	5141	1283	83
H(82B)	9163	5466	1423	83
H(82C)	9781	5706	1030	83
H(83A)	7455	5877	374	52
H(83B)	8359	6088	683	52
H(84A)	8988	6081	21	75
H(84B)	8707	5377	-23	75
H(84C)	9613	5589	287	75
H(85A)	6572	5571	979	52
H(85B)	7570	5710	1263	52
H(86A)	6412	5050	1600	84
H(86B)	7508	4712	1521	84
H(86C)	6512	4570	1236	84
H(87A)	7873	4632	255	52
H(87B)	7427	4315	658	52
H(88A)	6054	4482	204	76
H(88B)	6321	5190	188	76
H(88C)	5876	4896	600	76
H(91A)	5568	5066	4397	58
H(91B)	6465	4854	4709	58
H(92A)	5428	5613	5004	74
H(92B)	5726	6068	4642	74
H(92C)	6613	5851	4958	74
H(93A)	8614	5612	4193	52
H(93B)	7995	5850	4586	52
H(94A)	9281	5151	4783	88
H(94B)	8763	4647	4494	88
H(94C)	8141	4885	4888	88
H(95A)	6647	6193	4093	53

H(95B)	7309	5895	3731	53
H(96A)	5593	6065	3518	87
H(96B)	5154	5657	3885	87
H(96C)	5816	5351	3524	87
H(97A)	6483	4607	3871	59
H(97B)	7413	4410	4174	59
H(98A)	8004	4367	3488	82
H(98B)	8668	4867	3731	82
H(98C)	7739	5070	3429	82

Table VI.6. Torsion angles [°] for $C_{38}H_{48}FeN_4O_{10}V_2$, 1.3.

C(15)-N(1)-C(1)-V(1)	-14(12)	C(56)-Fe(2)-C(45)-N(31)	59.1(7)
C(10)-V(1)-C(1)-N(1)	-12(12)	C(57)-Fe(2)-C(45)-N(31)	20.8(7)
C(13)-V(1)-C(1)-N(1)	93(10)	C(55)-Fe(2)-C(45)-C(49)	34(18)
C(12)-V(1)-C(1)-N(1)	178(100)	C(48)-Fe(2)-C(45)-C(49)	38.9(4)
C(14)-V(1)-C(1)-N(1)	3(10)	C(59)-Fe(2)-C(45)-C(49)	178.0(4)
C(11)-V(1)-C(1)-N(1)	-92(10)	C(58)-Fe(2)-C(45)-C(49)	-143.2(4)
C(25)-N(2)-C(2)-V(2)	26(8)	C(47)-Fe(2)-C(45)-C(49)	82.4(4)
C(20)-V(2)-C(2)-N(2)	18(8)	C(46)-Fe(2)-C(45)-C(49)	120.5(5)
C(24)-V(2)-C(2)-N(2)	-11(7)	C(56)-Fe(2)-C(45)-C(49)	-60.8(5)
C(23)-V(2)-C(2)-N(2)	-100(7)	C(57)-Fe(2)-C(45)-C(49)	-99.0(4)
C(21)-V(2)-C(2)-N(2)	82(7)	C(55)-Fe(2)-C(45)-C(46)	-87(18)
C(22)-V(2)-C(2)-N(2)	174(7)	C(48)-Fe(2)-C(45)-C(46)	-81.6(4)
C(13)-V(1)-C(10)-O(10)	-114(12)	C(59)-Fe(2)-C(45)-C(46)	57.5(6)
C(12)-V(1)-C(10)-O(10)	161(12)	C(58)-Fe(2)-C(45)-C(46)	96.3(4)
C(14)-V(1)-C(10)-O(10)	-24(12)	C(47)-Fe(2)-C(45)-C(46)	-38.1(4)
C(11)-V(1)-C(10)-O(10)	71(12)	C(49)-Fe(2)-C(45)-C(46)	-120.5(5)
C(1)-V(1)-C(10)-O(10)	-10(13)	C(56)-Fe(2)-C(45)-C(46)	178.7(4)
C(10)-V(1)-C(11)-O(11)	34(14)	C(57)-Fe(2)-C(45)-C(46)	140.4(4)
C(13)-V(1)-C(11)-O(11)	-48(15)	N(31)-C(45)-C(46)-C(47)	-179.8(6)
C(12)-V(1)-C(11)-O(11)	-57(14)	C(49)-C(45)-C(46)-C(47)	0.6(7)
C(14)-V(1)-C(11)-O(11)	121(14)	Fe(2)-C(45)-C(46)-C(47)	59.9(4)
C(1)-V(1)-C(11)-O(11)	-153(14)	N(31)-C(45)-C(46)-Fe(2)	120.3(7)
C(10)-V(1)-C(12)-O(12)	51(11)	C(49)-C(45)-C(46)-Fe(2)	-59.3(4)
C(13)-V(1)-C(12)-O(12)	-41(11)	C(45)-Fe(2)-C(46)-C(47)	-117.8(6)
C(14)-V(1)-C(12)-O(12)	-26(13)	C(55)-Fe(2)-C(46)-C(47)	60.9(6)
C(11)-V(1)-C(12)-O(12)	138(11)	C(48)-Fe(2)-C(46)-C(47)	-36.6(4)
C(1)-V(1)-C(12)-O(12)	-130(11)	C(59)-Fe(2)-C(46)-C(47)	97.4(4)
C(10)-V(1)-C(13)-O(13)	23(29)	C(58)-Fe(2)-C(46)-C(47)	141.0(4)
C(12)-V(1)-C(13)-O(13)	114(29)	C(49)-Fe(2)-C(46)-C(47)	-80.7(4)
C(14)-V(1)-C(13)-O(13)	-64(29)	C(56)-Fe(2)-C(46)-C(47)	158(17)
C(11)-V(1)-C(13)-O(13)	105(28)	C(57)-Fe(2)-C(46)-C(47)	178.0(4)
C(1)-V(1)-C(13)-O(13)	-150(29)	C(55)-Fe(2)-C(46)-C(45)	178.7(4)
C(10)-V(1)-C(14)-O(14)	-45(25)	C(48)-Fe(2)-C(46)-C(45)	81.2(4)
C(13)-V(1)-C(14)-O(14)	47(25)	C(59)-Fe(2)-C(46)-C(45)	-144.8(4)

C(12)-V(1)-C(14)-O(14)	32(27)	C(58)-Fe(2)-C(46)-C(45)	-101.2(4)
C(11)-V(1)-C(14)-O(14)	-132(25)	C(47)-Fe(2)-C(46)-C(45)	117.8(6)
C(1)-V(1)-C(14)-O(14)	136(25)	C(49)-Fe(2)-C(46)-C(45)	37.0(4)
C(1)-N(1)-C(15)-C(16)	177.7(19)	C(56)-Fe(2)-C(46)-C(45)	-84(18)
C(1)-N(1)-C(15)-C(19)	-1(3)	C(57)-Fe(2)-C(46)-C(45)	-64.2(6)
C(1)-N(1)-C(15)-Fe(1)	-91(2)	C(45)-C(46)-C(47)-C(48)	-0.6(7)
C(18)-Fe(1)-C(15)-N(1)	157.4(7)	Fe(2)-C(46)-C(47)-C(48)	58.6(5)
C(17)-Fe(1)-C(15)-N(1)	-159.9(7)	C(45)-C(46)-C(47)-Fe(2)	-59.3(4)
C(25)-Fe(1)-C(15)-N(1)	-89(15)	C(45)-Fe(2)-C(47)-C(48)	-82.1(4)
C(27)-Fe(1)-C(15)-N(1)	21.6(7)	C(55)-Fe(2)-C(47)-C(48)	97.2(4)
C(16)-Fe(1)-C(15)-N(1)	-121.0(8)	C(59)-Fe(2)-C(47)-C(48)	140.6(4)
C(26)-Fe(1)-C(15)-N(1)	59.7(8)	C(58)-Fe(2)-C(47)-C(48)	177.6(4)
C(19)-Fe(1)-C(15)-N(1)	119.5(8)	C(49)-Fe(2)-C(47)-C(48)	-37.9(4)
C(29)-Fe(1)-C(15)-N(1)	-59.8(8)	C(46)-Fe(2)-C(47)-C(48)	-120.9(6)
C(28)-Fe(1)-C(15)-N(1)	-21.7(7)	C(56)-Fe(2)-C(47)-C(48)	59.6(6)
C(18)-Fe(1)-C(15)-C(16)	-81.6(5)	C(57)-Fe(2)-C(47)-C(48)	172(37)
C(17)-Fe(1)-C(15)-C(16)	-38.9(4)	C(45)-Fe(2)-C(47)-C(46)	38.8(4)
C(25)-Fe(1)-C(15)-C(16)	32(15)	C(55)-Fe(2)-C(47)-C(46)	-141.9(4)
C(27)-Fe(1)-C(15)-C(16)	142.6(4)	C(48)-Fe(2)-C(47)-C(46)	120.9(6)
C(26)-Fe(1)-C(15)-C(16)	-179.3(4)	C(59)-Fe(2)-C(47)-C(46)	-98.5(4)
C(19)-Fe(1)-C(15)-C(16)	-119.5(6)	C(58)-Fe(2)-C(47)-C(46)	-61.4(5)
C(29)-Fe(1)-C(15)-C(16)	61.2(6)	C(49)-Fe(2)-C(47)-C(46)	83.0(4)
C(28)-Fe(1)-C(15)-C(16)	99.3(5)	C(56)-Fe(2)-C(47)-C(46)	-179.5(4)
C(18)-Fe(1)-C(15)-C(19)	37.8(5)	C(57)-Fe(2)-C(47)-C(46)	-67(12)
C(17)-Fe(1)-C(15)-C(19)	80.6(5)	C(46)-C(47)-C(48)-C(49)	0.5(7)
C(25)-Fe(1)-C(15)-C(19)	152(15)	Fe(2)-C(47)-C(48)-C(49)	59.3(4)
C(27)-Fe(1)-C(15)-C(19)	-97.9(5)	C(46)-C(47)-C(48)-Fe(2)	-58.9(5)
C(16)-Fe(1)-C(15)-C(19)	119.5(6)	C(45)-Fe(2)-C(48)-C(47)	80.8(4)
C(26)-Fe(1)-C(15)-C(19)	-59.9(6)	C(55)-Fe(2)-C(48)-C(47)	-99.3(4)
C(29)-Fe(1)-C(15)-C(19)	-179.3(5)	C(59)-Fe(2)-C(48)-C(47)	-61.2(6)
C(28)-Fe(1)-C(15)-C(19)	-141.2(5)	C(58)-Fe(2)-C(48)-C(47)	-43(7)
N(1)-C(15)-C(16)-C(17)	-179.0(6)	C(49)-Fe(2)-C(48)-C(47)	119.5(6)
C(19)-C(15)-C(16)-C(17)	-0.4(7)	C(46)-Fe(2)-C(48)-C(47)	36.6(4)
Fe(1)-C(15)-C(16)-C(17)	59.7(4)	C(56)-Fe(2)-C(48)-C(47)	-143.7(4)
N(1)-C(15)-C(16)-Fe(1)	121.3(6)	C(57)-Fe(2)-C(48)-C(47)	-179.7(4)
C(19)-C(15)-C(16)-Fe(1)	-60.0(4)	C(45)-Fe(2)-C(48)-C(49)	-38.7(4)
C(18)-Fe(1)-C(16)-C(15)	80.9(5)	C(55)-Fe(2)-C(48)-C(49)	141.2(4)
C(17)-Fe(1)-C(16)-C(15)	117.3(6)	C(59)-Fe(2)-C(48)-C(49)	179.2(4)
C(25)-Fe(1)-C(16)-C(15)	-179.2(4)	C(58)-Fe(2)-C(48)-C(49)	-162(7)
C(27)-Fe(1)-C(16)-C(15)	-60.6(6)	C(47)-Fe(2)-C(48)-C(49)	-119.5(6)
C(26)-Fe(1)-C(16)-C(15)	152(20)	C(46)-Fe(2)-C(48)-C(49)	-83.0(4)
C(19)-Fe(1)-C(16)-C(15)	37.6(4)	C(56)-Fe(2)-C(48)-C(49)	96.8(4)
C(29)-Fe(1)-C(16)-C(15)	-141.0(4)	C(57)-Fe(2)-C(48)-C(49)	60.8(6)
C(28)-Fe(1)-C(16)-C(15)	-97.6(4)	N(31)-C(45)-C(49)-C(48)	-179.9(6)
C(18)-Fe(1)-C(16)-C(17)	-36.4(5)	C(46)-C(45)-C(49)-C(48)	-0.3(7)
C(15)-Fe(1)-C(16)-C(17)	-117.3(6)	Fe(2)-C(45)-C(49)-C(48)	-59.7(4)

C(25)-Fe(1)-C(16)-C(17)	63.5(6)	N(31)-C(45)-C(49)-Fe(2)	-120.3(6)
C(27)-Fe(1)-C(16)-C(17)	-178.0(5)	C(46)-C(45)-C(49)-Fe(2)	59.4(4)
C(26)-Fe(1)-C(16)-C(17)	34(20)	C(47)-C(48)-C(49)-C(45)	-0.1(7)
C(19)-Fe(1)-C(16)-C(17)	-79.7(5)	Fe(2)-C(48)-C(49)-C(45)	59.5(4)
C(29)-Fe(1)-C(16)-C(17)	101.6(5)	C(47)-C(48)-C(49)-Fe(2)	-59.6(5)
C(28)-Fe(1)-C(16)-C(17)	145.0(5)	C(55)-Fe(2)-C(49)-C(45)	-179.3(4)
C(15)-C(16)-C(17)-C(18)	-0.1(7)	C(48)-Fe(2)-C(49)-C(45)	-117.4(6)
Fe(1)-C(16)-C(17)-C(18)	59.7(5)	C(59)-Fe(2)-C(49)-C(45)	-134(9)
C(15)-C(16)-C(17)-Fe(1)	-59.8(4)	C(58)-Fe(2)-C(49)-C(45)	61.4(6)
C(15)-Fe(1)-C(17)-C(18)	-81.3(5)	C(47)-Fe(2)-C(49)-C(45)	-80.3(4)
C(25)-Fe(1)-C(17)-C(18)	99.7(5)	C(46)-Fe(2)-C(49)-C(45)	-37.1(4)
C(27)-Fe(1)-C(17)-C(18)	-7(12)	C(56)-Fe(2)-C(49)-C(45)	142.1(4)
C(16)-Fe(1)-C(17)-C(18)	-119.9(6)	C(57)-Fe(2)-C(49)-C(45)	98.9(4)
C(26)-Fe(1)-C(17)-C(18)	60.9(6)	C(45)-Fe(2)-C(49)-C(48)	117.4(6)
C(19)-Fe(1)-C(17)-C(18)	-37.1(4)	C(55)-Fe(2)-C(49)-C(48)	-61.8(6)
C(29)-Fe(1)-C(17)-C(18)	144.5(5)	C(59)-Fe(2)-C(49)-C(48)	-17(9)
C(28)-Fe(1)-C(17)-C(18)	-178.2(5)	C(58)-Fe(2)-C(49)-C(48)	178.9(4)
C(18)-Fe(1)-C(17)-C(16)	119.9(6)	C(47)-Fe(2)-C(49)-C(48)	37.1(4)
C(15)-Fe(1)-C(17)-C(16)	38.6(4)	C(46)-Fe(2)-C(49)-C(48)	80.3(4)
C(25)-Fe(1)-C(17)-C(16)	-140.4(4)	C(56)-Fe(2)-C(49)-C(48)	-100.4(4)
C(27)-Fe(1)-C(17)-C(16)	113(12)	C(57)-Fe(2)-C(49)-C(48)	-143.6(4)
C(26)-Fe(1)-C(17)-C(16)	-179.2(4)	C(53)-V(4)-C(50)-O(50)	-57(100)
C(19)-Fe(1)-C(17)-C(16)	82.8(5)	C(52)-V(4)-C(50)-O(50)	33(100)
C(29)-Fe(1)-C(17)-C(16)	-95.6(5)	C(54)-V(4)-C(50)-O(50)	-146(100)
C(28)-Fe(1)-C(17)-C(16)	-58.3(6)	C(51)-V(4)-C(50)-O(50)	124(100)
C(16)-C(17)-C(18)-C(19)	0.6(8)	C(32)-V(4)-C(50)-O(50)	46(100)
Fe(1)-C(17)-C(18)-C(19)	60.2(5)	C(53)-V(4)-C(51)-O(51)	-12(100)
C(16)-C(17)-C(18)-Fe(1)	-59.6(5)	C(50)-V(4)-C(51)-O(51)	157(100)
C(15)-Fe(1)-C(18)-C(17)	81.7(5)	C(52)-V(4)-C(51)-O(51)	-114(100)
C(25)-Fe(1)-C(18)-C(17)	-97.3(5)	C(54)-V(4)-C(51)-O(51)	70(100)
C(27)-Fe(1)-C(18)-C(17)	179.7(4)	C(32)-V(4)-C(51)-O(51)	-25(100)
C(16)-Fe(1)-C(18)-C(17)	37.8(4)	C(53)-V(4)-C(52)-O(52)	60(21)
C(26)-Fe(1)-C(18)-C(17)	-141.3(4)	C(50)-V(4)-C(52)-O(52)	-32(21)
C(19)-Fe(1)-C(18)-C(17)	120.1(7)	C(54)-V(4)-C(52)-O(52)	-15(25)
C(29)-Fe(1)-C(18)-C(17)	-58.2(7)	C(51)-V(4)-C(52)-O(52)	-125(21)
C(28)-Fe(1)-C(18)-C(17)	122(15)	C(32)-V(4)-C(52)-O(52)	148(21)
C(17)-Fe(1)-C(18)-C(19)	-120.1(7)	C(50)-V(4)-C(53)-O(53)	12(48)
C(15)-Fe(1)-C(18)-C(19)	-38.4(4)	C(52)-V(4)-C(53)-O(53)	-77(48)
C(25)-Fe(1)-C(18)-C(19)	142.6(4)	C(54)-V(4)-C(53)-O(53)	99(48)
C(27)-Fe(1)-C(18)-C(19)	59.7(6)	C(51)-V(4)-C(53)-O(53)	-180(100)
C(16)-Fe(1)-C(18)-C(19)	-82.3(5)	C(32)-V(4)-C(53)-O(53)	-167(100)
C(26)-Fe(1)-C(18)-C(19)	98.6(5)	C(53)-V(4)-C(54)-O(54)	-98(15)
C(29)-Fe(1)-C(18)-C(19)	-178.3(4)	C(50)-V(4)-C(54)-O(54)	-5(14)
C(28)-Fe(1)-C(18)-C(19)	2(15)	C(52)-V(4)-C(54)-O(54)	-23(18)
C(17)-C(18)-C(19)-C(15)	-0.8(8)	C(51)-V(4)-C(54)-O(54)	87(15)
Fe(1)-C(18)-C(19)-C(15)	59.1(4)	C(32)-V(4)-C(54)-O(54)	174(100)

C(17)-C(18)-C(19)-Fe(1)	-59.9(5)	C(32)-N(32)-C(55)-C(59)	-8(10)
N(1)-C(15)-C(19)-C(18)	179.4(6)	C(32)-N(32)-C(55)-C(56)	168(9)
C(16)-C(15)-C(19)-C(18)	0.7(7)	C(32)-N(32)-C(55)-Fe(2)	80(10)
Fe(1)-C(15)-C(19)-C(18)	-59.2(4)	C(45)-Fe(2)-C(55)-N(32)	25(18)
N(1)-C(15)-C(19)-Fe(1)	-121.4(6)	C(48)-Fe(2)-C(55)-N(32)	20.0(7)
C(16)-C(15)-C(19)-Fe(1)	59.9(4)	C(59)-Fe(2)-C(55)-N(32)	-119.7(7)
C(17)-Fe(1)-C(19)-C(18)	36.5(5)	C(58)-Fe(2)-C(55)-N(32)	-157.9(7)
C(15)-Fe(1)-C(19)-C(18)	118.2(7)	C(47)-Fe(2)-C(55)-N(32)	-23.3(7)
C(25)-Fe(1)-C(19)-C(18)	-61.0(7)	C(49)-Fe(2)-C(55)-N(32)	58.3(7)
C(27)-Fe(1)-C(19)-C(18)	-142.7(5)	C(46)-Fe(2)-C(55)-N(32)	-60.7(7)
C(16)-Fe(1)-C(19)-C(18)	80.8(5)	C(56)-Fe(2)-C(55)-N(32)	120.6(8)
C(26)-Fe(1)-C(19)-C(18)	-98.4(5)	C(57)-Fe(2)-C(55)-N(32)	158.2(7)
C(29)-Fe(1)-C(19)-C(18)	136(11)	C(45)-Fe(2)-C(55)-C(59)	145(18)
C(28)-Fe(1)-C(19)-C(18)	-179.9(5)	C(48)-Fe(2)-C(55)-C(59)	139.8(4)
C(18)-Fe(1)-C(19)-C(15)	-118.2(7)	C(58)-Fe(2)-C(55)-C(59)	-38.2(4)
C(17)-Fe(1)-C(19)-C(15)	-81.7(5)	C(47)-Fe(2)-C(55)-C(59)	96.5(4)
C(25)-Fe(1)-C(19)-C(15)	-179.3(4)	C(49)-Fe(2)-C(55)-C(59)	178.1(4)
C(27)-Fe(1)-C(19)-C(15)	99.1(5)	C(46)-Fe(2)-C(55)-C(59)	59.1(6)
C(16)-Fe(1)-C(19)-C(15)	-37.4(4)	C(56)-Fe(2)-C(55)-C(59)	-119.6(6)
C(26)-Fe(1)-C(19)-C(15)	143.4(4)	C(57)-Fe(2)-C(55)-C(59)	-82.1(4)
C(29)-Fe(1)-C(19)-C(15)	17(12)	C(45)-Fe(2)-C(55)-C(56)	-95(18)
C(28)-Fe(1)-C(19)-C(15)	61.8(6)	C(48)-Fe(2)-C(55)-C(56)	-100.6(4)
C(24)-V(2)-C(20)-O(20)	69(11)	C(59)-Fe(2)-C(55)-C(56)	119.6(6)
C(23)-V(2)-C(20)-O(20)	157(11)	C(58)-Fe(2)-C(55)-C(56)	81.5(4)
C(21)-V(2)-C(20)-O(20)	-24(11)	C(47)-Fe(2)-C(55)-C(56)	-143.9(4)
C(22)-V(2)-C(20)-O(20)	-116(11)	C(49)-Fe(2)-C(55)-C(56)	-62.3(6)
C(2)-V(2)-C(20)-O(20)	39(13)	C(46)-Fe(2)-C(55)-C(56)	178.7(4)
C(20)-V(2)-C(21)-O(21)	-1(7)	C(57)-Fe(2)-C(55)-C(56)	37.6(4)
C(24)-V(2)-C(21)-O(21)	-89(7)	N(32)-C(55)-C(56)-C(57)	-177.9(6)
C(23)-V(2)-C(21)-O(21)	17(9)	C(59)-C(55)-C(56)-C(57)	-0.7(7)
C(22)-V(2)-C(21)-O(21)	89(7)	Fe(2)-C(55)-C(56)-C(57)	-60.2(4)
C(2)-V(2)-C(21)-O(21)	-176(100)	N(32)-C(55)-C(56)-Fe(2)	-117.7(7)
C(20)-V(2)-C(22)-O(22)	-19(7)	C(59)-C(55)-C(56)-Fe(2)	59.5(4)
C(24)-V(2)-C(22)-O(22)	58(8)	C(45)-Fe(2)-C(56)-C(57)	-62.9(6)
C(23)-V(2)-C(22)-O(22)	71(7)	C(55)-Fe(2)-C(56)-C(57)	118.4(6)
C(21)-V(2)-C(22)-O(22)	-103(7)	C(48)-Fe(2)-C(56)-C(57)	-145.0(4)
C(2)-V(2)-C(22)-O(22)	163(7)	C(59)-Fe(2)-C(56)-C(57)	81.2(4)
C(20)-V(2)-C(23)-O(23)	-5(11)	C(58)-Fe(2)-C(56)-C(57)	37.4(4)
C(24)-V(2)-C(23)-O(23)	84(11)	C(47)-Fe(2)-C(56)-C(57)	178.0(4)
C(21)-V(2)-C(23)-O(23)	-23(12)	C(49)-Fe(2)-C(56)-C(57)	-100.6(4)
C(22)-V(2)-C(23)-O(23)	-95(11)	C(46)-Fe(2)-C(56)-C(57)	21(18)
C(2)-V(2)-C(23)-O(23)	170(11)	C(45)-Fe(2)-C(56)-C(55)	178.7(4)
C(20)-V(2)-C(24)-O(24)	35(11)	C(48)-Fe(2)-C(56)-C(55)	96.6(4)
C(23)-V(2)-C(24)-O(24)	-56(11)	C(59)-Fe(2)-C(56)-C(55)	-37.2(4)
C(21)-V(2)-C(24)-O(24)	119(11)	C(58)-Fe(2)-C(56)-C(55)	-81.0(4)
C(22)-V(2)-C(24)-O(24)	-42(13)	C(47)-Fe(2)-C(56)-C(55)	59.5(6)

C(2)-V(2)-C(24)-O(24)	-148(11)	C(49)-Fe(2)-C(56)-C(55)	140.9(4)
C(2)-N(2)-C(25)-C(26)	-178(2)	C(46)-Fe(2)-C(56)-C(55)	-98(17)
C(2)-N(2)-C(25)-C(29)	-1(3)	C(57)-Fe(2)-C(56)-C(55)	-118.4(6)
C(2)-N(2)-C(25)-Fe(1)	89(2)	C(55)-C(56)-C(57)-C(58)	0.6(7)
C(18)-Fe(1)-C(25)-N(2)	24.3(7)	Fe(2)-C(56)-C(57)-C(58)	-58.7(5)
C(17)-Fe(1)-C(25)-N(2)	-18.4(7)	C(55)-C(56)-C(57)-Fe(2)	59.3(4)
C(15)-Fe(1)-C(25)-N(2)	-89(15)	C(45)-Fe(2)-C(57)-C(56)	140.7(4)
C(27)-Fe(1)-C(25)-N(2)	160.1(7)	C(55)-Fe(2)-C(57)-C(56)	-38.6(4)
C(16)-Fe(1)-C(25)-N(2)	-57.5(8)	C(48)-Fe(2)-C(57)-C(56)	57.7(6)
C(26)-Fe(1)-C(25)-N(2)	121.8(8)	C(59)-Fe(2)-C(57)-C(56)	-82.3(4)
C(19)-Fe(1)-C(25)-N(2)	62.0(8)	C(58)-Fe(2)-C(57)-C(56)	-119.8(6)
C(29)-Fe(1)-C(25)-N(2)	-118.7(8)	C(47)-Fe(2)-C(57)-C(56)	-114(11)
C(28)-Fe(1)-C(25)-N(2)	-156.6(7)	C(49)-Fe(2)-C(57)-C(56)	96.2(4)
C(18)-Fe(1)-C(25)-C(26)	-97.5(5)	C(46)-Fe(2)-C(57)-C(56)	-179.5(4)
C(17)-Fe(1)-C(25)-C(26)	-140.2(4)	C(45)-Fe(2)-C(57)-C(58)	-99.5(4)
C(15)-Fe(1)-C(25)-C(26)	149(15)	C(55)-Fe(2)-C(57)-C(58)	81.2(4)
C(27)-Fe(1)-C(25)-C(26)	38.3(4)	C(48)-Fe(2)-C(57)-C(58)	177.6(4)
C(16)-Fe(1)-C(25)-C(26)	-179.3(4)	C(59)-Fe(2)-C(57)-C(58)	37.5(4)
C(19)-Fe(1)-C(25)-C(26)	-59.8(6)	C(47)-Fe(2)-C(57)-C(58)	6(12)
C(29)-Fe(1)-C(25)-C(26)	119.5(5)	C(49)-Fe(2)-C(57)-C(58)	-144.0(4)
C(28)-Fe(1)-C(25)-C(26)	81.6(4)	C(46)-Fe(2)-C(57)-C(58)	-59.7(6)
C(18)-Fe(1)-C(25)-C(29)	143.0(5)	C(56)-Fe(2)-C(57)-C(58)	119.8(6)
C(17)-Fe(1)-C(25)-C(29)	100.3(5)	C(56)-C(57)-C(58)-C(59)	-0.4(8)
C(15)-Fe(1)-C(25)-C(29)	30(15)	Fe(2)-C(57)-C(58)-C(59)	-59.4(5)
C(27)-Fe(1)-C(25)-C(29)	-81.2(4)	C(56)-C(57)-C(58)-Fe(2)	59.0(5)
C(16)-Fe(1)-C(25)-C(29)	61.2(6)	C(45)-Fe(2)-C(58)-C(59)	-142.1(4)
C(26)-Fe(1)-C(25)-C(29)	-119.5(5)	C(55)-Fe(2)-C(58)-C(59)	38.0(4)
C(19)-Fe(1)-C(25)-C(29)	-179.3(5)	C(48)-Fe(2)-C(58)-C(59)	-19(7)
C(28)-Fe(1)-C(25)-C(29)	-37.9(4)	C(47)-Fe(2)-C(58)-C(59)	-60.3(5)
N(2)-C(25)-C(26)-C(27)	178.2(6)	C(49)-Fe(2)-C(58)-C(59)	179.3(4)
C(29)-C(25)-C(26)-C(27)	0.1(7)	C(46)-Fe(2)-C(58)-C(59)	-97.7(4)
Fe(1)-C(25)-C(26)-C(27)	-59.3(4)	C(56)-Fe(2)-C(58)-C(59)	82.6(4)
N(2)-C(25)-C(26)-Fe(1)	-122.4(6)	C(57)-Fe(2)-C(58)-C(59)	119.5(6)
C(29)-C(25)-C(26)-Fe(1)	59.5(4)	C(45)-Fe(2)-C(58)-C(57)	98.4(4)
C(18)-Fe(1)-C(26)-C(25)	100.0(4)	C(55)-Fe(2)-C(58)-C(57)	-81.5(4)
C(17)-Fe(1)-C(26)-C(25)	63.4(6)	C(48)-Fe(2)-C(58)-C(57)	-139(7)
C(15)-Fe(1)-C(26)-C(25)	-179.2(4)	C(59)-Fe(2)-C(58)-C(57)	-119.5(6)
C(27)-Fe(1)-C(26)-C(25)	-118.6(6)	C(47)-Fe(2)-C(58)-C(57)	-179.8(4)
C(16)-Fe(1)-C(26)-C(25)	29(20)	C(49)-Fe(2)-C(58)-C(57)	59.8(6)
C(19)-Fe(1)-C(26)-C(25)	143.4(4)	C(46)-Fe(2)-C(58)-C(57)	142.8(4)
C(29)-Fe(1)-C(26)-C(25)	-38.0(4)	C(56)-Fe(2)-C(58)-C(57)	-37.0(4)
C(28)-Fe(1)-C(26)-C(25)	-81.4(4)	N(32)-C(55)-C(59)-C(58)	177.7(6)
C(18)-Fe(1)-C(26)-C(27)	-141.3(5)	C(56)-C(55)-C(59)-C(58)	0.4(7)
C(17)-Fe(1)-C(26)-C(27)	-178.0(5)	Fe(2)-C(55)-C(59)-C(58)	59.8(4)
C(15)-Fe(1)-C(26)-C(27)	-60.6(6)	N(32)-C(55)-C(59)-Fe(2)	117.8(7)
C(25)-Fe(1)-C(26)-C(27)	118.6(6)	C(56)-C(55)-C(59)-Fe(2)	-59.4(4)

C(16)-Fe(1)-C(26)-C(27)	148(20)	C(57)-C(58)-C(59)-C(55)	0.0(7)
C(19)-Fe(1)-C(26)-C(27)	-98.0(5)	Fe(2)-C(58)-C(59)-C(55)	-59.8(4)
C(29)-Fe(1)-C(26)-C(27)	80.7(5)	C(57)-C(58)-C(59)-Fe(2)	59.8(5)
C(28)-Fe(1)-C(26)-C(27)	37.2(4)	C(45)-Fe(2)-C(59)-C(55)	-179.2(4)
C(25)-C(26)-C(27)-C(28)	-0.5(7)	C(48)-Fe(2)-C(59)-C(55)	-62.7(5)
Fe(1)-C(26)-C(27)-C(28)	-59.9(5)	C(58)-Fe(2)-C(59)-C(55)	118.4(5)
C(25)-C(26)-C(27)-Fe(1)	59.4(4)	C(47)-Fe(2)-C(59)-C(55)	-99.8(4)
C(18)-Fe(1)-C(27)-C(28)	-178.2(5)	C(49)-Fe(2)-C(59)-C(55)	-46(9)
C(17)-Fe(1)-C(27)-C(28)	-172(38)	C(46)-Fe(2)-C(59)-C(55)	-143.0(4)
C(15)-Fe(1)-C(27)-C(28)	-97.6(4)	C(56)-Fe(2)-C(59)-C(55)	37.8(4)
C(25)-Fe(1)-C(27)-C(28)	81.3(4)	C(57)-Fe(2)-C(59)-C(55)	80.9(4)
C(16)-Fe(1)-C(27)-C(28)	-60.1(6)	C(45)-Fe(2)-C(59)-C(58)	62.4(5)
C(26)-Fe(1)-C(27)-C(28)	119.2(6)	C(55)-Fe(2)-C(59)-C(58)	-118.4(5)
C(19)-Fe(1)-C(27)-C(28)	-141.6(4)	C(48)-Fe(2)-C(59)-C(58)	178.9(4)
C(29)-Fe(1)-C(27)-C(28)	36.8(4)	C(47)-Fe(2)-C(59)-C(58)	141.8(4)
C(18)-Fe(1)-C(27)-C(26)	62.6(6)	C(49)-Fe(2)-C(59)-C(58)	-165(9)
C(17)-Fe(1)-C(27)-C(26)	69(12)	C(46)-Fe(2)-C(59)-C(58)	98.7(4)
C(15)-Fe(1)-C(27)-C(26)	143.2(4)	C(56)-Fe(2)-C(59)-C(58)	-80.6(4)
C(25)-Fe(1)-C(27)-C(26)	-37.9(4)	C(57)-Fe(2)-C(59)-C(58)	-37.5(4)
C(16)-Fe(1)-C(27)-C(26)	-179.3(4)	C(63)-N(6)-C(61)-C(62)	-178.5(7)
C(19)-Fe(1)-C(27)-C(26)	99.2(4)	C(61')-N(6)-C(61)-C(62)	-2.8(11)
C(29)-Fe(1)-C(27)-C(26)	-82.4(4)	C(65')-N(6)-C(61)-C(62)	118.5(9)
C(28)-Fe(1)-C(27)-C(26)	-119.2(6)	C(63')-N(6)-C(61)-C(62)	-125(7)
C(26)-C(27)-C(28)-C(29)	0.7(7)	C(67)-N(6)-C(61)-C(62)	-54.3(8)
Fe(1)-C(27)-C(28)-C(29)	-58.7(5)	C(65)-N(6)-C(61)-C(62)	59.6(8)
C(26)-C(27)-C(28)-Fe(1)	59.5(4)	C(67')-N(6)-C(61)-C(62)	-120.9(10)
C(18)-Fe(1)-C(28)-C(27)	59(15)	C(61)-N(6)-C(63)-C(64)	174.9(7)
C(17)-Fe(1)-C(28)-C(27)	179.7(4)	C(61')-N(6)-C(63)-C(64)	86(9)
C(15)-Fe(1)-C(28)-C(27)	99.1(4)	C(65')-N(6)-C(63)-C(64)	-123.1(9)
C(25)-Fe(1)-C(28)-C(27)	-81.9(4)	C(63')-N(6)-C(63)-C(64)	-0.1(10)
C(16)-Fe(1)-C(28)-C(27)	142.8(4)	C(67)-N(6)-C(63)-C(64)	51.8(8)
C(26)-Fe(1)-C(28)-C(27)	-38.1(4)	C(65)-N(6)-C(63)-C(64)	-65.4(8)
C(19)-Fe(1)-C(28)-C(27)	61.0(6)	C(67')-N(6)-C(63)-C(64)	118.0(9)
C(29)-Fe(1)-C(28)-C(27)	-120.7(6)	C(63)-N(6)-C(65)-C(66)	-61.7(8)
C(18)-Fe(1)-C(28)-C(29)	-180(100)	C(61)-N(6)-C(65)-C(66)	58.4(8)
C(17)-Fe(1)-C(28)-C(29)	-59.6(6)	C(61')-N(6)-C(65)-C(66)	120.4(9)
C(15)-Fe(1)-C(28)-C(29)	-140.2(4)	C(65')-N(6)-C(65)-C(66)	-1.8(9)
C(25)-Fe(1)-C(28)-C(29)	38.8(4)	C(63')-N(6)-C(65)-C(66)	-121.1(9)
C(27)-Fe(1)-C(28)-C(29)	120.7(6)	C(67)-N(6)-C(65)-C(66)	176.4(7)
C(16)-Fe(1)-C(28)-C(29)	-96.5(5)	C(67')-N(6)-C(65)-C(66)	51(12)
C(26)-Fe(1)-C(28)-C(29)	82.6(4)	C(63)-N(6)-C(67)-C(68)	61.2(8)
C(19)-Fe(1)-C(28)-C(29)	-178.3(4)	C(61)-N(6)-C(67)-C(68)	-60.8(8)
C(27)-C(28)-C(29)-C(25)	-0.7(7)	C(61')-N(6)-C(67)-C(68)	-116.2(10)
Fe(1)-C(28)-C(29)-C(25)	-59.3(4)	C(65')-N(6)-C(67)-C(68)	-163(7)
C(27)-C(28)-C(29)-Fe(1)	58.6(5)	C(63')-N(6)-C(67)-C(68)	113.2(9)
N(2)-C(25)-C(29)-C(28)	-177.8(6)	C(65)-N(6)-C(67)-C(68)	-177.3(7)

C(26)-C(25)-C(29)-C(28)	0.3(7)	C(67')-N(6)-C(67)-C(68)	-0.1(9)
Fe(1)-C(25)-C(29)-C(28)	59.9(4)	C(75')-N(7)-C(71)-C(72)	-128(9)
N(2)-C(25)-C(29)-Fe(1)	122.3(6)	C(75)-N(7)-C(71)-C(72)	179.8(9)
C(26)-C(25)-C(29)-Fe(1)	-59.6(4)	C(71')-N(7)-C(71)-C(72)	-4.9(9)
C(18)-Fe(1)-C(29)-C(28)	180.0(5)	C(73)-N(7)-C(71)-C(72)	51.9(12)
C(17)-Fe(1)-C(29)-C(28)	144.2(5)	C(77')-N(7)-C(71)-C(72)	-132.1(12)
C(15)-Fe(1)-C(29)-C(28)	62.6(6)	C(73')-N(7)-C(71)-C(72)	110.2(10)
C(25)-Fe(1)-C(29)-C(28)	-118.2(6)	C(77)-N(7)-C(71)-C(72)	-65.0(10)
C(27)-Fe(1)-C(29)-C(28)	-36.6(4)	C(75')-N(7)-C(73)-C(74)	-122.1(10)
C(16)-Fe(1)-C(29)-C(28)	100.1(5)	C(71)-N(7)-C(73)-C(74)	57.9(11)
C(26)-Fe(1)-C(29)-C(28)	-80.8(5)	C(75)-N(7)-C(73)-C(74)	-69.7(10)
C(19)-Fe(1)-C(29)-C(28)	46(12)	C(71')-N(7)-C(73)-C(74)	115.4(10)
C(18)-Fe(1)-C(29)-C(25)	-61.8(6)	C(77')-N(7)-C(73)-C(74)	27(7)
C(17)-Fe(1)-C(29)-C(25)	-97.7(4)	C(73')-N(7)-C(73)-C(74)	-1.9(8)
C(15)-Fe(1)-C(29)-C(25)	-179.3(4)	C(77)-N(7)-C(73)-C(74)	175.3(8)
C(27)-Fe(1)-C(29)-C(25)	81.6(4)	C(75')-N(7)-C(75)-C(76)	1.3(9)
C(16)-Fe(1)-C(29)-C(25)	-141.8(4)	C(71)-N(7)-C(75)-C(76)	177.0(9)
C(26)-Fe(1)-C(29)-C(25)	37.3(4)	C(71')-N(7)-C(75)-C(76)	58(8)
C(19)-Fe(1)-C(29)-C(25)	164(11)	C(73)-N(7)-C(75)-C(76)	-53.8(11)
C(28)-Fe(1)-C(29)-C(25)	118.2(6)	C(77')-N(7)-C(75)-C(76)	133.3(11)
C(45)-N(31)-C(31)-V(3)	46(60)	C(73')-N(7)-C(75)-C(76)	-116.7(10)
C(40)-V(3)-C(31)-N(31)	4(59)	C(77)-N(7)-C(75)-C(76)	61.2(10)
C(43)-V(3)-C(31)-N(31)	0(51)	C(75')-N(7)-C(77)-C(78)	117.6(9)
C(44)-V(3)-C(31)-N(31)	-91(51)	C(71)-N(7)-C(77)-C(78)	-57.7(9)
C(42)-V(3)-C(31)-N(31)	90(51)	C(75)-N(7)-C(77)-C(78)	61.0(9)
C(41)-V(3)-C(31)-N(31)	-180(100)	C(71')-N(7)-C(77)-C(78)	-119.3(9)
C(55)-N(32)-C(32)-V(4)	-147(21)	C(73)-N(7)-C(77)-C(78)	-179.9(8)
C(53)-V(4)-C(32)-N(32)	105(26)	C(77')-N(7)-C(77)-C(78)	-3.5(8)
C(50)-V(4)-C(32)-N(32)	2(33)	C(73')-N(7)-C(77)-C(78)	-146(9)
C(52)-V(4)-C(32)-N(32)	15(26)	C(85)-N(8)-C(81)-C(82)	-58.7(8)
C(54)-V(4)-C(32)-N(32)	-166(100)	C(87)-N(8)-C(81)-C(82)	179.7(6)
C(51)-V(4)-C(32)-N(32)	-77(26)	C(83)-N(8)-C(81)-C(82)	60.3(8)
C(43)-V(3)-C(40)-O(40)	21(100)	C(85)-N(8)-C(83)-C(84)	173.2(6)
C(44)-V(3)-C(40)-O(40)	113(100)	C(81)-N(8)-C(83)-C(84)	50.5(8)
C(42)-V(3)-C(40)-O(40)	-68(100)	C(87)-N(8)-C(83)-C(84)	-66.7(7)
C(41)-V(3)-C(40)-O(40)	-159(100)	C(81)-N(8)-C(85)-C(86)	-59.9(8)
C(31)-V(3)-C(40)-O(40)	18(100)	C(87)-N(8)-C(85)-C(86)	58.7(7)
C(40)-V(3)-C(41)-O(41)	-79(17)	C(83)-N(8)-C(85)-C(86)	177.7(6)
C(43)-V(3)-C(41)-O(41)	99(17)	C(85)-N(8)-C(87)-C(88)	48.5(7)
C(44)-V(3)-C(41)-O(41)	7(17)	C(81)-N(8)-C(87)-C(88)	170.9(6)
C(42)-V(3)-C(41)-O(41)	-166(17)	C(83)-N(8)-C(87)-C(88)	-68.2(7)
C(31)-V(3)-C(41)-O(41)	101(17)	C(97)-N(9)-C(91)-C(92)	179.7(6)
C(40)-V(3)-C(42)-O(42)	30(12)	C(95)-N(9)-C(91)-C(92)	-59.0(8)
C(43)-V(3)-C(42)-O(42)	-60(12)	C(93)-N(9)-C(91)-C(92)	60.1(8)
C(44)-V(3)-C(42)-O(42)	41(13)	C(97)-N(9)-C(93)-C(94)	-51.9(7)
C(41)-V(3)-C(42)-O(42)	123(12)	C(95)-N(9)-C(93)-C(94)	-173.4(6)

C(31)-V(3)-C(42)-O(42)	-149(12)	C(91)-N(9)-C(93)-C(94)	65.3(7)
C(40)-V(3)-C(43)-O(43)	-20(13)	C(97)-N(9)-C(95)-C(96)	57.1(8)
C(44)-V(3)-C(43)-O(43)	-106(13)	C(91)-N(9)-C(95)-C(96)	-61.2(7)
C(42)-V(3)-C(43)-O(43)	67(13)	C(93)-N(9)-C(95)-C(96)	178.0(6)
C(41)-V(3)-C(43)-O(43)	162(11)	C(95)-N(9)-C(97)-C(98)	56.8(8)
C(31)-V(3)-C(43)-O(43)	160(13)	C(91)-N(9)-C(97)-C(98)	178.0(6)
C(40)-V(3)-C(44)-O(44)	-7(8)	C(93)-N(9)-C(97)-C(98)	-62.3(7)
C(43)-V(3)-C(44)-O(44)	84(8)	C(1S)-Cl(2)-Cl(2')-C(2S)	-112(3)
C(42)-V(3)-C(44)-O(44)	-17(10)	Cl(2')-Cl(2)-C(1S)-Cl(1)	-91.5(9)
C(41)-V(3)-C(44)-O(44)	-99(8)	C(2S)-Cl(2')-C(1S)-Cl(2)	150.9(19)
C(31)-V(3)-C(44)-O(44)	172(8)	Cl(2)-Cl(2')-C(1S)-Cl(1)	103.6(7)
C(31)-N(31)-C(45)-C(49)	9(14)	C(2S)-Cl(2')-C(1S)-Cl(1)	-105.5(16)
C(31)-N(31)-C(45)-C(46)	-170(14)	C(1S)-Cl(2')-C(2S)-C(3S)	-140.8(18)
C(31)-N(31)-C(45)-Fe(2)	-81(14)	Cl(2)-Cl(2')-C(2S)-C(3S)	-47(3)
C(55)-Fe(2)-C(45)-N(31)	153(18)	Cl(2')-C(2S)-C(3S)-C(4S)	105(2)
C(48)-Fe(2)-C(45)-N(31)	158.8(6)	C(2S)-C(3S)-C(4S)-C(5S)	121.8(18)
C(59)-Fe(2)-C(45)-N(31)	-62.1(7)	C(3S)-C(4S)-C(5S)-C(6S)	-68(4)
C(58)-Fe(2)-C(45)-N(31)	-23.3(7)	C(4S)-C(5S)-C(6S)-C(9S)	157(4)
C(47)-Fe(2)-C(45)-N(31)	-157.7(7)	C(4S)-C(5S)-C(6S)-C(7S)	-70(5)
C(49)-Fe(2)-C(45)-N(31)	119.9(7)	C(4S)-C(5S)-C(6S)-C(8S)	-66(5)
C(46)-Fe(2)-C(45)-N(31)	-119.6(7)		

Appendix 4

VII. Crystallographic data for $C_{34}H_{28}N_2O_8$, 2.1c

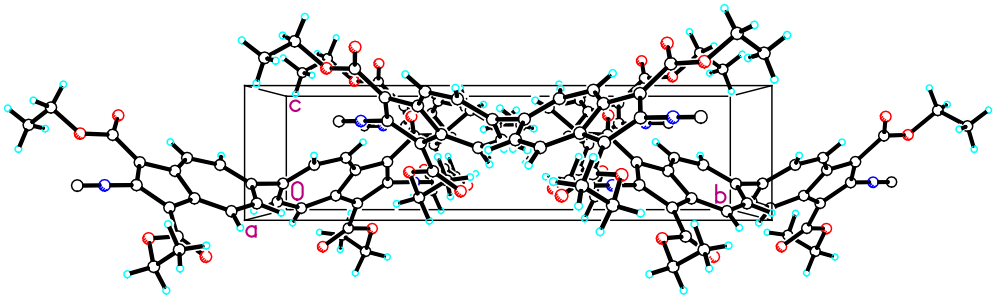

Figure VII.1. Packing diagram for $C_{34}H_{28}N_2O_8$.

Table VII.1. Atomic coordinates (x 10^4) and equivalent isotropic displacement parameters ($Å^2$ x 10^3) for $C_{34}H_{28}N_2O_8$, 2.1c. U(eq) is defined as one third of the trace of the orthogonalized U_{ij} tensor.

	x	y	z	U(eq)
C(1)	8262(1)	2584(1)	9259(4)	18(1)
C(2)	7605(1)	2605(1)	7500(1)	18(1)
C(3)	9413(1)	3404(1)	9603(4)	20(1)
C(4)	9869(1)	4034(1)	9027(4)	22(1)
C(5)	9697(1)	4697(1)	7500	20(1)
C(6)	8686(1)	3241(1)	8575(4)	18(1)
C(7)	8489(1)	2005(1)	11434(4)	18(1)
C(8)	8174(1)	810(1)	13573(4)	23(1)
C(9)	8729(1)	267(1)	12228(5)	27(1)
C(10)	6583(1)	1583(1)	7500	28(1)
N(1)	7049(1)	2049(1)	7500	19(1)
O(1)	7997(1)	1422(1)	11521(3)	22(1)
O(2)	9045(1)	2042(1)	12999(3)	23(1)

Table VII.2. Bond lengths [Å] for $C_{34}H_{28}N_2O_8$, 2.1c.

O(1)-C(7)	1.348(2)	C(2)-C(1)#1	1.407(2)
O(1)-C(8)	1.457(2)	C(3)-C(6)	1.394(2)
O(2)-C(7)	1.211(2)	C(3)-C(4)	1.397(2)
N(1)-C(2)	1.387(2)	C(4)-C(5)	1.393(2)
N(1)-C(10)	1.165(2)	C(5)-C(4)#1	1.393(2)
C(1)-C(2)	1.407(2)	C(5)-C(5)#2	1.512(4)
C(1)-C(6)	1.415(2)	C(6)-C(6)#1	1.475(3)
C(1)-C(7)	1.473(2)	C(8)-C(9)	1.500(2)

Symmetry transformations used to generate equivalent atoms:
#1: y+1/2, x-1/2, -z+3/2; #2: -x+2, -y+1, z

Table VII.3. Bond angles [°] for $C_{34}H_{28}N_2O_8$, 2.1c.

C(7)-O(1)-C(8)	116.5(1)	C(4)#1-C(5)-C(4)	127.7(2)
C(10)-N(1)-C(2)	180.0(2)	C(4)#1-C(5)-C(5)#2	116.2(1)
C(2)-C(1)-C(6)	107.0(1)	C(4)-C(5)-C(5)#2	116.2(1)
C(2)-C(1)-C(7)	128.2(2)	C(3)-C(6)-C(1)	125.7(2)
C(6)-C(1)-C(7)	124.8(1)	C(3)-C(6)-C(6)#1	126.8(1)
N(1)-C(2)-C(1)	124.4(1)	C(1)-C(6)-C(6)#1	107.4(1)
N(1)-C(2)-C(1)#1	124.4(1)	O(2)-C(7)-O(1)	123.2(2)
C(1)-C(2)-C(1)#1	111.1(2)	O(2)-C(7)-C(1)	124.9(1)
C(6)-C(3)-C(4)	129.3(2)	O(1)-C(7)-C(1)	112.0(1)
C(5)-C(4)-C(3)	129.5(2)	O(1)-C(8)-C(9)	111.0(2)

Symmetry transformations used to generate equivalent atoms:
#1: y+1/2, x-1/2, -z+3/2; #2: -x+2, -y+1, z

Table VII.4. Anisotropic displacement parameters ($Å^2$ x 10^3) for $C_{34}H_{28}N_2O_8$, 2.1c. The anisotropic displacement factor exponent takes the form: $-2\pi^2[h^2 a^{*2}U_{11} + ... + 2 h k a^* b^* U_{12}]$

	U11	U22	U33	U23	U13	U12
C(1)	15(1)	16(1)	22(1)	-1(1)	1(1)	1(1)
C(10)	23(1)	23(1)	39(1)	7(1)	-7(1)	-3(1)
C(2)	14(1)	14(1)	25(1)	-3(1)	3(1)	-3(1)
C(3)	18(1)	15(1)	26(1)	2(1)	0(1)	2(1)
C(4)	15(1)	18(1)	32(1)	0(1)	-3(1)	-1(1)
C(5)	16(1)	16(1)	27(1)	-3(1)	3(1)	-3(1)
C(6)	16(1)	14(1)	24(1)	-2(1)	1(1)	2(1)
C(7)	16(1)	14(1)	24(1)	-1(1)	4(1)	1(1)
C(8)	23(1)	17(1)	28(1)	5(1)	0(1)	-2(1)
C(9)	31(1)	16(1)	34(1)	3(1)	3(1)	-1(1)
N(1)	16(1)	16(1)	25(1)	2(1)	-2(1)	0(1)
O(1)	21(1)	15(1)	30(1)	5(1)	-3(1)	-4(1)
O(2)	20(1)	19(1)	29(1)	3(1)	-5(1)	-1(1)

Table VII.5. Hydrogen coordinates (x 10^4) and isotropic displacement parameters ($Å^2$ x 10^3) for $C_{34}H_{28}N_2O_8$, 2.1c.

	x	y	z	U(eq)
H(3)	9628	3034	10878	24
H(4)	10370	4005	9789	26
H(8A)	7703	536	14096	27
H(8B)	8390	1024	15417	27
H(9A)	8538	92	10307	41
H(9B)	8796	-169	13550	41
H(9C)	9217	521	11947	41

Table VII.6. Torsion angles [°] for $C_{34}H_{28}N_2O_8$, 2.1c.

C(10)-N(1)-C(2)-C(1)	0(100)	C(2)-C(1)-C(6)-C(3)	-173.2(2)
C(10)-N(1)-C(2)-C(1)#1	0(100)	C(7)-C(1)-C(6)-C(3)	7.1(3)
C(6)-C(1)-C(2)-N(1)	178.9(1)	C(2)-C(1)-C(6)-C(6)#1	2.8(2)
C(7)-C(1)-C(2)-N(1)	-1.3(2)	C(7)-C(1)-C(6)-C(6)#1	-177.0(2)
C(6)-C(1)-C(2)-C(1)#1	-1.1(1)	C(8)-O(1)-C(7)-O(2)	-1.7(2)
C(7)-C(1)-C(2)-C(1)#1	178.7(2)	C(8)-O(1)-C(7)-C(1)	179.1(1)
C(6)-C(3)-C(4)-C(5)	6.5(3)	C(2)-C(1)-C(7)-O(2)	-175.8(1)
C(3)-C(4)-C(5)-C(4)#1	-5.2(2)	C(6)-C(1)-C(7)-O(2)	4.0(3)
C(3)-C(4)-C(5)-C(5)#2	174.8(2)	C(2)-C(1)-C(7)-O(1)	3.5(2)
C(4)-C(3)-C(6)-C(1)	179.7(2)	C(6)-C(1)-C(7)-O(1)	-176.8(2)
C(4)-C(3)-C(6)-C(6)#1	4.5(3)	C(7)-O(1)-C(8)-C(9)	-82.8(2)

Symmetry transformations used to generate equivalent atoms:
#1: y+1/2, x-1/2, -z+3/2; #2: -x+2, -y+1, z

Appendix 5

VIII. Crystallographic data for $C_{32}H_{30}O_8$, 1,1',3,3'-tetraethoxycarbonyl-2,2'-biazulene

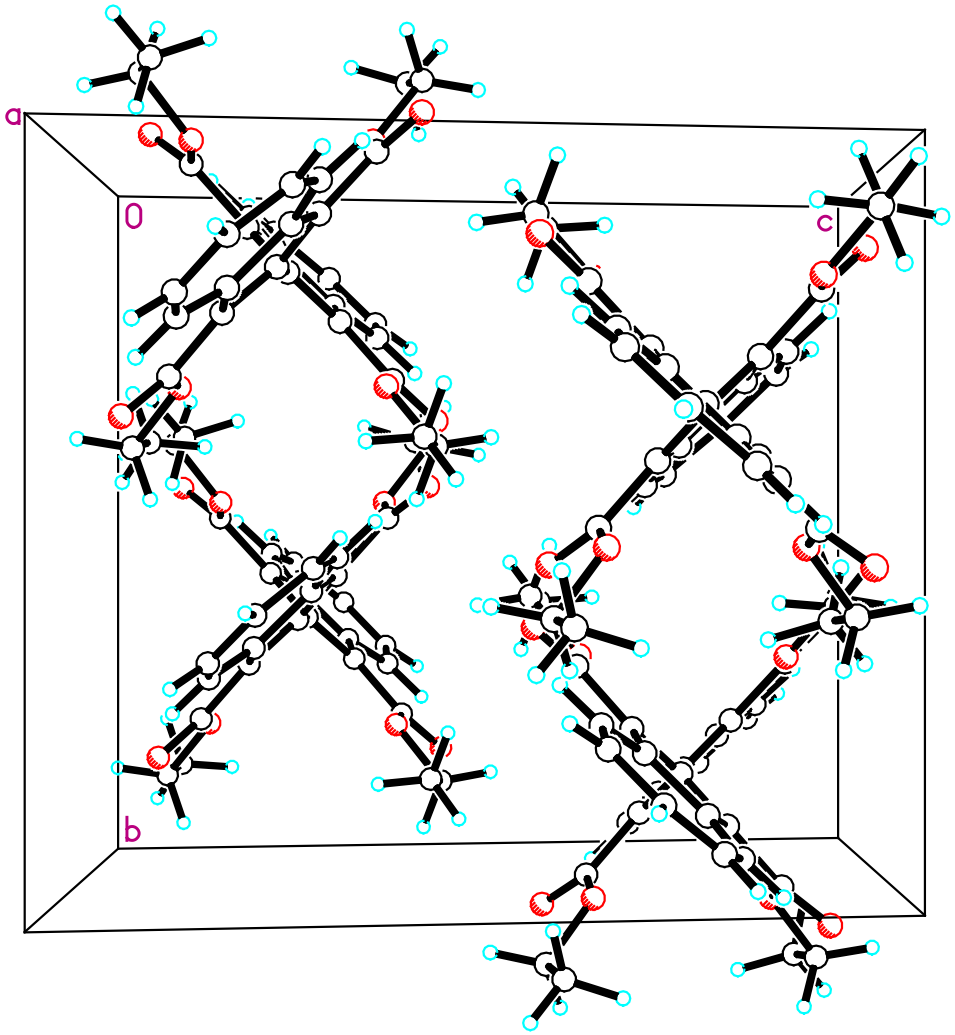

Figure VIII.1. Packing diagram for $C_{32}H_{30}O_8$ (polymorph I).

Table VIII.1. Atomic coordinates (x 10^4) and equivalent isotropic displacement parameters ($Å^2$ x 10^3) for $C_{32}H_{30}O_8$ (polymorph I). U(eq) is defined as one third of the trace of the orthogonalized U_{ij} tensor.

	x	y	z	U(eq)
O(1)	5415(1)	3110(1)	3795(1)	26(1)
O(2)	4247(1)	3553(1)	4392(1)	31(1)
O(3)	4867(1)	-310(1)	1375(1)	27(1)
O(4)	3471(1)	-547(1)	750(1)	29(1)
C(1)	4162(1)	2144(1)	3177(1)	20(1)
C(2)	4539(1)	1481(1)	2543(1)	19(1)
C(3)	3902(1)	801(1)	1998(1)	20(1)
C(4)	2325(1)	507(2)	1920(2)	25(1)

C(5)	1533(1)	658(2)	2193(2)	28(1)
C(6)	1320(1)	1324(2)	2918(2)	28(1)
C(7)	1838(1)	2032(2)	3551(2)	28(1)
C(8)	2697(1)	2289(2)	3602(2)	24(1)
C(9)	3277(1)	1867(2)	3056(1)	21(1)
C(10)	3107(1)	1021(1)	2291(1)	21(1)
C(11)	4585(1)	2996(2)	3849(1)	21(1)
C(12)	5896(1)	3948(2)	4413(2)	27(1)
C(13)	6812(1)	3843(2)	4286(2)	31(1)
C(14)	4032(1)	-70(1)	1308(1)	21(1)
C(15)	5087(1)	-1201(2)	775(2)	26(1)
C(16)	6046(1)	-1282(2)	981(2)	32(1)

Table VIII.2. Bond lengths [Å] for $C_{32}H_{30}O_8$ (polymorph 1).

O(1)-C(11)	1.339(2)	C(6)-H(6)	0.98(2)
O(1)-C(12)	1.452(2)	C(7)-C(8)	1.385(3)
O(2)-C(11)	1.210(2)	C(7)-H(7)	0.94(2)
O(3)-C(14)	1.342(2)	C(8)-C(9)	1.393(3)
O(3)-C(15)	1.448(2)	C(8)-H(8)	0.97(2)
O(4)-C(14)	1.211(2)	C(9)-C(10)	1.467(3)
C(1)-C(2)	1.407(3)	C(12)-C(13)	1.499(3)
C(1)-C(9)	1.421(3)	C(12)-H(12A)	0.98(2)
C(1)-C(11)	1.468(3)	C(12)-H(12B)	1.01(2)
C(2)-C(3)	1.410(3)	C(13)-H(13A)	0.97(2)
C(2)-C(2)#1	1.486(4)	C(13)-H(13B)	0.99(2)
C(3)-C(10)	1.418(3)	C(13)-H(13C)	0.97(2)
C(3)-C(14)	1.468(3)	C(15)-C(16)	1.494(3)
C(4)-C(5)	1.390(3)	C(15)-H(15A)	0.98(2)
C(4)-C(10)	1.396(3)	C(15)-H(15B)	0.99(2)
C(4)-H(4)	0.94(2)	C(16)-H(16A)	1.04(2)
C(5)-C(6)	1.382(3)	C(16)-H(16B)	0.96(2)
C(5)-H(5)	0.96(2)	C(16)-H(16C)	0.97(3)
C(6)-C(7)	1.384(3)		

Symmetry transformations used to generate equivalent atoms:
#1: -x+1, y, -z+1/2.

Table VIII.3. Bond angles [°] for $C_{32}H_{30}O_8$ (polymorph 1).

C(11)-O(1)-C(12)	116.83(15)	C(3)-C(10)-C(9)	106.78(16)
C(14)-O(3)-C(15)	117.61(15)	O(2)-C(11)-O(1)	122.05(17)
C(2)-C(1)-C(9)	108.47(16)	O(2)-C(11)-C(1)	126.02(17)
C(2)-C(1)-C(11)	127.19(17)	O(1)-C(11)-C(1)	111.93(15)
C(9)-C(1)-C(11)	124.33(16)	O(1)-C(12)-C(13)	106.39(17)

C(1)-C(2)-C(3)	108.99(16)	O(1)-C(12)-H(12A)	108.1(12)
C(1)-C(2)-C(2)#1	126.07(17)	C(13)-C(12)-H(12A)	113.3(12)
C(3)-C(2)-C(2)#1	124.94(17)	O(1)-C(12)-H(12B)	106.2(13)
C(2)-C(3)-C(10)	108.68(16)	C(13)-C(12)-H(12B)	112.6(13)
C(2)-C(3)-C(14)	126.76(17)	H(12A)-C(12)-H(12B)	109.9(18)
C(10)-C(3)-C(14)	124.33(17)	C(12)-C(13)-H(13A)	108.7(14)
C(5)-C(4)-C(10)	128.6(2)	C(12)-C(13)-H(13B)	112.3(14)
C(5)-C(4)-H(4)	116.0(13)	H(13A)-C(13)-H(13B)	109(2)
C(10)-C(4)-H(4)	115.4(13)	C(12)-C(13)-H(13C)	111.5(13)
C(6)-C(5)-C(4)	129.3(2)	H(13A)-C(13)-H(13C)	108.2(18)
C(6)-C(5)-H(5)	116.4(12)	H(13B)-C(13)-H(13C)	106.9(19)
C(4)-C(5)-H(5)	114.4(12)	O(4)-C(14)-O(3)	122.38(17)
C(5)-C(6)-C(7)	129.04(19)	O(4)-C(14)-C(3)	125.98(17)
C(5)-C(6)-H(6)	115.4(12)	O(3)-C(14)-C(3)	111.63(16)
C(7)-C(6)-H(6)	115.6(12)	O(3)-C(15)-C(16)	106.53(16)
C(6)-C(7)-C(8)	129.2(2)	O(3)-C(15)-H(15A)	106.8(11)
C(6)-C(7)-H(7)	114.7(13)	C(16)-C(15)-H(15A)	113.7(11)
C(8)-C(7)-H(7)	116.1(13)	O(3)-C(15)-H(15B)	110.1(12)
C(7)-C(8)-C(9)	129.1(2)	C(16)-C(15)-H(15B)	111.8(12)
C(7)-C(8)-H(8)	117.2(11)	H(15A)-C(15)-H(15B)	107.8(16)
C(9)-C(8)-H(8)	113.7(11)	C(15)-C(16)-H(16A)	111.3(12)
C(8)-C(9)-C(1)	125.82(18)	C(15)-C(16)-H(16B)	109.0(13)
C(8)-C(9)-C(10)	127.06(18)	H(16A)-C(16)-H(16B)	111.6(18)
C(1)-C(9)-C(10)	107.04(16)	C(15)-C(16)-H(16C)	108.9(14)
C(4)-C(10)-C(3)	125.66(18)	H(16A)-C(16)-H(16C)	106.7(19)
C(4)-C(10)-C(9)	127.55(18)	H(16B)-C(16)-H(16C)	109.3(18)

Symmetry transformations used to generate equivalent atoms:
#1: -x+1, y, -z+1/2.

Table VIII.4. Anisotropic displacement parameters ($Å^2$ x 10^3) for $C_{32}H_{30}O_8$ (polymorph I). The anisotropic displacement factor exponent takes the form: $-2\pi^2[h^2 a^{*2}U_{11} + ... + 2 h k a^* b^* U_{12}]$

	U_{11}	U_{22}	U_{33}	U_{23}	U_{13}	U_{12}
O(1)	20(1)	27(1)	32(1)	-10(1)	5(1)	-4(1)
O(2)	28(1)	29(1)	39(1)	-13(1)	11(1)	-2(1)
O(3)	23(1)	26(1)	32(1)	-10(1)	8(1)	-1(1)
O(4)	25(1)	27(1)	34(1)	-9(1)	1(1)	-1(1)
C(1)	19(1)	18(1)	23(1)	3(1)	4(1)	2(1)
C(2)	20(1)	17(1)	21(1)	5(1)	3(1)	1(1)
C(3)	20(1)	19(1)	21(1)	3(1)	4(1)	0(1)
C(4)	26(1)	21(1)	26(1)	3(1)	3(1)	-3(1)
C(5)	21(1)	27(1)	33(1)	3(1)	3(1)	-4(1)
C(6)	16(1)	30(1)	37(1)	6(1)	7(1)	1(1)

C(7)	24(1)	29(1)	34(1)	3(1)	11(1)	7(1)
C(8)	24(1)	23(1)	27(1)	1(1)	4(1)	3(1)
C(9)	23(1)	19(1)	22(1)	5(1)	3(1)	2(1)
C(10)	24(1)	17(1)	22(1)	5(1)	3(1)	0(1)
C(11)	20(1)	19(1)	24(1)	4(1)	4(1)	3(1)
C(12)	24(1)	27(1)	30(1)	-6(1)	2(1)	-5(1)
C(13)	26(1)	32(1)	35(1)	0(1)	0(1)	-5(1)
C(14)	22(1)	19(1)	22(1)	3(1)	5(1)	-1(1)
C(15)	29(1)	21(1)	31(1)	-7(1)	11(1)	-3(1)
C(16)	32(1)	28(1)	38(1)	-7(1)	14(1)	0(1)

Table VIII.5. Hydrogen coordinates (x 10^4) and isotropic displacement parameters (Å^2 x 10^3) for $C_{32}H_{30}O_8$ (polymorph I).

	x	y	z	U(eq)
H(4)	2341(13)	-17(18)	1426(16)	31(6)
H(5)	1079(13)	218(17)	1833(15)	25(5)
H(6)	720(14)	1278(17)	3002(15)	28(5)
H(7)	1563(14)	2385(17)	4007(16)	28(6)
H(8)	2949(12)	2818(15)	4095(13)	15(5)
H(12A)	5820(12)	3822(16)	5086(16)	23(5)
H(12B)	5633(15)	4674(19)	4171(16)	38(6)
H(13A)	7148(15)	4420(20)	4664(17)	41(6)
H(13B)	6871(15)	3907(19)	3591(19)	43(7)
H(13C)	7054(14)	3138(19)	4519(15)	32(6)
H(15A)	4801(12)	-1859(16)	958(13)	17(5)
H(15B)	4859(13)	-1050(17)	77(17)	30(6)
H(16A)	6275(14)	-1525(18)	1699(18)	38(6)
H(16B)	6283(13)	-587(18)	839(15)	29(6)
H(16C)	6220(15)	-1840(20)	563(18)	44(7)

Table VIII.6. Torsion angles [°] for $C_{32}H_{30}O_8$ (polymorph 1).

C(9)-C(1)-C(2)-C(3)	1.4(2)	C(14)-C(3)-C(10)-C(4)	-4.9(3)
C(11)-C(1)-C(2)-C(3)	-177.8(2)	C(2)-C(3)-C(10)-C(9)	-0.6(2)
C(9)-C(1)-C(2)-C(2)#1	-178.1(2)	C(14)-C(3)-C(10)-C(9)	174.2(2)
C(11)-C(1)-C(2)-C(2)#1	2.7(3)	C(8)-C(9)-C(10)-C(4)	3.6(3)
C(1)-C(2)-C(3)-C(10)	-0.5(2)	C(1)-C(9)-C(10)-C(4)	-179.4(2)
C(2)#1-C(2)-C(3)-C(10)	179.0(2)	C(8)-C(9)-C(10)-C(3)	-175.6(2)
C(1)-C(2)-C(3)-C(14)	-175.2(2)	C(1)-C(9)-C(10)-C(3)	1.5(2)
C(2)#1-C(2)-C(3)-C(14)	4.3(3)	C(12)-O(1)-C(11)-O(2)	-0.7(3)
C(10)-C(4)-C(5)-C(6)	-2.4(4)	C(12)-O(1)-C(11)-C(1)	178.7(2)
C(4)-C(5)-C(6)-C(7)	1.4(4)	C(2)-C(1)-C(11)-O(2)	-179.6(2)
C(5)-C(6)-C(7)-C(8)	2.5(4)	C(9)-C(1)-C(11)-O(2)	1.3(3)

C(6)-C(7)-C(8)-C(9)	-2.9(4)	C(2)-C(1)-C(11)-O(1)	1.0(3)
C(7)-C(8)-C(9)-C(1)	-177.6(2)	C(9)-C(1)-C(11)-O(1)	-178.1(2)
C(7)-C(8)-C(9)-C(10)	-1.0(3)	C(11)-O(1)-C(12)-C(13)	175.1(2)
C(2)-C(1)-C(9)-C(8)	175.3(2)	C(15)-O(3)-C(14)-O(4)	-2.2(3)
C(11)-C(1)-C(9)-C(8)	-5.5(3)	C(15)-O(3)-C(14)-C(3)	176.5(2)
C(2)-C(1)-C(9)-C(10)	-1.8(2)	C(2)-C(3)-C(14)-O(4)	-169.4(2)
C(11)-C(1)-C(9)-C(10)	177.5(2)	C(10)-C(3)-C(14)-O(4)	16.7(3)
C(5)-C(4)-C(10)-C(3)	177.9(2)	C(2)-C(3)-C(14)-O(3)	11.9(3)
C(5)-C(4)-C(10)-C(9)	-1.1(3)	C(10)-C(3)-C(14)-O(3)	-162.0(2)
C(2)-C(3)-C(10)-C(4)	-179.8(2)	C(14)-O(3)-C(15)-C(16)	179.3(2)

Symmetry transformations used to generate equivalent atoms:
#1: -x+1; y; -z+1/2.
.

Appendix 6

IX. Crystallographic data for 2,2’-biazulene, $C_{20}H_{14}$

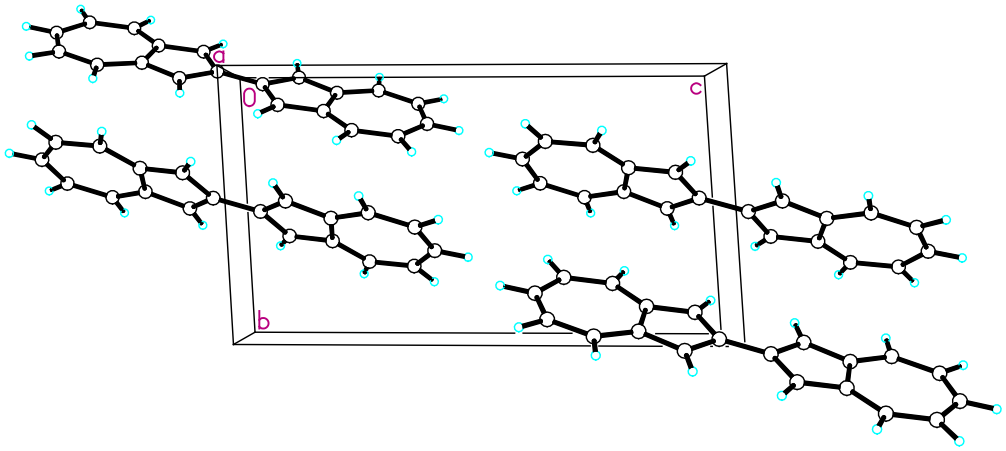

Figure IX.1. Packing diagram for $C_{20}H_{14}$.

Table IX.1. Atomic coordinates coordinates (x 10^4) and equivalent isotropic displacement parameters ($Å^2$ x 10^3) for $C_{20}H_{14}$. U(eq) is defined as one third of the trace of the orthogonalized U_{ij} tensor.

	x	y	z	U(eq)
C(1)	-1635(4)	-77(3)	1232(2)	22(1)
C(2)	39(4)	255(3)	487(2)	20(1)
C(3)	1810(4)	1133(3)	852(2)	21(1)
C(4)	2677(4)	2142(3)	2420(2)	22(1)
C(5)	2328(4)	2368(3)	3390(2)	24(1)
C(6)	509(4)	1846(3)	4003(2)	24(1)
C(7)	-1442(4)	992(3)	3818(2)	24(1)
C(8)	-2083(4)	435(3)	2959(2)	23(1)
C(9)	-940(4)	564(3)	2066(2)	20(1)
C(10)	1310(4)	1359(3)	1814(2)	20(1)
C(11)	3369(4)	6187(3)	999(2)	22(1)
C(12)	5059(4)	5250(3)	487(2)	20(1)
C(13)	6856(4)	4861(3)	1085(2)	20(1)
C(14)	7593(4)	5290(3)	2770(2)	23(1)
C(15)	7095(4)	5817(3)	3684(2)	25(1)
C(16)	5187(4)	6709(3)	4041(2)	26(1)
C(17)	3289(4)	7324(3)	3575(2)	24(1)
C(18)	2792(4)	7169(3)	2633(2)	22(1)
C(19)	4036(4)	6365(3)	1915(2)	21(1)
C(20)	6311(4)	5497(3)	1976(2)	19(1)

Table IX.2. Bond lengths [Å] for $C_{20}H_{14}$.

C(1)-C(9)	1.393(3)	C(11)-C(19)	1.388(3)
C(1)-C(2)	1.414(3)	C(11)-C(12)	1.410(3)
C(1)-H(1)	1.00(2)	C(11)-H(11)	0.99(2)

C(2)-C(3)	1.406(3)	C(12)-C(13)	1.412(3)
C(2)-C(2)#1	1.455(4)	C(12)-C(12)#2	1.455(4)
C(3)-C(10)	1.388(3)	C(13)-C(20)	1.392(3)
C(3)-H(3)	0.97(2)	C(13)-H(13)	0.98(2)
C(4)-C(10)	1.389(3)	C(14)-C(15)	1.387(3)
C(4)-C(5)	1.391(3)	C(14)-C(20)	1.389(3)
C(4)-H(4)	0.99(2)	C(14)-H(14)	0.98(2)
C(5)-C(6)	1.390(3)	C(15)-C(16)	1.393(3)
C(5)-H(5)	1.01(2)	C(15)-H(15)	0.99(2)
C(6)-C(7)	1.394(3)	C(16)-C(17)	1.394(3)
C(6)-H(6)	0.99(2)	C(16)-H(16)	0.98(2)
C(7)-C(8)	1.388(3)	C(17)-C(18)	1.389(3)
C(7)-H(7)	0.99(2)	C(17)-H(17)	0.96(2)
C(8)-C(9)	1.389(3)	C(18)-C(19)	1.385(3)
C(8)-H(8)	0.94(2)	C(18)-H(18)	0.97(2)
C(9)-C(10)	1.497(3)	C(19)-C(20)	1.494(3)

Symmetry transformations used to generate equivalent atoms:
#1: -x, -y, -z; #2: -x+1, -y+1, -z.

Table IX.3. Bond angles [°] for $C_{20}H_{14}$.

C(9)-C(1)-C(2)	109.1(2)	C(19)-C(11)-C(12)	109.1(2)
C(9)-C(1)-H(1)	127(1)	C(19)-C(11)-H(11)	127(1)
C(2)-C(1)-H(1)	124(1)	C(12)-C(11)-H(11)	124(1)
C(3)-C(2)-C(1)	108.4(2)	C(11)-C(12)-C(13)	108.4(2)
C(3)-C(2)-C(2)#1	125.9(3)	C(11)-C(12)-C(12)#2	125.5(3)
C(1)-C(2)-C(2)#1	125.7(3)	C(13)-C(12)-C(12)#2	126.0(2)
C(10)-C(3)-C(2)	109.4(2)	C(20)-C(13)-C(12)	109.2(2)
C(10)-C(3)-H(3)	127(1)	C(20)-C(13)-H(13)	126(1)
C(2)-C(3)-H(3)	124(1)	C(12)-C(13)-H(13)	125(1)
C(10)-C(4)-C(5)	129.4(2)	C(15)-C(14)-C(20)	129.1(2)
C(10)-C(4)-H(4)	116(1)	C(15)-C(14)-H(14)	119(1)
C(5)-C(4)-H(4)	115(1)	C(20)-C(14)-H(14)	112(1)
C(6)-C(5)-C(4)	128.3(2)	C(14)-C(15)-C(16)	129.0(2)
C(6)-C(5)-H(5)	118(1)	C(14)-C(15)-H(15)	118(1)
C(4)-C(5)-H(5)	114(1)	C(16)-C(15)-H(15)	113(1)
C(5)-C(6)-C(7)	130.1(2)	C(15)-C(16)-C(17)	129.4(2)
C(5)-C(6)-H(6)	115(1)	C(15)-C(16)-H(16)	117(1)
C(7)-C(6)-H(6)	115(1)	C(17)-C(16)-H(16)	113(1)
C(8)-C(7)-C(6)	128.7(2)	C(18)-C(17)-C(16)	128.7(2)
C(8)-C(7)-H(7)	116(1)	C(18)-C(17)-H(17)	117(1)
C(6)-C(7)-H(7)	115(1)	C(16)-C(17)-H(17)	114(1)
C(7)-C(8)-C(9)	129.1(2)	C(19)-C(18)-C(17)	129.3(2)
C(7)-C(8)-H(8)	117(1)	C(19)-C(18)-H(18)	117(1)
C(9)-C(8)-H(8)	114(1)	C(17)-C(18)-H(18)	114(1)
C(8)-C(9)-C(1)	126.5(2)	C(18)-C(19)-C(11)	125.9(2)

C(8)-C(9)-C(10)	127.1(2)	C(18)-C(19)-C(20)	127.2(2)
C(1)-C(9)-C(10)	106.4(2)	C(11)-C(19)-C(20)	106.9(2)
C(3)-C(10)-C(4)	126.0(2)	C(14)-C(20)-C(13)	126.4(2)
C(3)-C(10)-C(9)	106.7(2)	C(14)-C(20)-C(19)	127.2(2)
C(4)-C(10)-C(9)	127.3(2)	C(13)-C(20)-C(19)	106.4(2)

Symmetry transformations used to generate equivalent atoms:
#1: -x, -y, -z; #2: -x+1, -y+1, -z.

Table IX.4. Anisotropic displacement parameters ($Å^2 x 10^3$) for $C_{20}H_{14}$. The anisotropic displacement factor exponent takes the form: $-2\pi^2[h^2 a^{*2} U_{11} + ... + 2 h k a^* b^* U_{12}]$

	U_{11}	U_{22}	U_{33}	U_{23}	U_{13}	U_{12}
C(1)	20(1)	17(1)	28(1)	3(1)	-3(1)	0(1)
C(2)	22(1)	15(1)	23(1)	3(1)	-2(1)	3(1)
C(3)	18(1)	18(1)	26(1)	2(1)	-1(1)	0(1)
C(4)	20(1)	15(1)	30(2)	1(1)	-1(1)	1(1)
C(5)	23(1)	21(1)	29(2)	-1(1)	-8(1)	0(1)
C(6)	29(2)	22(1)	22(1)	0(1)	-5(1)	5(1)
C(7)	23(1)	23(1)	24(1)	2(1)	2(1)	3(1)
C(8)	17(1)	17(1)	33(2)	5(1)	0(1)	2(1)
C(9)	21(1)	14(1)	25(1)	4(1)	-4(1)	4(1)
C(10)	21(1)	13(1)	25(1)	3(1)	-2(1)	4(1)
C(11)	20(1)	17(1)	28(1)	5(1)	-1(1)	2(1)
C(12)	19(1)	14(1)	24(1)	5(1)	0(1)	0(1)
C(13)	18(1)	17(1)	25(1)	2(1)	1(1)	1(1)
C(14)	22(1)	17(1)	30(2)	1(1)	-3(1)	-1(1)
C(15)	27(1)	23(1)	25(2)	1(1)	-6(1)	-3(1)
C(16)	33(2)	24(1)	23(2)	-3(1)	0(1)	-2(1)
C(17)	24(1)	20(1)	28(2)	-2(1)	3(1)	-1(1)
C(18)	20(1)	16(1)	31(2)	2(1)	-1(1)	-1(1)
C(19)	22(1)	13(1)	27(1)	5(1)	-3(1)	-2(1)
C(20)	17(1)	14(1)	27(1)	4(1)	0(1)	-2(1)

Table IX.5. Hydrogen coordinates ($x 10^4$) and isotropic displacement parameters ($Å^2 x 10^3$) for $C_{20}H_{14}$.

	x	y	z	U(eq)
H(1)	-3060(40)	-710(30)	1162(14)	16(6)
H(3)	3150(40)	1520(30)	472(15)	21(6)
H(4)	4140(40)	2570(30)	2128(15)	21(6)
H(5)	3580(40)	2990(30)	3671(15)	19(6)
H(6)	620(30)	2110(30)	4677(15)	11(5)
H(7)	-2510(40)	760(30)	4378(16)	23(6)
H(8)	-3450(40)	-160(30)	2971(16)	24(6)
H(11)	1910(40)	6580(30)	739(16)	30(7)

H(13)	8230(40)	4210(30)	906(15)	23(6)
H(14)	9040(40)	4680(30)	2631(15)	26(6)
H(15)	8210(40)	5540(30)	4175(15)	14(6)
H(16)	5120(40)	6950(30)	4716(16)	17(6)
H(17)	2220(40)	7950(30)	3966(15)	15(6)
H(18)	1330(40)	7670(30)	2471(15)	21(6)

Table IX.6. Torsion angles [°] for $C_{20}H_{14}$.

C(9)-C(1)-C(2)-C(3)	-0.6(3)	C(19)-C(11)-C(12)-C(13)	-1.4(3)
C(9)-C(1)-C(2)-C(2)#1	178.3(3)	C(19)-C(11)-C(12)-C(12)#2	177.8(3)
C(1)-C(2)-C(3)-C(10)	0.3(3)	C(11)-C(12)-C(13)-C(20)	1.5(3)
C(2)#1-C(2)-C(3)-C(10)	-178.6(3)	C(12)#2-C(12)-C(13)-C(20)	-177.6(3)
C(10)-C(4)-C(5)-C(6)	0.7(4)	C(20)-C(14)-C(15)-C(16)	-0.8(4)
C(4)-C(5)-C(6)-C(7)	-1.0(4)	C(14)-C(15)-C(16)-C(17)	-0.8(4)
C(5)-C(6)-C(7)-C(8)	0.0(4)	C(15)-C(16)-C(17)-C(18)	1.7(4)
C(6)-C(7)-C(8)-C(9)	0.8(4)	C(16)-C(17)-C(18)-C(19)	0.1(4)
C(7)-C(8)-C(9)-C(1)	177.6(2)	C(17)-C(18)-C(19)-C(11)	176.5(2)
C(7)-C(8)-C(9)-C(10)	-0.1(4)	C(17)-C(18)-C(19)-C(20)	-2.2(4)
C(2)-C(1)-C(9)-C(8)	-177.5(2)	C(12)-C(11)-C(19)-C(18)	-178.2(2)
C(2)-C(1)-C(9)-C(10)	0.5(2)	C(12)-C(11)-C(19)-C(20)	0.7(2)
C(2)-C(3)-C(10)-C(4)	178.7(2)	C(15)-C(14)-C(20)-C(13)	-176.5(2)
C(2)-C(3)-C(10)-C(9)	0.0(2)	C(15)-C(14)-C(20)-C(19)	0.3(4)
C(5)-C(4)-C(10)-C(3)	-177.8(2)	C(12)-C(13)-C(20)-C(14)	176.3(2)
C(5)-C(4)-C(10)-C(9)	0.6(4)	C(12)-C(13)-C(20)-C(19)	-1.0(2)
C(8)-C(9)-C(10)-C(3)	177.7(2)	C(18)-C(19)-C(20)-C(14)	1.8(4)
C(1)-C(9)-C(10)-C(3)	-0.3(2)	C(11)-C(19)-C(20)-C(14)	-177.1(2)
C(8)-C(9)-C(10)-C(4)	-0.9(4)	C(18)-C(19)-C(20)-C(13)	179.1(2)
C(1)-C(9)-C(10)-C(4)	-179.0(2)	C(11)-C(19)-C(20)-C(13)	0.2(2)

Symmetry transformations used to generate equivalent atoms:
#1: -x, -y, -z; #2: -x+1, -y+1, -z .

Appendix 7

X. Cartesion Coordinates from DFT Optimized Structures of 8,16,24,32-Tetraisocyano[2.2.2.2]metacyclophane

Table X.1. Cartesian coordinates for the DFT optimized structure of 3.3 (as shown in Figure III.14).

Atom	X	Y	Z	Atom	X	Y	Z
N1	1.9302	1.0716	1.7151	H12	-5.642	-0.0938	-1.3053
N2	-2.0609	1.0297	-1.5701	C20	-4.6044	-1.3341	0.1192
N3	-2.8014	-3.2108	-1.1019	H13	-5.2691	-1.0536	0.9449
N4	3.6857	-2.4945	1.007	H14	-5.0429	-2.2197	-0.3534
C1	1.5425	0.3579	2.5686	C21	-2.3736	-2.5892	0.0668
C2	-1.3662	0.4947	-2.3571	C22	-3.2442	-1.6698	0.6926
C3	-3.1769	-3.7371	-2.0873	C23	-2.808	-1.0715	1.8794
C4	4.2075	-2.937	1.9667	H15	-3.4629	-0.3676	2.3864
C5	2.3768	1.975	0.7585	C24	-1.553	-1.3626	2.4117
C6	3.7358	1.965	0.3897	H16	-1.2173	-0.8784	3.3238
C7	4.1653	2.9558	-0.5023	C25	-0.7127	-2.272	1.7702
H1	5.2136	2.9879	-0.7912	H17	0.261	-2.4761	2.2019
C8	3.272	3.8873	-1.028	C26	-1.0997	-2.9121	0.5884
H2	3.6265	4.6518	-1.7145	C27	-0.2245	-3.964	-0.0738
C9	1.9155	3.8309	-0.6936	H18	-0.4945	-4.0571	-1.1292
H3	1.2283	4.5429	-1.1402	H19	-0.4723	-4.9405	0.3684
C10	1.4354	2.8711	0.2004	C28	1.2997	-3.7795	0.0669
C11	-0.0285	2.7242	0.5666	H20	1.5805	-3.7761	1.1241
H4	-0.193	3.0855	1.5921	H21	1.7737	-4.6819	-0.3472
H5	-0.2612	1.6543	0.6008	C29	3.0899	-1.9726	-0.1364
C12	-1.0397	3.4143	-0.3777	C30	1.9022	-2.567	-0.6227
H6	-1.0141	4.5011	-0.237	C31	1.3446	-2.0238	-1.7844
H7	-0.7614	3.2166	-1.4186	H22	0.4258	-2.436	-2.1877
C13	-2.8967	1.6965	-0.6817	C32	1.9413	-0.9478	-2.4411
C14	-2.4435	2.9116	-0.1183	H23	1.4766	-0.5421	-3.3343
C15	-3.3166	3.5988	0.7283	C33	3.1118	-0.3838	-1.9386
H8	-2.9952	4.5403	1.1676	H24	3.5696	0.4591	-2.4495
C16	-4.589	3.0962	1.0112	C34	3.7063	-0.8722	-0.77
H9	-5.2591	3.6512	1.6625	C35	4.95	-0.2091	-0.2164
C17	-4.9989	1.8828	0.4608	H25	5.4935	0.2503	-1.0505
H10	-5.9885	1.4934	0.6895	H26	5.6187	-0.9556	0.2263
C18	-4.1623	1.1486	-0.3902	C36	4.6838	0.8853	0.8639
C19	-4.6126	-0.1896	-0.9371	H27	4.3024	0.4116	1.7718
H11	-3.9989	-0.4829	-1.7925	H28	5.651	1.3346	1.1215

Table X.2. Cartesian coordinates for the DFT-optimized structure 1 of 3.3 on gold(111) (shown in Figure III.16).

Atom	X	Y	Z	Atom	X	Y	Z
C1	-4.5148	-1.3251	-2.0181	H16	3.1374	3.9924	1.1109
C2	-3.8	-2.4175	-1.5243	C18	3.1706	2.374	-0.2748
C3	-3.1706	-2.374	-0.2748	C19	3.8	2.4175	-1.5244
C4	-3.2888	-1.171	0.4557	C20	4.5148	1.325	-2.0182
C5	-3.9915	-0.04	-0.0192	C21	4.609	0.1524	-1.2699
C6	-4.609	-0.1524	-1.2699	C22	3.9914	0.04	-0.0192
H1	-5.0069	-1.3929	-2.9849	C23	3.2888	1.171	0.4557
H2	-3.7442	-3.3318	-2.1109	N3	2.7254	1.1118	1.7192
C7	-2.5139	-3.6358	0.2785	C24	4.1319	-1.2141	0.8288
H3	-2.5932	-4.4064	-0.498	H17	3.4752	-1.1472	1.6986
H4	-3.1374	-3.9925	1.1109	H18	5.1563	-1.2497	1.2269
N1	-2.7254	-1.1118	1.7192	C25	3.8673	-2.5662	0.1125
C8	-4.1319	1.2141	0.8287	H19	4.5773	-2.6969	-0.7122
H5	-5.1564	1.2497	1.2269	H20	4.0844	-3.3595	0.8363
H6	-3.4753	1.1472	1.6986	H21	5.1815	-0.6854	-1.6591
H7	-5.1815	0.6853	-1.6591	H22	5.0068	1.3928	-2.985
C9	-3.8673	2.5662	0.1125	H23	3.7441	3.3317	-2.111
H8	-4.5772	2.6969	-0.7122	C26	2.4627	-2.7228	-0.4274
H9	-4.0844	3.3595	0.8363	C27	2.1943	-2.4338	-1.7712
C10	-2.4626	2.7227	-0.4275	C28	0.9054	-2.532	-2.2866
C11	-2.1943	2.4337	-1.7712	C29	-0.1514	-2.9092	-1.4576
C12	-0.9054	2.5319	-2.2866	C30	0.0564	-3.2157	-0.1099
C13	0.1514	2.9092	-1.4576	C31	1.3835	-3.1403	0.3816
C14	-0.0563	3.2157	-0.1099	H24	3.0128	-2.1277	-2.4162
C15	-1.3835	3.1403	0.3816	H25	0.7185	-2.306	-3.3332
H10	-3.0127	2.1276	-2.4162	H26	-1.1521	-2.9589	-1.8687
H11	-0.7184	2.3058	-3.3332	C32	-1.064	-3.6278	0.8225
H12	1.1522	2.9589	-1.8687	H27	-0.8667	-4.6532	1.1672
C16	1.064	3.6279	0.8225	H28	-1.0044	-3.0186	1.728
H13	0.8667	4.6533	1.1671	N4	1.6344	-3.5232	1.6996
H14	1.0044	3.0187	1.728	C33	-2.2541	-1.0695	2.7969
N2	-1.6344	3.5233	1.6995	C34	-1.8525	3.9042	2.7968
C17	2.514	3.6358	0.2785	C35	2.2541	1.0696	2.7969
H15	2.5932	4.4064	-0.4979	C36	1.8525	-3.9041	2.7969

Table X.3. Cartesian coordinates for the DFT-optimized structure 2 of 3.3 on gold(111) (shown in Figure III.16).

Atom	X	Y	Z	Atom	X	Y	Z
C1	2.6124	-2.6965	-2.2683	C18	-3.6505	1.5598	-0.3863
C2	3.5733	-1.8279	-1.7574	C19	-3.5735	1.8279	-1.7573
C3	3.6504	-1.5599	-0.3864	C20	-2.6128	2.6966	-2.2682
C4	2.7381	-2.2308	0.4579	C21	-1.6785	3.285	-1.4162
C5	1.6994	-3.0554	-0.0375	C22	-1.6995	3.0553	-0.0375
C6	1.6782	-3.2849	-1.4162	C23	-2.7381	2.2307	0.4579
H1	2.5803	-2.9068	-3.3341	H17	-4.2861	1.3574	-2.4295
H2	4.2858	-1.3574	-2.4297	H18	-2.5808	2.907	-3.334
C7	4.6912	-0.5976	0.1542	H19	-0.9288	3.942	-1.8368
H3	5.4054	-0.3724	-0.646	N2	-2.9151	2.1214	1.8339
H4	5.2699	-1.0904	0.9458	N3	-2.4089	-2.6882	1.8201
N1	2.9152	-2.1218	1.8339	C24	-0.6931	3.6722	0.9213
H5	0.9283	-3.9418	-1.8367	H20	-0.3907	2.9126	1.6514
C8	0.6931	-3.6723	0.9214	H21	-1.204	4.4448	1.5139
H6	1.2041	-4.4449	1.5139	C25	0.5788	4.3256	0.3163
H7	0.3908	-2.9127	1.6515	H22	0.2941	5.0958	-0.4097
C9	-0.5788	-4.3256	0.3165	H23	1.0705	4.8568	1.14
H8	-0.2942	-5.0959	-0.4094	C26	1.5846	3.3894	-0.3326
H9	-1.0705	-4.8569	1.1402	C27	1.7597	3.3544	-1.7207
C10	-1.5847	-3.3895	-0.3323	C28	2.6862	2.4978	-2.3125
C11	-1.7601	-3.3548	-1.7204	C29	3.4448	1.631	-1.5259
C12	-2.6867	-2.4983	-2.3122	C30	3.3252	1.6254	-0.1333
C13	-3.4451	-1.6313	-1.5256	C31	2.4199	2.5505	0.4375
C14	-3.3252	-1.6255	-0.133	H24	1.1754	4.0214	-2.3481
C15	-2.4198	-2.5504	0.4378	H25	2.8124	2.4991	-3.392
H10	-1.1759	-4.0219	-2.3478	H26	4.1482	0.9607	-2.006
H11	-2.8131	-2.4998	-3.3916	C32	4.1446	0.7169	0.7671
H12	-4.1487	-0.9611	-2.0057	H27	5.007	1.2822	1.1507
C16	-4.1446	-0.7169	0.7674	H28	3.5516	0.4718	1.6524
H13	-3.5515	-0.4717	1.6526	N4	2.4095	2.6887	1.8198
H14	-5.0069	-1.2822	1.1511	C33	3.1895	-2.0854	2.9815
C17	-4.6912	0.5975	0.1545	C34	-2.5185	-2.8587	2.9819
H15	-5.4055	0.3722	-0.6458	C35	-3.1885	2.0861	2.9818
H16	-5.2699	1.0903	0.946	C36	2.5195	2.8596	2.9815